CHARACTERIZATION OF GLAZES OF THE 11-14th-CENTURY POTSHERDS AND TILES FROM COMANA PONTICA IN TOKAT, TURKEY

A THESIS SUBMITTED TO
THE GRADUATE SCHOOL OF NATURAL AND APPLIED SCIENCES
OF
MIDDLE EAST TECHNICAL UNIVERSITY

BY

CANBERK ALTUNDAL

IN PARTIAL FULFILLMENT OF THE REQUIREMENTS
FOR
THE DEGREE OF MASTER OF SCIENCE
IN
ARCHAEOMETRY

SEPTEMBER 2023

Approval of the thesis:

CHARACTERIZATION OF GLAZES OF THE 11-14th-CENTURY POTSHERDS AND TILES FROM COMANA PONTICA IN TOKAT, TURKEY

submitted by **CANBERK ALTUNDAL** in partial fulfillment of the requirements for the degree of **Master of Science** i**n Archaeometry, Middle East Technical University** by,

Prof. Dr. Halil Kalıpçılar

Dean, Graduate School of **Natural and Applied Sciences**

Assoc. Prof. Dr. Ayşe Tavukçuoğlu

Head of the Department, **Archaeometry**

Prof. Dr. Deniz Burcu Erciyas

Supervisor, **Archaeometry, METU**

Assoc. Prof. Dr. Gülsu Şimşek Franci

Co-Supervisor, **KUYTAM, Koç University**

Examining Committee Members:

Assoc. Prof. Dr. Evangelia Pişkin

Archaeometry, METU

Prof. Dr. Deniz Burcu Erciyas

Archaeometry, METU

Assoc. Prof. Dr. Meryem Acara Eser

Art History, Sivas Cumhuriyet University

Date: 08.09.2023

I hereby declare that all information in this document has been obtained and presented in accordance with academic rules and ethical conduct. I also declare that, as required by these rules and conduct, I have fully cited and referenced all material and results that are not original to this work.

Name Last name: Canberk Altundal

Signature:

ABSTRACT

CHARACTERIZATION OF GLAZES OF THE 11-14th-CENTURY POTSHERDS AND TILES FROM COMANA PONTICA IN TOKAT, TURKEY

Altundal, Canberk
Master of Science, Archaeometry
Supervisor: Prof. Dr. Deniz Burcu Erciyas
Co-Supervisor: Assoc. Prof. Dr. Gülsu Franci Şimşek

September 2023, 222 pages

Comana Pontica, the ancient settlement in Tokat, Turkey, was one of the intersection points on the main ancient road connecting the inland cities of the Black Sea Region to the coastal cities. Archaeological findings from the layers of the Ottomans, the Seljuks-Danishmendids, the Byzantines, the Romans and the Greeks were revealed by the excavations from 2009 till present day. Totally 1479 glazed ceramic samples, 1842 unglazed cooking utensils and 2223 unglazed storage containers were unearthed from the Seljukid-Danishmendids' layers until 2018. In this thesis, within these 5544 ceramic samples, totally 106 glaze spacimens with different colors on sides, together with 6 paste and 3 slip spacimens from the inner sides of 71 glazed potsherds and 2 glazed tiles, which were collected from the 11-14th-century Seljukid-Danishmendids' layers, were analyzed by Fourier-Transform Infrared (FT-IR), X-Ray Powder Diffraction (XRD), Raman Spectroscopy, and X-Ray Fluorescence (XRF) Spectrometry. The aim was to find the composition of glaze colorants and production technologies of the glazes, to reveal the estimated firing temperatures of the ceramics and to characterize the

samples with the help of the percentages of the oxide contents of the glazes. Moreover, these XRF oxide data were shown in bivariate and ternary plots, and then compared with the literature data in order to display whether the contents of materials used in the glazes of pottery and tile samples represent the characteristics of their period.

As a result, with the help of the wavenumber positions of their Si-O asymmetric stretching peaks, firing temperature range of the Comana Pontica ceramics was estimated as changing between 600 and 925 °C, with a majority fired in the range of 800-900 °C. Brown glazes were determined to be applied in a reducing atmosphere and fired around 700-750 °C, followed by turquoise glazes in 725-800 °C, yellow and green glazes in 750-800 °C, orange glazes around 850 °C, and the black glaze around 900 °C. Red pastes were discovered to be fired around 850-900 °C, while white pastes behind the turquoise glazed potsherd and tiles, and the white slip layers around 900 °C, which can be suggested that the initial firing was done to the all potsherds except the turquoise one and at around 900 °C, then glazed and re-fired to 700-850 °C in an oxidating atmosphere for the light-colored glazes, as well as to colder temperatures in an reducing environment for the darker glazes.

Furthermore, according to the vibrations around 3600-3700 cm^{-1} in an FTIR spectrum, the clay minerals in the glazes were identified as mainly in kaolinit (dickite, halloysite, kaolinite, nacrite) and montmorillonit-smectite (bentonite, montmorillonite, saponite, smectite, vermiculite) groups. On the other hand, exceptionally, paste of K104 was also including illite and sepiolite. In the rest of the slips and pastes, the peaks are almost not observed, probably due to the dehydroxylation, dehydration, and decarbonation occurred at higher firing temperature values such as 850-925 °C. Moreover, inclusions of slaked lime [$Ca(OH)_2$], quicklime (CaO) and calcite ($CaCO_3$ also provide information about the possible firing temperatures with signals at 3648 cm^{-1}, 1647 cm^{-1} and 1430-1450 cm^{-1}, recpectively, probably all taken from the crushed shells and bones. If $CaCO_3$ peak is observed, it means the temperature was below 600 °C, CaO between 600-800 °C,

$Ca(OH)_2$ between 800-900 °C and disapperance of all the calcite peaks and -OH bands corresponds to the temperature above 900 °C. Additionally, due to the positive slope of the trend line in the chart of estimated average firing temperatures of the glazed ceramics differentiated by periods of production dates, the firing temperatures of the glazed ceramics of Comana Pontica were estimated to be increasing from the 12^{th} till 14^{th} centuries.

Moreover, the colorant for the yellow glazes was considered mostly to be lead antimonate ($Pb_2Sb_2O_7$) and green glazes as copper oxide, according to the XRF analysis results. By Raman spectrum, the presence magnetite and hematite were identified in the brown-glazed potsherd sample of K146. Moreover, XRF data showed that manganese is responsible for the color of the black tile, copper (3% for the turquoise potsherd glaze) and 6.7% SnO_2 +1.6% CuO are the reasons for the turquoise coloring together with the high content of calcium oxide. By XRF, it could be seen that most of the samples contain high levels of lead up to 50%. The two tile samples are determined to be in the group of tin-opacified lead-alkali glaze, whereas the glazed potsherds are in the high lead and lead-alkali types. The results of XRF analysis of the glazes of both the potsherds and tiles showed that lead-oxide was preferred as the fluxing agent with natron. If the tin-opacified lead alkali type glaze is desired to be turquoise, then lead also should be in the medium, as could be understood from XRF data for the tiles. CuO is attributed to be responsible for the turquoise and green colors of the glazes as well as the yellow glaze is the result of Fe_2O_3 together with $Pb_2Sb_2O_7$ and Sb_2O_3. This information is also supported by XRD spectrum of the turquoise glaze of the potsherd sample of K223, where Plagioclase [$Na(AlSi_3O_8)$,$Ca(Al_2Si_2O_8)$], Portlandite [$Ca(OH)_2$], Quartz (SiO_2) and Verdigris [$Cu(CH_3COO)_2.H_2O$] might be possibly included in the glaze. For the turquoise color, the paste was preferred to be rich in calcite. For the color tones of green, it could be stated that increase in concentration of CuO could result in the yellow color of the glaze to turn into green. Yellow color of the glazes could be proposed to be reached with very low concentration (around 0.5%) of Fe_2O_3 in the

oxidizing atmosphere and by addition of Sb_2O_3, PbO and TiO_2. If the Fe_2O_3 concentration is increased to twice and 0.5% CuO and 0.06% As_2O_3 added in an oxidative environment, then its color turns into green. Glaze color of orange could be arisen from about 4% Fe_2O_3, 0.5% TiO_2 and 0.13% CdO. CuO addition between 1.5-3.4% is thought to be the reason for the turquoise glaze and on a calcite paste. Purple color on the glaze of K117 potsherd could be due to the mixture of colors of red due to the reduced Cu_2O and bluish green due to the oxidized CuO. Brown color could probably be occurred by FeO in the reductive atmosphere at lower temperatures together with around 0.2% TiO_2, and also related with the high CO_2 content. Likewise, black color could be gathered by MnO and FeO, also by contributions of Na_2O and MgO. In tiles, SnO_2 was used for the opacification. Cobalt is known to be responsible for the dark turquoise color of the glaze, but no cobalt is detected in any sample.

Gas bubbles observed on the turquoise glaze, which could lead to consider no bisque-firing was applied prior to the glazing. Reddish color of the paste, occurred due to the clay and iron oxide, is an indicator for the atmosphere used in an oxidizing way in the kilns and its homogeneity is the result of the bisque-firing applied under high temperatures, whose temperature was estimated as around 900-925 °C from the FTIR Spectroscopy wavenumber data. Moreover, the glazes were determined to be produced using quartz, from not only calcareous but also non-calcareous clays. PbO is thought to be added most probably to lower the firing temperature, which was supported by FTIR spectroscopy that it was as low as 600-700 °C for some pottery samples. Firing temperatures estimated by FTIR spectra were mostly consistent with those determined by the positions of samples on the isothermal curves in the bivariate chart of PbO vs. (Na_2O+K_2O) acquired by XRF spectrometry.

Binary and ternary diagrams also contributed to the possibility of the turquoise glazed sample K223 to be brought from Egypt or Iraq. From the ternary diagrams, the yellow glaze of K149 from the 13th century was found to be closer to Islamic glazes of Iran from the 10-11th centuries. On the other hand, since all the clay

minerals were detected to be similar for the potsherds with respect to the 3600-3700 cm^{-1} region in FTIR spectra, it might be possible to produce all the pottery locally from the basin of Iris River, but influenced by different traditions or made by different potters.

And by XRD spectroscopy, olivine, epidote and siderite were examined in both tiles, additionally with augite and fayalite in K002 black tile, which also supports the idea that glazing traditions in the Seljukids-Danishmendids periods were a mixture of those of the Byzantines and the Ottomans, since olivine, epidote, augite and fayalite were typical mostly to the Byzantines as well as siderite to the Ottomans. XRD spectra of the potsherd glazes were amorphous, which supports the information that they were transparent and formed by fast cooling of the glaze also affected by the addition of Al_2O_3 and MgO. On the other hand, XRD signals of the tiles were easily identified with the help of their crystalline content in the glaze probably contributed by ZnO, TiO_2, CaO, Fe_2O_3, SiO_2, opacified by SnO_2, and formed by the slowly-cooling process. Those oxides were also checked by the XRF analysis. Anatase, calcite, albite, quartz, graphite, epidote, carbon iron silicon, siderite, magnetoplumbite, ramsdellite were identified in the turquoise tile by XRD spectroscopy. Due to the observance of anatase and calcite signals in XRD, the firing temperature was estimated between 600-850 °C, which is also parallel with the temperature found as 600-700 °C by FTIR spectroscopy. Moreover, pyroxene, quartz, graphite, albite, tin oxide, carbon iron silicon, tridymite, magnetoplumbite and ramsdellite were discovered by XRD spectrum of the glaze of the black tile, in which pyroxene and tridymite are formed at temperatures higher than 870-900 °C, which was also relevant to the same temperature range calculated as 900-925 °C by FTIR spectroscopy.

From the biplot of SnO_2/PbO ratios, K002 black tile was found to be extremely similar to the Iznik (Nicaea) tiles of the Ottoman Empire from the 17th century and K001 turquoise tile was observed to be similar to the tiles of an Ottoman mosque (1429) in Edirne and those of the Timurids (2nd half of the 14th century – first quarter

of the 16th century) where Iran might be the possible origin of influence. With respect to the biplot of ratios of Pb/Si vs. Sn/Si, the potsherd K149 with yellow glaze from 13th century was determined to be close to the tiles from the mosques of the 15th and 16th centuries in Edirne, while K161 with green glaze and K172 with orange glaze from the 12-13th centuries were found to be close to the 15th century mosque in Edirne, which could bring the consideration that pottery making tradition with addition of similar proportions of lead and quartz might have continued from the periods of Seljukids in the 12th century to the Ottomans in the 16th century. This consideration is consistent with the information that continued workshop of ceramic arts and techniques of the Seljuks initiated the tile production in the Ottoman Empire. Also the locations of the Comana potsherds and tiles in the biplots were consistent with the other previously analyzed glazes from Seljukid Era and the same time periods were condensed in close positions, which could make the glazes found in the layer of the Seljukids unique and its differentiation possible with respect to the oxide contents. Also this uniqueness could be seen from Figure 12 that the FTIR and Raman spectra of the potsherds display both high PbO content similar to Byzantine Era as well as specified by addition of more NaO that also cause a change in the shape with a shoulder in the wavenumber region on the stretching modes. Furthermore, with the help of the biplots, mineral natron was also identified to be added as the flux during firing the glazes, that is also consistent with the traditional method in Anatolia in that period. From the characterization biplot of PbO/SiO_2 vs. CaO/SiO_2, both tiles were closest to the 12th century Islamic Iran and the turquoise - glazed K223 was closest to the 11-12th century Islamic Syria which could find an estimation where it could be imported from if this is the case as recommended from Dr. Bilgi Er. The locations of the Comana potsherds in the biplots were consistent with the other previously analyzed Seljukid glazes and the same time periods were condensed in close positions, which could make the glazes found in the layer of the Seljukids unique and its differentiation possible with respect to the oxide contents.

The firing temperatures of the glazes of some potsherds samples are also estimated from I_p calculation of the Raman spectra, whose results are in accordance with the ones gathered by FTIR analyses, but if one method was to be preferred most probably it would be Raman I_p values since they are more accurate with sharper signals compared to the larger area under the maximum point of the curves of FTIR spectra that seems to be more misleading.

Analysis of ceramics and glazes are important in not only describing and dating the archaeological remains, but also providing information about the sociocultural structure and economic relationship.

Keywords: Comana Pontica, FTIR, XRF, XRD, Raman.

ÖZ

TÜRKİYE TOKAT'TAKİ KOMANA PONTİKA'DA BULUNAN 11-14. YÜZYIL SERAMİK VE ÇİNİ PARÇALARININ SIRLARININ KARAKTERİZASYONU

Altundal, Canberk
Yüksek Lisans, Arkeometri
Tez Yöneticisi: Prof. Dr. Deniz Burcu Erciyas
Ortak Tez Yöneticisi: Doç. Dr. Gülsu Şimşek Franci

Eylül 2023, 222 sayfa

Tokat'ta bulunan Komana Pontika Antik Kenti, Karadeniz Bölgesi'nin iç ve denize kenarı olan şehirlerini birbirine bağlayan antik ana yol üzerinde bulunan kesişim noktalarından biriydi. Osmanlılar, Selçuklu-Danişmendliler, Bizanslılar, Romalılar ve Yunanlılar dönemlerine ait arkeolojik buluntular, 2009 yılında başlayıp günümüzde de devam eden kazı çalışmalarında gün yüzüne çıkarıldı. 2018 yılına kadar, Selçuklu-Danişmendli dönemlerine ait toplamda 1479 sırlı seramik örneği, 1842 sırsız pişirme kabı ve 2223 sırsız saklama kabı kazıda çıkarılmıştır. Bu tezde, bu 5544 seramik örneği içinden, 2011-2012 kazı sezonlarında açığa çıkarılan ve 11.-14. yüzyıllara tarihlenen Selçuklu-Danişmendli katmanlarında bulunan 71 adet sırlı çanak çömlek kırığı parçası ile 2 adet sırlı çini örneği seçilmiş ve bu örneklerin hem dış hem iç yüzeylerindeki farklı renklerdeki toplam 106 sır, 6 seramik hamuru ve 3 astar örneği, Fourier Dönüşümlü Kızılötesi (FT-IR), X Işını Kırınımı (XRD), Raman Spektroskopisi ile X Işını Floresansı (XRF) Spektrometrisi ile analiz edilmiştir. Sır boyar maddelerinin yapılarının ve sırların üretim teknolojilerinin belirlenmesi,

seramiklerin pişirilme sıcaklıklarının bulunması ve sır içeriğindeki metal oksit yüzdelerinden yararlanılarak örneklerin karakterizasyonu amaçlanmıştır. Ayrıca, elde edilen bu XRF oksit verileri iki değişkenli ve üçgen grafiklerde gösterilmiş ve literatürdeki benzer diğer çalışmalardan elde edilen veriler ile karşılaştırılarak, seramik kap ve çini örneklerinin sırlarında kullanılan malzemelerin içeriklerinin kendi dönemlerinin özelliklerini taşıyıp taşımadıkları konusunda bir sonuca varılmaya çalışılmıştır.

Sonuç olarak, Si-O asimetrik gerilme tepe noktalarının dalga numarası konumları yardımıyla, Comana Pontica seramiklerinin pişirilme sıcaklık aralığının 600 ile 925 °C arasında değiştiği ve çoğunluğunun 800-900 °C aralığında pişirildiği tahmin edilmiştir. Kahverengi sırların 700-750 °C civarında, ardından mavi sırların 725-800 °C'de, sarı ve yeşil sırların 750-800 °C'de, turuncu sırların 850 °C civarında ve siyah sırrın 900 °C civarında pişirildiği bulunmuştur. Kırmızı hamurların 850-900 °C civarında, mavi sırların ve Osmanlı çinilerinin altındaki beyaz hamurların ve civarında beyaz astar tabakalarının 900 °C'de pişirildiği keşfedilmiştir, ki bu da mavi dışındaki sırlı çanak çömlek parçalarının önce yaklaşık 900 °C'de, daha sonra sırlanmalarının ardından açık renkli sırlar için yükseltgeyici bir atmosferde 700-850 °C'de ve koyu renkli sırlar için indirgeyici bir ortamda biraz daha soğuk bir sıcaklıkta yeniden fırınlandığı öne sürülmektedir.

Ayrıca FTIR spektrumunda 3600-3700 cm^{-1} civarındaki titreşimlere göre sırlardaki kil mineralleri, başlıca kaolinit (dikit, halloysit, kaolinit, nakrit) ve montmorillonit-simektit (bentonit, montmorillonit, saponit, simektit, vermikülit) grupları olarak tanımlanmıştır. Öte yandan, istisnai olarak K104 hamuru ayrıca illit ve sepiyolit içermektedir. Astar ve hamurların geri kalanında ise, 850-925 °C gibi daha yüksek pişirme sıcaklık değerlerinde meydana gelen büyük olasılıkla dehidroksilasyon, dehidrasyon ve dekarbonasyon nedeniyle tepe noktaları neredeyse gözlenmemiştir. Ayrıca sönmüş kireç [$Ca(OH)_2$] sönmemiş kireç (CaO) ve kalsit ($CaCO_3$) içerikleri aynı zamanda sırasıyla 3648 cm^{-1}'de, 1647 cm^{-1}'de ve 1430-1450 cm^{-1}'de bir sinyal vererek olası pişirilme sıcaklıkları hakkında bilgi

verir ki muhtemelen hepsi de ezilmiş deniz kabuklardan ve kemiklerden elde edilmiştir. Eğer $CaCO_3$ tepe noktası gözlemlenirse, bu durum sıcaklığın 600 °C'nin altında olduğunu; eğer CaO'nınki gözlemlenirse, bu sıcaklığın 600-800 °C arasında olduğunu, $Ca(OH)_2$'ninkinin gözlenmesi durumunda sıcaklığın 800-900 °C arasında olduğunu ve tüm kalsit tepe noktalarının ve -OH bantlarının kaybolması durumunda da sıcaklığın 900 °C'nin üzerinde olduğu anlamına gelir. Ek olarak, sırlı seramiklerin tahmini ortalama pişirilme sıcaklıklarının üretim dönemlerine göre ayrılmış tablosundaki eğilim çizgisinin pozitif eğiminden dolayı, Comana Pontica sırlı seramiklerinin pişirilme sıcaklıklarının 12. yüzyıldan 14. yüzyıla kadar arttığı bulunmuştur.

Üstelik, XRF analiz sonuçlarına göre, sarı sırlar için renklendirici maddenin büyük olasılıkla kurşun antimonat ($Pb_2Sb_2O_7$) ve yeşil sırlar için de bakır oksit olduğu düşünülmektedir. Kahverengi sırlı K146 seramik örneğinin Raman spektrumuna bakıldığında ise, jakobsit, manyetit ve hematitin varlığı tespit edilmiştir. Ayrıca, XRF verileri, siyah çininin kendi renginden manganezin sorumlu olduğunu, bakırın (mavi çanak çömlek parçası sırrı için %3 olmak üzere) ve %6,7 SnO_2 + %1,6 CuO içeriklerinin yüksek kalsiyum oksit içeriği ile birlikte mavi rengin sebebi olduğunu göstermiştir. XRF ile örneklerin çoğunun %50'ye varan yüksek seviyelerde kurşun içerdiği görülmektedir. İki çini örneğinin de kalayla opaklaştırılmış kurşun-alkali sır grubunda olduğu, sırlı çanak çömlek parçalarının ise yüksek kurşun ve kurşun-alkali tiplerinde olduğu belirlenmiştir. Hem çanak çömlek parçalarının hem de çinilerin sırlarının XRF analizi sonuçları, eritici etmen olarak natron ile kurşun oksitin tercih edildiğini göstermiştir. Kalayla opaklaştırılmış kurşun alkali tip bir sırrın turkuaz renkli olması isteniyorsa, çiniler için XRF verilerinden de anlaşılacağı gibi, kurşunun da ortamda olması gerekmektedir. CuO, sırların mavi ve yeşil renklerinden sorumlu olduğu gibi, sarı sır da içerikte $Pb_2Sb_2O_7$ ve Sb_2O_3 ile birlikte Fe_2O_3'ün de olmasının sonucudur. Bu bilgi de K223 turkuaz sırlı seramik örneğinin XRD spektrumuyla desteklenmiştir, ki sır yapısının içinde büyük ihtimalle Plagioclase [$Na(AlSi_3O_8)$,$Ca(Al_2Si_2O_8)$], Portlandite [$Ca(OH)_2$], Quartz (SiO_2) and Verdigris

[$Cu(CH_3COO)_2.H_2O$]'in yer aldığı düşünülmektedir. Mavi rengin oluşması için, hamurun kalsitçe zengin olması tercih edilmiştir. Yeşilin renk tonları için ise, CuO konsantrasyonunun artmasının sırrın sarı renginin yeşile dönüşmesine neden olacağı ifade edilebilir. Sırların sarı renginde kalabilmesinin, oksitleyici atmosferde (yaklaşık %0.5 gibi) çok düşük bir konsantrasyonda Fe_2O_3, Sb_2O_3, PbO ve TiO_2 ilavesi ile ulaşılabileceği önerilebilir. Eğer Fe_2O_3 konsantrasyonu iki katına çıkarılıp oksidatif ortamda %0.5 CuO ve %0.06 As_2O_3 eklenirse, sırrın rengi yeşile döner. Turuncu sır rengi ise yaklaşık %4 Fe_2O_3, %0.5 TiO_2 ve %0.13 CdO'dan elde edilebilir. Kalsit hamur üzerine %1.5-3.4 arasında CuO ilavesinin mavi sırra neden olduğu düşünülmektedir. K117 çanak çömlek parçasının sırındaki mor renk ise, Cu_2O'nun indirgenmesi sonucunda oluşan kırmızı renkle ve CuO'nun yükseltgenmesi sonucu oluşan mavimsi yeşil rengin karışımından kaynaklanmaktadır. Kahverengi renk de büyük ihtimalle indirgeyici atmosferde daha düşük sıcaklıklarda oluşan FeO ile yaklaşık %0,2 TiO_2'nin birleşmesinden oluşmaktadır ve ayrıca yüksek CO_2 içeriği ile de bağlantılıdır. Siyah renk ise MnO ve FeO'nun, ve bazen de Na_2O ve MgO'nun katkılarıyla oluşmaktadır. Çinilerde, opaklaştırma için SnO_2 kullanılmıştır. Sırın koyu mavi renginden kobaltın sorumlu olduğu bilinmektedir, ancak hiçbir örnekte kobalt tespit edilmemiştir.

Mavi sır üzerinde gözlenen gaz kabarcıkları, sırlamadan önce hiç bisküvi pişirimi yapılmadığını düşündürmektedir. Hamurun kil ve demir oksit nedeniyle oluşan kırmızımsı rengi, fırınlarda oksitleyici bir şekilde kullanılan atmosferin bir göstergesidir ve homojenliği de, sıcaklığı FTIR Spektroskopisi dalga numarası verilerinden yararlanılarak yaklaşık 900-925 °C olarak tahmin edilen yüksek sıcaklıklarda uygulanan bisküvi pişiriminin bir sonucudur. Ayrıca sırların hem kalkerli hem de kalkersiz killerden ve de kuvars kullanılarak üretildiği belirlenmiştir. PbO'nun büyük olasılıkla pişirme sıcaklığını düşürmek için eklendiği düşünülmektedir, ki bu da bazı çanak çömlek parçalarının pişirilme sıcaklıklarının FTIR spektroskopisi ile 600-700 °C kadar düşük olduğunun bilinmesiyle desteklenmektedir. FTIR spektrumları tarafından tahmin edilen pişirilme

sıcaklıkları, XRF spektrometrisi ile elde edilen iki değişkenli PbO'ya karşı (Na_2O+K_2O) grafiğindeki eşsıcaklık eğrileri üzerindeki örneklerin konumları tarafından belirlenen değerlerle çoğunlukla tutarlı olmuştur.

İkili ve üçlü diyagramları da mavi sırlı K223 örneğinin Mısır veya Irak'tan getirilmiş olma olasılığına katkıda bulunmuştur. Üçlü diyagramlardan da 13. yüzyıla ait olan K149 sarı sırlı örneğinin, 10-11. Yüzyıllara tarihlenen İran İslami sırlarına daha yakın olduğu bulunmuştur. Öte yandan, çanak çömlek parçalarının tüm kil minerallerinin FTIR spektrumlarının 3600-3700 cm^{-1} bölgesine göre benzer olduğu tespit edildiğinden, seramiklerin tamamının İris (Yeşilırmak) Nehri havzasından yerel olarak üretilmiş olmaları mümkün olabilir, ancak farklı geleneklerden etkilenmiş veya farklı çömlekçiler tarafından yapılmış olabilirler.

XRD spektroskopilerine bakıldığında ise, olivin, epidot ve sideritin her iki çini de olmasına rağmen, K002 siyah çinisinde ayrıca ojit ve fayalit olduğu bulunmuştur, ki bu da Selçuklu-Danişmendli dönemlerindeki sırlama geleneklerinin aslında Bizans ve Osmanlı sırlarının bir karışımı olduğu fikrini de desteklemektedir; çünkü olivin, epidot, ojit ve fayalit, çoğunlukla Bizanslılar için tipik olduğu gibi, siderit de Osmanlılar için de tipiktir. Çömlek parçası sırlarının XRD spektrumlarının amorf olması, onların şeffaf oldukları ve sırrın hızlı soğumasıyla oluşmuş olabilecekleri bilgisini desteklerken, ayrıca Al_2O_3 ve MgO ilavesinden de etkilenmiş olabilir. Öte yandan, çiniler için, muhtemelen ZnO, TiO_2, CaO, Fe_2O_3, SiO_2'nin eklenmelerinin de etkilediği, SnO_2 ile opaklaştırılmış ve yavaş soğutma işlemiyle oluşan sırdaki kristal içeriği sayesinde XRD sinyalleri kolaylıkla tanımlanabilmiştir. Bu oksitler ayrıca XRF analizi ile de kontrol edilmiştir. XRD spektroskopisi ile mavi çini parçasında anataz, kalsit, albit, kuvars, grafit, epidot, karbon demir silikon, siderit, manyetoplumbit ve ramsdellit tanımlanmıştır. XRD'de anataz ve kalsit sinyallerinin gözlenmesinden dolayı, pişirilme sıcaklığı 600-850 °C arasında tahmin edilmiştir ve bu da FTIR spektroskopisi ile 600-700 °C olarak bulunan sıcaklık ile paraleldir. Ayrıca, XRD spektrumu ile siyah çini sırında piroksen, kuvars, grafit, albit, kalay oksit, karbon demir silikon, tridimit, manyetoplumbit ve ramsdellit olduğu

keşfedilmiştir, ki piroksen ve tridimit 870-900 °C 'den yüksek sıcaklıklarda oluşmaktadır ve bu sıcaklık değerleri de FTIR spektroskopisi ile 900-925 °C olarak hesaplanan pişme sıcaklığına yakın bir sıcaklık aralığındadır.

SnO_2/PbO oranlarının iki değişkenli çizelgesinde K002 siyah çinisinin 17. yüzyıldan kalma Osmanlı İmparatorluğu'nun İznik (Nicaea) çinilerine aşırı derecede benzediği ve K001 mavi çininin de Edirne'de 1429 yılılndan kalan bir Osmanlı cami çinisi ile 14. yüzyılın 2. yarısı - 16. yüzyılın ilk çeyreği arasında hüküm süren Timurlular'ın arasında bir yere denk geldiği, olası etki kaynağının İran olabileceği gözlemlenmiştir. Pb/Si ve Sn/Si oranlarının iki değişkenli çizelgesine göre ise, 13. yüzyıla ait sarı sırlı K149 çanak çömlek parçasının Edirne'deki 15. ve 16. yüzyıl cami çinilerine yakın olduğu, 12-13. yüzyıllara ait yeşil sırlı K161 ve turuncu sırlı K172'nin ise Edirne'deki bir 15. yüzyıl camisinin çinilerine yakın olduğu belirlenmiştir, ki bu da benzer oranlarda kurşun ve kuvars ilavesiyle çanak çömlek yapma geleneğinin 12. yüzyıldaki Selçuklular döneminden 16. yüzyıldaki Osmanlılara kadar devam etmiş olabileceği düşüncesini akıllara getirebilir. Bu düşünce, Selçuklular'ın devam eden seramik sanatları ve teknikleri atölyelerinin Osmanlılar'da çini üretimini başlattığı bilgisi ile de tutarlıdır. Aynı zamanda Komana seramik ve çini örneklerinin bu iki değişkenli çizelgelerdeki yerleri de yan yana toplanmış bulunmaktadır, ki bu da selçuklu tabakalarında bulunan sorların ne kadar da benzersiz ve oksit bileşenlerinin oranına bağlı olarak tek tipleşmeye yatkın ve ayırt edilebilir olduğunu gösterir. Bu benzersizlik de 11. Figür'de görüldüğü gibi, seramiklerin yüksek PbO oranı içermesi bakımından Bizans Dönemi eserlerine benzemesine rağmen içine daha fazla NaO eklenmesiyle özelleşmiştir, ki bu da spektrumun dalga boyunun gerilme modları alanında yeni bir omuz oluşturarak biçimini farklılaştırmıştır. Ayrıca, o dönemde Anadolu'da uygulanan geleneksel yöntemle de uyumlu olarak, sırların pişirilmesi sırasında eritici etken olarak natron mineralinin eklendiği tespit edilmiştir. PbO/SiO_2 ve CaO/SiO_2 arasındaki karakterizasyon iki değişkenli çizelgesinde, her iki çini de 12. yüzyıl İslami İran'ınkilere en yakındı ve mavi sırlı K223 örneği de, 11-12. yüzyıl İslami

Suriye'sininkilere en yakındı, ki bu şayet bu Dr. Er'in önerdiği gibi bir durumsa, ithal edilebileceği yerin tahmini yapılabilir. İki değişkenli çizelgelerdeki Comana çanak çömlek parçalarının konumları, daha önce incelenen diğer Selçuklu sırları ile uyumluydu ve aynı zaman periyotları birbirine yakın konumlarda yoğunlaşmıştı, bu da Selçuklular tabakasında bulunan sırları benzersiz kılabilir ve onun oksit içerikleri özelinde farklılaşmasını mümkün kılabilir.

Bazı seramik sır örneklerinin Raman spektrumları ile elde edilen I_p (polimerleşme endeksi) değerlerinden yola çıkılarak pişirilme sıcaklıkları hesaplandı, ki bu sonuçlar FTIR analizleri ile hesaplananlar ile tutarlıdır, ama ikisi arasında tek bir yöntem seçilecek olsaydı bu kesinlikle Raman spektrumları aracılığıyla polimerleşme endeksi hesaplanması olurdu, çünkü onlar FTIR spektrumlarının sinyalleriyle karşılaştırılınca daha keskin oldukları için göre daha doğru sonuçlar verir, FTIR spektrumlarında tepe noktasının altında kalan eğrinin alanı çok geniş olduğu için daha az doğru olan sonuca götürmektedir.

Seramik ve sırların analizi, arkeolojik kalıntıların tanımlanması ve tarihlendirilmesinin yanı sıra sosyokültürel yapı ve ekonomik ilişkiler hakkında bilgi vermesi açısından da önemlidir.

Anahtar Kelimeler: Komana Pontika, FTIR, XRF, XRD, Raman.

To my family

ACKNOWLEDGMENTS

I sincerely would like to thank my supervisor and the Chair of the Department of Settlement Archaeology at Middle East Technical University (METU), Prof. Dr. Deniz Burcu Erciyas, for helping to reveal the pottery samples, enlightening with the significant archaeological information, encouraging me to discover what type of features of the glazed artefacts could be come to light and giving me the power whenever I need.

I would like to thank genuinely my co-supervisor, Assoc. Prof. Dr. Gülsu Şimşek Franci from Koç University Surface Science and Technology Center, for the valuable contributions on the characterization of the samples with spectroscopic techniques, giving me priceless instructions as well as contributions and also for giving me the chance to finish writing this thesis in depth.

I would like to thank Prof. Dr. Gülay Ertaş, the ex-Chair of the Department of Archaeometry and the Vice Chair of the Department of Chemistry at METU, for letting me be involved in her research group, letting me use the multiple analytical laboratory instruments.

I would like to send my sincerest condolences to the deceased Prof. Dr. Osman Yavuz Ataman, from the Department of Chemistry at METU, who had a great influence on leading me to this field after his lecture "Archaeometry Stories in Anatolia" during the inter-semester seminars in 2017.

I would like to express my deep gratitude to Assoc. Prof. Dr. Zeynep Işıl Kalaylıoğlu, from the Department of Statistics at METU, for her contributions on statistical methods in addition to her motivating yoga sessions.

I would like to thank Assoc. Prof. Dr. Çiğdem Atakuman and Assoc. Prof. Dr. Evangelia Ioannidou-Pişkin, from the Department of Settlement Archaeology at METU, together with the research assistants Dr. Deniz Erdem, Dr. İlham Sakarya

and Dr. Nadire Atıcı from the Centre of Research and Assessment of Historical Environment (TAÇDAM) at METU for their supports in archaeological knowledge.

I would like to show courtesy to Prof. Dr. Ömür Bakırer, Prof. Dr. Emine Caner-Saltık, Prof. Dr. Ay Melek Özer, Prof. Dr. Asuman Günal Türkmenoğlu, Prof. Dr. Şahinde Demirci, Prof. Dr. Musa Doğan and Prof. Dr. Ali Kalkanlı from the Department of Archaeometry of METU profoundly for their endless supports throughout my education.

I would like to show appreciation to Prof. Dr. Ayşen Yılmaz for providing me with the access to XRD instrument in the Department of Chemistry at METU, as well as Mehmet Burak Uzun and the research assistant Özde Ceren Abacı for their assistance during my XRD analyses.

I would also like to thank Dr. Leyla Molu from the Central Laboratory at METU for the help to perform the analyses of XRF Spectrometry.

I would like to offer my thanks to Asu Pelin Akköse, Ayşe Efran Boz, Deniz Yılmaz, Ecem Yıldız and Ege Duran, as well as the research assistants Sezin Atıcı Özdemir and Canan Höçük Özkan from C-49; together with Eda Akın and the research assistants Begüm Avcı and Dr. Yeliz Akpınar from C-50 research laboratories at METU Chemistry Department, for their not only friendship but also assistance in using various laboratory instruments.

I would like to owe a debt of gratitude to Ayşen Elşen Aydın for her friendship, Dr. Mehmet Bilgi Er for sampling and Dr. Yunus Emre Karasu for sampling and dating.

I also would like to be obliged to the archaeologists took part in Komana Archaeological Research Project (KARP) for their patient scrutinization and efforts.

At last but not least, I would like to extend my thanks to my mother Satı Gençer, my father Zeynel Altundal and my sister Beril Altundal for their affection and precious supports every time I need.

TABLE OF CONTENTS

LIST OF TABLES

TABLES

LIST OF FIGURES

FIGURES

LIST OF ABBREVIATIONS

ABBREVIATIONS

BCE: Before Common Era

bk: black

bl: blue

br: brown

CE: Common Era

ch: champlevé

cm: centimeter

deco: decoration

ex: exterior

FTIR: Fourier-Transform Infrared

gn: green

gy: gray

ICP-MS: Inductively Coupled Plasma Mass Spectrometry

in: interior

I_p: polymerization index

KARP: Comana Archaeological Research Project

KUYTAM: Koç University Surface Science and Technology Center (in Turkish: Koç Üniversitesi Yüzey Teknolojileri Araştırma Merkezi)

ν: stretching vibrational frequency (Greek small letter Nu)

ND: not detected

NIST: National Institute of Standards and Technology

or: orange

pa: paste

re: red

res: resolution

S/N: signal to noise ratio

sg: sgraffito

δ: bending frequency (Greek small letter Delta)

sl: slip

sp: slip painted

T: Transmittance

TAÇDAM: the Centre of Research and Assessment of Historical Environment (in Turkish: Tarihsel Çevre Değerlerini Araştırma Merkezi)

TUBITAK: Scientific Technological Research Council of Turkey (in Turkish: Türkiye Bilimsel ve Teknolojik Araştırma Kurumu)

ti: tile

tq: turquoise

wh: white

XRD: X-Ray Powder Diffraction

XRF: X-Ray Fluorescence

ye: yellow

CHAPTER 1

INTRODUCTION

In this thesis, there are five chapters. Initially chemistry and the history of both pottery and glazes will be explored and then, the ancient settlement Comana Pontica will be briefly introduced together with the period of its exploration and excavation. After giving some information about the previously conducted studies about Comana Pontica, the second chapter with literature review part will be encountered. In that part, the studies based on Si-O stretching peak in FTIR will be mentioned to determine firing temperature of the ceramic samples. Then, the effect of the temperature on the wavenumber values will be identified with the help of an experiment conducted in the laboratory conditions, and coloring reagents in glazes will be studied. Then, it will be going on with the third chapter about sampling. Then the analytical techniques of FTIR spectroscopy, XRF spectrometry, XRD and Raman spectroscopy will be studied in the third part of this thesis, together with the instruments and reagents. After the results and discussion part, the thesis will end with conclusion part, references and appendices.

1.1 Pottery and Glaze

The ceramic wares, that are made of clay and then fired in order to be hardened, are called as pottery [2]. The typical clay mineral is kaolinite, $Al_2O_3.2SiO_2.2H_2O$, including aluminosilicate particles that are produced by feldspar group minerals, $K_2O.Al_2O_3.6SiO_2$, covering most of the crust of the Earth, being eroded through water [3]. Crystals of kaolinite are made up of stacked layers of tetrahedral SiO_4 sheet, whose oxygen is bonded via hydrogen bonding to the hydrogen of the octahedral sheet of AlO_6 in which some oxygens might be replaced with hydroxide groups. In reality, when the clay is wet and a force is applied on it, either by hands or by the potter's wheel that is thought to be invented about 4500 BCE, the plasticity of the

clay is increased with respect to the separation of the stacked layers by formation of a new thin layer composed of molecules of water, which also creates hydrogen bonding to keep the clay in shape [3-4].

Then, when the wet clay is heated in a kiln and its temperature is increased to larger values than 550 °C, water is removed, hydrogen bond is replaced with stronger bridges of oxygen and, at the end, an irreversible chemical reaction occurs, as seen in Equation 1 to yield disordered amorphous metakaolin, $Al_2Si_2O_7$, [3].

$$2\ (\text{Clay-OH}) \rightarrow (\text{Clay-O-Clay}) + H_2O \qquad \text{Equation (1)}$$

Moreover, beyond 925 °C, hydroxide group is lost entirely and γ-alumina type Al-Si spinel, $Al_4Si_3O_{12}$, is produced. Finally, above 1050 °C, transformation to mullite, $3Al_2O_3.2SiO_2$, is observed, whose configurational and molecular changes could be detected by XRD analysis [6].

The oldest pottery sample is the 11-cm-high Dolní Věstonice Venus figurine from today's Brno, Czechia, in 1925. Being dated back to around 28,000 years ago, it is revealed that it was made from clay fired to around 500-800 °C and probably produced for ritual purposes [7]. Additionally, some pottery vessels dating to 20,000 years ago were found out in China [8]. In the Middle East, the first pottery sample appeared around 9,000 years ago in Northern Mesopotamia [9].

In Anatolia, the earliest proofs of pottery were found in Boncuklu Höyük (Konya) and dated back to 10,500 years ago [10]. Moreover, it is known that there are 8000-year-old pottery samples, without any glaze or paint on them collected in Çatalhöyük (Konya) excavations and estimated to be fired up to 800 °C due to observing aluminum diopside and gehlenite by the XRD analysis [11].

Pottery alone was very fragile and not very capable of holding liquids for long times due to its porous structure when it is used as a tableware. Therefore, the glaze, which is a vitreous substance fused on to the surface of pottery to form a hard and impervious coating, was discovered first in Egypt in the 5th millennium BCE, most likely by coincidence from the deposits, near the Nile River and Red Sea, and source was mainly steatite, $Mg_3(Si_4O_{10})(OH)_2$, a kind of talc with particles smaller than 75 microns, making it impermeable to water, and very difficult to fuse, dissolve or melt,

moreover it can be hardened by being dehydrated and glassy naturally with the increase in temperature [12].

Besides waterproofing and strengthening, the other aim was to make the wares unique to its culture in the ways of decorating and coloring them, which has also become popular in time. This coating of glaze is typically applied by dipping, brushing, spraying, pouring, etc. of the sample after an initial bisque firing, and then may be strengthened with a second firing to a temperature appropriate for both the clay body and glaze being used, finally getting cooled fast or slowly which also contributes to the brightness of the glaze by insolubility of opacifiers (such as SnO_2, $ZrSiO_4$, TiO_2, Al_2O_3, CaO, ZnO, $Ca_3(PO_4)_2$) and colorants (Co_3O_4, Cr_2O_3, Fe_2O_3, CuO, MnO_2), if added, and precipitation of newly-produced crystalline compounds formed in the melted glaze due to its interaction with the surface of the ceramic [13].

The surface of the glaze becomes smooth after sudden cooling, so specular reflection occurs from the surface. Whereas, due to the crystals formed during the slowly-cooling step, the surface becomes too rough that makes the glaze surface matte, which causes the diffuse reflection of incoming light [14].

If the cooling process of the glaze is fast, then it solidifies transparently, whereas slow cooling makes the crystals to grow. Likewise, existence of oxides of zinc, titanium, calcium, iron (III), silicon, barium and boron also contribute to the formation of crystalline structure. On the other hand, presence of the oxides of aluminum, zirconium and magnesium hardens the melt so that transparent glazes can be formed on the surface of the ceramic samples [15].

However, these discoveries were presumed to be improved slowly and by chance. Because early potters probably did not have the technology to increase the firing temperatures to very high degrees and did not know which materials should be used for getting the high-quality glazes. Around 3500 BCE, it is thought that most probably the glass producing technology was first used in Ancient Egypt by firing limestone ($CaCO_3$), sand and natron ($Na_2CO_3.10H_2O$) mixture [16]. In 1200 BCE, oldest known glazed bricks were made in Ancient Mesopotamia, which evolved into the tiles in time [17]. Next, in around 300 BCE, the first mosaics were seen in Rome

by combination of multiple tiles and became popular in sacred places in Byzantines and Egyptians [18]. Then, it spread through Iran in 900 CE and started to be observed in many mosques, public places and palaces of Seljuks and Ottomans, too [19]. Especially İznik tiles of the Ottoman Empire were produced during 1500-1600 CE and it was known that cobalt blue was used as a colorant like in Chinese Ceramics and that is why it is named as "çini", translation of "tile" in Turkish that means "of China" [20].

In time, after many trials they had to add the compounds of sodium, potassium and especially lead to lower the melting point of the glaze [16]. The other reasons for preference of lead are that they could be prepared easily, its glaze suspension could be applied easily, its susceptibility for the glaze to be crazed and crawled is low, its optical brilliance is very high, and it is cheap. On the other hand, lead is poisonous, which was probably not known at that time.

According to the ratios of oxides of some elements, the glazes could be classified. For example, if PbO content is greater than 45%, then it is called high lead type, it is called lead-alkali type if its PbO content is 20-40% together with its alkali content 5-12%, it is called low lead-alkali type if PbO content is 2-10% [21] and the one without PbO is called alkaline. Likewise, depending on the calcite ($CaCO_3$) content, the paste could be either calcareous (with calcite content being greater than 10%) or non-calcareous (with less than 10%) [1].

In case either the paste or the glaze is rich in carbonate and fired between 600-850 °C, calcite decomposes in the clay matrix. So, if any calcite was put into the sample, then the firing temperature would not be larger than 850 °C [22].

Initially during the Roman times, lead glazes were used to make the exterior parts of the pottery green and interior parts yellow in color, to resemble the ceramics to the vessels made of copper alloys. During the 1st century BCE, lead glazes started to be observed initially in Anatolia and Italy in Roman Empire and then it is thought to be examined that they were made by mixing silica and calcareous clay with lead oxide (PbO) and the colorants of oxides of copper and iron . After three centuries up to 10th century, non-calcareous clay was used without any colorants. Between the 8th to 14th

centuries CE, the Byzantines and the Seljuks used both the non-calcareous and calcareous lead glazes together in production of pottery [23-24].

Sgraffito, which is a decoration technique applied by carving into the thin coating of slip (liquidified clay) with the help of a sharp instrument, first appeared in Islamic pottery in the 8th century, became popular during the 10-11th centuries in Anatolia and then spread to the Byzantines from the 12th century [25]. Moreover, tin was invented to be added as an opacifier in the 9th century by Islamic potters in today's Iraq. In here, determinants for such a change into the start of using the tin-opacified lead-alkali glazes could be as the results of its high availability of being produced via melting lead and tin together, the risk of reduction of PbO to Pb, which causes blackening of the glaze, being low, and once more the susceptibility of the glaze to be crazed and crawled being low [21]. After the invention of addition of tin to the glaze, overglaze painting on tin-opacified white glazes by using metallic lusters was invented for the first time again in Iraq in the same century. Then, lusters have been substituted with enamels in the 12th century starting from Persia, spreading to Spain and Italy, finally to throughout world with the name "majolica" [26-27]. It has been accepted that pottery samples with the techniques special to the 12-13th centuries, such as painted with brown and yellow, slip painted and champlevé were initially invented in a limited numbered specialized workshops before being distributed to all of the Mediterranean region [28]. After 1150 CE, high lead type of glaze is spread through China and caused the invention of colored overglaze enamels applied first on to the high-fired stoneware glazes, which eventually turns into the discovery of the first white porcelains [21].

If the ingredients of the glaze are investigated, it could be said that it is made of glass (also known as sand or quartz) that has been modified to melt onto the clay. According to the theory of Zachariasen, multiply-charged ions, such as P^{5+}, Si^{4+} and B^{3+}, occupy the centers of the polyhedral in the vitreous state and then form random three dimensional glass network with oxygen ions [29].

Even though quartz (silica, SiO_2) is one of the most abundant minerals composing the earth, glass cannot be used alone to make glazes since its melting point is greater than 1700 °C [30]. Therefore, modifications need to be made to the silica to lower its

melting temperature. The chemicals added to the silica to lower its melting point, such as PbO, $CaCO_3$, borax, frit, dolomite, organic ash and feldspar, are called fluxes. So, the percentage of the flux ingredients was increased to decrease the firing temperature further. Additionally, in order to acquire the glaze to shrink suitably or to prevent shrinkage and cracking during both drying and firing processes by increasing the viscosity and stability of the glaze, alumina (Al_2O_3) is also added, such as bone, wood ash, charcoal, limestone, sand, plant fiber, etc. [31].

Traditional glazes are categorized into different groups like lead, tin, etc. glazes depending on the type of main ceramic fluxing agents used. Here, the study of glazed pottery and tile samples from the Seljukid layers is revealed as to be mostly lead and lead-alkali glaze whose category belongs to the earthen ware. Initially, the raw and soft clay is converted into the hard ceramic by being fired for a long time, then the lead glaze is added with some colorants on to the ceramic surface, fired again and cooled as fast as possible in order to get the transparent and shiny glaze. In the early thirteenth century, the Byzantine and Seljuk workshops changed their method of firing glazed wares by stacking them on the top of each other separated by tripod stilts and started facilitating the mass production [28].

Previous studies of lead-glazed pottery have mostly focused on determining the provenance of the ceramics based on elemental analysis results of the body parts [32]. Indeed, the minor element ingredients of local soil deposits make the glaze or paste unique to its region, and by checking the ratios of some metal oxides it is possible to distinguish which civilizations were there, how the compositions changed in time and influenced from which cultures by trades [33]. Moreover, the elemental and oxide compositions can be determined by using spectrometric techniques such as XRF and the firing temperatures could be estimated by the changes in the structure of silica by using molecular spectroscopic techniques such as FTIR and Raman spectroscopy. In addition, XRD spectroscopy provides information about the crystallographic structure of the materials under investigation.

1.2 Comana Pontica

Since Anatolia has been in the crossing point between Europe and Asia, it has a strategic role to become the center of multiple civilizations emerging from prehistory. Comana Pontica[1] as seen in the map in Figure 1 was one of the temple-states in ancient Pontus with a sanctuary site dedicated to the local Anatolian divinity Ma. It was located near Yeşilırmak (Iris) River in Southern Black Sea Region, more specifically at 9 km northeast of the modern city Tokat in Turkey. The main ancient road passed from Dazimon (in Tokat) through Comana to Neocaesarea (Niksar) and used to have and still has today an important role in connecting the inland cities of the Black Sea Region with each other. Starting with the Greeks in the colonization period to the Hellenistic period, then with the Romans, Byzantines, Danishmendids, Seljuks to Ottomans, many civilizations were present there [34].

According to Strabo, "Kome" meant "hair" in ancient Greek and was derived from the real story of two sisters leaving their hair as means to show their sorrow after they introduced their homeland's holy rituals to Cappadocia [35]. Strabo also suggested that Comana Pontica, the population of which was more than 6000 in 64 BCE, was a cosmopolitan and populous city as well as an important festival, trade and sacred prostitution center for people of Armenia in around the first century CE.

It was founded later than Comana Cappadocia where people shared the same practices [35]. In the 2nd century, the city was enlarged and became an ordinary city of the Roman Empire. There are archives with inscriptions, such as limestone blocks on the collapsed Roman bridge on the Iris River and fragments dedicated to the Roman emperors such as Trajan [36], as well as two coins, demonstrating the loyalty of the city to the emperors with the depictions of the tetra-style temple dated to around 3rd century CE whose dating was figured out from the inscriptions dedicated

[1] Comana Pontica in Latin, or Pontic Comana in English, is formed by the addition of Pontic, meaning belonging to Pontus, in which Pontus represents the Black Sea (Pontus Euxinus) Region, is done on purpose to prevent possible confusions with the other site named as Comana, that is Comana Cappadocia [113]

Figure 1. Location of Comana Pontica in Anatolia during the Greco-Roman period (4th century CE) [2].

to Septimius Severus. Later, Christianity spread throughout Anatolia, which was not good news for Comana Pontica since people living there were still in tendency to pursue their rituals to Anatolian deities. In the 7th century CE, an Arabian-Byzantine battle broke out at Sebastopolis resulting with the defeat of the Byzantines [35]. During the 11th and 12th centuries, the area near Comana was conquered by Danishmendids, Byzantines, Komnenians, Seljuks a few times again and again during the wars of the Crusades between Christian and Muslim authorities. In 1175, Comana Pontica was annexed by Sultan Kılıç Arslan along with other surrounding cities, thence the period of Danishmendids was over and that of Seljuks started. In the next year, with the Battle of Myriokephalon, Byzantine reign ended. During the 11th and 12th centuries, an economic growth was observed in Anatolia. After the Mongol invasion in 1241, administration was maintained by a number of small principalities and the Battle of Kösedağ between the Seljuks and the Mongols in 1243 resulted with the loss of the Seljuks. The decline of the Seljuks in the 13th

[2] Adapted from [114]

century resulted in the collapse of the Seljukid reign in the 14th century at Comana. Finally, the city was ruled by the Eretna Principality in 1328, followed by the Ottomans till the first quarter of the 20th century [37].

1.3 Archaeological Explorations and Excavations at Comana Pontica

After 1830s, the ruins of the ancient settlement of Comana Pontica was visited mostly by the American and European travelers [40-41]. Hamilton describes a well-preserved Roman bridge, an ancient structure in the shape of a rectangle and a colossal tomb. After 50 years of visits, other travelers also came to Comana Pontica. The great temple was mentioned by others and the future excavations were recommended [40]. Also, Anderson wrote about a mound, described the monolith rock-cut tomb in details and identified the name of the nearby village Gümenek must have been derived from Comana [41] .

In 2004, the ancient city was revisited by Prof. Dr. Erciyas and then the archaeological and geophysical surveys have been conducted on Hamamtepe and the villages Kılıçlı, Bula and others until 2009. During the surveys, a Byzantine basilica in Kılıçlı and a stone quarry in Bula were discovered [44-45]. Then the excavations were started in 2009 at seven distinct locations with the supports of METU and the Scientific Technological Research Council of Turkey (TUBITAK), and continued to date. Excavations revealed a wide chronological span from the Late Iron Age through the Ottoman period. Following the Middle Byzantine Period, when there were two churches and a cemetery on Hamamtepe, the region was conquered by the Danishmendids during the 12th century, then the Seljuks reigned between the 12th and 14th centuries, and finally the Ottomans after the 16th century. During excavations, an archaeological phase was recognized to be a workshop with storages, ovens, pits for firing, tripod stilts and sherds including glazed and unglazed samples. This period was attributed to the Danishmendids and the Seljuks [36].

The 30-m-high mound, which is 640 m above sea level and is approximately 200 m x 250 m, constitutes the center of Comana Pontica and is named as Hamamtepe. Here in Figure 2, the four areas where excavations concentrated on are indicated by

different colors. The main area, HTP01, is in the middle (yellow), HTP02 is in the west (red), HTP03 is in the east (in blue) and HTP04 in the north (purples) [44].

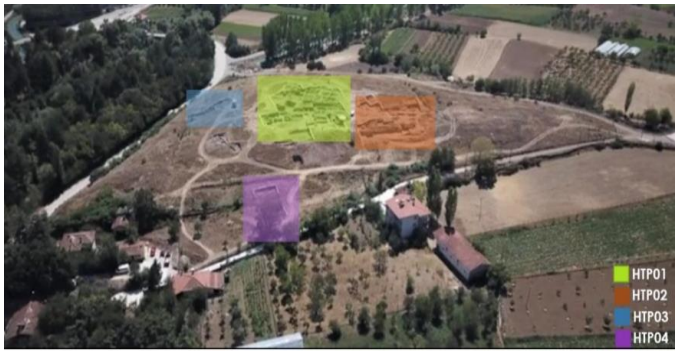

Figure 2. The aerial photograph of four main excavation areas of Hamamtepe [3].

The depicted plan of HTP01 and HTP02 are shown in Figure 3. On the plan, HTP01 is on the right-hand side and represents the center of the citadel of Hamamtepe along with its most elevated point. It has been understood that this area was used as a church and a graveyard from the 10th century till the 12th century during the Byzantine Era, and then as a workshop and a possible domestic area for the next century in the Medieval times. Finally, it was a village neighborhood between the 16th-18th centuries in the period. HTP02 was excavated in order to reveal the fortification wall along with some potsherds [35].

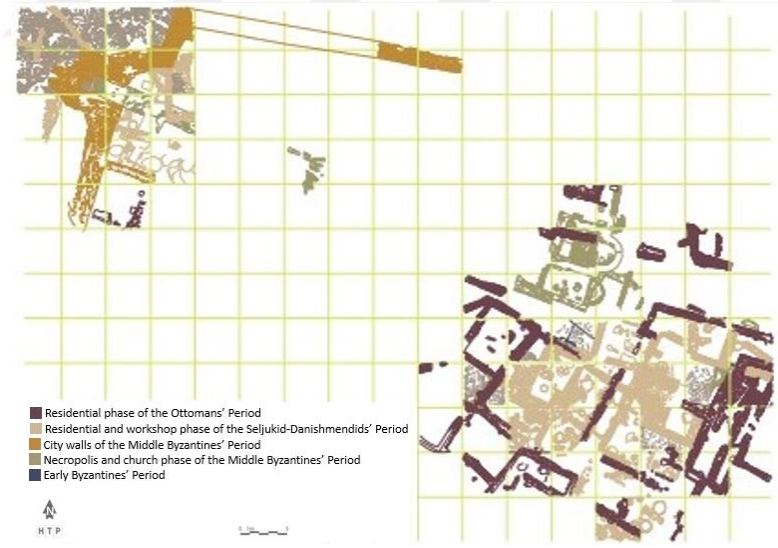

Figure 3. Plan of HTP02 on the left and HTP01 on the right [4].

[3] Received from [44].
[4] Adapted from [35].

Most of the finds were recovered from HTP01 and its trenches were numbered as seen in the plan provided below in Figure 4.

Figure 4. Trench distribution of the HTP01 area in 2017 [5].

The different chronological phases at HTP01 are shown in Figure 5 below. Besides HTP01 and HTP02, there were five more excavation areas, among which HTP06 was also really important since a workshop area, together with multiple ovens and pipes used for air circulation, were discovered [35]. Twenty-four semi-finished pottery pieces, 31 tripods and some burned ceramic cooking pots near the ovens also supported the idea that firing was most probably done locally [44]. Therefore, the possible firing temperatures and conditions of the glazed pottery and tile samples were studied by multi-analytical techniques in this thesis.

[5] Adapted from [44]

Figure 5. Layers of the Byzantines, the Danishmendid-Seljukids and the Ottomans of the HTP01 sector of Comana Pontica [6].

1.4 Former Studies about Comana Pontica

An archaeological study could help to interpret the excavated artefacts according to the comparisons of their decorations, functional usage and utilized technology. The assemblage as a whole can be studied in order to crosscheck the proposed dates and interpretations. Radiocarbon dating and other archaeometric methods could become

[6] Adapted from [44]

useful. In this manner, an archaeometric research is a convenient way to assist the archaeological study through not only age determination and provenance analysis, but also investigation of whether the samples are copies of the original or not, along with the characterization processes of the objects in the way to relate them with some periods and cultures.

Previously, spatial analysis of archaeological data for the identification of both organization and operation of Comana Pontica was carried out [36, 46-47]. As a result of the excavations from 2009 to 2017, archaeological artefacts from the layers of the Ottomans, the Seljuks-Danishmendids, the Byzantines, the Romans and the Greeks, respectively from top to the bottom, were revealed. Most of these artefacts were from the HTP01 sector and totally 1479 glazed ceramic samples, 1842 unglazed cooking utensils and 2223 unglazed storage containers were unearthed from the Seljukid-Danishmendids' layers during 2009-2017. The total 5544 ceramic samples were examined in detail by Karasu, by comparing them with the other Medieval Period ceramics both from Anatolia and the nearby regions and a map with the similarities in the forms of the glazed potsherds of Comana Pontica was created as seen in Figure 6. This map also provides information about the possible trade routes during the Medieval Period. Within those 1479 glazed ceramic samples, Sgraffito technique was applied on 21% of them and 20% of all the glazed ceramics consisted of glaze with one color [44]. In this thesis, 71 glazed potsherds and 2 glazed tiles from the Seljukid-Danishmendids' layers were studied.

Dating of the objects were performed by several methods. Animal bones discovered in the ovens were analyzed by using Carbon-14 dating. Ceramics were compared with the other samples with respect to the similarities of the figures and forms on their surfaces [44]. There are also coins discovered in the Danishmendids' and Seljukids' layers of HTP01 belonging respectively to the time periods of 1143-1166 and 12-14th centuries, mostly to the reign of Keyqubad I (1219-1236) for the latter period [46].

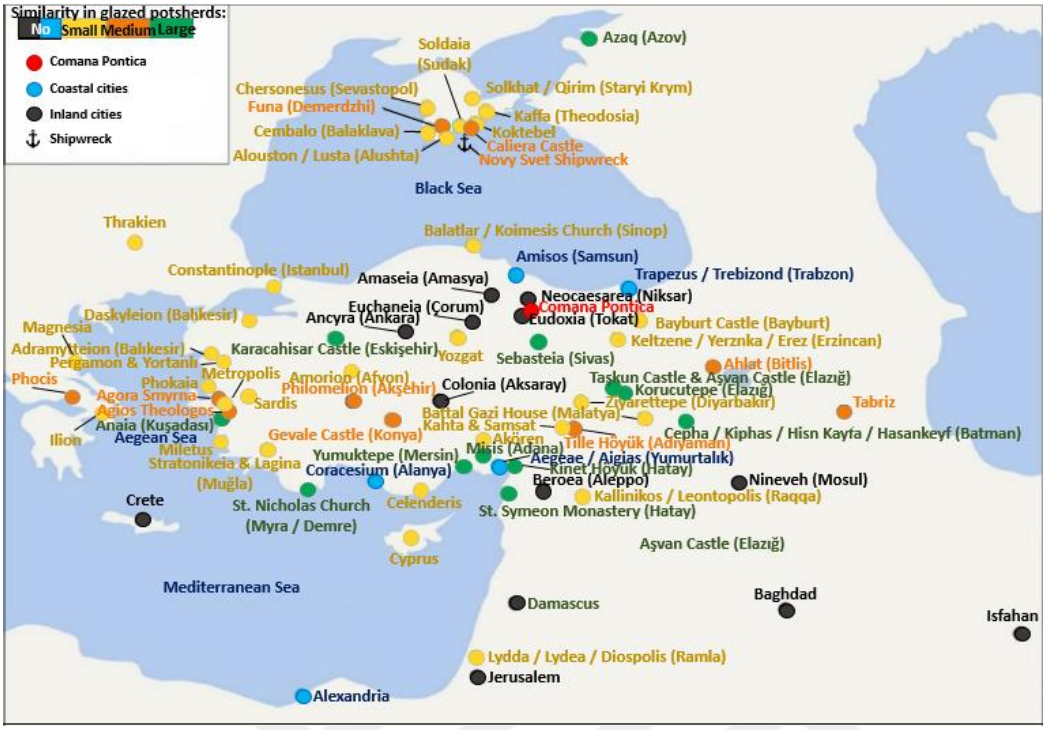

Figure 6. Map with the similar forms of the glazed potsherds of Comana Pontica [7].

Provenance analysis of ceramic samples from Comana excavation was completed by Mehmet Bilgi Er [47]. A second Master's thesis was completed on the archaeometallurgical properties of the Byzantine coins from Comana excavation [48].

1.5 Purpose of the Study

The aim of this thesis is to characterize the glazes of the potsherds and tiles found in Comana Pontica, to investigate which components are responsible for the differentiation in colors and whether the glazes were applied on an oxidizing or reducing atmosphere, as well as to determine the firing temperature of those pottery samples with the help of their glaze parts, using the analytical techniques of FTIR, XRD and Raman spectroscopy and XRF spectrometry. After getting the

[7] Adapted from [44].

XRF analysis results of the glazes, this information can also be valuable in characterization, such as drawing the ternary diagrams of oxide analyses that would enlighten whether the pottery sherds and tiles are representing its time that falls in the Seljuks' periods.

CHAPTER 2

LITERATURE REVIEW

To characterize the glaze of an archaeological pottery sample, various techniques can be performed. For example, Fourier Transform Infrared Spectroscopy (FTIR) can identify the characteristic vibrations of the glaze components, providing information on the type of bonding between the atoms present in the glaze. It is used to determine the functional groups present in a material by measuring the absorption of infrared radiation. Infrared radiation is passed through the sample, and the amount of radiation absorbed is measured. This absorption corresponds to the vibrational frequency of the different chemical bonds in the sample, making it possible to identify specific functional groups. Moreover, any organic compounds that may be present due to post firing usage of the pot could be determined, which can provide information on any potential usage of the pottery besides the manufacturing process of the pottery. Alternatively X-Ray Diffraction (XRD) can identify the crystallographic structure of minerals making up the glaze, which works by directing an X-ray beam to the sample and analyzing the angle and intensity of the reflected X-rays. These patterns can then be compared to known mineral databases to identify the minerals present in the sample which helps determining the type of the glaze, its chemical components, the geographical origin of the pottery, as well as the technological level of the civilization that has made it. Furthermore, XRF (X-ray Fluorescence) can also be used for determining the elemental composition of a sample of the pottery glaze, which works by irradiating the sample with X-rays, causing the atoms to emit their characteristic energy signatures when they return to their ground state, where these signatures can then be analyzed to identify the elemental composition of the sample. Compared to other analytical techniques, XRF is relatively fast and non-destructive. It can provide qualitative and quantitative information about the elemental composition of the glaze, including major, minor, and trace elements.

While XRF provides good chemical fingerprinting information that can help to identify the geographical origin of the pottery, on the other hand it does not give much information about the crystal phase of the glaze. Hence a combination of those abovementioned methods can be used together to get a comprehensive characterization of archaeological pottery samples. That is why all of these techniques are used one by one in this research to support each other.

Besides, there are a few more techniques which were not preferred here but can also contribute to the glaze analyses, such as Scanning Electron Microscopy (SEM) to identify and describe the microstructure and morphology of the glaze, as well as to show the elemental composition of the glaze. Hence, Thermal Analysis (TA) can measure the changes in the physical and chemical properties of the glaze from high temperatures to provide information about the melting point, chemical composition and also firing condition of the glaze. By using a combination of these techniques, a comprehensive characterization of the glaze on an archaeological pottery sample can be achieved, and more information about the composition and manufacturing technique of the ancient pottery can be determined.

To start with, to find the production technology of the glaze of the pottery and tile samples, the information about the type of crystallites developed during the firing process and their distribution in the ceramic object are really important and they are affected by:

a. The body composition (earthenware, stoneware clays or porcelain),

b. The glaze composition (lead, lead-alkali or alkaline),

c. Type of the initial materials (raw or mixed),

d. Firing temperature and conditions (whether the furnace atmosphere was oxidizing or reducing, and whether the bisque-firing was applied before the glaze firing) [13].

A glaze consists of mainly silica and then, oxides of several elements such as lead, potassium, sodium, boron and magnesium to provide a flux in order to decrease the melting point of the mixture. Afterwards, some colorants, like oxides of metals of

iron, chromium, lead, calcium, zirconium, cadmium and zinc can be added to the glaze in order to increase the stability before the final steps, drying and firing processes, take place [49].

Firing has an important role in the preparation of ceramic objects since it converts the matrix of the clay mineral inclusions into its more favorable polymorphs which are more stable, by their undergoing chemical modifications or structural transformations, such as vitrification, new phase formation, decomposition, dehydration and dehydroxylation [50].

So, as seen in **Figure 7**, linkages between silicon and oxygen are broken down with firing according to equation below as follows:

$$O_3Si\text{-}O\text{-}SiO_3 \leftrightarrow O_3Si^{+} + {}^{-}O\text{-}SiO_3 \quad (2)$$

Then the repeating anion ($^{-}OSiO_3$), which is shown at the right end in the upper equation (2), reacts at increased temperature with a metal cation from any metal oxide, such as $M^{2+}O^{2-}$ or $(M^{+})_2O^{2-}$, to increase its stability to form $MO\text{-}SiO_3$ compound. Then, the reaction further produces the compound of $MO\text{-}Si(O)_2\text{-}OM$ which is more stable than $MO\text{-}SiO_3$ [49].

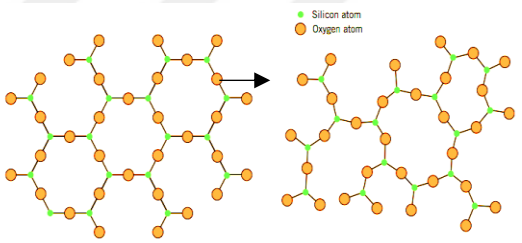

Figure 7. Structure of crystalline SiO_2 (a) and non-crystalline (amorphous) silica-based glass (b). Green dots symbolize Silicon atoms and orange ones are Oxygens. Adapted from [115].

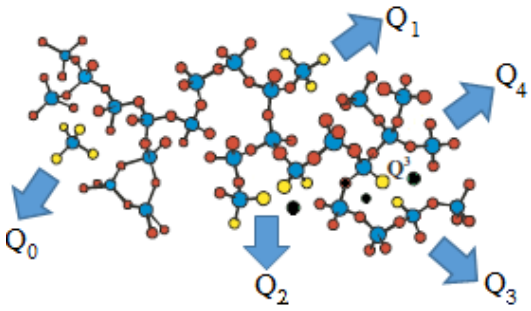

Figure 8. Illustrative representation of the polymerized network of the glaze. Yellows are H, reds are O, blues are Si and blacks are any metal like Al, Pb, Mg, Mn, etc.; and isolated (Q_0), bonded with one (Q_1), two (Q_2), three (Q_3) and four (Q_4) Si-O-Si tetrahedral bridge(s). Adapted from [53].

Since both the glass and glaze consist of silicates, if any network modifier is added during firing, Si-O linkages would be broken down by the interchanging metals as well as the change in the degree of polymerization

according to the altering bending (δ) and stretching (ν) modes of Si-O yielded from the analysis of Spectral Q_n components, as seen in the **Figure 8** [51].

Furthermore, as indicated in **Figure 9**, the intensity of the transmittance peak of the spectrum between the wavenumber range of 800-1300 cm^{-1}, both in FTIR[52] and Raman spectra[53], is composed of five sub-peak components and could be detected by the signals of proportions of molecules with different numbers of Si-O bridges. Moreover, the detailed structural schemes of the Si-O bridges of each component (Q_n) are added to **Figure 10**. If the pottery sample is not fired at all, then most of the silicon molecules are expected to be a tetrahedron as shown in **Figure 10.a** and the spectrum will be like the component 0, symbolized by the band Q_0, the sub-peak on the left end of the groups of stretching (ν) peaks on the right of **Figure 9**, corresponding roughly to 800 cm^{-1}. If the firing temperature is low enough in the kiln, then the isolated molecules begin connecting with each other to produce pairs as seen in **Figure 10.b** as well as its spectrum will predominantly be with the sub-peak 1 in **Figure 9** and the band is named as Q_1 corresponding to 800-850 cm^{-1}. Likewise, if more heat is given to the silicate, then configuration turns into forming single chains, as could be seen in

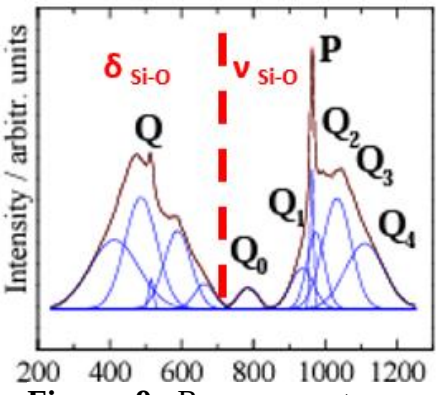

Figure 9. Raman spectrum of transmittance intensity versus wavenumber of a pottery in which the bending (δ) peak, denoted with Q, observed between 300-700 cm^{-1} and stretching (ν) peak consisting of different sub-peaks (Q_1, Q_2, Q_3, Q_4, Q_5) resulted from different Si-O bridges, observed between 800-1300 cm^{-1}. P peak may be observed because of the superimposed α-quartz and calcium phosphate crystalline phases on the glaze. Adapted from [51-52].

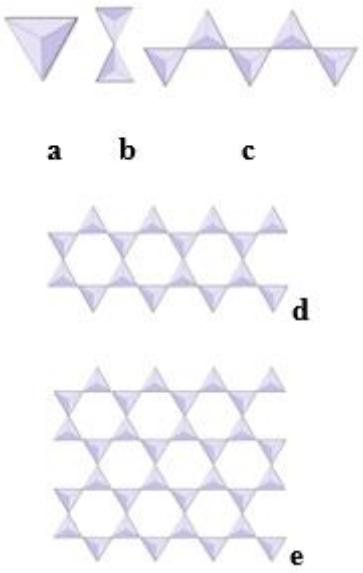

Figure 10. Schematic diagram of the structural Si-O bridges, in **a.** isolated SiO_4^{4-} units, **b.** pairs, **c.** chains, **d.** double chains, **e.** sheet formation.

Figure 10.c with the major peak of 2 in **Figure 9**, whose chemical band is known as mostly Q_2 corresponding to 950-1000 cm^{-1}. Further heating will cause with a shift of the major sub-peak towards 3 above in the **Figure 9**, denoted as the band Q_3, that results from the double chains as represented with the framework of d in **Figure 10** above corresponding to 1050-1100 cm^{-1}. Finally, if the glazed pottery sample is put in the furnace with up to 1200°C, then the sheet formation is observed as seen in **Figure 10.e** whose spectrum signals would be overpowering in the area shown with number 4 in **Figure 9**, and the area of four bridging oxygens are symbolized as Q_4 and the wavenumber shifted to approximately 1100-1200 cm^{-1} [54]. Indeed, in the presence of some fluxes, like oxides of Pb, Ca, K, Na, these metals are ionized and the cations start incorporating into the silica sheets by breaking the Si-O linkages, which results in a decrease in the polymerization of the Si-O network, finally yielding to a shift to the lower wavenumbers and firing temperatures could decrease to around 600 °C [55-56]. Vice versa, they could move to the higher wavenumber side if the metal oxides are glass formers such as oxides of Si and Al [57-58].

At the end, checking the ratios of the areas of the two maxima sub-peak positions, namely the area of bending multiplet, A_{500}, observed around 400-600 cm^{-1} divided by the area of stretching (900-1100 cm^{-1}) multiplet, A_{1000}, in Raman spectrum, gives information about the measure of the change in network and about the firing temperature of the glaze and the technology used for firing [54]. This calculation of area ratios (A_{500}/A_{1000}), called as the polymerization index (I_p), is more accurate in Raman spectroscopy, since Raman signals are generally narrower compared to those of its analogue of FTIR bands [57, 59].

Baseline subtraction is preferred for eliminating the Boson peak contribution and just to observe the silica peaks clearly. Moreover, as I_p increases, Q_n wavenumber also increases due to the silica structure becoming more strongly bonded and compact. The location of the silica stretching and bending Q_n components together with I_p values can give information about assigning the materials in the glaze as shown in **Figure 11** [53] and the shape of the Raman spectra can also give information about the characterization of the glaze as seen in **Figure 12** [59].

Furthermore, according to plots of I_p values versus the wavenumber of the maximum Si-O stretching component, as seen in **Figure 13.a**, can give information about the type of the samples whether they are porcelain, stoneware or glass, as well as their contents are rich in which oxides. Moreover, I_p values versus the area ratio of Q_2/Q_1 as seen in **Figure 13.b** can also give information about characterization of the samples such as in which civilization and in which century they were produced [53].

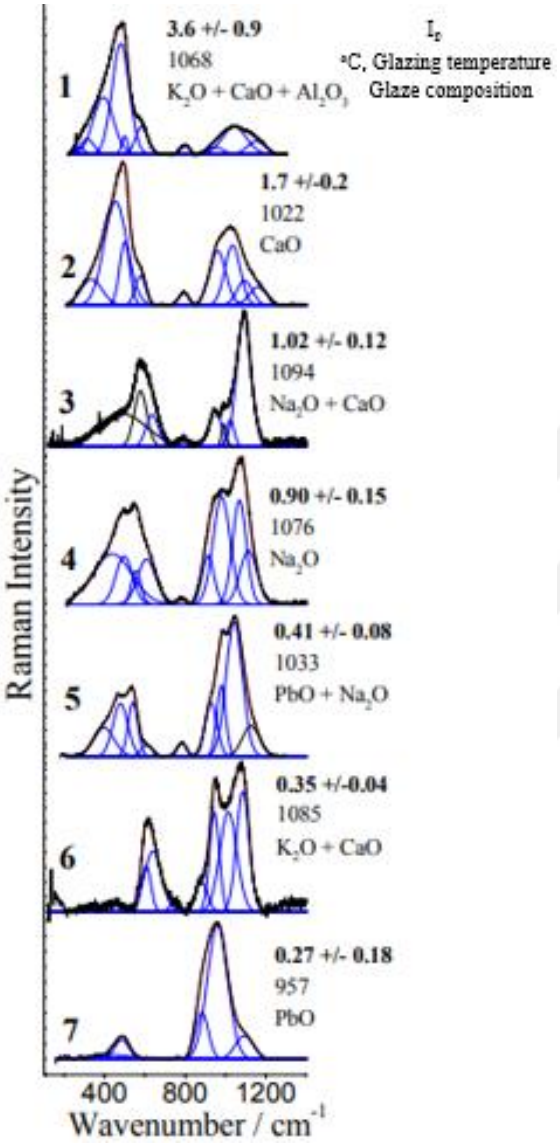

Figure 11. The polymerization indices and shapes of the stretching and bending Q_n components of Si-O can give information about assigning the materials in the glaze. From [53].

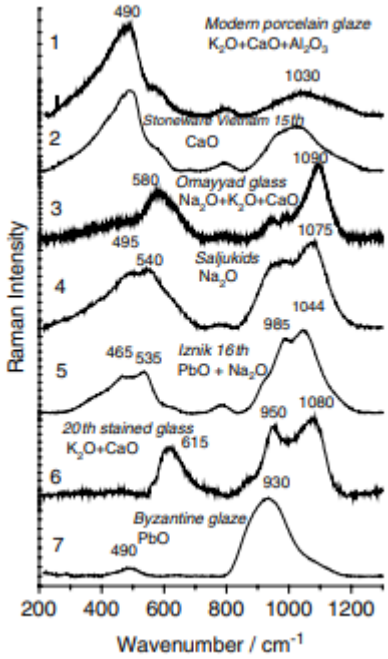

Figure 12. Representative Raman spectra of some identified families after the application of baseline substraction. From [59].

If the glaze is Pb-rich, then its I_p value will mostly be less than 0.3-0.5. If the glaze is rich in Na- or Pb-mixed glassy enamels, then I_p value will be between 0.5 and 0.8. Soft-paste porcelain enamels and ancient Roman glasses will yield the I_p as between 0.8 and 1.1. If the glaze is enriched with Ca, then the I_p becomes between 1.3 and 2.5. Glazes of the K-based hard-paste porcelains gives an Ip greater than 2.5 [60]. Besides the glassy composition, I_p value can also give information about the glazing temperature in such a way that I_p is around 0.3 for the glazes fired around 600 °C or less, around 1 for 1000 °C and around 7 for 1400 °C [60]. According to this information, Figure 14 could be plotted, in which the equation of the first part between 600-1000 °C is y = 66.667x + 933.33 and that of the second part between 1000-1400 °C is y = 571.43x + 428.57. If the logarithmic equation is calculated, it is found as y = 249.37ln(x) + 938.33.

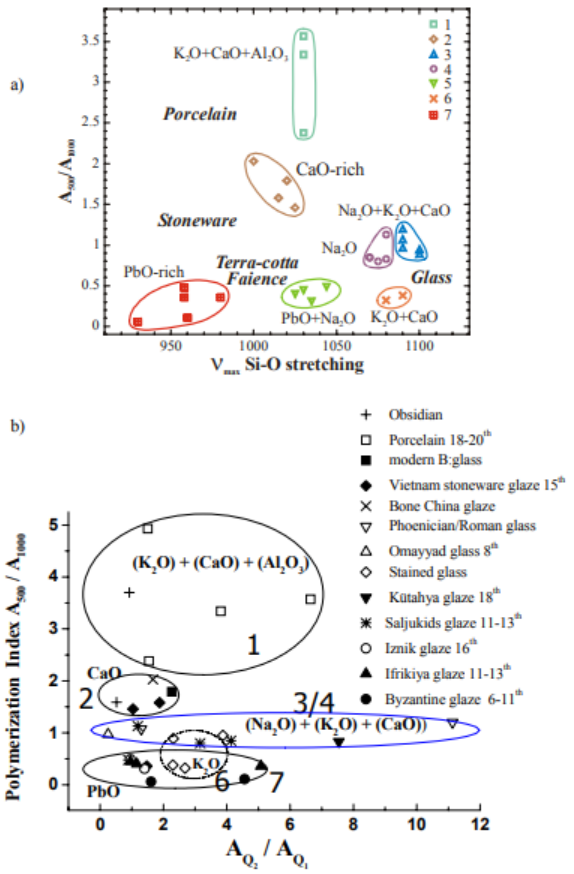

Figure 13. Plots of I_p vs wavenumber of maximum Si-O stretching (a) and area ratio of Q_2/Q_1 (b). From [53]

This estimation of firing temperatures from I_p values calculated from areas in Raman spectra can also be supported with the wavelength location of the major bands in

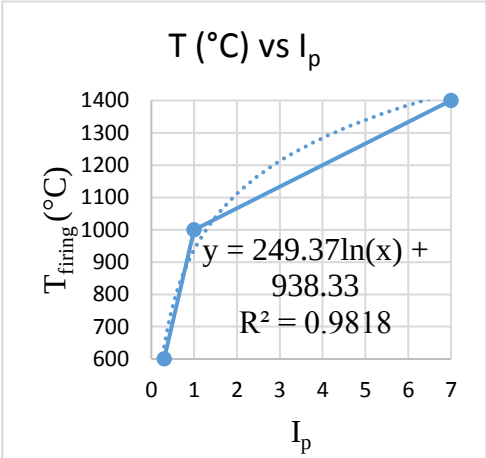

Figure 14. The graph of firing temperatures (°C) vs. Raman I_p values, drawn according to [60].

the FTIR spectra. A detailed information about the kinds of bands is given in **Figure 15** [61].

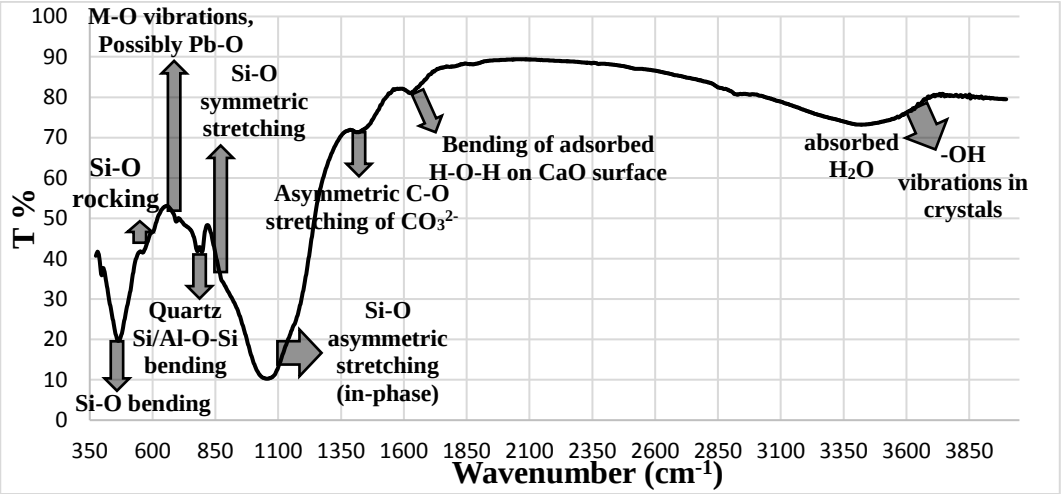

Figure 15. Vibrational bands shown on the FTIR spectrum of the yellow glaze of potsherd K108 in this study.

As could be seen in Figure 15, the maximum peak around approximately 900-1100 cm^{-1} is due to the in-phase asymmetric stretching vibrations of Si-O in silica. The shoulder around 1160 cm^{-1} is as a result of out-of-phase Si-O stretching, likewise the signals at 700, 780, 800 cm^{-1} are resulted from Al/Si-O-Si bending vibrations [49]. The shoulder at around 500-600 cm^{-1} is due to Si-O rocking vibrations, likewise the local maximum peak at around 460-470 cm^{-1} is due to a Si-O bending [62]. The broad band between 3000-3700 cm^{-1} reveals the hydroxyl group (-OH) either in the crystallized form in the glaze or the absorbed water due to the long times staying of the samples under the earth [49]. Moreover, Si-O-Ti vibration is observed at 935-960 cm^{-1}; Si-O-Al vibration at 1000 cm^{-1}; Si-O-Zr vibration at 950 cm^{-1} [63]. Additionally, Al-OH-Al bending is seen at 915 cm^{-1}; Al-OH-Fe bending at 884 cm^{-1}; Al-OH-Mg bending at 842 cm^{-1} [64]. Likewise, Si-O-Fe vibrations are at 680 and 900 cm^{-1}; Si-O-Fe vibrations at 680 cm^{-1} [65]. The signals at around 584, 646 and 725 cm^{-1} are characteristic vibrations of Metal-O bonds, most probably Pb-O. Likewise, the ones at around 713, 876, 1430-1450 and 1775-1820 cm^{-1} are due to the calcite ($CaCO_3$) present in the glaze [62-63] and those at 531 and 685 cm^{-1} are thought to belong to Sn-O vibrations.

Furthermore, the region around 3600-3700 cm^{-1} is used to characterize the clay type [64-65]. It is considered that there are three types of clay, kaolinitic (dickite, halloysite, kaolinite, nacrite), montmorillonitic-smectitic (nontronite, montmorillonite, pyrophyllite, saponite, sauconite, talc, vermiculite) and illitic (mica), by excluding chlorite and sepiolite classified not as a clay but a separate group in phyllosilicates [69].

Moreover, the peak at 3648 cm^{-1} is known to belong to the slaked lime, $Ca(OH)_2$, and the peak at around 1647 cm^{-1} occurs due to the bending vibrations of adsorbed water on the surface of CaO [70], both of which also provide information about the firing temperature of the sample in such a way that above 600 °C microcrystalline calcite ($CaCO_3$) decomposes and the quicklime (CaO) is formed, after 800 °C calcareous clay minerals are rehydroxylated to $Ca(OH)_2$, above 900 °C dehydroxylation [56], dehydration and decarbonation occur up to 1000 °C with disappearance of all the calcite peaks and -OH bands [61].

It is known that the Si-O bending and Si-O stretching peak positions are also dependent on both the firing temperature [71] and type of the glaze additives [57]. To investigate the shifts in these Si-O bending and Si-O stretching peak positions in general, pottery samples are prepared in the laboratory conditions at various firing temperatures. The ceramic samples have been found to be fired at specific temperatures, such as for the various studies with 800 °C, the measured wavenumbers fluctuate from one study to another in a way that a single peak was measured at 1079 cm^{-1} from the unglazed cooking pots in Tel Hadar [56], a single peak at 1050 cm^{-1} from the unglazed storage jar in Tel Hadar [71], a double peak at 1045 and 1080 cm^{-1} from a raw clay in Caricin Grad [72], a single peak at around 1059 cm^{-1} from the ceramic body of glazed Byzantine potsherds in Skopsko Kale [73], and a double peak at 1050 cm^{-1} (with the one with a little bit greater in volume) and 1078 cm^{-1} from the raw material in Tel Michal [74].

Therefore, as the firing temperature increases, SiO_4 tetrahedra tends to become interlinked from the corners of each other to form a sheet as depicted in **Figure 10.e** and this effect is resulted in a shift of the wavenumber of the maximum peak in the spectrum, which corresponds to the Si-O stretching signal, starting from 1028 cm^{-1}

after being heated at 100 °C for 6 hours to 1073 cm^{-1} at 1000 °C as in the Caricin Grad experiments [72]. The wavenumber intervals correspond to Si-O stretching peak are listed in **Table 1**. Since the wavenumber locations of FTIR spectra of the frits and glazes mostly do not change [72] with additions of modifier elements, such as Ba, Si, Al, K and Mg, to the glassy network [75], the laboratory experiments of fired raw clays could also be appropriate as those of glazes.

Table 1. Wavenumbers of the Si-O stretching peaks (cm^{-1}) vs. the specified temperatures (°C) drawn by the results of FTIR spectra of the fired raw clay [72].

T (˚C)	100	600	650	700	750	800	850	900	1000
ν (cm^{-1})	1028	1035	1037	1040	1040	1045 & 1080	1047 & 1080	1077	1073

Figure 16 shows the wavenumbers of the Si-O stretching peaks shift to the higher wavenumbers when the firing temperature is increased. The graph is divided into 7 parts, considering the change in the slope values for temperature ranges between 100 to 900 °C. Then, the line equations for each part are listed in Table 2. Using these line equations, calculated firing temperatures are listed

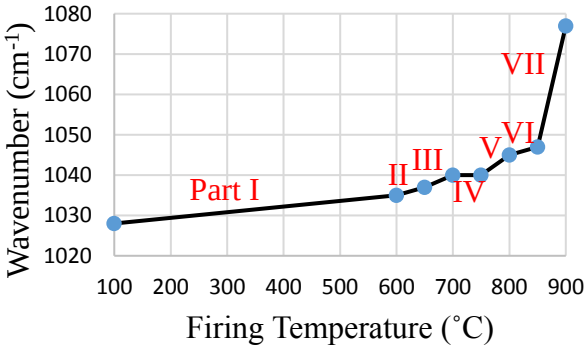

Figure 16. Graph of firing temperatures (°C) vs. wavenumber (cm^{-1}). Data are taken from Table 1.

Table 2. Line equations found from Figure 16.

Part	Equation	ν (cm^{-1})	T (˚C)
I	y = 0.014x + 1026.6	1028-1035	100-600
II	y = 0.04x + 1011	1035-1037	600-650
III	y = 0.06x + 998	1037-1040	650-700
IV	y = 1040	1040	700-750
V	y = 0.1x + 965	1040-1045	750-800
VI	y = 0.04x + 1013	1045-1047	800-850
VII	y = 0.6x + 537	1047-1077	850-900

in Table 3 between 1027-1093 cm^{-1}.

Since the slope of the part IV is zero, even 50 °C of an increase in temperature does not cause any change in the wavelength value in this region. On the other hand, the slope of the part VII is greater than the other parts, the wavenumbers in that region are increasing rapidly, so the larger shifts in wavenumbers results in small change in firing temperature values.

Table 3. Estimation of the firing temperatures with respect to the shifts in the wavenumbers of the Si-O stretching peaks according to Table 2.

ν (cm^{-1})	T (°C)	ν (cm^{-1})	T (°C)	ν (cm^{-1})	T (°C)	ν (cm^{-1})	T (°C)
1027	30	1036	625	1045	800	1067-1069	885
1028	100	1037	650	1046	825	1070-1072	890
1029	170	1038	670	1047-1048	850	1073-1075	895
1030	240	1039	685	1049-1051	855	1076-1078	900
1031	315	1040	700-750	1052-1054	860	1079-1081	905
1032	385	1041	760	1055-1057	865	1082-1084	910
1033	460	1042	770	1058-1060	870	1085-1087	915
1034	530	1043	780	1061-1063	875	1088-1090	920
1035	600	1044	790	1064-1066	880	1091-1093	925

According to the laboratory research done, the spectra of the glazes, also some slips and pastes of the Comana Pontica samples can be analyzed, the wavelength numbers of the maximum peaks could be compared with the values in the upper table to reveal the estimated firing temperatures.

Then XRF can reveal whether there is lead in the glaze or not. In case lead is added to the glaze, the glaze starts to melt at lower temperatures around as 600 °C. Afterwards, lead is oxidized and then reacts with the clay minerals such as Al and K. Finally, lead crystallizes in the interface layer and then precipitates as lead feldspar ($PbAl_2Si_2O_8$) and lead-potassium feldspar [$(Pb,K)AlSi_3O_8$] [26, 70]. So, the estimated firing temperatures could be checked for the lead glazes whether they are fired at lower temperatures as 600 °C.

Moreover, pottery can be colored for decorative purposes with the addition of some types of additives. When the colorant is added to the sample, volatile compounds are

released from the structure with the increase in the temperature. In this case, as well as the temperature, condition of the kiln is also important in the formation of colors. If there is enough oxygen around the kiln (in oxidizing atmosphere), oxides of the elements are formed, which could also be detected with the help of the XRF technique. If there is no oxygen around (in reducing atmosphere), oxygen will be released from the sample in the form of CO_2 with the help of free carbons occurred from the fuel that could not be burned and the surface color of the glaze becomes darker, in the way that green color becomes red and purple after Cu^{2+} of CuO is reduced to Cu^{+} of Cu_2O, yellow color turns into green and brown after Fe^{3+} of Fe_2O_3 is reduced to Fe^{2+} of FeO, and brown color becomes black after Mn^{4+} of MnO_2 is reduced to Mn^{2+} of MnO [77], which means also the colors can give information about the way how and in which conditions the ceramics are fired.

Besides those colors, it is known that 1.5% Co as $CoCO_3$ is enough for the intense blue color independent from the firing atmosphere. Together with Co, if there is also Mg and fired at 920 °C, then the color becomes pink and with the increase in concentration of Co, blue-violet color would be obtained on the surface. If there are Mn and Fe with Co, then the color becomes black [78].

In more details, the color of the iron oxide is red in the form of ferric oxide (Fe_2O_3), black in the form of ferrous oxide (Fe_3O_4) and rarely yellow in the form of Fe_2O_3 [78]. The color becomes green if Fe^{2+} ions are present in the reducing atmosphere [79]. On the other hand, if the glaze having Fe^{3+} ions is fired under an oxidating atmosphere, then the color can be between amber to brown depending on the concentration of iron; otherwise, under reducing atmosphere it could give green color in the presence of 2% Fe_2O_3, yellow between 2-3%, orange at 3-4%, red at 4-5% and brown-black above 5%. If the glaze is heated at around 1300 °C, presence of Fe_2O_3 and bone ash make the color orange and Fe_2O_3 with Sn produces cream color [78].

Likewise, 2-3% copper, which is volatile at 950 °C, gives red and purple depending on the concentration of the copper under reductive atmosphere and blue/turquoise to green under oxidative environment. If the glaze is alkaline, then Cu makes the color turquoise. If Pb and Cu coexist, then green color is observed [78].

Moreover, addition of 2-3% chromium gives green color under reductive and brown to red and then yellow under oxidative conditions. Besides chromium, if lead is immersed and fired up to 950 °C, then its color is observed as red. If there is also soda ($NaHCO_3$) besides lead and chromium, then its color changes into yellow up to 950 °C and becomes green above this temperature. If there is Zn and Cr, the glaze would appear brown. Chromium is volatile at 1000 °C and addition over this temperature causes smoky effects [78].

Five to ten percent manganese makes the color of the sample purple and black under reductive and honey-brown under oxidative atmosphere up to 1000 °C. If the glaze is high in alkali, then the color is observed as blue-purple. Lead and manganese produce the purple softer with traces of brown color [78].

Furthermore, addition of nickel oxide provides the color gray-brown [78]. Titanium causes an increase in both the crystal growth and opacity, and dyes the glaze to tan color in the oxidative atmosphere and gray in the reductive atmosphere [78]. In addition, antimony gives the yellow color, selenium and cadmium give red, gold makes pink-red-purple and finally platinum dyes to gray color [78].

Pigments are also dispersed in the matrix such as, there is no green and light blue shades in the Ottoman Era Iznik pottery with the help of the black lines of chromite. Chromite traps copper and cobalt ions so that color of copper and cobalt ions are more intensified in those regions [58].

FTIR analysis of the samples does not provide fully characterization of the ingredients added to the glaze if there is colorant added, such as Verona green $\{K[(Al,Fe^{3+}),(Fe^{2+},Mg](AlSi_3,Si_4)O_{10}(OH)_2)\}$, Naples yellow ($Pb_2Sb_2O_7$), lead-tin-yellow ($Pb_2SnO_4$), smalt ($SiO_2.K_20.Al_2O_3.CoO$), manganese black ($MnFe_2O_4$), lead white [$2PbCO_3.Pb(OH)_2$] or malachite [$Cu_2CO_3(OH)_2$], but FTIR supports the presence of silica, lead, carbonate, carbon dioxide and water in the glaze [64, 74].

Furthermore, by boiling of the crust or the substances in some parts of the animals, also by softening of wood, roots, leaves, vegetables, fruits, after evaporation and drying; natural pigments with organic origins can be produced. The most common pigments are ochre (with yellow clay minerals $Fe_2O_3.H_2O$), sienna [yellow raw

goethite FeO(OH) or its burnt state], red ochre (hematite), vermilion red (HgS), chrome red [$PbCrO_4.Pb(OH)_2$)], ultramarine blue (lapis lazuli, $3Na_2O.3Al_2O_3.6SiO_2.2Na_2S$), Prussian blue {$Fe_4[Fe(CN)_6]_3$}, Cobalt blue ($CoO.Al_2O_3$), umber brown either raw or burnt ochre with MnO_2, chrome green (Cr_2O_3), chalk white ($CaCO_3$), gypsum sulphate ($CaSO_4.2H_2O$), white marble dust or could be black (either by graphite, carbon black, bone black of calcined bone, or MnO)[81].

Besides coloring agents, to make the transparent glaze becoming opaquer, opacifiers can be added. Tin oxide (SnO_2) or Zircon sand cannot be solved into the glaze melt, so they lower the thermal expansion and increase the hardness, particles start getting suspended in the glaze and scattering light. Opacification can also be achieved if the crystallizing component is too saturated as observed in TiO_2, or if the glaze is slowly cooled then less saturated oxides as Borax ($Na_2H_{20}B_4O_{17}$) derivative Boron blue crystallizes easily [82]. Furthermore, antimony oxide (Sb_2O_3) can be produced as a byproduct after refining of Sb metal or Pb-Sb alloys, and gives the Naples yellow color if the glaze is rich in Pb [83].

Moreover, by detecting the type of the clay in the paste and in the glaze, estimation of the firing temperature could be double checked. It is known that if the temperature is elevated up to 550 °C then kaolinite turns into metakaolinite. If the temperature is increased up to 920-940 °C, then alumina, metakaolinite, mullite, spinel and amorphous silica phases are observed in the matrix. Finally, at 1200 °C mullite and cristobalite are observed and could be detected with XRD measurements [84].

In most of the pottery samples, quartz (SiO_2), hematite (Fe_2O_3), maghemite (γ-Fe_2O_3), magnetite ($FeO.Fe_2O_3$), anatase (TiO_2 stable up to 550 °C), rutile (TiO_2 between 550-1000 °C), calcite ($CaCO_3$), albite ($NaCa_{0-0.1}AlSi_3O_8$), graphite (crystalline C's arranged in hexagonal structure), carbon black (paracrystalline C), microcline ($KAlSi_3O_8$), apatite [$Ca_5(PO_4)_3(F,Cl,OH)$], titanite ($CaTiSiO_5$) and hornblende [$(Ca,Na)_{2-3}(Mg,Fe,Al)_5(Al,Si)_8O_{22}(OH,F)_2$] are added to the glaze and identified using XRD [73]. Additionally, there are minerals specifically used by Byzantines, such as olivine [$(Mg^{2+},Fe^{2+})_2SiO_4$], baryte ($BaSO_4$), augite $(Ca,Na)(Mg,Fe,Al,Ti)(Si,Al)_2O_6$, epidote [$Ca_2Al_2(Fe^{3+},Al)(SiO_4)(Si_2O_7)O(OH)$],

fayalite (Fe_2SiO_4), sphalerite [(Zn,Fe)S] and phlogopite [$KMg_3(AlSi_3O_{10})(F,OH)_2$] [73]. Dolomite [$CaMg(CO_3)_2$], diopside [$FeCaSi_2O_6$], spessartine [$Mn^{2+}{}_3Al_2(SiO_4)_3$] and siderite ($FeCO_3$) minerals are detected in the Ottomans' ceramic samples [73].

CHAPTER 3

EXPERIMENTAL

3.1 Sampling

From the excavations of Comana Pontica, 73 glazed samples, 71 of which are potsherds and the rest 2 are tiles, were chosen to be analyzed. Some pottery glazes consist of more than one color, so totally 115 colored samples, including 106 from potsherd glazes (with 51 green, 36 yellow, 9 brown, 7 orange and 1 turquoise), 2 from tile glazes (1 black and 1 turquoise), 6 from pastes (indicated as red or white here depending on the paste color) and 3 from underglaze slips (indicated with white), are displayed by some codes (tiles start with K0 and the potsherds with K1-K2) in the Table 4 below and by photographs and features like their dating, decoration types, colors, inclusions, together with the representation of interior and exterior parts, in the Appendix A.1. For more details about the potsherd samples, including their drawings, excavation rings, dates, heights, radii, ratios of forms of the glazed pottery, Dr. Karasu's article could be addressed [44]. Lastly, two tiles, which have been discovered in the layers of 262/593 trench of HTP01 of Comana Pontica, were added to this study to make more comparisons.

Table 4. Colors and codes of glazed tile and potsherd samples (#: number, bk: black, bl: blue, br: brown, ex: exterior, gr: green, in: interior, or: orange, pa: paste, re: red, sl: slip, ti: tile, tq: turquoise, wh: white, ye: yellow).

Sample #	Sample Code	Sample Color	Analysis #		Sample #	Sample Code	Sample Color	Analysis #
1	K001	bl/tq (ti)	1		4	K102	br	8
		wh (pa)	2		5	K103	gr	9
2	K002	bk (ti)	3		6	K104	ye	10
		wh (pa)	4				gr	11
3	K101	gr	5				re (pa)	12
		re (pa)	6				wh (sl)	13
4	K102	ye	7		7	K105	gr	14

Table 4 (Cont'd)

Sample #	Sample Code	Sample Color	Analysis #		Sample #	Sample Code	Sample Color	Analysis #
8	K106	gr	15		34	K148	ye	54
		ye	16				gr	55
		re (pa)	17		35	K149	ye	56
		wh (sl)	18				gr	57
9	K108	ye	19				re (pa)	58
		gr	20				wh (sl)	59
		br	21		36	K150	gr	60
10	K109	gr	22		37	K151	ye	61
11	K110	gr	23		38	K152	ye	62
12	K111	ye	24		39	K153	gr	63
		gr	25		40	K154	ye	64
13	K112	ye	26				gr	65
		gr	27		41	K155	gr	66
14	K113	gr	28				ye	67
		ye	29		42	K156	ye	68
15	K114	gr	30				gr	69
16	K115	ye	31		43	K157	gr	70
		gr	32		44	K158	gr	71
17	K117	br	33		45	K159	gr	72
18	K118	br	34		46	K160	ye	73
19	K119	gr	35				gr	74
20	K122	ye	36		47	K161	gr	75
		gr	37		48	K164	or	76
21	K123	gr.in	38				br	77
		gr.ex	39		49	K167	ye	78
22	K124	gr	40		50	K168	ye	79
23	K125	ye	41				gr	80
24	K128	ye	42		51	K169	gr	81
25	K129	ye	43				br	82
		br	44		52	K170	ye	83
26	K130	ye	45				gr	84
27	K131	ye	46		53	K171	or	85
		gr	47		54	K172	or.in	86
28	K132	ye	48				or.ex	87
29	K143	gr	49		55	K173	or.in	88
30	K144	gr	50				or.ex	89
31	K145	gr	51		56	K184	ye	90
32	K146	br	52				gr	91
33	K147	gr	53				br	92

Table 4 (Cont'd)

Sample #	Sample Code	Sample Color	Analysis #	Sample #	Sample Code	Sample Color	Analysis #
57	K185	ye	93	66	K213	gr	105
58	K199	ye	94	67	K215	ye	106
		gr	95	68	K220	ye	107
59	K200	ye	96			gr	108
60	K201	gr.in	97	69	K221	ye	109
		gr.ex	98	70	K222	gr.in	110
61	K203	ye	99			gr.ex	111
		or	100	71	K223	bl	112
62	K204	gr	101	72	K226	gr	113
63	K210	gr	102	73	K228	ye	114
64	K211	ye	103			gr	115
65	K212	gr	104				

All the glazed potsherds were used as the tableware. These samples were analyzed with multiple analytical techniques and the type of the technique used to analyze the sample is shown in the Table 5.

Table 5. Analytical techniques (I: FTIR spectroscopy, F: XRF spectrometry, D: XRD spectroscopy and R: Raman spectroscopy) used to analyze the glazed tiles and potsherd samples represented according to their visual features like their codes (tiles: starting with K0 and potsherds: starting with K1-K2), colors (bk: black, br: brown, gr: green, gy: gray, or: orange, re: red, tq: turquoise, wh: white, ye: yellow), dating, decoration types (ch: champlevé, sg: sgraffito, sp: slip painted), places (interior or exterior side, pa: paste, sl: slip) and whether including any inclusions or not; #: number, ?: not known, deco: decoration.

#	Sample	Dating (century)	Interior Surface			Interior Glaze						Exterior Surface		Exterior Glaze				Paste		
			Deco	Slip	wh	ye	gn	or	br	tq	bk	Deco	Slip	ye	gn	or	br	pa	Color	Inclusions
1	K001	14th	none	none						IFD		none	none					I	wh	wh
2	K002	14th	none	none							IFD	none	none					I	wh	wh
3	K101	13th	sg	wh			I					none	none					I	re	wh
4	K102	13th	sg	wh								sg	wh	I			I		or	none
5	K103	13th	sg	wh			I					none	wh						re, br	wh
6	K104	13th	sg	wh	I		I					sp	wh	I				I	re	none
7	K105	13th	sg	wh								none	wh		I				re	none
8	K106	12-13th	sg	wh	I		I					sg	wh	I				I	re	none
9	K108	13th	sg	wh		I			IF			sg	wh		I				re, br	wh (few)
10	K109	13th	sg	wh								sg	wh		I				br	wh
11	K110	12-13th	sg	wh			I					sg	wh						re, br	wh (few)
12	K111	13th	sg	wh		I						sg	wh		I				or	none
13	K112	13th	sg	wh		I						none	wh		I				re, br	wh
14	K113	12-13th	sg	wh		I						sg	wh		I				re, br	wh
15	K114	13th	sg	wh								sg	wh		I				re	none

Table 5 (Cont'd)

#	Sample	Dating (century)	Interior Surface			Interior Glaze						Exterior Surface		Exterior Glaze				Paste		
			Deco	Slip	wh	ye	gn	or	br	tq	bk	Deco	Slip	ye	gn	or	br	pa	Color	Inclusions
16	K115	12th	sg	wh		IR						sg	wh		ID				or	none
17	K117	13th	sp	wh					I			sp	wh						re, or	none
18	K118	12-13th	sg	wh					I			sg	wh						re, br	none
19	K119	13th	sg	wh								sg	wh		I				re	dark
20	K122	13th	sg	wh		I						sg	wh		I				re, br	none
21	K123	12-13th	sg	wh			I					sg	wh		I				re, br	none
22	K124	12-13th	sg	wh			I					none	wh						re, br	none
23	K125	13th	sg	wh		I						none	none						re, br	none
24	K128	12-13th	sg	wh		ID			R			none	wh						re	wh (few)
25	K129	13th	sg, sp	wh		I			IDR			none	wh						re, br	wh
26	K130	13th	sg	wh		I						ch, sg	wh						re	dark
27	K131	13th	ch, sg	wh		I						sg	wh		I				re, br	wh
28	K132	13th	sg	wh		I						none	trace wh						re	wh
29	K143	12-13th	sg	wh			I					sg	wh						re, br	none
30	K144	12-13th	none	wh			I					none	wh						re	none
31	K145	13th	sg	wh			I					sg	wh						gy	wh (few)
32	K146	13th	sp	wh					IR			sp	wh						re,br	wh
33	K147	13th	ch, sg	wh								sg, sp	wh		I				re	wh
34	K148	13th	sg	wh		I						sg	wh		I				re, br	wh
35	K149	13th	sg	wh	I	IFD						sg	wh		IR			I	re, br	wh
36	K150	12-13th	sg	wh			I					none	none						re	wh
37	K151	12-13th	none	wh		I						none	none						re, br	wh
38	K152	12-13th	none	wh		IDR						none	wh						re	wh
39	K153	12-13th	none	wh								sg	wh		I				re	wh, dark
40	K154	13th	sg	wh		I						none	wh		I				re, br	none
41	K155	13th	sg	wh			I					sp	wh	I					or	dark
42	K156	13th	none	wh			I					sg	wh	I					re, br	none
43	K157	13th	none	wh			IDR					none	none						re	none
44	K158	13th	sg	wh			I					none	none						re, br	wh
45	K159	13th	sg	wh			I					none	none						re, br	wh
46	K160	13th	sg	wh		IR						sg	wh		IDR				re	none
47	K161	12-13th	none	wh			IFR					none	none						re	wh
48	K164	13th	sg	wh				I	I			none	wh						light re	none
49	K167	13th	sg	wh		I						sg	wh						re, br	light
50	K168	13th	sg	wh		I						sg	wh		I				re, br	wh
51	K169	12-13th	sg	wh								sg	wh		I		I		re, br	wh
52	K170	13th	sg	wh		I			I			sg	wh		I				re	wh
53	K171	12-13th	sg	wh				I				none	none						re	wh
54	K172	12-13th	sg	wh				I				none	wh			IFD			re, br	wh
55	K173	12-13th	none	wh				I				none	wh			I			re	wh
56	K184	12-13th	ch, sg	wh		I			I			none	wh		I				re, br	wh
57	K185	12-13th	sg	wh		I						none	wh						re, br	wh
58	K199	13th	sg	wh		I	I					none	wh						re	wh
59	K200	13th	sg	wh		I						none	wh				I		re, br	none
60	K201	13th	sg	wh			I					none	wh		I				re	none
61	K203	13th	sg	wh		I		I				none	none						re, br	wh
62	K204	12-13th	sg	wh								none	wh		I				re	wh
63	K210	12-13th	none	none, wh			I					none	wh						or	wh (few)
64	K211	13th	sg	wh		I						none	none						br	wh
65	K212	13th	sg	wh								sg	wh		I				or	wh
66	K213	13th	sg	wh			I					none	none						re, br	wh (few)
67	K215	13th	sg	wh		I						sg, sp	wh						re	none
68	K220	13-14th	ch, sg	wh		I			I			none	wh		I				re, br	wh
69	K221	12-13th	none	wh		I						none	re br						light br	wh (few)
70	K222	12-13th	sg	wh			I					none	wh		I				re	?
71	K223	12-13th	none	none						IFD		none	none						wh	?
72	K226	12-13th	sg	wh			I					sg	wh						or	none
73	K228	13th	sg	wh		I						sg	wh		I				re, br	none

The different colors of glazes on each sample are indicated by filling the squares with the same color of each glaze according to their location either on the interior or exterior part of the sample, as seen in the Table 5. The colored squares without a letter inside mean that the tile or potsherd is is colored, however colored area was too small to get enough sample for the analysis of the glaze using FTIR, XRD, XRF or Raman techniques.

3.2. Fourier-Transform Infrared (FTIR) Spectroscopy

Sample holders, glass slides, the utility knife, the agate mortar and the grinder were cleaned before each step with ethanol (Merck 100983).

Initially, each glaze layer, together with the colorants adhered to it, of chosen potsherd samples was pulled out with the help of a utility knife, grinded with an agate mortar. Then, these powdered samples were mixed with spectroscopic grade KBr (Merck 1.04907) with a wt.% ratio of 1:100 in order to prepare pellets. Among these ratios, the best S/N ratio was obtained with 1.75/100 and this ratio was used throughout FTIR experiments.

Bruker ALPHA FTIR spectrometer was used and the spectra were recorded within the range of 4000–400 cm^{-1} with 128 scans at a resolution of 4 cm^{-1} under the double-sided forward-backward acquisition mode with velocity of 7.5 kHz.

Furthermore, the scan number is also changed from 16 to 32, 64, 128, 256 and 512 in order to find best S/N with minimum analysis time. Signal to noise ratio does not get better above 128 scans so throughout FTIR scans 128 was used as the number of scans.

Moreover, all the experiments of each glaze samples were repeated three times by collecting samples from different parts of the glazed area of ceramic sample.

Potassium bromide (KBr) was kept at 100 °C temperature for 2 hours in order to get rid of humidity and then, stored in a desiccator.

3.3. X-Ray Fluorescence (XRF) Spectrometry

Two tiles and representative five potsherd samples, each with different glaze colors, namely turquoise and black tiles, and potsherds with glaze colors of brown, yellow, green, orange and turquoise, with the sample codes K001, K002, K108, K149, K161, K172 and K223, respectively, were analyzed with XRF spectrometer. Since the surface area of the yellow, turquoise and brown glazed pottery samples were very small, each of them was put into 10-mm sample holders. The other potsherd samples with green and orange glazes were put into 20-mm sample holders and the two tiles were put into 30-mm holders separately.

The trademark of the X-Ray Fluorescence (XRF) spectrometer in the Chemical Analysis Laboratory of the Central Laboratory at METU is Rigaku ZSX Primus II and it was used to determine elemental composition of the glazes sampled from ceramic surfaces.

3.4. X-Ray Powder Diffraction (XRD) Spectroscopy

Glaze samples of the potsherds with the colors of 3 yellow (K128, K149 and K152), 3 green (K115, K157, K160), one orange (K172), one turquoise (K223) and one brown (K129), together with the tile samples (K001 and K002) were chosen to be examined due to their relatively large surface area. In here, the potsherd samples of K149 with yellow, K172 with orange and K223 with turquoise glazes, and the tiles were chosen to be analyzed with XRD to compare the results with XRF.

Initially about 3 grams of each of the glaze layers of the aforementioned potsherd and tile samples were pulled out with the help of a utility knife, grinded in an agate mortar. Then, these powdered samples were smeared uniformly, randomly and in the un-oriented way on the glass slide, placed into the sample holder and the intensities of the diffracted X-rays were recorded continuously while both the detector and the sample rotated with scan speed of 2 degrees per minute within the 2Θ range of 5-90° under CuKα radiation with the wavelength of 0.1542 nm with the instrument Rigaku Miniflex X-ray diffractometer. The scattering was continuous with the X-rays of

30kV/15mA, scattering slit with 4.2 degree and the receiving slit 0.3 mm. At the end of the analysis, the spectra were drawn as peak positions at 2Θ versus peak height (intensity) of X-rays using Microsoft Excel© 2019 program.

For the calculations, Equation of Bragg's Law below could be used, where d is the spacing between diffracting planes, Θ is the incident angle, n is any integer and λ is the wavelength of the beam [85]:

$$2d.\sin\Theta = n.\lambda \quad (3)$$

3.5. Raman Spectroscopy

Initially at least one sample from different colors of glazes, namely yellow, orange, green, turquoise, brown and black were chosen and their pastes were also analyzed without any sample preparation. The first measurements were carried out by Horiba-Jobin Yvon LABRAM Raman spectrometer in METU Chemistry Department using a 20 mW He–Ne laser at 632.8 nm with a spot size around 1 mm^2 using a microscope with a 50x objective lens, 10 s integration time and 2 accumulations were used to take spectra of the ceramic samples. Whereas no Raman signals except a brown glazed potsherd were able to be measured from these glaze parts of these samples because of the laser wavelength of 632.8 nm.

In Koç University Surface Science and Technology Center (KUYTAM), Renishaw inVia confocal Raman microscope which is completely automated was used with a 532-nm (green) laser excitation and a power of 112.5 mW. The laser power on the sample was measured without any objective and found 18.3 mW. A Leica long working distance objective, 50×, NPlan, NA 0.50, was used, and in order to prevent any phase transformation and analysis area blackening due to the intense laser irradiation, the exit power on the sample was gradually decreased. The spectrum recording time was ranged between 10 and 60 s. The data were kept with the original software of the instrument, WIRE Version 4.4. For the peak fitting and data processing, linear baseline was initially subtracted using LabSpec Software (Version 5.25.15), using Origin 6.0 software peak-fitting module (Microcal Software), which

allows the investigation of the bending and stretching envelopes. The index of polymerization, I_p, is calculated from the ratio of bending to stretching areas of the molecular Si–O Raman signature, as already described in the literature. The integral areas were calculated for some of the samples. At first, the spectrum was imported by choosing "Import as Single ASCII", then all the y-axis (Raman intensity) values were chosen and clicked on the "Peak Fitting" icon. From the window of "Set Baseline", "Line" was chosen and in the "Set Peak Function" area the Gaussian shape was chosen for all assigned Raman lines since Gaussian is preferred for amorphous samples whereas Lorentzian is for crystals. And then from the option of "Estimate Peaks' Center and Height", spectrum massive areas were divided into sub-divisions by clicking on "Start Fitting Session". The maximum bandwidths were set to be equal to 120 cm^{-1}, and until the fitted value became constant, it was kept on fitting process. Finally by clicking "Results" and "Plot", peak analyses reports were gathered, from whose frequency and area values were used to calculate the I_p values [86].

CHAPTER 4

RESULTS AND DISCUSSION

In this chapter, some graphics and tables are created from the results of the spectra of FTIR, XRF, XRD and Raman. Initially by FTIR spectroscopy, firing temperatures of the samples will be investigated with respect to the wavenumber values of asymmetric Si-O stretching peaks. Then, with the results of XRF spectrometry, percentages of the oxide contents will be examined for each type of different colors of glaze, together with the contribution of bivariate and ternary characterization diagrams and their statistical interpretations. Finally, XRD and Raman spectra will give information about the structure and chemicals of the glazes and pastes.

4.1 Results and Discussion of FTIR Spectroscopy

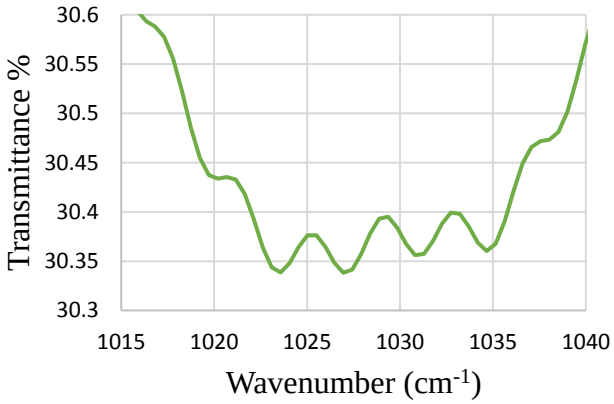

Figure 17. FTIR spectrum of the green glaze of K101 potsherd between 1015-1040 cm^{-1}.

FTIR spectrum of the green glaze from K101 sample is shown in the Figure 17. The peak maximum around 1027 cm^{-1} shows that the firing temperature is around 600 °C as calculated from the Table 3. It is known that minimum 600 °C is needed to produce glaze layer on top of the ceramic surface [87].

Furthermore, it is known that by checking the vibrations around 3600-3700 cm^{-1} in an FTIR spectrum, the clay minerals could be identified [64]. As shown for the yellow glaze of K108 potsherd in Figure 18; peaks at 3620, 3650-3652, 3671 and 3692-3696 cm^{-1} correspond to the stretching vibrations of hydroxy of kaolinite, and the peak at

around 3628-3630 cm^{-1} stands for O-H stretching vibration of smectite and H-O-H bending vibration of halloysite. Likewise, the peak at 3594 cm^{-1} results from Na-vermiculate; 3600 cm^{-1} from illite; 3607 cm^{-1} from Fe bearing kaolinite; 3622 cm^{-1} from smectite; 3624 cm^{-1} from montmorillonite; 3625 cm^{-1} from bentonite; 3670 cm^{-1} from saponite; 3670 and 3580 cm^{-1} from chlorite; 3675 cm^{-1} from Mg-vermiculite; 3686 cm^{-1} from lizardite; 3701 and 3647 cm^{-1} from nacrite; 3708, 3654 and 3628 cm^{-1} from dickite; 3719 and 3689 cm^{-1} from sepiolite; 3740, 3670 and 3570 cm^{-1} from saponite [67].

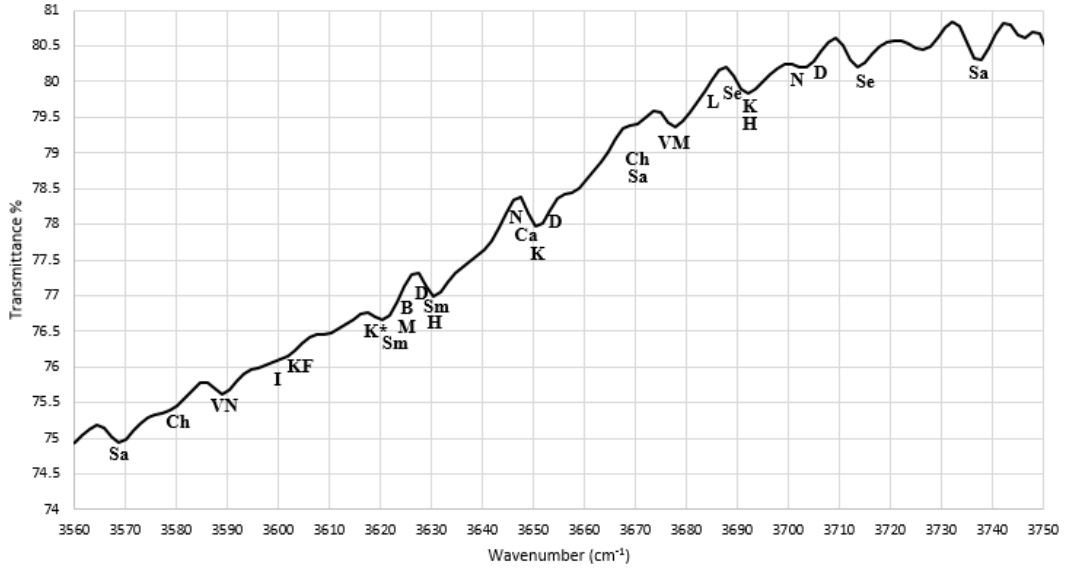

Figure 18. FTIR spectrum of the yellow glaze of K108 potsherd around 3600-3700 cm^{-1} with the vibration peaks of characterized clay minerals; **B:** Bentonite $[(Ca,Na)_{0.3}(Al,Mg)_2Si_4O_{10}(OH)_2 \cdot nH_2O]$, **Ca:** O-H stretching of slaked lime $[Ca(OH)_2]$, **Ch:** Chlorite $(Fe^{+2},Fe^{+3},Mg^{+2},Mn^{+2},Ni^{+2},Zn^{+2},Al^{+3},Li^{+1},Ti^{+4}.)_{4-6}(Si,Al)_4O_{10}(OH,O)_8$, **D:** Dickite $[Al_2Si_2O_5(OH)_4]$, **H:** H-O-H bending of halloysite $(Al_2O_3 \cdot 2SiO_2 \cdot 2H_2O)$, **I:** Illite $(K,H_3O)(Al,Mg,Fe)_2(Si,Al)_4O_{10}[(OH)_2,(H_2O)]$, **K:** Surface O-H stretching of kaolinite $(Al_2O_3 \cdot 2SiO_2 \cdot 2H_2O)$, **K*:** Inner O-H stretching of kaolinite $(Al_2O_3 \cdot 2SiO_2 \cdot 2H_2O)$, **KF:** Stretching of AlFeOH in Fe-kaolinite $[Al_{3.91-3.96}Si_{4-4.04}Fe_{0.03-0.13}Ti_{0.01-0.1}O_5(OH)_4]$, **L:** Lizardite $[Mg_3(Si_2O_5)(OH)_4]$, **M:** Montmorillonite $(Na,Ca)_{0.33}(Al,Mg)_2(Si_4O_{10})(OH)_2 \cdot nH_2O$, **N:** Nacrite $[Al_2Si_2O_5(OH)_4]$, **Sa:** Saponite $[Ca_{0.25}(Mg,Fe)_3((Si,Al)_4O_{10})(OH)_2 \cdot n(H_2O)]$, **Se:** Sepiolite $[Mg_4Si_6O_{15}(OH)_2 \cdot 6H_2O]$, **Sm:** O-H stretching of smectite $[(Na,Ca)_{0.33}(Al,Mg)_2(Si_4O_{10})(OH)_2 \cdot nH_2O]$, **VM:** Mg-vermiculite $[(Mg,Al,Fe^{2+})_3(Si,Al)_4\ O_{10}(OH)_2 \cdot nH_2O]$, **VN:** Na-vermiculite $[(Na,\ Al,\ Fe^{2+})_3\ (Si,Al)_4O_{10}(OH)_2 \cdot nH_2O]$

The peaks in Figure 18 were similar for all the potsherds, including the turquoise-glazed potsherd of K223, as well as the white slip of K104 and the red paste of K106. Therefore, the main groups of the clays in the potsherds were both kaolinitic (dickite, halloysite, kaolinite, nacrite) and montmorillonitic-smectitic (bentonite, montmorillonite, saponite, smectite, vermiculite).

The exceptional spectra whose peaks in the range around 3600-3700 cm^{-1} were different than the ones in Figure 18, namely the rest of the red pastes and white slips, and all the white pastes, are shown in Figure 19.

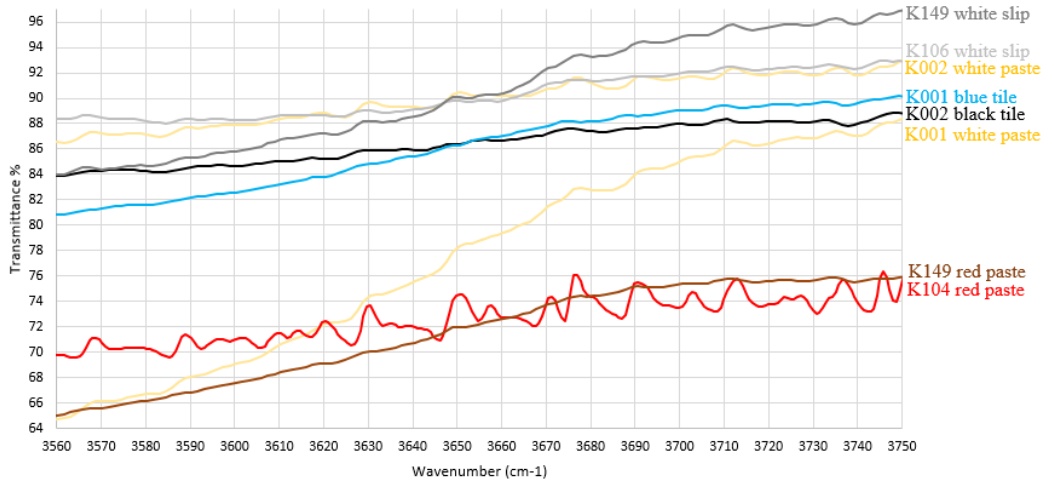

Figure 19. FTIR spectra of the rest of the red pastes and white slips, and all the white pastes, around 3600-3700 cm^{-1} with the vibration peaks of characterized clay minerals.

It could be seen in Figure 19 that illite peak at around 3600 cm^{-1}, Fe-kaolinite peak at 3607 cm^{-1}, dickite peaks at 3654 and 3708 cm^{-1}, saponite peak at 3668-3670 cm^{-1}, Mg-vermiculite peak at 3675 cm^{-1}, sepiolite peak at 3689 cm^{-1} , and nacrite peak at 3701 cm^{-1} [67] are more intense for the red paste of K104. For the rest of the white slips, red paste and all the white pastes, the peaks are almost not observed, probably due to the dehydroxylation, dehydration, and decarbonation occurred at higher firing temperature values such as 850-925 °C [54, 62]. When the almost-flattened peaks of the slips and white pastes are checked in the same figure, little peaks could still be observed at around 3565, 3622, 3624, 3625, 3648, 3670, 3740 cm^{-1}, indicating saponite $[Ca_{0.25}(Mg,Fe)_3((Si,Al)_4O_{10})(OH)_2 \cdot n(H_2O)]$, smectite $[(Na,Ca)_{0.33}(Al,Mg)_2(Si_4O_{10})(OH)_2 \cdot nH_2O]$, montmorillonite $[(Na,Ca)_{0.33}(Al,Mg)_2$

$(Si_4O_{10})(OH)_2 \cdot nH_2O$], bentonite [$(Ca,Na)_{0.3}(Al,Mg)_2Si_4O_{10}(OH)_2 \cdot nH_2O$], slaked lime [$Ca(OH)_2$], and again saponite and saponite [67] respectively, which are all derivatives of minerals containing calcium, probably taken from crushed shells and bones [88].

Moreover, the peak at 3648 cm^{-1} is known to belong to the slaked lime, $Ca(OH)_2$, and the peak at around 1647 cm^{-1} occurs due to the bending vibrations of adsorbed water on the surface of CaO [70], both of which also provide information about the firing temperature of the sample in such a way that above 600 °C microcrystalline calcite ($CaCO_3$) decomposes and the quicklime (CaO) is formed, after 800 °C calcareous clay minerals are rehydroxylated to $Ca(OH)_2$, above 900 °C dehydroxylation [56], dehydration and decarbonation occur up to 1000 °C with disappearance of all the calcite peaks and -OH bands [61].

The results of the clay minerals determined by the region around 3600-3700 cm^{-1} in FTIR spectra of this research are also consistent with those of pastes of the same potsherds analyzed by the optical microscope, XRD and ICP-MS by Dr. Bilgi Er [47]

Moreover, the firing temperature range calculated by the wavenumbers of asymmetric stretching peaks at around 1010-1090 cm^{-1} in Figure 16 is divided to 600-700, 700-800, 800-900 and 900-925 °C intervals, since the slope in the beginning values of the same graph is not so steep that ±4 cm^{-1} changes in wavenumber, due to the resolution, was affecting almost 100 °C change in temperature, on the other hand, beyond 850 °C, its slope becomes so great that even small amounts of change in wavenumber causes jumps in the estimated temperatures. FTIR spectra of all the samples were taken, some of which are shown in Figure 20, and with the help of line equations in each step, possible firing temperatures are calculated, using the Table 3 with respect to the wavenumbers of the maximum peak points of Si-O asymmetric stretching in the FTIR spectra for each sample. FTIR spectra of all the individual glaze samples of the potsherds and tiles are given in the Appendix A.2. The firing temperature values are calculated for each sample using the line equations given in the Table 2.

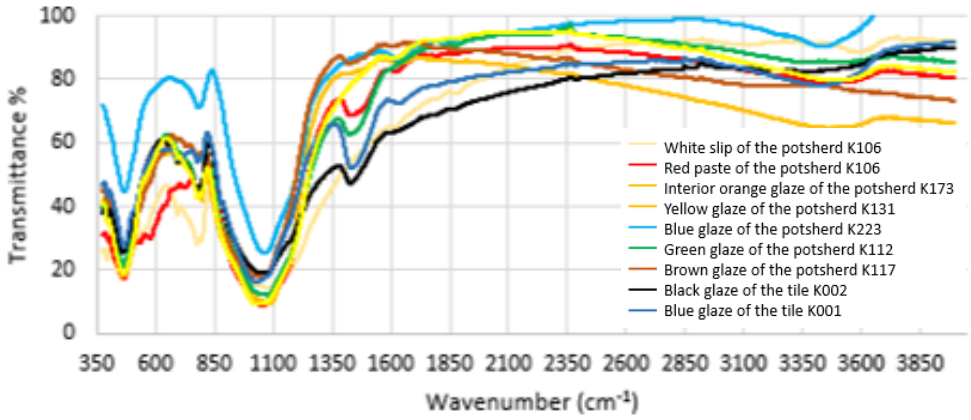

Figure 20. FTIR spectra of representative different colors of glazes, pastes and slips.

Due to the fact that the resolution was chosen as large as 4 cm^{-1}, the maximum peak points were observed to have changed in the repeated analyses of the same glaze from different points. Similarly, if the area around the maximum peak point is enlarged as shown in the boxes put on the right below corners of the spectra in Appendix A.2, their shape was also changing, for example from doublet to triplet, within the range of ±4 cm^{-1}, which can affect the determination of the firing temperatures. Even though, in this time, more spectra were collected by increasing the number of scans and decreasing the resolution, the more accurate decision on the estimation of the firing temperatures were made after by comparisons. Finally, even though the sampling number was increased a lot, estimated temperature range stayed large, sometimes as much as 100 °C.

Since the asymmetric Si-O stretching peak positions corresponding to certain wavenumbers as stated in the Table 3 were very wide, there is not just one wavenumber assigned for each of the peak positions. Minimum and maximum firing temperatures were also calculated based on the ±4 FTIR wavenumber range (cm^{-1}).

According to the calculated firing temperatures of the ceramic samples added to the Appendix A.2, Table 6 is produced. Colored rectangles without any number indicate that the amount of glaze is too small to take sample from those areas.

Table 6. Estimated firing temperatures (°C) calculated by Si-O asymmetric stretching vibration bands at around 1010-1080 cm^{-1} in FTIR spectra, using Table 3.

#	Sample	Paste	In. Slip	Interior Glaze Temperatures (°C)						Exterior Glaze Temperatures (°C)			
			White	Yellow	Green	Orange	Brown	Blue	Black	Yellow	Green	Orange	Brown
1	K001	850-900						600-700					
2	K002	900-925							900-925				
3	K101	850-900			600-700								
4	K102									700-800			850-900
5	K103				850-900								
6	K104	850-900	900-925		900-925					900-925			
7	K105										775-825		
8	K106	850-900	900-925		800-850					900-925			
9	K108			850-900			600-700				850-900		
10	K109										775-850		
11	K110				850-900								
12	K111			600-700							600-700		
13	K112			775-825							900-925		
14	K113			600-700							775-850		
15	K114										600-700		
16	K115			600-700							600-700		
17	K117						850-900						
18	K118						600-700						
19	K119										600-700		
20	K122			850-900							600-700		
21	K123				600-700						600-700		
22	K124				700-800								
23	K125			900-925									
24	K128			600-700									
25	K129			900-925			600-700						
26	K130			600-700									
27	K131			700-800							900-925		
28	K132			900-925									
29	K143				850-900								
30	K144				900-925								
31	K145				650-750								
32	K146						850-900						
33	K147										850-900		
34	K148			750-800							600-700		
35	K149	850-900	900-925	775-850							850-900		
36	K150				900-925								
37	K151			700-800									
38	K152			775-825									
39	K153										600-700		
40	K154			600-700							850-900		
41	K155				900-925					675-775			
42	K156				600-700					600-700			
43	K157				850-900								
44	K158				750-800								
45	K159				675-775								
46	K160			600-700							900-925		
47	K161				675-775								
48	K164					850-900	600-700						
49	K167			675-775									
50	K168			700-800							850-900		
51	K169										600-700		600-700
52	K170			600-700							700-800		

Table 6 (Cont'd)

#	Sample	Paste	In. Slip	Interior Glaze Temperatures (°C)						Exterior Glaze Temperatures (°C)			
			White	Yellow	Green	Orange	Brown	Blue	Black	Yellow	Green	Orange	Brown
53	K171					850-900							
54	K172					850-900						850-900	
55	K173					900-925						900-925	
56	K184			700-800			600-700				600-700		
57	K185			850-900									
58	K199			900-925	900-925								
59	K200			600-700									
60	K201				700-800						650-750		
61	K203			700-800		600-700							
62	K204										600-700		
63	K210				600-700								
64	K211			850-900									
65	K212										650-750		
66	K213				850-900								
67	K215			775-825									
68	K220			675-775							600-700		
69	K221			850-900									
70	K222				850-900						850-900		
71	K223							850-900					
72	K226				850-900								
73	K228			750-800							675-775		

The column graphs of estimated firing temperatures of thirty-six yellow-glazed and fifty one green-glazed samples, drawn with regard to the wavenumber shifts of the maximum peak points on FTIR spectra, are shown in the Figure 21 and Figure 22 respectively, and the rest of the colored glazes, pastes and slips can be seen in the Figure 23. The colored columns in the front line represent the estimated minimum temperatures of each glaze and are painted to the same color of the glaze observed, for example columns in the front are painted in yellow for all the yellow glazes. On the other hand, the estimated maximum temperatures are colored in black for all the samples and placed at the back.

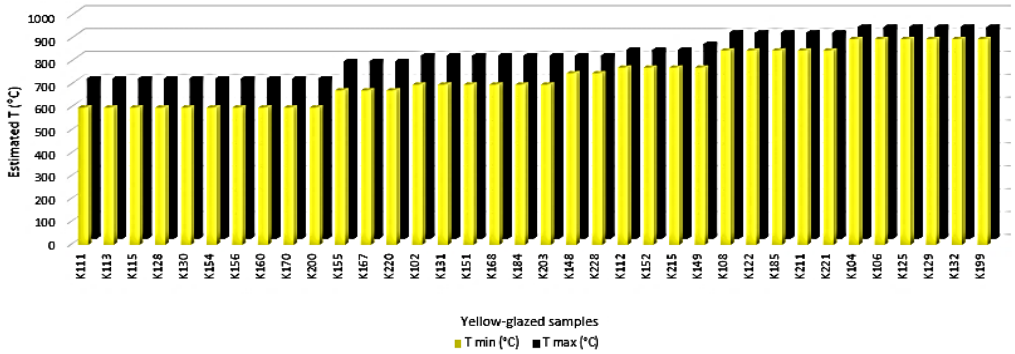

Figure 21. Estimated firing temperatures of the yellow glazes.

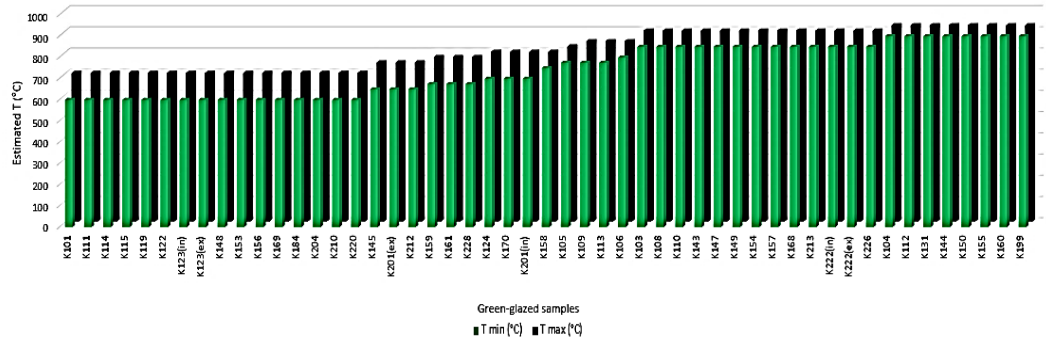

Figure 22. Estimated firing temperatures of the green glazes.

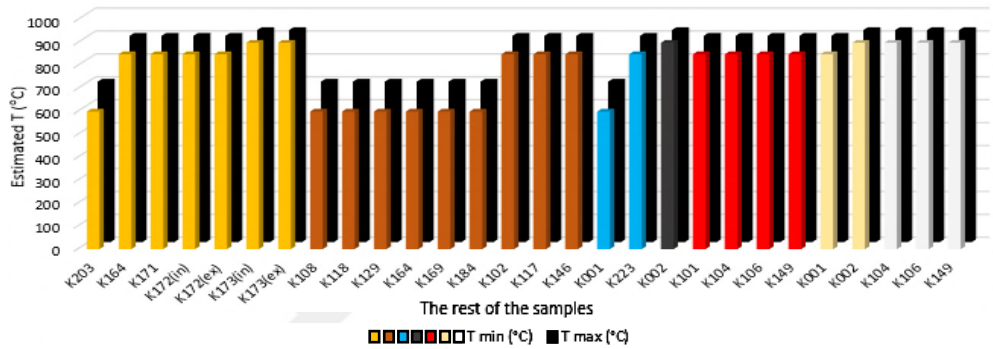

Figure 23. Estimated firing temperatures of the rest of the glazes, from left to right, orange, brown, turquoise, black glazes and red pastes, white pastes and white slips.

In Figure 21-23, each column is painted to the same glaze color, and potsherds are symbolized with circles and the tiles with the shape of diamonds. The minimum and maximum temperature values calculated by FTIR spectra are found as 600 and 915 °C respectively. The estimated average firing temperature is 786 °C for all the samples including the glazes, pastes and slips; 782 °C for all the glazed potsherds and tiles; and 777 °C for just the glazes and excluding the pastes and slips; which could be rounded to the range of 750-800 °C for all.

Then, the average values of the estimated all minimum and maximum firing temperatures are calculated for each group of samples with the same color and then compared with each other as seen in Figure 24.

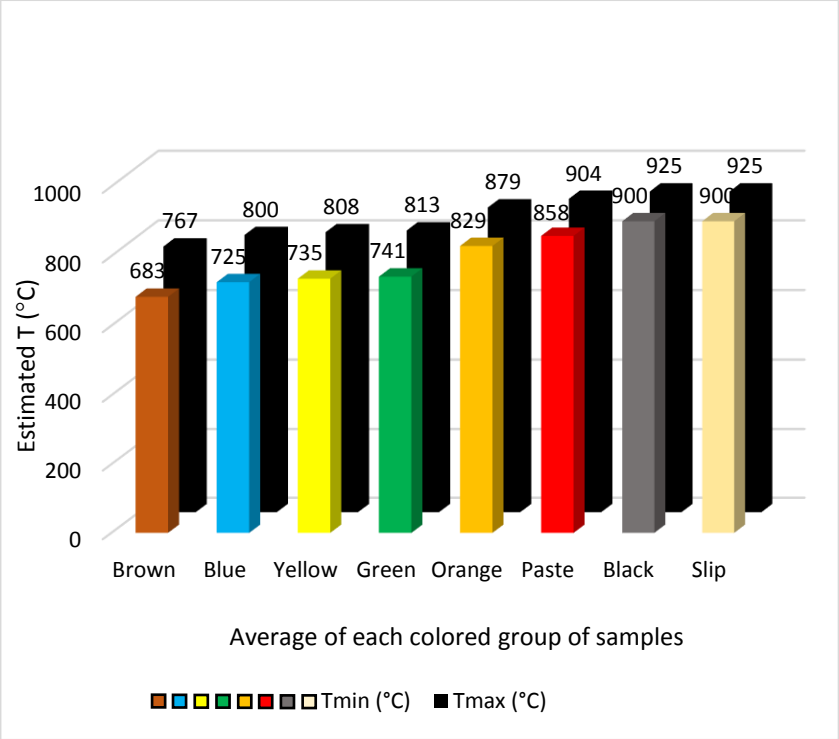

Figure 24. Comparison of the average of minimum and maximum firing temperatures of colored glazes, pastes and slips.

According to the Figure 24, brown glazes are found to be applied in the lowest estimated firing temperatures in the range around 700-750 °C, followed by turquoise glazes at 725-800 °C, yellow and green glazes at 750-800 °C, orange glazes around 850 °C, and the black glaze around 900 °C. Likewise, red pastes were discovered to be fired around 850-900 °C, while white pastes behind the tiles and the white slip layers around 900 °C.

Furthermore, the average numbers of estimated maximum and minimum firing temperatures calculated for each glaze sample could be divided into four subgroups with the ranges of 600-700, 700-800, 800-900 or 900-925 °C. Then, the number density of temperatures ranges of all the samples are shown in Figure 25.

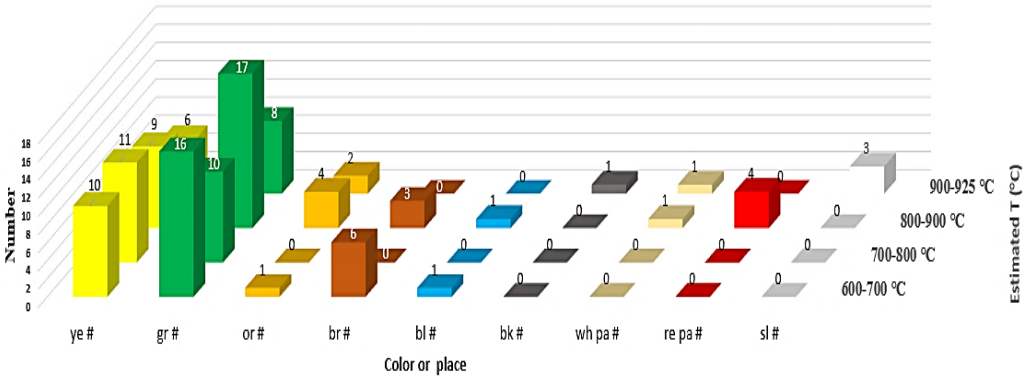

Figure 25. Number density of temperature ranges of all the samples, from left to right, **ye:** yellow, **gr:** green, **or:** orange, **br:** brown, **bl:** blue/turquoise and **bk:** black glazes, **wh pa:** white and **re pa:** red pastes, and **sl:** white slips, **#:** number density; utilized by Table 6.

As shown by Figure 25, most of the samples (51%) were from the green glazes, and followed by 31% of the samples from yellow, 8% from brown, 6% from orange, 2% from turquoise and 1% from black glazes. Likewise, 4% of the samples were from the red pastes, 3% from white slips and 2% from white pastes. Moreover, it could be investigated that majority of the samples (34%) were calculated to be fired in the temperature range of 800-900 °C, followed by 30% at 600-700 °C, 18% at 600-700 °C and 18% at 900-915 °C. Majority of the yellow glazes (31%) were found to be fired at 700-800 °C, followed by 28% at 600-700 °C, 25% at 800-900 °C and 17% at 900-925 °C; whereas majority of the green glazes (33%) were discovered to be fired at 800-900 °C, followed by 31% at 600-700 °C, 20% at 700-800 °C and 16% at 900-925 °C. It could be said that most of the orange glazes (57%) were estimated to be fired at 800-900 °C, followed by 29% at 900-925 °C and 14% at 600-700 °C; but most of the brown glazes (67%) were fired at 600-700 °C and the other 33% was in the range of 800-900 °C for the brown glazes. turquoise glaze on the tile could be explicated to be fired at 600-700 °C and the turquoise glaze on the K223 potsherd sample at 850-900 °C. The black glaze of the tile was appointed to be fired at 900-925 °C.

Moreover, according to the plot of the ratio of the peak position of Si-O stretching vibration in the range of 1010-1090 cm^{-1} divided by the peak position of Si-O bending vibration in the 459-472 cm^{-1} range versus the peak position of Si-O

stretching vibration, samples fired at higher temperatures could be grouped in higher frequencies, while the ones with lower temperature ranges lie in the lower frequencies [73]. These plots of [ν(Si–O)/δ(Si–O–Si)] versus ν(Si–O) are shown for the yellow glazes in Figure 26, green glazes in Figure 27, and the rest of the samples in Figure 28.

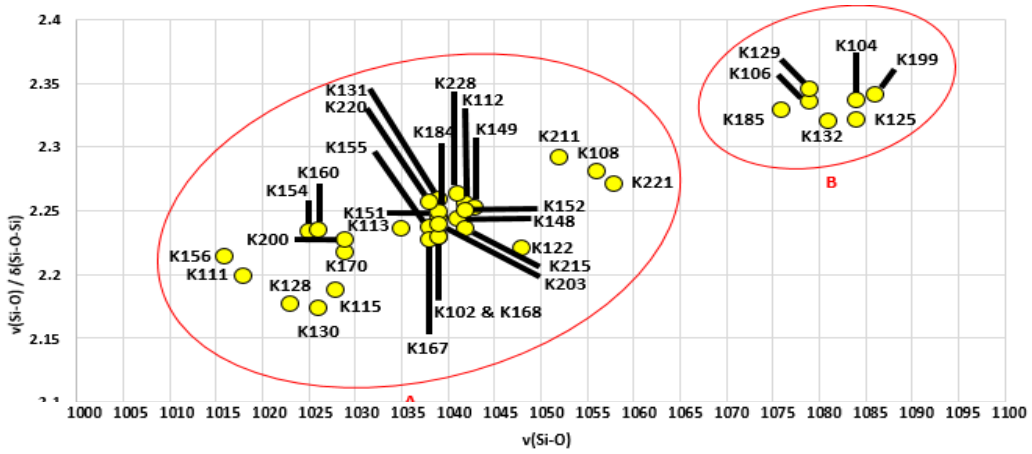

Figure 26. Plot of [ν(Si–O)/δ(Si–O–Si)] versus ν(Si–O) for the yellow glazes. Group A symbolizes the glazes fired at low temperatures, mostly observed in the Byzantine glazes, whereas B denotes the ones fired at higher temperatures, both in which are observed in the Ottoman Era glazes [73].

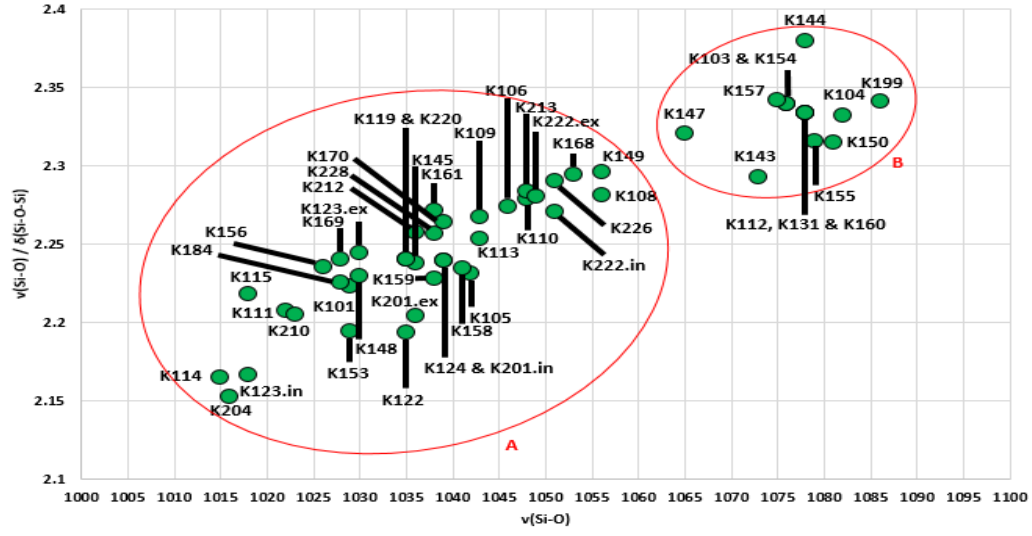

Figure 27. Plot of [ν(Si–O)/δ(Si–O–Si)] versus ν(Si–O) for the green glazes. Group A symbolizes the glazes fired at low temperatures, mostly observed in the Byzantine glazes, whereas B denotes the ones fired at higher temperatures, both in which are observed in the Ottoman Era glazes [73].

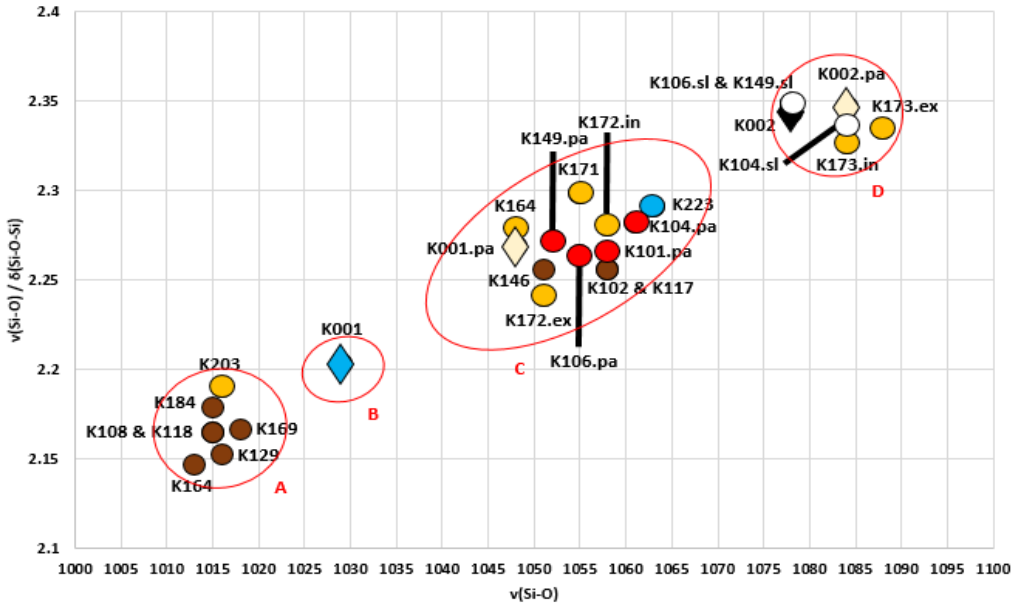

Figure 28. Plot of [ν(Si–O)/δ(Si–O–Si)] versus ν(Si–O) for the brown, orange and turquoise glazes, together with the pastes and slips. Tiles are shown in the shape of diamonds and the potsherds in circles. Whites are slip layers, cream colors and reds are pastes.

The results of the samples identified in the higher temperatures, namely the ones in the Group B in Figure 26-27 and Group D in Figure 28, are consistent with the estimated temperature ranges of samples in Table 6 and Figure 21-23. Moreover, this type of grouping also gives information about the civilizations of the ceramic samples [73]. The Byzantine pottery mostly has only the Group A, whereas the samples from the Ottoman Era have all the groups A to D in Figure 28 and A and B in the Figure 26-27 [73]. The results could support that the tiles and pottery samples of Comana Pontica were mostly similar to each other.

It could also be deduced from Figure 26-28 that there might be at least two types of pottery workshops in Comana Pontica or potters living in or visiting the city, one applying the traditions of the Byzantines and the one with those of the Danishmendids-Seljukids, the latter of which could make the grounds of the Ottomans in time.

After the estimated firing temperatures of the glazed samples are associated with the potsherd and tile samples, and the average temperatures are calculated for the two different glaze samples on a single sherd, then Table 7 was prepared. In this table,

brown-colored lines are excluded to avoid possible confusions could be resulted because of their estimated lower temperatures since they were displayed by scraping the outer glaze layer which was fired at higher temperatures. Dating century information of the ceramics was taken from Table 5 and were obtained according to the samples revealed from the same layers of each trenches by comparing the similarities of the figures and forms on their surfaces with the other samples in literature [44].

Table 7. Potsherd and tile samples with the dating periods and estimated average firing temperatures after excluding the brown glazes on the layers revealed by sgraffito; ave: average.

Sample Code	Included		Excluded T	Taken T_{ave}	Dating (century)
	T_1	T_2			
K001	600-700			650	14th
K002	900-925			913	14th
K101	600-700			650	13th
K102	700-800		850-900	750	13th
K103	850-900			875	13th
K104	900-925	900-925		913	13th
K105	775-825			800	13th
K106	800-850	900-925		869	12-13th
K108	850-900	850-900	600-700	875	13th
K109	775-850			813	13th
K110	850-900			875	12-13th
K111	600-700	600-700		650	13th
K112	775-825	900-925		856	13th
K113	600-700	775-850		731	12-13th
K114	600-700			650	13th
K115	600-700	600-700		650	12th
K117	850-900			875	13th
K118	600-700			650	12-13th
K119	600-700			650	13th
K122	850-900	600-700		763	13th
K123	600-700	600-700		650	12-13th
K124	700-800			750	12-13th

Table 7 (Cont'd)

Sample Code	Included		Excluded T	Taken T_{ave}	Dating (century)
	T_1	T_2			
K125	900-925			913	13th
K128	600-700			650	12-13th
K129	900-925		600-700	913	13th
K130	600-700			650	13th
K131	700-800	900-925		831	13th
K132	900-925			913	13th
K143	850-900			875	12-13th
K144	900-925			913	12-13th
K145	650-750			700	13th
K146	850-900			875	13th
K147	850-900			875	13th
K148	750-800	600-700		713	13th
K149	775-850	850-900		844	13th
K150	900-925			913	12-13th
K151	700-800			750	12-13th
K152	775-825			800	12-13th
K153	600-700			650	12-13th
K154	600-700	850-900		763	13th
K155	900-925	675-775		819	13th
K156	600-700	600-700		650	13th
K157	850-900			875	13th
K158	750-800			775	13th
K159	675-775			725	13th
K160	600-700	900-925		781	13th
K161	675-775			725	12-13th
K164	850-900		600-700	763	13th
K167	675-775			725	13th
K168	700-800	850-900		813	13th
K169	600-700	600-700		650	12-13th
K170	600-700	700-800		700	13th
K171	850-900			875	12-13th
K172	850-900	850-900		875	12-13th
K173	900-925	900-925		913	12-13th
K184	700-800	600-700	600-700	700	12-13th
K185	850-900			875	12-13th
K199	900-925	900-925		913	13th
K200	600-700			650	13th
K201	700-800	650-750		725	13th
K203	700-800	600-700		700	13th

Table 7 (Cont'd)

Sample Code	Included		Excluded T	Taken T_{ave}	Dating (century)
	T_1	T_2			
K204	600-700			650	12-13th
K210	600-700			650	12-13th
K211	850-900			875	13th
K212	650-750			700	13th
K213	850-900			875	13th
K215	775-825			800	13th
K220	675-775	600-700		688	13-14th
K221	850-900			875	12-13th
K222	850-900	850-900		875	12-13th
K223	850-900			875	12-13th
K226	850-900			875	12-13th
K228	750-800	675-775		750	13th

Using the data from Table 7, Figure 29 is prepared based on estimated firing temperatures of the potsherd and tile samples in the increasing order per time periods to show the relationship between firing temperatures and dating periods, colors and the positions of the glazes either on the interior or exterior side, or on both sides.

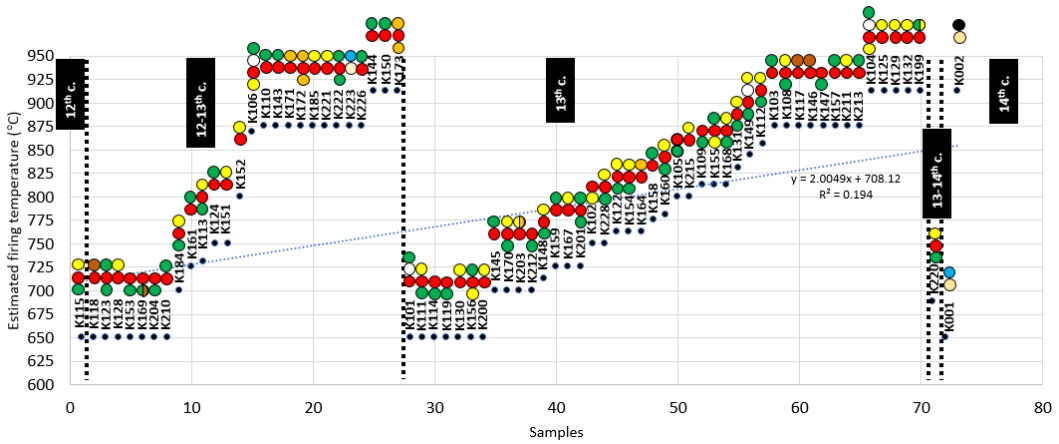

Figure 29. Glazed potsherd and tile samples ordered according to the estimated average firing temperatures, glaze and paste colors indicated in circles, together with the dating periods, written above. Data are taken from Table 6.

Black dots show the estimated firing temperatures of each glazed ceramic samples with the sample code, the colored circles and the dating periods above. In these circles, the middle one with mostly colored in red and rarely white resembles the paste under the glazed sample. If there is slip layer, between the paste and the glaze, whose sample was also analyzed by FTIR, then it is shown by one more circle painted in white. The circles above the red or white circles represent the glaze in the interior part of the ceramic, whereas the colored circles below the middle red or white circles mean the glazed samples taken from the exterior parts. If the glaze on one side is bicolored, then it is indicated by semi-circles. Each circle is colored according to the color of the glaze sample taken to the FTIR analysis. Moreover, the trend line for Figure 29 is calculated as $y=2.0049x+708.12$ (with $R^2=0.194$) whose slope is greater than 0, which proves that firing temperatures of the glazed ceramics of Comana Pontica were estimated to be increasing from the 12th till 14th centuries.

The results of the calculated firing temperatures associated with the glaze colors and time periods are consistent with the literature information that between the 9-13th centuries, pale yellow, green and polychrome glazes were preferred mostly, whereas orange and dark green colors in glaze became popular in the 13-15th centuries [89]. Polychrome was determined to be used on the potsherds dated to 12-13th and orange color was observed to be used mostly after the 13th century.

Table 8. Distribution of number density and percentage (in parenthesis) of glazed ceramics in time periods with respect to the increasing estimated firing temperatures (°C).

Temperature	12th	12-13th	13th	13-14th	14th	Total
600-699 °C	1	7 (27%)	7	1	1	17
700-799 °C	0	5 (19%)	15	0	0	20
800-899 °C	0	11 (42%)	16	0	0	27
900-925 °C	0	3 (12%)	5	0	1	9
Total #	1	26	43	1	2	73
Total %	1.4%	35.6%	58.9%	1.4%	2.7%	100%

Number density and percentage of the glazed tiles and potsherds are given in Table 8 in the order of increasing estimated firing temperatures. According to the same table and Figure 29, it could be detected that there is only one sample from 12th

century and potsherd of this sample consists of the yellow interior and green exterior with brown lines, and firing temperature estimated as around 650 °C from FTIR analysis. In the 12-13th centuries, majority of the pottery fired at around 650 °C (71%) were identified being in the form of green interior and green exterior, whereas 14% with just yellow interior and 14% with yellow glaze both on the interior and exterior parts. In the samples of glazed pottery fired at 700-799 °C, 33% of them were with yellow interior and green exterior, another 33% were with just a yellow glaze on the interior and the final 33% were with just green on the interior. For those fired at 800-899 °C, majority of them (30%) were with green interior and yellow exterior, 20% with green interior and green exterior, and the rest consist of just orange on the interior, orange glazes both on the interior and exterior, just yellow on the interior, yellow glazes both on the interior and exterior, and turquoise glaze on the interior, 10% for each. Last part of the 12-13th century were the ones fired at 900-925 °C, with 67% just green interior and 33% orange glazes both on the interior and exterior sides. For the 13th century potsherds fired at 650 °C, 57% were the ones with yellow interior and green exterior, the rest were with green interior and brown exterior, green interior and green exterior, and green interior and yellow exterior, all with 14%. For the range between 700-800 °C in the 13th-century potsherds, 53% were with yellow interior and green exterior, 13% with green interior and yellow exterior, and the rest were with yellow-yellow, green-green, green-orange, just green in the interior and orange green on the interior, all with 7%. In the 800-899 °C, yellow interior and green exterior ones were consisting the majority.

Furthermore, from Table 8, it could be deduced that most of the glazed ceramics (59%) were detected to be produced in the 13th century, followed by 36% in the 12-13th centuries, 3% in the 14th, 1% in the 12th and 1% in the 13-14th centuries. It could be stated that majority of the glazed ceramics belonging to the 12-13th and 13th centuries were estimated to be fired at 800-899 °C and minority of the glazed ceramics (12%) were fired to be at 900-925 °C. The second major temperature ranges were 600-699 °C for the ones in the 12-13th centuries and 700-799 °C in the 13th century.

When not the individual glazes but the combinations of multi-colored glazes on single potsherds are considered and the average firing temperatures are calculated for the potsherd and tile samples, it is found that majority (37%) of the glazed ceramics were estimated to be fired at 800-899 °C, followed by 27.4% at 700-799, 23.3% at 600-699 °C and 12.3% at 900-925 °C.

Even though the firing temperature estimation could be gathered from FTIR spectra, it could not be used for identifying the coloring pigments. So, Raman spectroscopy, that is based on not absorbance but scattering, could be an alternative method to be applied, since it is non-destructive, easy to use and measurements could also be done on-site and with no sample preparation needed, as well as easy to calculate the firing temperature of the samples with respect to the polymerization indices. In case of my experiments, Raman spectroscopy was applied initially, but since there was no signal acquired except from one glazed potsherd, the XRF and XRD analyses had to be applied.

It could be stated that 4% of all the glazed samples consisted of the colors of green, yellow and orange at the same time placed side by side, quarter of which had multi-colors on both sides, and most of the glazed ceramic samples (68%) were glazed on both sides with only one kind of color on each side. Almost quarter (26%) of all the samples were found to be glazed just on a single side, most of which (95%) were on the interior side. It could be deduced that, almost half of the single-colored glazes on one side of the ceramic samples (47%) are colored in green, almost quarter (26%) of them in yellow, 11% in turquoise, 5% in black, 5% in brown and 5% in orange. Most of the glazed pottery samples (around three quarters) were preferred to be glazed on both sides.

4.2. Results and Discussion of XRF Spectrometry

The results of oxide contents obtained by XRF spectrometry could be seen in

Table 9 XRF spectrometry data in found out that there is no tin in the potsherd samples but just in the tiles, which could make some of the characterization charts[33] not to be used. Furthermore, XRF analysis could not detect the oxides of elements

up to boron and those besides the uranium, which causes the accuracy of the elemental analysis could not be so high.

However, XRF oxide analysis is still one of the best ways to characterize both the time period and the civilization with unique cultures since some rare metal oxides in the glaze structure and ratios of distinct metal oxides could give a fixed place on the charts [33]. For example, as could be seen in Figure 30, Şimşek and Colomban showed the tin/lead ratios of tiles corresponding to specific locations that indicate both the time period and civilization.

XRF spectra for the selected potsherd and tile samples with different colors of glaze are given in Appendix A.3.

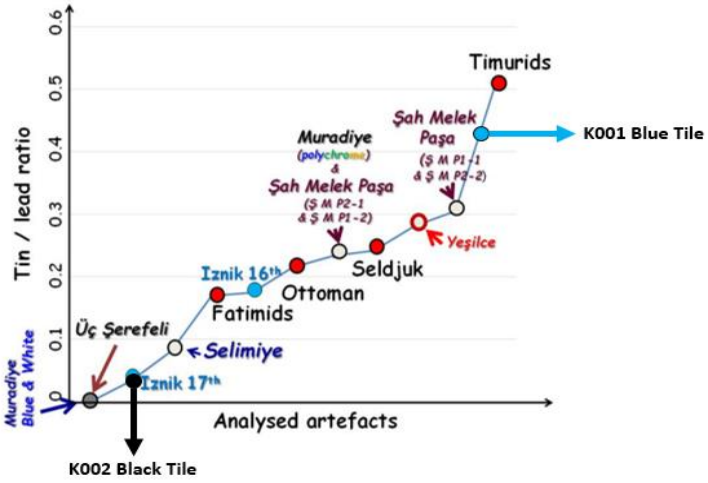

Figure 30. Characterization of the tile samples with respect to tin/lead ratios, using the data of XRF spectrometry. Adapted from [33].

Table 9. Oxide contents of the glazes and tiles obtained by XRF spectrometry. CO_2 data are excluded; ND: Not detected.

Na_2O	0.503	9.57	0.137	0.227	0.189	0.333	1.7
TiO_2	0.222	0.185	0.231	0.234	0.188	0.524	0.117
CuO	1.63	0.106	0.162	0.341	1.12	0.052	3.1

Rb_2O	ND	0.004	ND	ND	ND	ND	ND
SnO_2	6.71	0.084	ND	ND	ND	ND	ND
V_2O_5	ND	0.025	ND	ND	ND	ND	ND

Sample	PbO	SiO_2	Br	Al_2O_3	K_2O	CaO	Fe_2O_3	MgO	Sb_2O_3
K001 turquoise tile	15.3	43.9	ND	6.92	1.01	5.04	2.16	0.593	ND
K002 black tile	1.67	54.2	ND	4.13	1.23	4.68	2.5	1.67	ND
K108 brown glaze	32.2	7.08	0.02	0.87	0.692	9.78	1.34	0.607	0.167
K149 yellow glaze	49.7	28.9	ND	2.76	0.688	0.687	0.458	0.367	0.361
K161 green glaze	21.6	27.2	0.009	3.32	1.24	3.63	0.815	0.833	0.198
K172 orange glaze	23.3	34.2	ND	5.39	1.06	2.77	4.17	0.847	ND
K223 turquoise glaze	4.24	53	ND	4.56	2.2	3.85	1.08	0.764	ND

Sample	Cl	SO_3	P_2O_5	As_2O_3	MnO	CdO	NiO	SrO	ZnO
K001 turquoise tile	0.129	0.23	0.668	ND	0.077	ND	0.011	ND	ND
K002 black tile	0.116	0.19	0.414	ND	3.93	ND	0.028	0.06	0.014
K108 brown glaze	0.847	0.3	11.9	ND	ND	ND	ND	ND	ND
K149 yellow glaze	ND	ND	0.095	ND	ND	ND	ND	ND	ND
K161 green glaze	0.5	0.2	5.37	0.063	0.028	ND	ND	ND	ND
K172 orange glaze	0.067	ND	0.285	ND	0.139	0.129	0.015	ND	ND
K223 turquoise glaze	0.861	2.55	0.494	ND	0.139	ND	ND	0.026	0.023

Even though the potsherd samples did not contain tin, they are included in Figure 31 with zero contribution. Moreover, by using the Pb/Si vs. Sn/Si ratios, a new characterization chart could be drawn as could be seen in Figure 31.

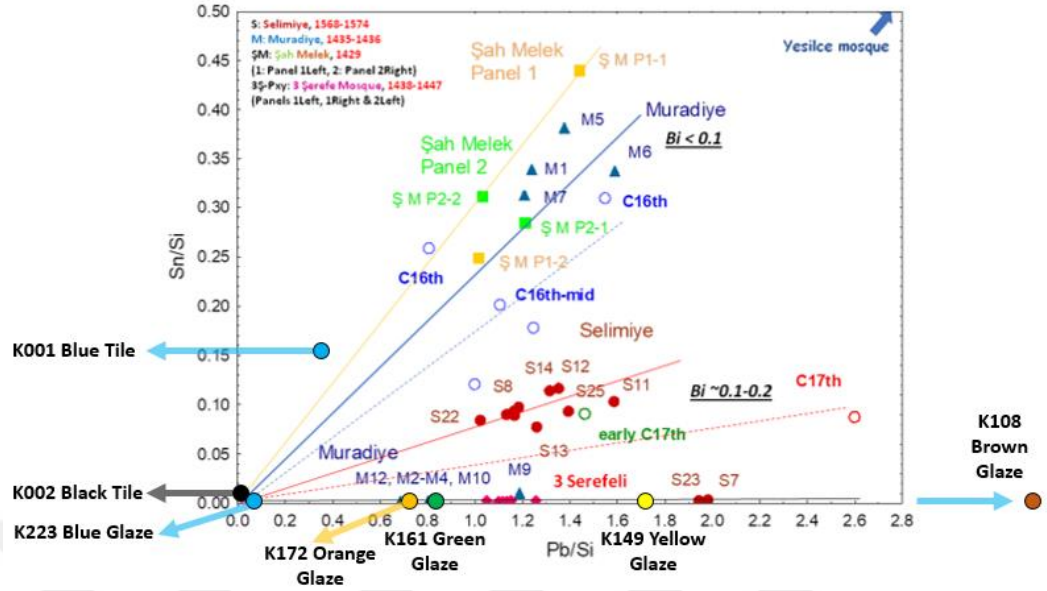

Figure 31. Characterization of the tile and potsherd samples with respect to Pb/Si vs. Sn/Si ratios, using the data from XRF, adapted from [33].

Besides, XRF is a powerful tool, since it gives information both qualitatively and quantitatively and the oxide content investigation could yield to the characterization processes. From Figure 31 K002 black tile was found to be extremely similar to the Iznik (Nicaea) tiles of the Ottoman Empire from the 17th century and K001 turquoise tile fell between Şah Melek Paşa Mosque (1429) from Edirne (formerly Adrianople) and the Timurids (2nd half of the 14th century – first quarter of the 16th century) where Iran might be the possible origin [90].

From the Figure 31, it could be stated that tiles of Muradiye Mosque (1435-1436) in Edirne were similar to the orange glaze of K172 and green glaze of K161. The K149 sample with the yellow glaze was determined to be close to the tiles of Üç Şerefeli Mosque (1410-1447) in Edirne and two tile samples (S23 and S7) of Selimiye Mosque (1569-1575) in Edirne [33].

Another bivariate diagram, wt.% (MgO+CaO) vs. wt.% Al_2O_3, as stated Walton (p. 101) [24], could be drawn for Comana Pontica samples as shown in Figure 32.

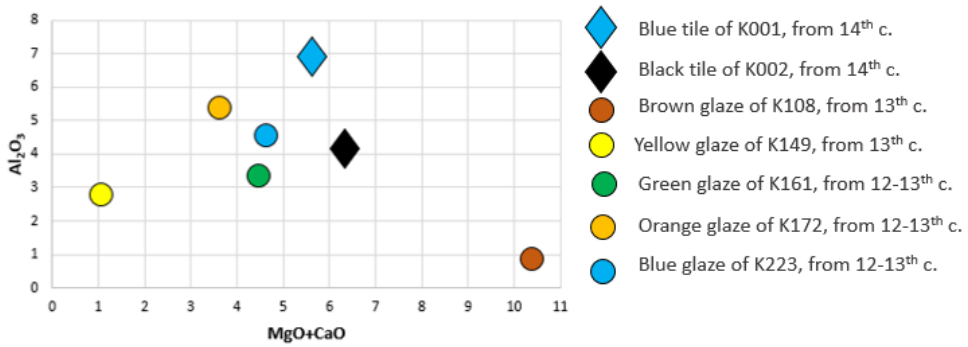

Figure 32. Bivariate diagram of wt.% (MgO+CaO) vs. wt.% Al_2O_3, comparing the Comana Pontica glazed samples with each other, data are taken from XRF spectrometry.

The literature data of the results of XRF spectrometry of the glazed potsherds of Diana and Singidunum (Serbia); Gaul, Lezoux and Vichy (France); London (England); Apulum Partos (Romania); Roman Forum, Ostia and Carlino (Italy); Byzantine and Chinese sancai [21]; Littlemore, Colchester, Silchester and Gloucester (England); Pozzuoli and Campania (Italy); Alexandria (Egypt); Paphos and Kition (Cyprus); Dura Eiropos (Syria); Xanthos, Smyrna, Clazomenae, Tarsus, Ain Tab (Anatolia) [91]; Jordan [92]; Sasanian and Parthian [93]; Iznik tiles [51]; Roman Italy, Islamic Iraq, Islamic Egypt, Islamic Iran, Islamic Spain, Hispano-Moresque, Anglo-Saxon, Byzantine, Medieval England, St. Porchaire, Palissy, English, Islamic Iznik and Maiolica [21]; Fustat (Egypt) and Maarrat al Numan (Syria) [94], Ain Sinu (Iraq) [95] are used to prepare the characterization chart as shown in Figure 33. Data points for this chart is given in Appendix A.4.

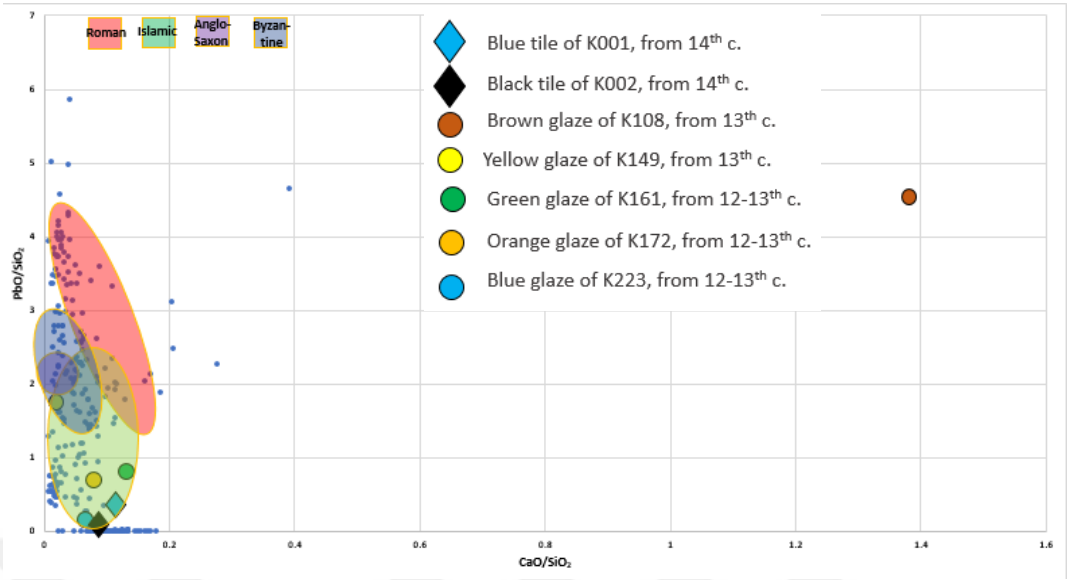

Figure 33. The PbO/SiO_2 vs CaO/SiO_2 characterization biplot of the literature data of oxide contents of some glazes from various studies [20, 83-88]. Tiles are represented with diamond symbol and glazes with circles, each colored with the same as its own color. Area of Roman, Islamic, English and Byzantine glazes are shown in the ellipses of red, green, purple and blue, respectively.

Points in more details are shown in Figure 34-39.

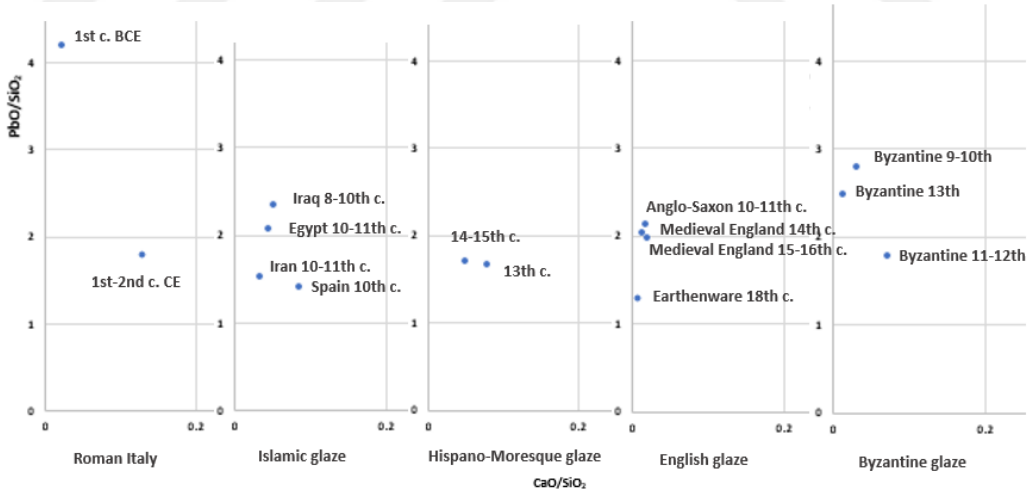

Figure 34. Details of characterization points.

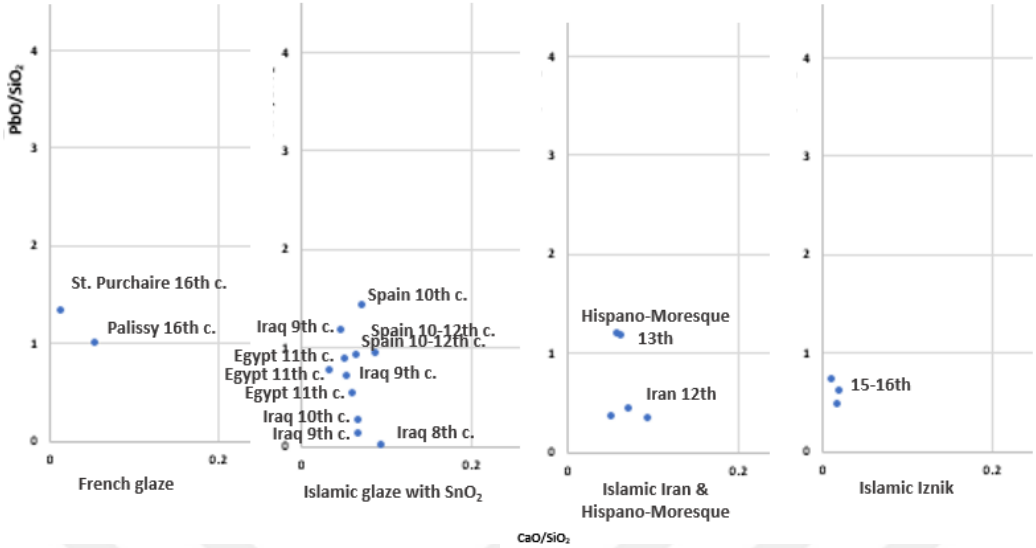

Figure 35. Details of characterization points.

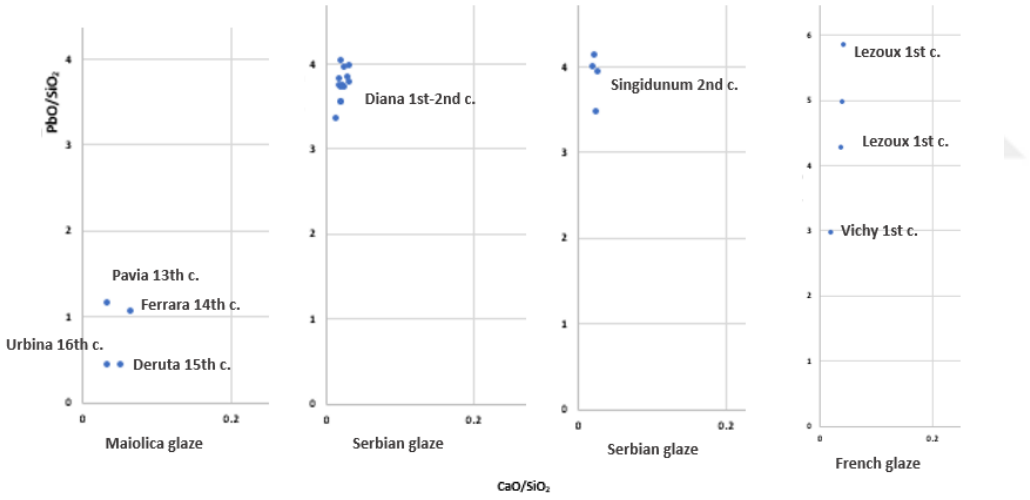

Figure 36. Details of characterization points.

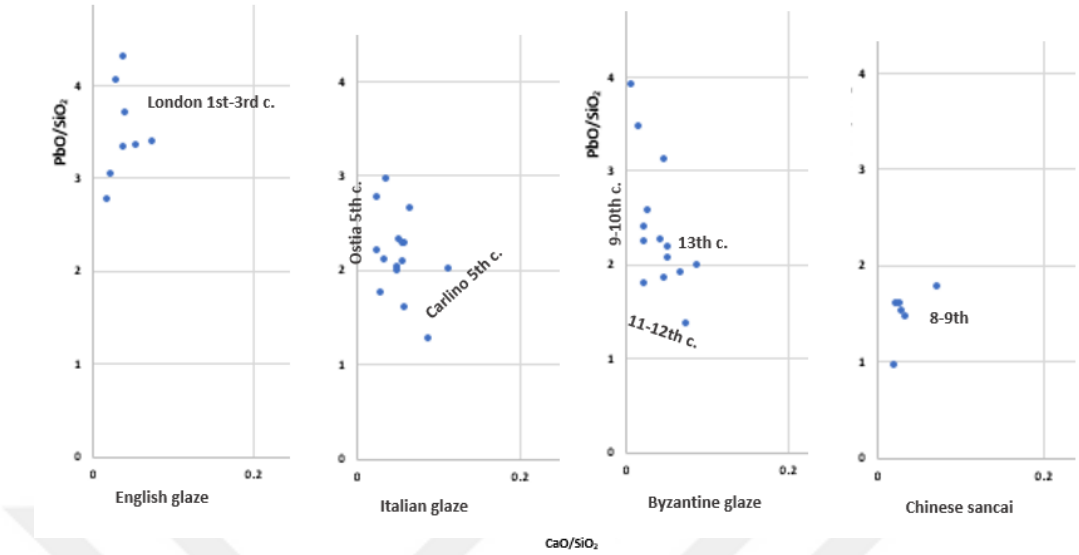

Figure 37. Details of characterization points.

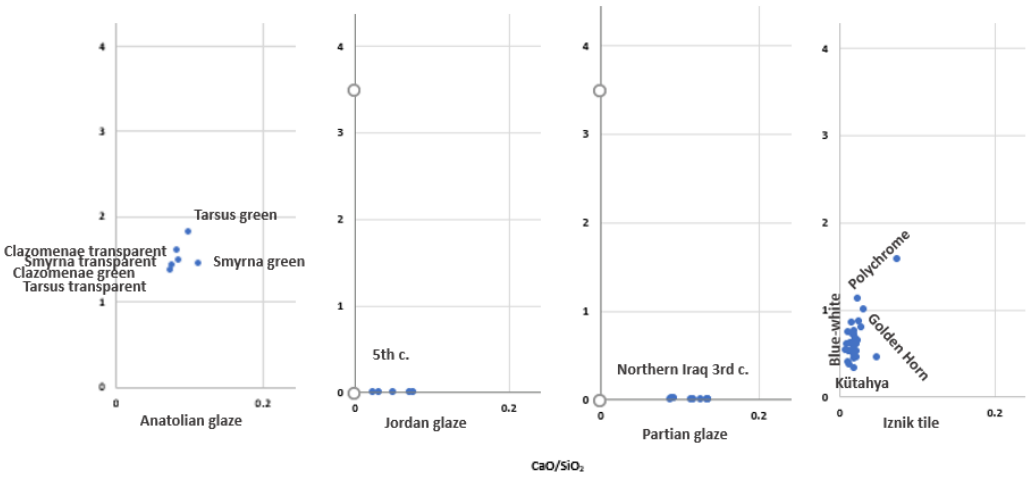

Figure 38. Details of characterization points.

From the characterization biplot of PbO/SiO_2 vs. CaO/SiO_2 in Figure 33 and the detailed characterization points from Figure 35, both tiles were closest to the 12th century Islamic Iran (with the coordination of 0.068, 0.128) and the turquoise-glazed K223 was closest to the 11-12th century Islamic Syria (with the coordination of 0.0692, 0.261).

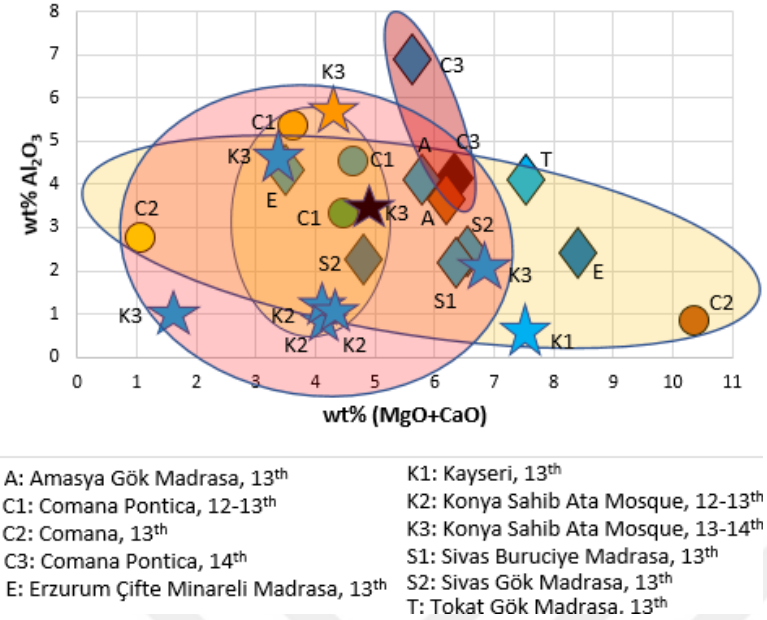

Figure 39. Characterization biplot for the glazes from Seljukid Era. Stars symbolize the previously analyzed Seljukid glazes taken from [96], tiles are shown with diamonds and potsherd glazes with circles. Each shape is colored with the same color of its glaze. Ellipses colored in yellow mean the samples were from 12-13th centuries, orange for the 13th, red for 13-14th and the purple for the 14th century.

As seen in the Figure 39, determining oxide contents of the potsherd samples are compatible with the other glazed samples from Seljukid times that have been analyzed previously [96]. Turquoise tile seems to be an outlier and could be excluded, which supports the information of its being exported most probably.

From Figure 39, it can be said that Comana Pontica potsherds have a characteristics of high amount of silica (36%) and lead (around more than 20%) with a low (around 0.8+4.3%) MgO+CaO content and about 4% Al_2O_3, as well as 1.8% Fe_2O_3, 1% CuO, 2% Na, 3% P_2O_5 determined by XRF spectrometry in this study, together with 3.4% SnO_2 for the tiles, which values are also similar to the averages at 20% PbO, 8% Na_2O, 0.6% MgO, 4% CaO, 2.3% Al_2O_3, 1.7% K_2O, 1.4% Fe_2O_3, and 2.4% SnO_2.

Moreover, in order to determine what type of flux was added during the firing of the glaze, a biplot of K_2O% in content vs. MgO% could be drawn as seen in the Figure 40 and that of P_2O_5% vs. MgO% contents in the Figure 41 according to the locations of the data points, it could be discovered whether plant ashes or mineral natron were added as a flux [96].

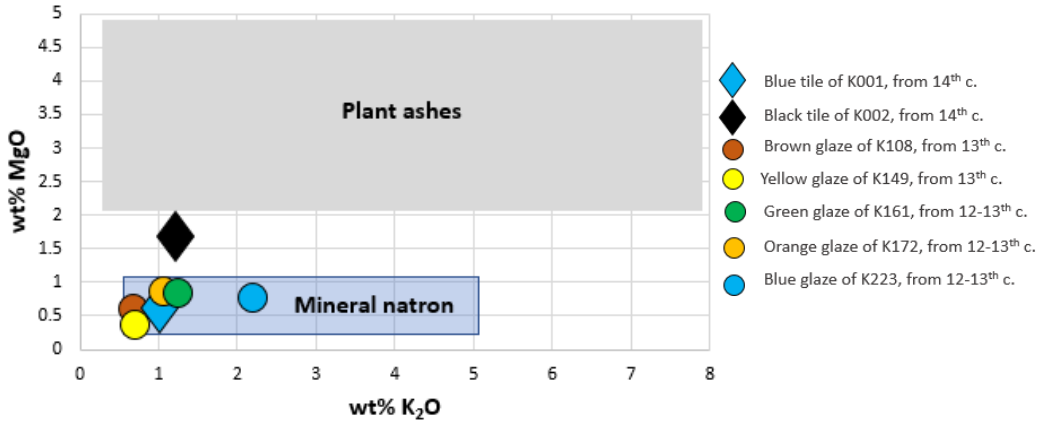

Figure 40. Discrimination method on biplot of wt.% K_2O vs. wt.% MgO contents to determine whether mineral natron or plant ashes added as a flux on the glaze, adapted from [96]. Tiles are shown with diamonds and potsherd glazes with circles. Each shape is colored with the same color of its glaze.

From the Figure 40, it could be understood that mineral natron was added as a flux during the firing of the glazes, since most of the samples stay in the area restricted by blue rectangle, which is consistent with the information that it was the traditional method at that period in Anatolia [96].

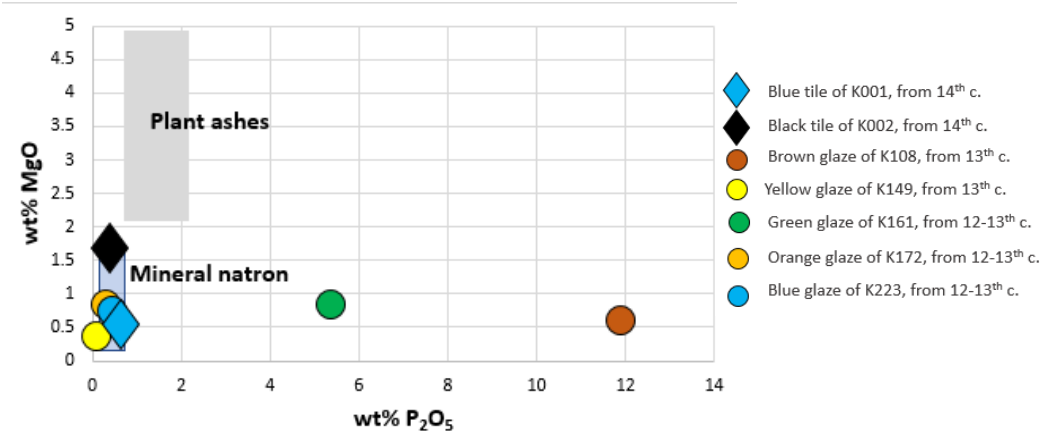

Figure 41. Discrimination method on biplot of wt.% P_2O_5 vs. wt.% MgO contents to support the determination whether mineral natron or plant ashes added as a flux on the glaze, adapted from [96]. tiles are shown with diamonds and potsherd glazes with circles. Each shape is colored with the same color of its glaze.

On the other hand, the usage of biplots could be improved in a way that its number of components can be increased to get more information about dating and

civilizations of samples collected from Comana excavation. It is the plot whose location of a point in the coordinate system is determined by reference to the three parameters on a triangular plane where the summation is a fixed number, which is represented as 100%. Three major groups namely lead, silica and some metal oxides, cause a differentiation in the glazes. After being placed on the corners, each oxide is represented by the ratio bar on their left. The distance between the samples on ternary plots gives information about how close the data points are to each other. If the gap between the sample points in the triangle is increased, it could be deduced that the samples are originally different to each other [21]. The ternary plots for the glazed potsherds and tiles compared with each other and with literature data, without tin oxide contribution for the potsherds and with tin oxide addition for the tiles are shown in Figure 42-45.

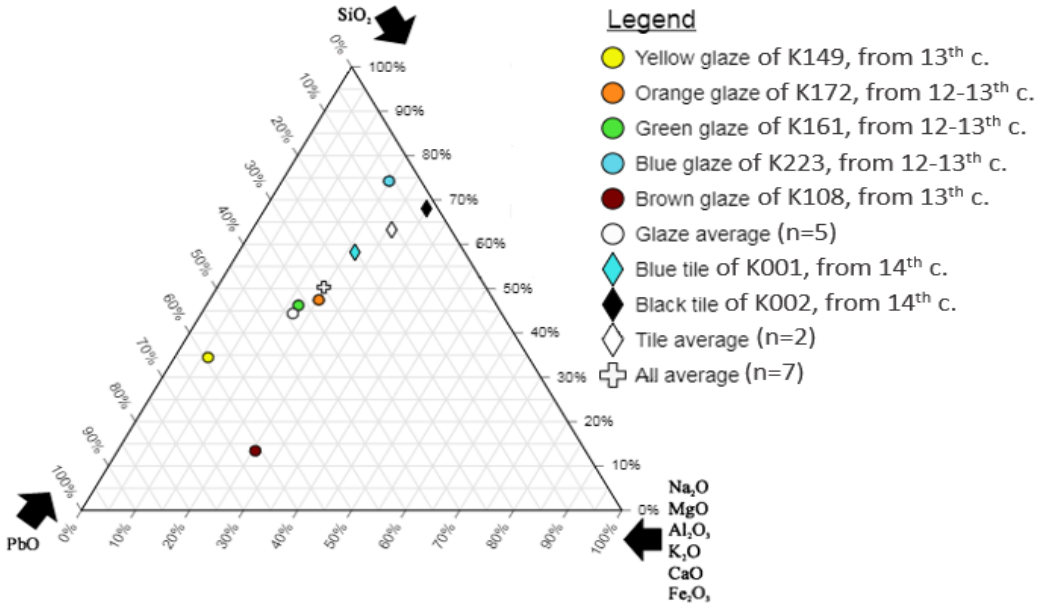

Figure 42. Ternary diagram of Comana Pontica glazes and tiles.

From the ternary diagram of Figure 42, it could be stated that K161 potsherd sample with green glaze and K172 sample with orange glaze are close to each other, while K149 sample with yellow glaze and K108 sample with brown glaze are situated towards the higher percentage of lead content. Tiles are away from the glazed potsherd samples with their relatively lower lead contents. K223 potsherd sample with the turquoise glaze is found to be different from the rest of the potsherds as well.

This result is consistent with the explanation of Er [47], in which K223 was proposed to be imported probably from Egypt.

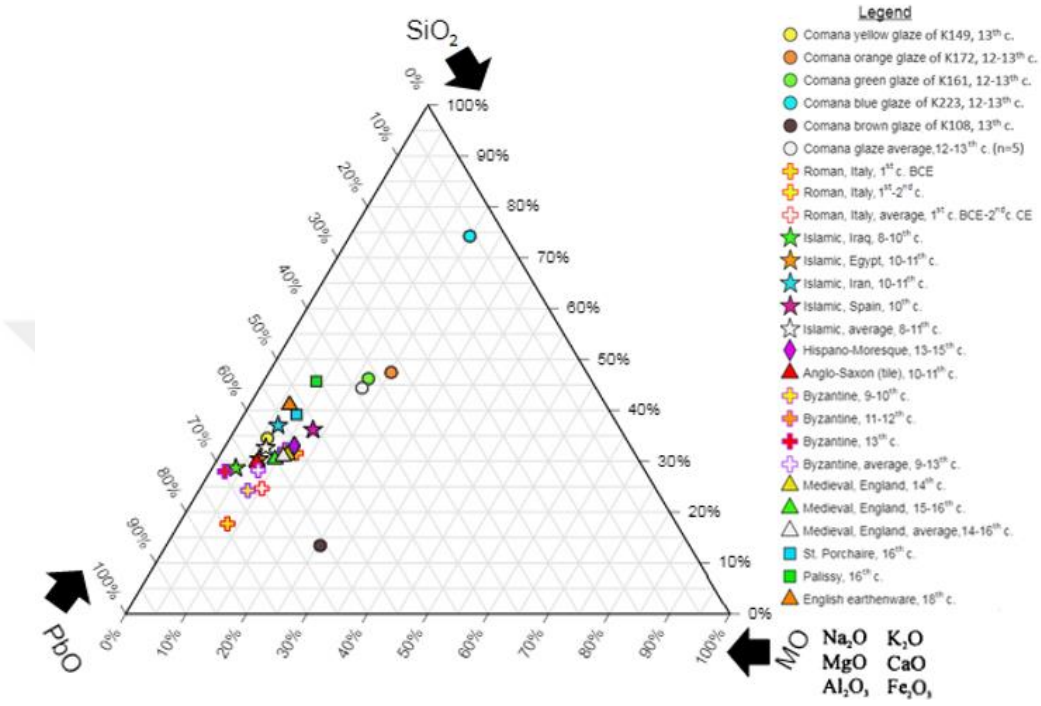

Figure 43. Ternary diagram for the glazed pottery samples excluding SnO_2; M: metal, c: century.

From the Figure 43, it could be said that green, orange and brown glazes of K161, K172 and K108 respectively are distinct from the glazes of other civilizations, turquoise glaze was mentioned to possibly be from different origin, and the yellow glaze of K149 from the 13th century is found to be close to Islamic glazes of Iran from the 10-11th centuries that is represented with the blue star in the figure. As could be identified by the closeness of the points on the same ternary diagram, K149 yellow-glazed potsherd is close to the blue star, which symbolizes the Islamic Iran glazes from 10-11th centuries.

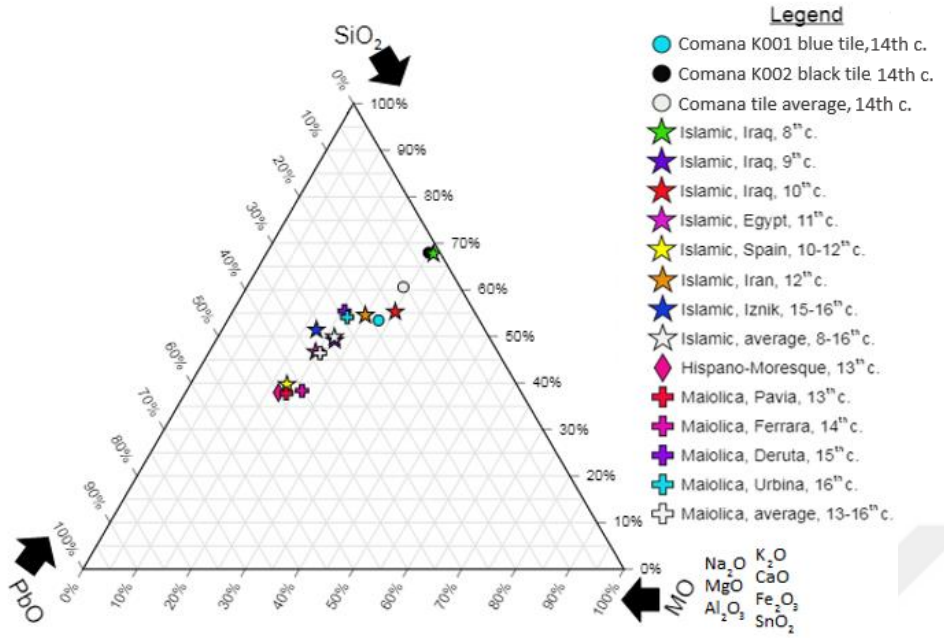

Figure 44. Ternary diagram for the glazed tiles after addition of SnO_2.

From the Figure 44, blue/turquoise tile could be seen close to the 12th-century Iranian and 10th-century Iraqi glazes. Black tile is found to be similar to Islamic glazes in Iraq from 8th century. Moreover, it could be stated that K002 black tile as seen in **Figure 44** and K223 turquoise-glazed pottery as seen in **Figure 43** might be imported to Comana Pontica or produced with different techniques in different time periods since both of them lie very far away from the rest of the glazed samples. One of the possible reasons for that could be the inclusion of tin oxide. On the other hand, as shown in FTIR spectra in Figure 18, clay minerals of K223 were almost same with the other potsherds, which may support the idea that those pottery samples were made in Comana Pontica with different ingredients and techniques, instead of being imported from anywhere else.

Since in literature, the glazes are called as types of "high-lead", "lead-alkali", "low lead-alkali" or "alkaline"; if their PbO contents exceed 45%, stays between 20-40% (together with its alkali content 5-12%), 2-10% or less than 2%, respectively [21]. Likewise, the paste could be either calcareous or non--calcareous depending on its calcite content being greater or lower than 10% respectively [1]. From the data of XRF analysis, it is observed that Comana Pontica glazes are mostly high-lead and

lead type, with the PbO content changes in the range 20-50% for most of the potsherd samples. Moreover, as revealed by FTIR analysis, some samples are calcareous. Also calcareous samples give information that the firing temperature is below 850 °C [22]. Moreover, it is known that addition of sodium, potassium and especially lead is known to lower the melting point of the glaze [16]. By XRF analysis, PbO was detected mostly within 20-50%, and Na_2O content was around 9.6% for the K002 black tile, which could lead to the consideration of Pb and Na could probably be preferred on purpose to cause the melt of the glaze started in the lower temperatures towards 600-700 °C. Estimated firing temperatures calculated with respect to the results of FTIR analysis could also support this proposal since for most of the samples the firing temperatures were not exceeding 900 °C.

The types of the glazed samples could also be determined according to their XRF spectrometry data. As shown in

Table 9, K149 potsherd sample can be classified as high-lead with 49.7% PbO; whereas K108, K161 and K172 glazes are called as lead glazes with 32.2, 21.6 and 23.3% respectively. Furthermore, it could be recognized that the alkali contents of K108, K161 and K149 potsherds were below 2%, which makes them not categorized as lead-alkali, but instead just as lead glazes. To go on, if the PbO content of the turquoise tile, K001, is checked, it can also be counted from the side of the lead glazes, again with low alkali content. The other turquoise glazed sample, K223, could be considered as low lead-alkali, and leaving the last glazed sample, the black tile of K002, behind the alkaline type.

Furthermore, if the CaO content is considered, just K108 sample is called calcareous, the rest of the samples are non-calcareous since their CaO content is less than 10%. Hence for the turquoise color to be observed, mostly the white paste is preferred, which is also the same for the turquoise-glazed samples of K001 and K223. Main reason for their pastes to seem as white is as the result of the higher calcite contents.

In case either the paste or the glaze is rich in carbonate and fired between 600-850 °C, calcite decomposes in the clay matrix [22]. So, if any calcite is investigated in the

sample, such as by FTIR spectroscopy, it could be deduced that the firing temperature was not greater than 850 °C. This situation can be supported by not only the observation of the calcite peaks in FTIR spectra around 1430-1450 cm^{-1} and 1775-1820 cm^{-1}, together with H-O-H bending of CaO at 1650-1800 cm^{-1}, but also from the estimated firing temperatures of the wavenumbers of asymmetric Si-O stretching in FTIR spectra. It is known that involvement of calcite to the glaze will lower the firing temperature to the range of 600-850 °C [22]. When the calculated firing temperatures are compared with the calcite contents of the samples, CaO and CO_2 would be considered as forming calcite and a converse relationship between the calcite content and firing temperatures is observed as shown in Figure 45.

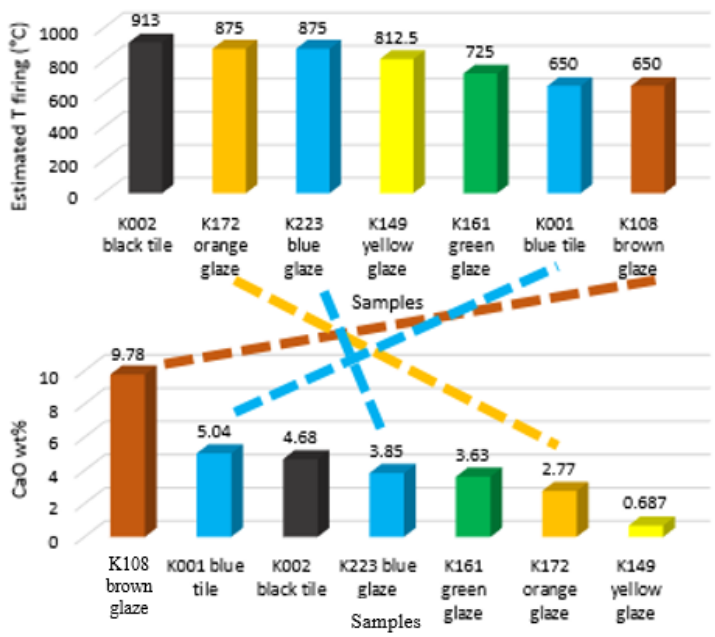

Figure 45. Comparison of the relationship between the estimated firing temperatures and calcite contents of the samples.

The two samples with the lowest firing temperatures (in the range of 600-700 °C), K108 and K001, have the highest CaO contents. Likewise, 600-700 °C range is below the literature value of 850 C [22]. Furthermore, it could be checked from the Appendix A.2 that the spectra with calcite peaks (1430-1450 cm^{-1}) are generally the ones whose firing temperatures are calculated as low, such as those of the yellow glazes of K167, K170, green glazes of K114, K184, K220, K228 and the turquoise tile K001, whose spectra could be found in the Appendix A.2. Indeed, the paste of the turquoise tile is known to have calcite since its color is white. However, even though K002 black tile is also calcareous known not only from its white paste but also from its FTIR spectrum with the calcite peak in the same appendix, its firing temperature is

calculated as 900-925 °C, which could sometimes make predictions harder just by checking the FTIR spectra. There are also other examples, like as seen in the spectra of the green glaze of K155, yellow glazes of K132, K134, K185, K221, in which the firing temperatures might be high enough instead of still observing the calcite peak. Vice versa, there are also spectra, as seen in the yellow glazes of K111, K113, K131, without an apparent calcite peak around 1430-1450 cm^{-1} but with estimations of low firing temperatures, which may be as the result of the other factors like high amounts of PbO put in the glaze to lower the firing temperature.

For the determination of glaze colorants, it is known that 1.0-3.2% Fe_2O_3 + 0.1-1.3% MnO gives the black color [94]. 2.5% FeO and 3.93% MnO were determined by XRF spectrometry for the black-glazed tile K002 and Fe and Mn oxides could be the main contributors for the occurring of black color, together with the matting ability of MgO that is 1.67%. Moreover, black color could be observed on the alkali-lime type of glazes better[94], which could explain the existence of 9.57% Na_2O in the black tile. CO_2 in the glaze might be produced as the reason of the reductive atmosphere, which is consistent with the information that brown color occurs by Fe_2O_3 turning to FeO in the reductive environment, and CO_2 percentage was the highest with 33.7% in the brown glaze of K108. Fe_2O_3 in the oxidizing atmosphere results in the existence of yellow color. If Fe_2O_3% content is low, such as 0.458% in the yellow glaze of K149, its color is observed light. However, if its amount is increased, as could be seen with 0.815% in K161 green glaze, then its color becomes green and around 4% its color becomes orange, which is consistent with the 4.17% content in the orange glaze of K172. CuO is responsible for the green and blue/turquoise colors if its content is greater than 0.5% and between 1.5-3.4% respectively. If CuO content is below 0.5%, then the green color is occurred by Fe_2O_3 [94]. This information is also satisfied since the highest CuO was maintained in the turquoise glazed samples of K223 (3.1%) and K001 (1.63%), following the green glazed K161 with 1.12% CuO. Sb_2O_3 is an uncommon ceramic oxide, which is responsible with the occurrence of yellow color under low Fe_2O_3 content and if combined with titanium or lead. It is consistent with the highest Sb_2O_3 content seen in the yellow glaze of K149 with 0.361% and with 0.234% TiO_2 and 49.7% PbO.

Copper can give the blue color with azurite, $2CuCO_3.Cu(OH)_2$, and green color with malachite, $CuCO_3.Cu(OH)_2$, whose hydroxyl groups could be the main reason of the occurrence of the band at 3000-3700 cm^{-1} [97]. Also, the usage of the paste of calcite for the turquoise glazes could be to observe these colorants. In an oxidative atmosphere, CuO gives green color, if some of CuO is reduced to Cu_2O which gives red color in the reductive environment, then the mixture of the colors is observed as purple, which was observed on the interior side of K117. TiO_2 is observed with the highest amounts in the orange glaze K172 (as %0.524) and the yellow glaze of K149 (as 0.234%) which may contribute to the intensifying and stabilizing the colors in yellow to orange, furthermore into brown if combined with FeO, as could be seen in the brown glaze of K108 with 0.231% TiO_2 and 1.34% Fe_2O_3. As_2O_3 contributes to the occurrence of the light green color [98], which is also parallel with the XRF spectrometry results that only the green glaze of K161 had As_2O_3 with 0.0634%. CdO together with sulfur makes the glaze yellowish [98], likewise only in the content of the orange glaze CdO was observed with 0.129%. SnO_2 was probably used for the opacification [98].

Finally, the estimated firing temperatures from the FTIR spectra could be checked by using a new biplot of PbO vs. (Na_2O+K_2O) acquired by the data of XRF spectrometry. On the diagram of Figure 46, the firing temperatures could be calculated with the help of a coordination system of theoretical isothermal curves [96], and a similar biplot is created on it with the samples analyzed by XRF spectrometry.

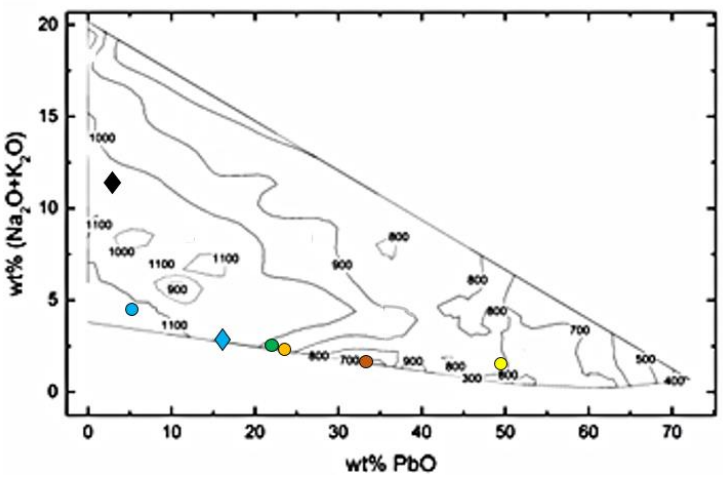

Figure 46. Biplot of wt.% PbO vs. wt.% (Na_2O+K_2O), with estimated thermal isothermal curves of firing temperatures and coordination of samples whose data were acquired by XRF spectrometry.

As seen in Table 6 based on wavenumber values of the Si-O stretching vibration mode, the firing temperatures of the samples of K001 turquoise tile, K002 black tile, K108 brown glaze, K149 yellow glaze, K161 green glaze, K172 orange glaze and K223 turquoise glaze were estimated to be around 600-699, 900-924, 600-699, 775-849, 675-774, 850-899 and 850-899 °C, respectively. Mostly the similar ranges could be found from the positions of points of samples on the isothermal curves in Figure 46, such as around 950, 1050, 650, 800, 1000, 950 and 1000 °C, respectively in the same order, with an exception of the turquoise tile that has a significant difference between values. Thermal isothermal curves are found generally 50-100 °C higher than the firing temperatures estimated by FTIR spectra.

4.3. Results and Discussion of XRD Spectroscopy

Another contribution to the firing temperature estimation of the glazes could be achieved by XRD spectroscopy, since illite, gehlenite and hematite could specifically exist around 850 °C after the vitrification [99]. Thesis completed by Dr. Er [47] on the pastes of the same potsherd samples of Comana Pontica, the possible firing temperature was detected to be around 800-900 °C due to the existence of pyroxene whether in the form of diopside or wollastonite in the paste. Likewise, XRD spectra of the K001 turquoise and K002 black tiles are shown in the Figure 47 and Figure 48 respectively. The XRD spectra for the rest of the ceramic glazes, as well as the reference data and calculations for identification of the compounds in the glazes are given in Appendices E and F.

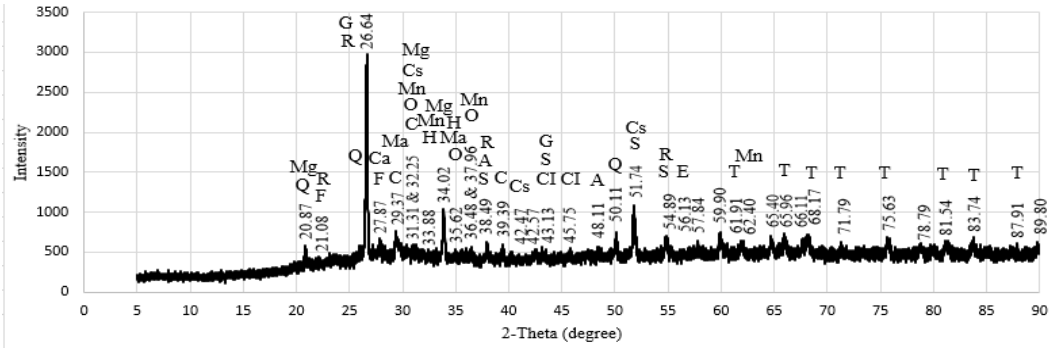

Figure 47. XRD spectrum of the turquoise tile of K001. **A:** Anatase (TiO_2), **C:** Calcite ($CaCO_3$), **Ca:** Calcian albite [$(Na,Ca)(Si,Al)_4O_8$], **CI:** Carbon iron silicon

[$C_{0.12}Fe_{0.79}Si_{0.09}$], **Cs:** Calcian siderite [$Ca_{0.1}Mg_{0.33}Fe_{0.57}(CO_3)$], **E:** Epidote [$Ca_2(Al,Fe)_3(Si_2O_7)(SiO_4)(OH)_2$], **F:** Feldspar [$KAlSi_3O_8$–$NaAlSi_3O_8$–$CaAl_2Si_2O_8$], **G:** Graphite (C), **H:** Hematite (Fe_2O_3), **Ma:** Maghemite (Fe_2O_3), **Mg:** Magnetoplumbite [$PbO(Fe_2O_3)_6$], **Mn:** Manganoan magnetoplumbite [$Pb(Fe^{3+},Mn^{3+})_{12}O_{19}$], **R:** Ramsdellite ($MnO_2$) (Card no: 42-1316), **S:** Tin oxide (SnO_2), **T:** Tenorite (CuO), **O:** Olivine [$Mg_{1.8}Fe_2(SiO_4)$], **Q:** Quartz (SiO_2)

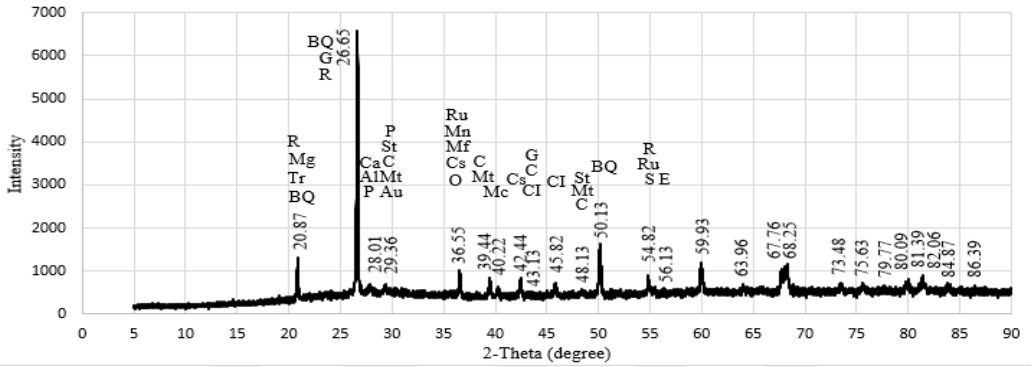

Figure 48. XRD spectrum of the black tile of K002. **Al:** Albite ($NaAlSi_3O_8$), **Au:** Augite [$Ca(Fe,Mg)Si_2O_6$], **BQ:** Beta-Quartz (SiO_2), **C:** Calcite ($CaCO_3$), **Ca:** Calcian albite [$(Na,Ca)(Si,Al)_4O_8$], **CI**: Carbon iron silicon [$C_{0.12}Fe_{0.79}Si_{0.09}$], **Cs:** Calcian siderite [$Ca_{0.1}Mg_{0.33}Fe_{0.57}(CO_3)$], **Cs:** Calcian siderite [$Ca_{0.1}Mg_{0.33}Fe_{0.57}(CO_3)$], **E:** Epidote [$Ca_2(Al,Fe)_3(Si_2O_7)(SiO_4)(OH)_2$], **G:** Graphite (C), **Mc:** Manganoan calcite, $(Ca,Mg)CO_3$, **Mf:** Magnesian fayalite, $(Fe,Mg)_2(SiO_4)$, **Mg:** Magnetoplumbite [$PbO(Fe_2O_3)_6$], **Mn:** Manganoan magnetoplumbite [$Pb(Fe^{3+},Mn^{3+})_{12}O_{19}$], **Mt:** Magnesian calcite [$(Ca,Mg)CO_3$], **O:** Olivine [$Mg_{1.8}Fe_2(SiO_4)$], **P:** Pyroxene [$(Na,Ca,Fe^{2+},Mg,Zn,Mn,Li)(Mg,Fe^{3+},Fe^{2+},Cr,Al,Co,Mn,Sc,Ti,Vn)(Si,Al)_2O_6$], **R:** Ramsdellite ($MnO_2$) (Card no: 42-1316), **Ru:** Rutile (TiO_2), **S:** Tin oxide (SnO_2), **St:** Sphalerite (ZnS), **Tr:** Tridymite (SiO_2).

When the Figure 47 is checked, it could be seen that the turquoise tile may consist of anatase (TiO_2), calcite ($CaCO_3$), calcian albite $(Na,Ca)(Si,Al)_4O_8$, quartz (SiO_2), graphite (C), tenorite (CuO), epidote [$Ca_2(Al,Fe)_3(Si_2O_7)(SiO_4)(OH)_2$], carbon iron silicon ($C_{0.12}Fe_{0.79}Si_{0.09}$), calcian siderite [$Ca_{0.1}Mg_{0.33}Fe_{0.57}(CO_3)$], magnetoplumbite [$PbO(Fe_2O_3)_6$], ramsdellite ($MnO_2$), manganoan magnetoplumbite [$Pb(Fe^{3+},Mn^{3+})_{12}O_{19}$], as revealed by XRD spectroscopy. The compounds are consistent with the content displayed by XRF spectrometry since the sample is formed of 44% SiO_2, 15% PbO, 15% CO_2, 7% Al_2O_3, 5% CaO, 2% Fe_2O_3, 1.6% CuO, 0.6% MgO, 0.2% TiO_2, 0.08% MnO. Moreover, titanium oxide was found to be in the form of anatase which could be seen up until 600 °C and existence of calcite is observed if the sample is fired below 600-850 °C [73]. These results are parallel with the estimated firing temperature which was found to be at 600-700 °C by FTIR

spectroscopy. Moreover, the XRD spectroscopy results of the black tile mention that there were pyroxene, quartz, graphite, albite, tin oxide, carbon iron silicon, tridymite, magnetoplumbite and ramsdellite in the glaze. Pyroxene is known to occur at around 900 °C [100], and since it is observed by XRD, it could be said that the black tile was fired above 900 °C, which is also consistent with the FTIR spectroscopy results which estimated it to be fired at around 900-925 °C. Likewise, tridymite is the polymorph of SiO_2 that occurs at high temperatures starting from 870 °C [101], which is also relevant to the same temperature range. XRF spectrometry data were also compatible with those found by XRD spectroscopy.

Even though the problem of compositional differentiation of the same molecules and compounds could be resolved by XRD, almost all the potsherd glazes were determined to be amorphous with thick signals by XRD analysis as shown in Appendix A.5. On the other hand, the tiles were crystalline, since most probably they were opacified by SnO_2, which was determined as 6.7% in K001 and 0.084% in K002. It is known in literature that yellow glazes with lead antimonate (Naples yellow, $Pb_2Sb_2O_7$) and green glazes with copper will be opaque [94].

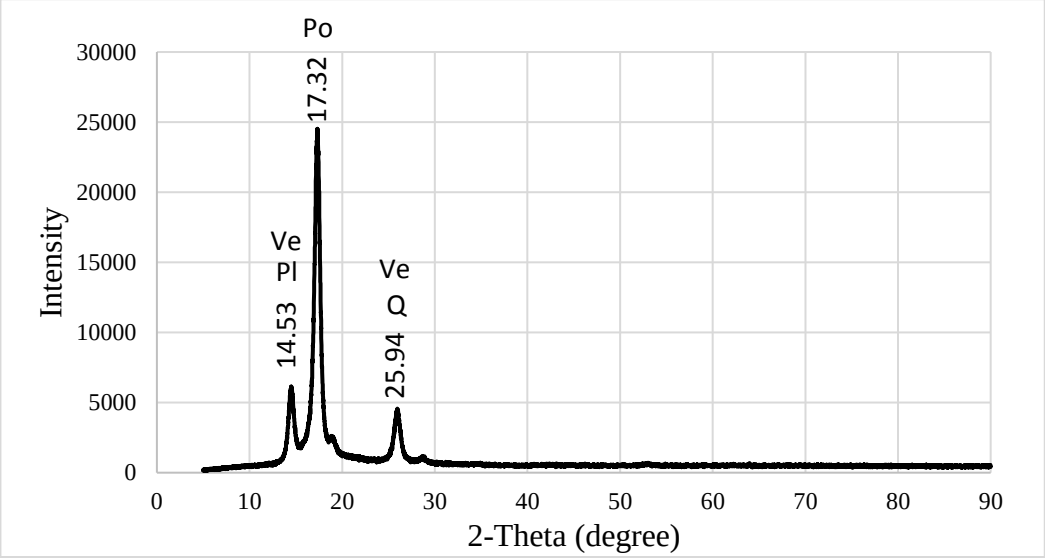

Figure 49. XRD spectrum of the turquoise glaze of the potsherd sample of K223, where Pl: Plagioclase [$Na(AlSi_3O_8)$,$Ca(Al_2Si_2O_8)$], Po: Portlandite [$Ca(OH)_2$], Q: Quartz (SiO_2), Ve: Verdigris [$Cu(CH_3COO)_2.H_2O$].

From the XRD spectrum of the turquoise glaze of the potsherd sample of K223 as seen in **Figure 49**, it could be deduced that the turquoise color comes from the pigment of Verdigris [$Cu(CH_3COO)_2.H_2O$] also mixed with Plagioclase [$Na(AlSi_3O_8)$,$Ca(Al_2Si_2O_8)$] and Quartz (SiO_2).

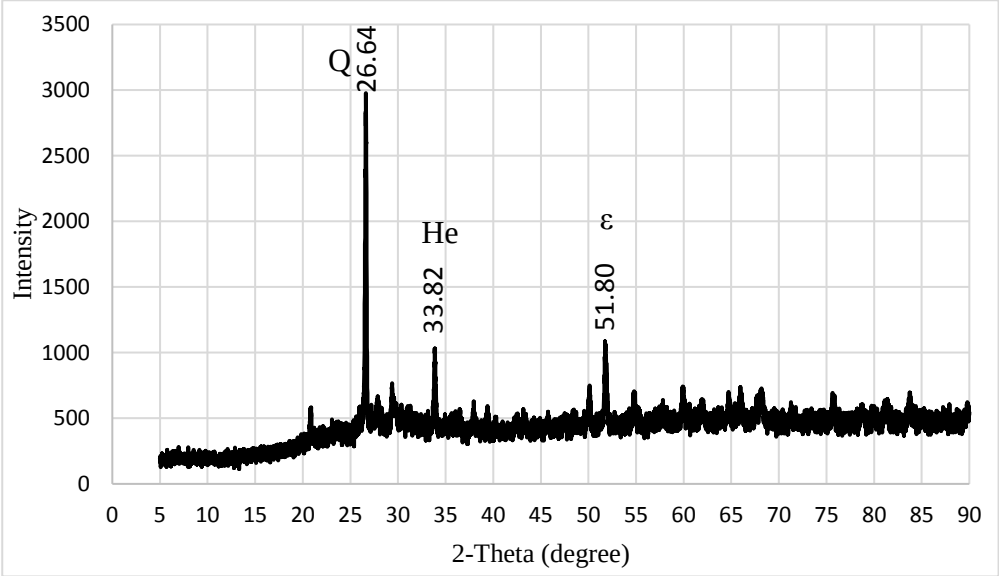

Figure 50. XRD spectrum of the brown glaze of the potsherd sample of K129 without a baseline correction, where ε: ε-Fe_2O_3, He: Hematite (α-Fe_2O_3), Q: Quartz (SiO_2).

As revealed by the XRD spectrum of the brown glaze of the potsherd sample of K129 as seen in **Figure 50**, brown color is created by both α and ε polymorphs of Fe_2O_3 together with Quartz (SiO_2). Observing the ε polymorphs also gives information about the firing temperature of the glaze that once exceeded 900 °C [102].

According to the XRF analysis results shown in

Table 9, both the most PbO (with 49.7%) and the most Sb_2O_3 was (with 0.361%) were determined in the yellow glaze of K149, as well as 1.12% CuO in the green glaze of K161. So, supported by the oxides found by XRF spectrometry, the colorants were suggested to be lead antimonate ($Pb_2Sb_2O_7$) for the yellow and copper oxide for the green glazes. Although these two colorant are crystalline, their XRD spectra in Appendix A.5 were amorphous, which can be explained by the possibility of the cooling process of the glazing to be fast [15].

Moreover, pyroxene [(Na,Ca,Fe^{2+},Mg,Zn,Mn,Li)(Mg,Fe^{3+},Fe^{2+},Cr,Al,Co,Mn,Sc, Ti,Vn)$(Si,Al)_2O_6$] was observed in the XRD spectrum of the K002 black tile and XRF results showed that Na_2O and MgO contents were 9.6% and 1.7%, respectively, which also supports the possibility of the presence of magnesium-rich pyroxene.

It is known that the minerals of olivine, epidote, baryte, augite, fayalite, sphalerite and phlogopite were special to the Byzantines (B), whereas dolomite, diopside, spessartine and siderite were mostly preferred by the Ottomans (O) [73]. The compounds determined by XRD spectroscopy were olivine (B), epidote (B) and siderite (O) in both tiles, plus with augite (B) and fayalite (B) in K002 black tile, which could be concluded that pottery glazing tradition in the period of Seljukids-Danishmendids was a mixture of the Byzantines and the Ottomans.

It is known that fast cooling process of the glaze and addition of Al, Zr and Mg increase its transparency and make it amorphous, whereas cooling slowly and adding Zn, Ti, Ca, Fe^{3+}, Si, Ba, B make it opaque, with the crystal formation [15]. As shown by the XRD spectra in Appendix A.5, it could be stated that almost all the potsherd glazes were amorphous, whereas the tiles were crystalline and opaque, which could also be supported by the XRF data in

Table 9 that Al_2O_3 was 4-7% in tiles, 0.87 in K108 and 2.8-5.4 for the rest of the potsherds; and MgO was changing from 0.6 to 1.7 for the tiles and 0.37- 0.65 for the potsherds. Whereas ZnO was determined to be 0.014 in K002 and 0.023 in K223; TiO_2 as 0.222 in K001, 0.185 in K002, 0.231 in K108, 0.234 in K149, 0.188 in K161, 0.524, in K172, 0.117 in K223; CaO as 5.04 in K001, 4.68 in K002, 9.78 in K108, 0.69 in K149, 3.63 in K161, 2.77 in K172, 3.85 in K223; Fe_2O_3 as 2.16 in K001, 2.5 in K002, 1.34 in K108, 0.46 in K149, 0.82 in K161, 4.17 in K172, 1.08 in K223; SiO_2 as 43.9 in K001, 54.2 in K002, 7.08 in K108, 28.9 in K149, 27.2 in K161, 34.2 in K172, 53 in K223. So, it could be deduced that pottery glazes were probably cooled fast while the tiles were cooled slowly.

Almost all the pastes of potsherd samples were reddish and homogeneous, which clarifies a biscuit firing was applied with high temperatures before the glaze is put [47]. Whereas exceptionally for the tile samples of K001 and K002, and the turquoise

glaze of K223 potsherd, the pastes were more white, indicating the addition of calcite to the pastes and observed bubbles in the surface of the K223 could give the information that this sample could be fired really fast that there was probably not enough time for the release of the occurred CO_2 [103].

4.4. Results and Discussion of Raman Spectroscopy

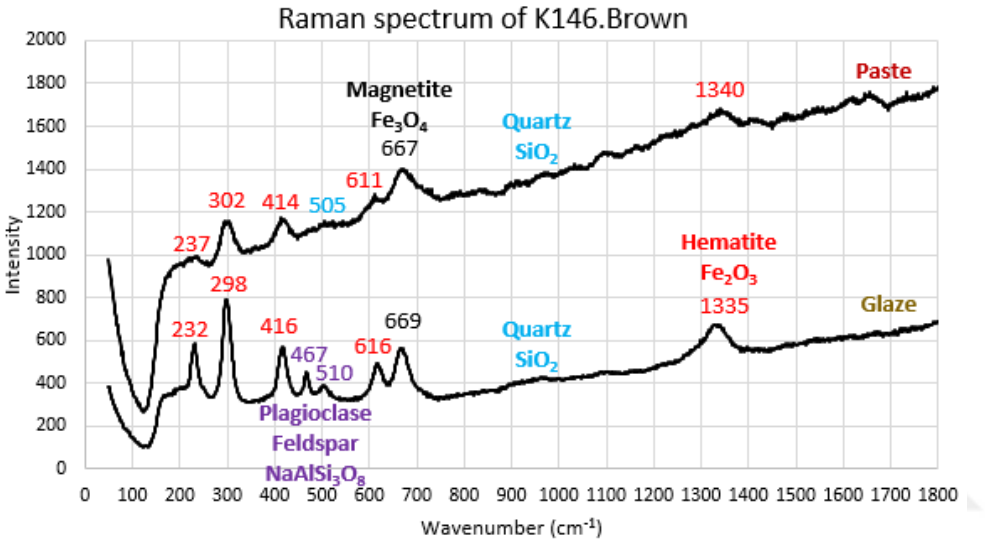

Figure 51. Raman spectrum of the paste (above) and the colorants in the glaze (below) of K146.

Raman spectra of the paste and the brown glaze of the potsherd K146 are given in Figure 51. Brown glaze of K146 consists of plagioclase feldspar and this shows that the firing temperature was not that much [26], could be less than 980 °C [104], which is also consistent with 850-900 °C calculated for K146 from its FTIR spectrum. Since the glaze starts melting first on the intersection points with the paste, Si-Pb might be in the crystal lattice [26].

It was expected initially to determine the firing temperatures of the glazed samples by calculating their polymerization indices, however except from just one point on the only one glazed sample, which is the brown-colored potsherd K146, the Raman signals could not be received. Then Raman spectrum of K146 glaze sample is compared with that of the paste as could be seen in Figure 51 and found out that both hematite, as depicted as red signals at 1335 cm^{-1}, magnetite, as shown as black at

667 cm^{-1}, plagioclase feldspar as purple at 467 ad 510 cm^{-1}, and silica signals (indicated by blue) at around 500 and 1000 cm^{-1} were collected [103-104]. Plagioclase feldspar are observed only on the glaze. Then, in the literature review it is mentioned that these extra signals might probably be because of the existence of plagioclase feldspar [107]. Information about the diffraction lines and corresponding d-values are given in Appendix A.6 with the following formula.

From the Bragg's Law, $2d\sin\Theta=n\lambda$

$(2)(\text{d-spacing})(\sin\frac{2\Theta}{2}) = (1)(0.15418\ \text{nm})$

$$d = \frac{0.15418\ nm}{2sin\Theta}$$

Moreover, to go on getting Raman signals, the 532-nm (green) laser at KUYTAM, in Istanbul, is beneffitted from. Raman spectra of some signals reveal the ingredients and pigments such as:

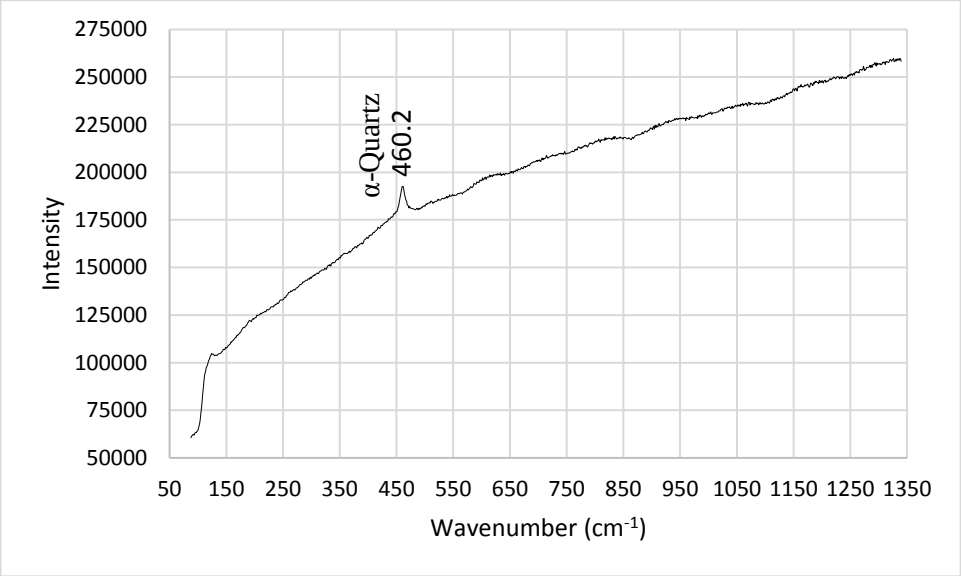

Figure 52. Raman spectrum of the white slip sample of K161 potsherd.

From the Raman spectrum of the white slip of K161 potsherd as seen in Figure 52 above, the signal around 460.2 cm^{-1} could reveal that the slip is made of only α-Quartz [108].

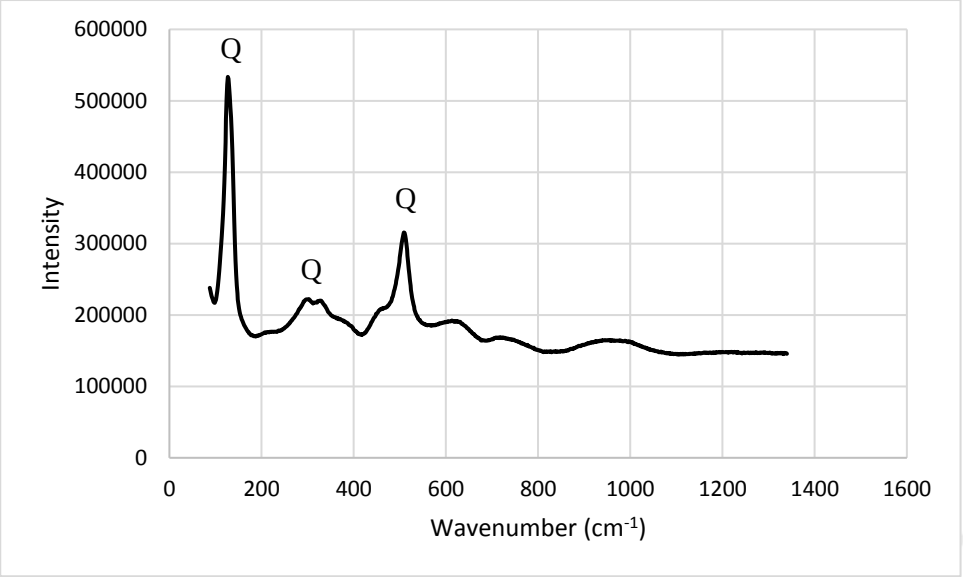

Figure 53. Raman spectrum of the green glaze on the interior side of K161 potsherd. Q: Quartz

Furthermore, from Raman spectra of the green glaze on the interior side of K161 potsherd, again quartz signals were delivered.

Another advantage of Raman spectra is that it allows us to compare the shape of the spectra to assign the materials in the glaze [53]. And if the below figures of Raman spectra are compared with the ones in **Figure 11**, it could easily be observed that shapes of the spectra of the Comana Pontica potsherds are fitting the same as the last group with "PbO" category in Figure 11, also supporting the information of low I_p.

Then, if the **Figure 122** is compared with the Raman spectra of Comana Pontica potsherds below, Byzantine influence could easily be seen, together with the Seljukid shapes similar to some of the FTIR spectra.

On the other hand, Raman spectra could also be used to calculate I_p values to reveal firing temperatures as follows:

Chi^2=14961.30273	COD=0.99564	# of Data Points=804
SS=11699738.74	Corr Coef=0.99782	Degree of Freedom=782

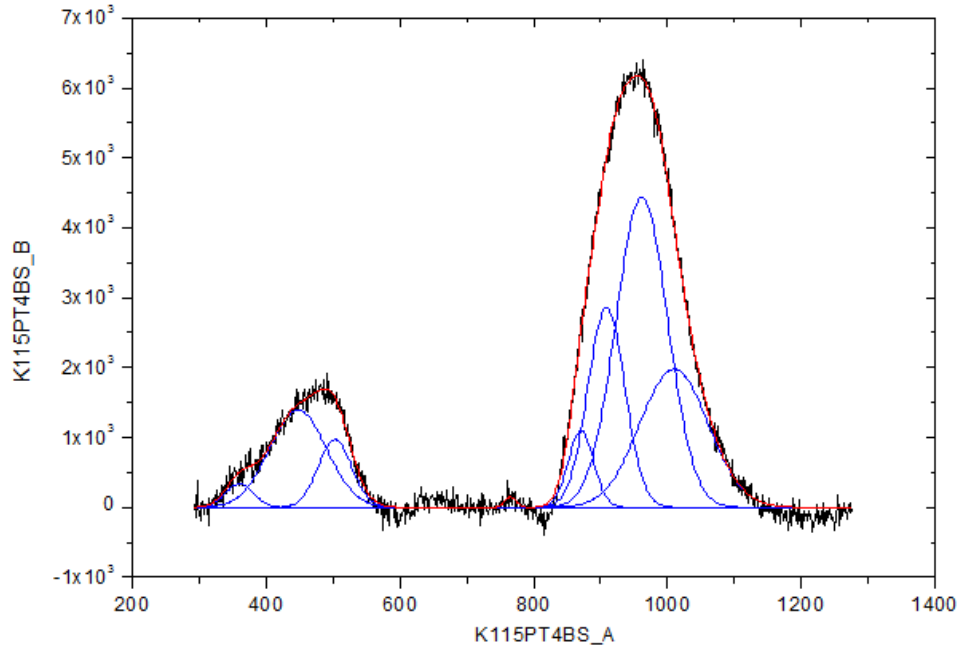

Fitting Results

Peak #	Peak Type	AreaFitT	FWHM	MaxHeight	CenterGrvty	AreaFitTP
1	Gaussian	3208.85426	20.2175	149.10449	765.69912	0.27574
2	Gaussian	52299.94208	44.44401	1105.49354	870.61579	4.49419
3	Gaussian	197851.98541	65.01131	2859.0365	908.66428	17.00165
4	Gaussian	430665.75927	91.19002	4436.71181	961.66136	37.00761
5	Gaussian	148494.79063	100	1395.20257	447.69576	12.76033
6	Gaussian	60758.79496	58.67509	972.80001	503.05368	5.22107
7	Gaussian	17694.49188	48.96738	339.6868	359.95088	1.52051
8	Gaussian	252747.57131	120	1978.6714	1010.125	21.71889

Figure 54. Raman spectrum of the yellow glaze on the interior side of K115 with Q_n drawings.

Figure 55. Image of the point on the yellow glaze on the interior side of K115 where the Raman signals taken

Source File: K128PT2BS | Data Set: K128PT2BS_B | Date:23

Chi^2=78220.66355 | COD=0.99905 | # of Data Points=728

SS=55145567.80 | Corr Coef=0.99952 | Degree of Freedom=705

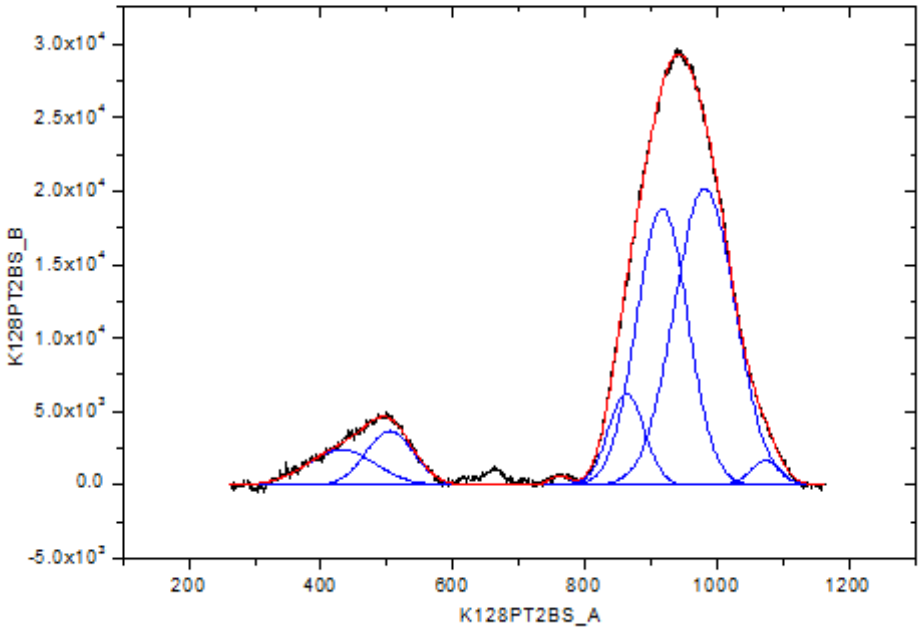

Fitting Results

Peak #	Peak Type	AreaFitf	FWHM	MaxHeight	CenterGruty	AreaFitfP
1	Gaussian	22573.96041	33.21497	638.47226	761.54112	0.42472
2	Gaussian	422533.68953	63.98334	6203.86879	863.18214	7.94981
3	Gaussian	1824729.5013	91.19192	18797.95495	917.31906	34.33159
4	Gaussian	2315505.8859	107.88473	20163.66183	981.62429	43.56536
5	Gaussian	93779.06202	53.04441	1660.92248	1073.75681	1.76442
6	Gaussian	138.28015	0.34009	381.97045	498.64649	0.0026
7	Gaussian	306569.7492	120	2401.16019	430.99771	5.76799
8	Gaussian	329185.95176	84.08839	3677.67712	504.13141	6.19351
		5315016.0803				

Figure 56. Raman spectrum of the brown glaze on the interior side of K128 with Q_n drawings.

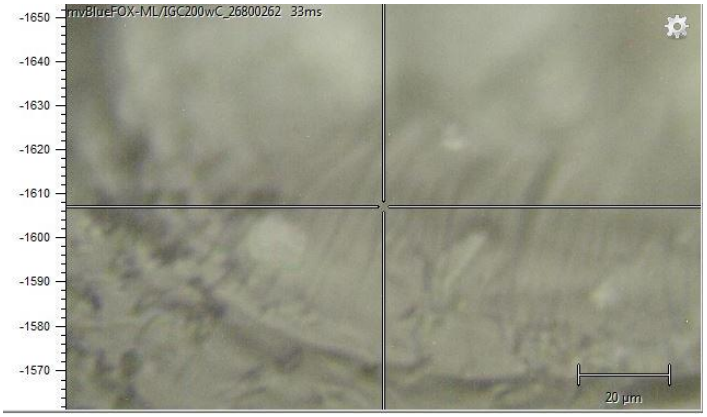

Figure 57. Image of the point on the brown glaze on the interior side of K128 where the Raman signals taken

Source File: K129PT4BS | Data Set: K129PT4BS_B | Date:23

Chi^2=16019.98517 | COD=0.99685 | # of Data Points=762

SS=11854789.02 | Corr Coef=0.99842 | Degree of Freedom=740

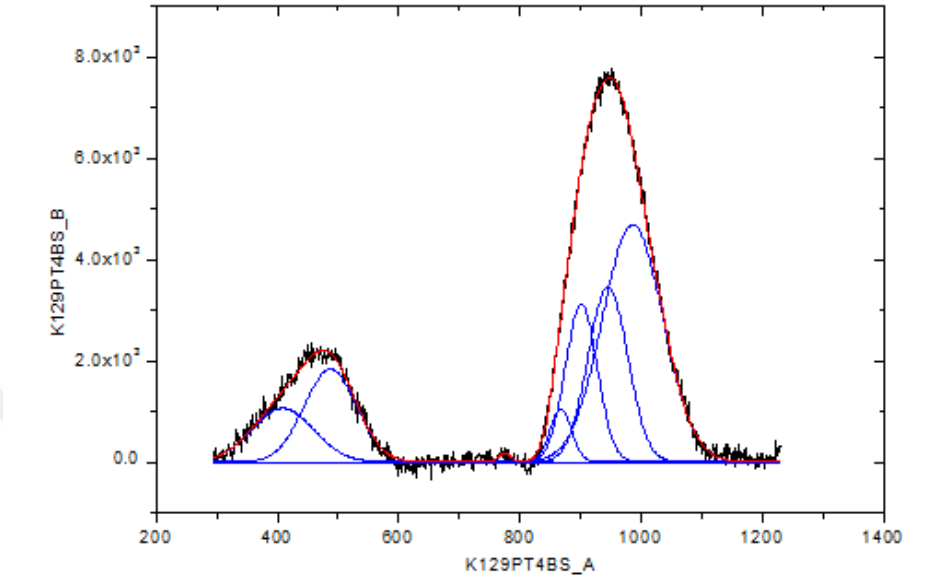

Fitting Results

Peak #	Peak Type	AreaFitT	FWHM	MaxHeight	CenterGrvty	AreaFitTP
1	Gaussian	4332.96056	23.59138	172.54387	774.60066	0.29669
2	Gaussian	46437.33073	41.71591	1045.76403	867.67568	3.17974
3	Gaussian	204787.96105	61.6403	3121.10145	901.40707	14.02259
4	Gaussian	282423.12803	76.63148	3462.27229	945.28964	19.33856
5	Gaussian	590127.90158	118.15138	4692.18678	986.31594	40.40825
6	Gaussian	133822.11501	120	1061.02928	408.39909	9.1633
7	Gaussian	198483.01035	101.72087	1833.08447	487.44687	13.59087
8	Gaussian	3.3815E-157	120	2.6475E-159	487.44687	2.3154E-161

1460414.4073

Figure 58. Raman spectrum of the brown glaze on the interior side of K129 with Q_n drawings.

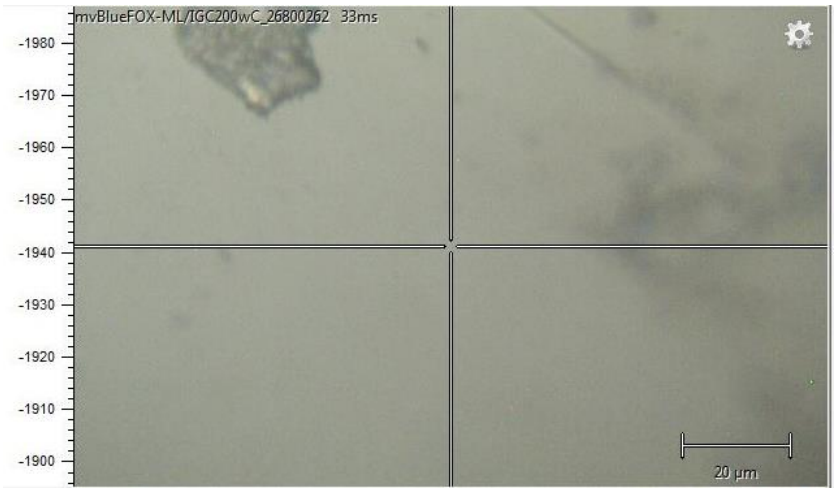

Figure 59. Image of the point on the brown glaze on the interior side of K129 where the Raman signals taken

Chi^2=88829.65727 COD=0.9916 # of Data Points=609

SS=52498327.44 Corr Coef=0.99579 Degree of Freedom=591

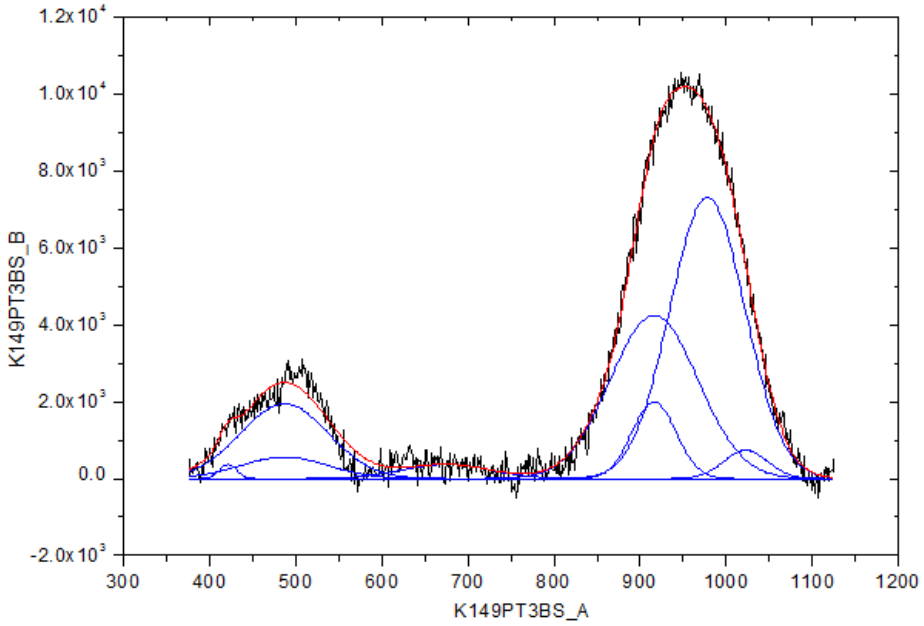

Fitting Results

Peak #	Peak Type	AreaFitT	FWHM	MaxHeight	CenterGrvty	AreaFitTP
1	Gaussian	47490.54035	120	371.78701	674.8592	2.51962
2	Gaussian	542038.53174	120	4243.51467	916.51341	28.75799
3	Gaussian	127444.67438	60	1995.43984	916.51341	6.76161
4	Gaussian	797562.65836	102.52673	7310.7565	978.4419	42.31489
5	Gaussian	46860.25053	60	733.72525	1022.50109	2.48618
6	Gaussian	9003.60134	23.13678	365.57936	421.1986	0.47769
7	Gaussian	244494.13754	120	1942.64786	486.81027	12.9717
8	Gaussian	69933.18293	120	555.65971	486.81033	3.71032
		1884827.5771				

Figure 60. Raman spectrum of the yellowish green glaze on the exterior side of K149 with Q_n drawings.

Figure 61. Image of the point on the yellowish green glaze on the exterior side of K149 where the Raman signals taken

Source File: K152PT4BS | Data Set: K152PT4BS_B | Date:23

Chi^2=646472.5550 | COD=0.99813 | # of Data Points=695

SS=433783084.4 | Corr Coef=0.99906 | Degree of Freedom=671

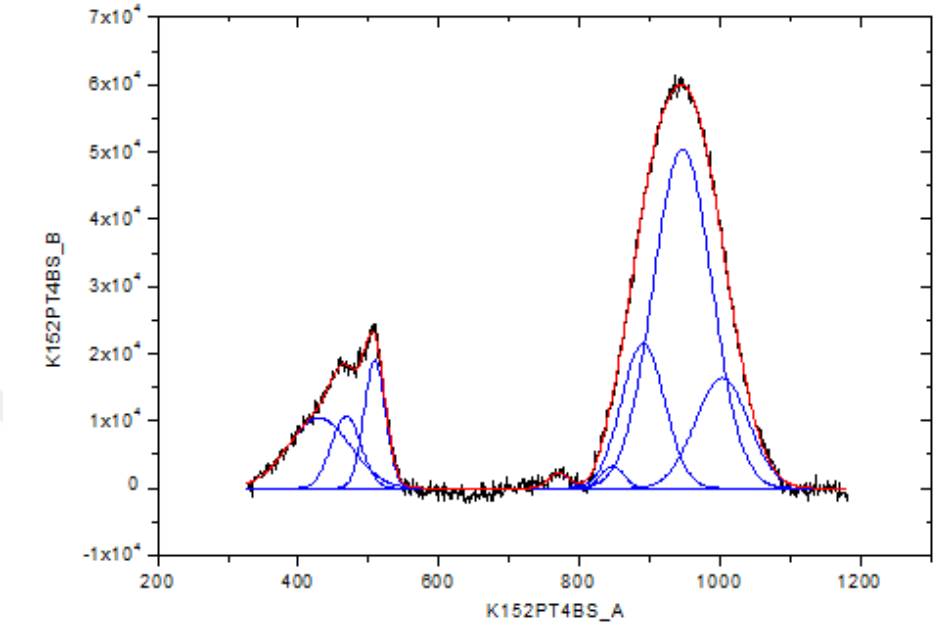

Fitting Results

Peak #	Peak Type	AreaFitT	FWHM	MaxHeight	CenterGrvty	AreaFitTP
1	Gaussian	81766.29446	33.89776	2266.06024	770.41392	0.7348
2	Gaussian	134122.66326	38.66731	3258.56497	846.85055	1.2053
3	Gaussian	1655158.0331	72.49975	21447.22603	890.79895	14.87413
4	Gaussian	5268539.2193	98.14545	50429.9133	947.01246	47.3459
5	Gaussian	1557311.6470	89.37026	16370.07394	1003.07227	13.99483
6	Gaussian	1143667.2003	104.10297	10428.07434	429.66683	10.2776
7	Gaussian	564521.53976	49.5911	10694.12229	468.21378	5.07309
8	Gaussian	722675.31322	35.55501	19094.59936	508.7581	6.49435
		11127761.910				

Figure 62. Raman spectrum of the yellow glaze on the interior side of K152 with Q_n drawings.

Figure 63. Image of the point on the yellow glaze on the interior side of K152 where the Raman signals taken

Chi^2=57799.33512	COD=0.98317	# of Data Points=769
SS=43291702.00	Corr Coef=0.99155	Degree of Freedom=749

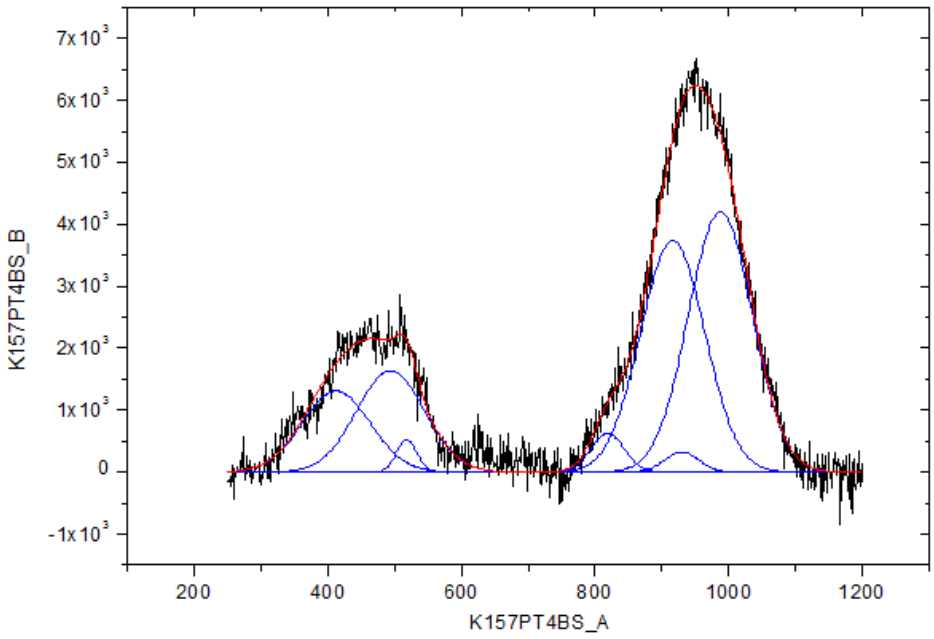

Fitting Results

Peak #	Peak Type	AreaFitT	FWHM	MaxHeight	CenterGrvty	AreaFitTP
1	Gaussian	15.56052	0.01179	1240.38615	1023.75562	0.0011
2	Gaussian	39037.65953	58.40121	627.95734	818.61938	2.76712
3	Gaussian	451006.90733	113.37385	3737.13378	916.2554	31.96886
4	Gaussian	20822.91144	60	326.03063	929.62088	1.476
5	Gaussian	504472.26462	112.91019	4197.33564	987.76636	35.75866
6	Gaussian	166915.91626	120	1307.69718	412.47415	11.83155
7	Gaussian	208677.97427	120	1633.66638	494.05004	14.79179
8	Gaussian	19820.10751	35.37449	526.36143	518.26468	1.40491
		1410769.3014				

Figure 64. Raman spectrum of the green glaze on the interior side of K157 with Q_n drawings.

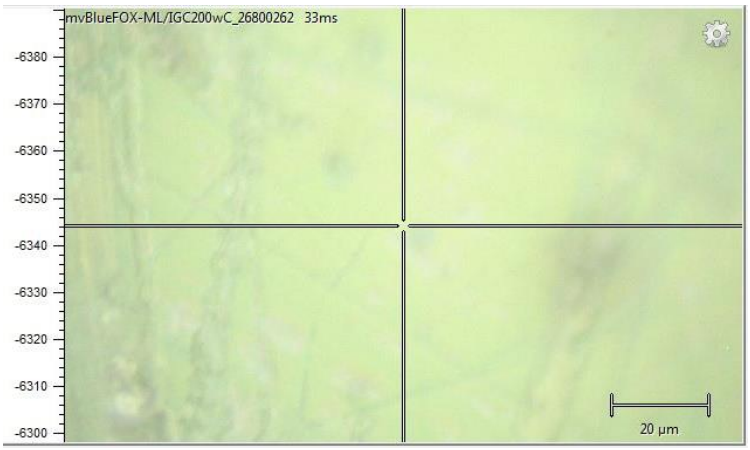

Figure 65. Image of the point of the green glaze on the interior side of K157 where the Raman signals taken

Chi^2=120957.5918 COD=0.99058 # of Data Points=769

SS=90234363.49 Corr Coef=0.99528 Degree of Freedom=746

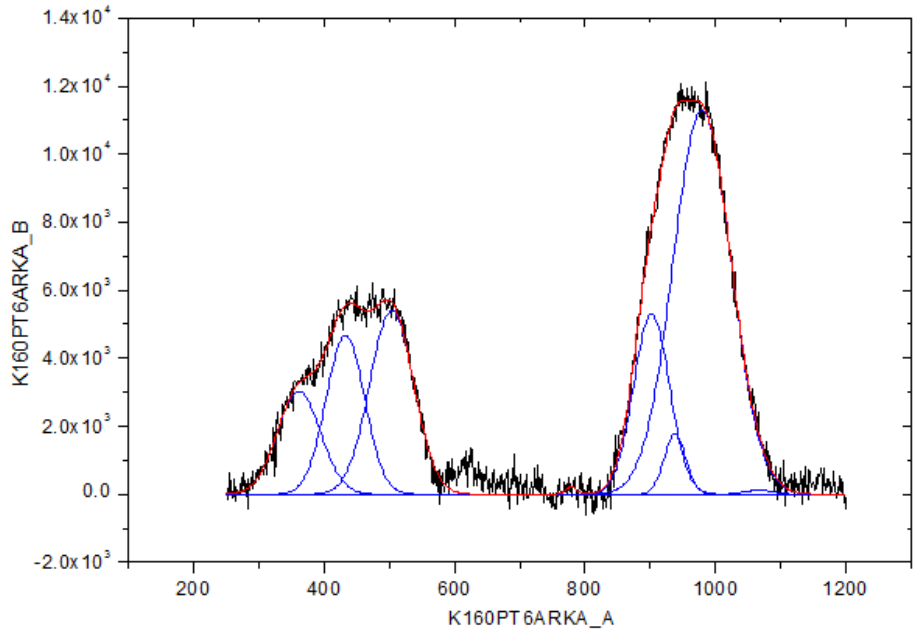

Fitting Results

Peak #	Peak Type	AreaFitT	FWHM	MaxHeight	CenterGrvty	AreaFitTP
1	Gausslan	4529.35829	19.96227	213.15473	778.39052	0.16387
2	Gausslan	366315.86902	64.95778	5297.76601	901.92328	13.25324
3	Gausslan	73741.00564	39.06962	1773.11996	938.0224	2.66794
4	Gausslan	1259125.0675	104.74706	11292.6246	979.5587	45.55491
5	Gausslan	251890.51589	78.30371	3023.27241	361.70914	9.11335
6	Gausslan	345725.83219	69.45422	4676.29267	432.81939	12.5083
7	Gausslan	455947.6506	79.40191	5394.51275	503.80502	16.4961
8	Gausslan	6696.82247	49.44664	127.2332	1066.77102	0.24229
		2763972.1216				

Figure 66. Raman spectrum of the green glaze on the exterior side of K160 with Q_n drawings.

Figure 67. Image of the point on the green glaze on the exterior side of K160 where the Raman signals taken

Chi^2=54377.35924 COD=0.98914 # of Data Points=762

SS=40130491.12 Corr Coef=0.99455 Degree of Freedom=738

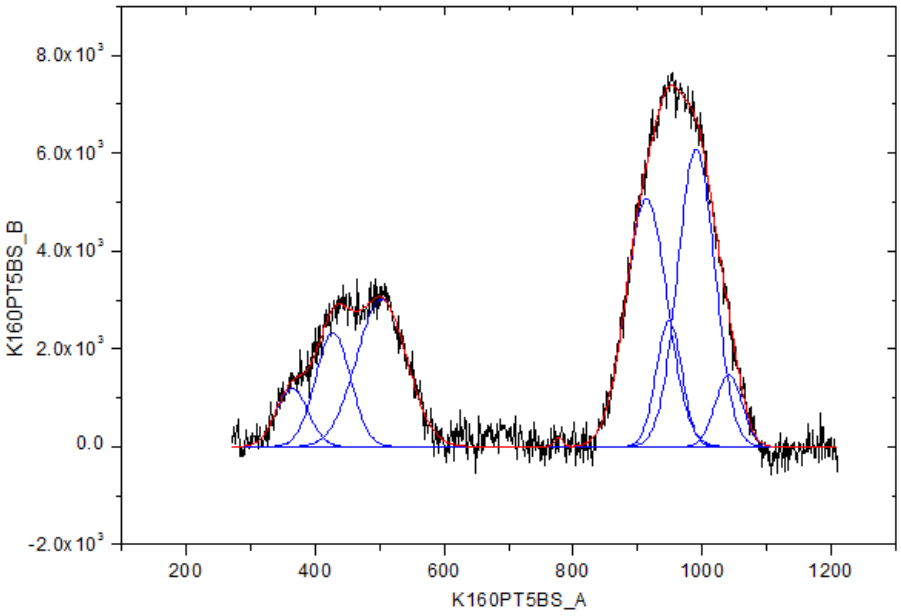

Fitting Results

Peak #	Peak Type	AreaFitT	FWHM	MaxHeight	CenterGrvty	AreaFitTP
1	Gaussian	2957.48404	15.04026	184.72904	777.41902	0.18838
2	Gaussian	406385.96481	75.36528	5065.65475	913.32104	25.88505
3	Gaussian	127660.65721	46.5331	2577.29027	948.5697	8.13144
4	Gaussian	433364.52019	67.01318	6075.21036	990.6761	27.60347
5	Gaussian	76637.73436	48.77683	1476.03723	1041.05609	4.8815
6	Gaussian	73307.16785	58.06079	1186.22513	364.64889	4.66935
7	Gaussian	158556.37289	64.0434	2325.82781	427.82288	10.09936
8	Gaussian	291094.10289	90.97143	3006.05407	503.01615	18.54145
		1569964.0042				

Figure 68. Raman spectrum of the yellow glaze on the interior side of K160 with Q_n drawings.

Figure 69. Image of the point of the yellow glaze of the interior side of K160 where the Raman signals taken

Chi^2=61348.90327 COD=0.99692 # of Data Points=658

SS=39140600.29 Corr Coef=0.99846 Degree of Freedom=638

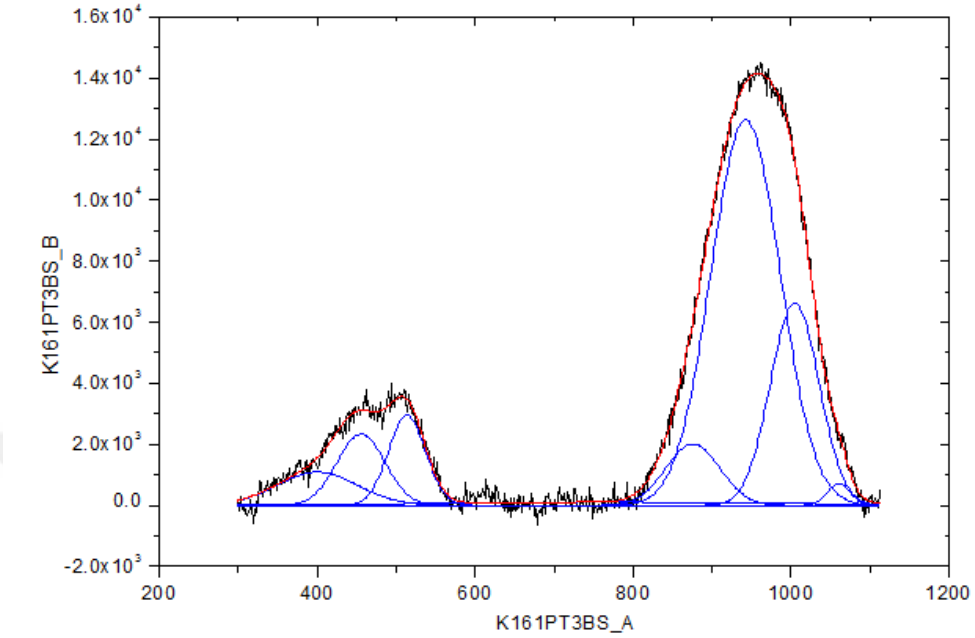

Fitting Results

Peak #	Peak Type	AreaFitT	FWHM	MaxHeight	CenterGrvty	AreaFitTP
1	Gaussian	177791.86727	71.49275	2336.24182	455.45929	6.73575
2	Gaussian	174160.42785	55.45778	2950.22553	513.77769	6.59818
3	Gaussian	136252.37853	120	1091.79212	400	5.16201
4	Gaussian	55368.90504	532.41009	106.53797	770	2.09769
5	Gaussian	172512.21835	80.45393	2014.37746	875.65439	6.53573
6	Gaussian	1386286.0742	103.12158	12629.65879	942.48676	52.52031
7	Gaussian	511676.52058	72.42182	6638.72174	1004.75028	19.38518
8	Gaussian	25475.60584	33.92235	705.60008	1060.37073	0.96516
		2639523.9977				

Figure 70. Raman spectrum of the green glaze on the interior side of K161 with Q_n drawings.

Figure 71. Image of the point on the green glaze of the interior side of K161 where the Raman signals taken

Table 10. Comparison of the estimated firing temperatures calculated by I_p values of Raman spectra with the ones calculated through FTIR spectra wavenumber values of the maximum peaks. N.D.: No data.

Sample	I_p (Raman)	$T_{calculated}$ (°C) (Raman)	$T_{estimated}$ (°C) (Raman)	$T_{estimated}$ (°C) (FTIR)	T_{ave} (FTIR)
K128.brown	0.1359	440	600-650	N.D.	N.D.
K149.green	0.207142	545	600-650	850-900	875
K161.green	0.226933	570	600-650	675-775	725
K115.yellow	0.242266	585	600-650	600-700	650
K152.yellow	0.279509	620	600-700	775-825	800
K129.brown	0.294568	635	600-700	600-700	650
K157.green	0.389434	705	700-800	850-900	875
160.yellow.int	0.499479	765	700-800	600-700	650
160.green.ext	0.615972	820	800-900	900-925	913

According to the I_p values calculated with the Origin program, the upper chart in **Table 10** is prepared. According to equations of **Figure 14**, in which if the I_p is less than 0.3 then the equation of the first part (between 600-1000 °C) is taken as $y = 66.667x + 933.33$, whereas for the I_p values greater than 1, the second part (between 1000-1400 °C) is taken as $y = 571.43x + 428.57$. On the other hand, since the limitations of I_p calculation in the chart is not including the values less than 0.3, but 6 of the samples here fall behind this scope, the calculated logarithmic equation, $y = 249.37\ln(x) + 938.33$, is preferred in calculation of the estimated firing temperature according to the Raman spectra. At the same time, the values of calculated firing temperatures that are below 600 °C are assumed as fired above 600 °C, namely preferred to be written here as 600-650 °C, since the minimum firing temperature of the glaze is greater than 600 °C [109].

Even though the results of the logarithmic equation of Raman spectra are not as same as the ones calculated from FTIR spectra, it can be said that Raman calculations are more trustworthy because of the broader areas of the maximum peaks of FTIR spectra may be misleading about the estimation of the firing temperatures, whereas sharper signals and Q_n calculations in Raman spectroscopy are more preferred [75].

CHAPTER 5

CONCLUSION

FTIR spectroscopy revealed that all of the samples compose of silica, some of which are carbonated and/or hydrated. Even though distinctive colorant molecules could not be observed most of the time with FTIR spectroscopy, it is a good tool to estimate the firing temperatures of the samples with respect to the changes occurring in the wavenumber positions of their Si-O asymmetric stretching peaks. According to the data of the estimated firing temperatures, it could be stated that temperature range is changing from 600 to 925 °C for the glazed samples, with a majority fired in the range of 800-900 °C. Moreover, if the colored glazes are ranked with respect to the increasing estimated firing temperatures, brown ones are found to be applied in the lowest in the range around 700-750 °C, followed by turquoise glazes in 725-800 °C, yellow and green glazes in 750-800 °C, orange glazes around 850 °C, and the black glaze around 900 °C. Likewise, red pastes were discovered to be fired around 850-900 °C, while white pastes behind the turquoise glazes and tiles, and the white slip layers around 900 °C, which can make the suggestion that the initial firing was done to the all potsherds except the turquoise one and at around 900 °C, then glazed and re-fired to 700-850 °C in an oxidative atmosphere for the light-colored glazes and to 700-750 °C in a reductive medium for the brown glazes. All of the turquoise glazes on the tile and pottery were on a white paste and glazed without a bisque-firing that could be understood from the bubbles in and under the glaze parts. The turquoise tile can be said to be fired in lower temperatures and the black tile was determined to be fired around 900 °C. Most of the brown glazes were calculated to be fired at 600-700 °C, majority of the yellow glazes were estimated to be fired at 700-800 °C, whereas it was 800-900 °C for majority of the green and most of the orange glazes. The second major firing temperature ranges were 600-700 °C for all of the yellow, green and orange glazes and minority of all of the yellow, green and orange glazes were in the range 900-925 °C.

Furthermore, the clay minerals in the glazes could be identified by the vibrations around 3600-3700 cm^{-1} in an FTIR spectrum. It was found that all the clays in the potsherds, together with the slip of K104 and the paste of K106 were similar to each other, constituted mainly by kaolinit (dickite, halloysite, kaolinite, nacrite) and montmorillonit-smectite (bentonite, montmorillonite, saponite, smectite, vermiculite) groups of clays. On the other hand, paste of K104 was also including illite and sepiolite. In the rest of the slips and pastes, the peaks are almost not observed, probably due to the dehydroxylation, dehydration, and decarbonation occurred at higher firing temperature values such as 850-925 °C. Moreover, inclusions of slaked lime [$Ca(OH)_2$], quicklime (CaO) and calcite ($CaCO_3$), probably taken from the crushed shells and bones, also provide information about the possible firing temperatures. The peak at 3648 cm^{-1} is known to belong to the slaked lime, the peak at around 1647 cm^{-1} occurs due to the bending vibrations of adsorbed water on the surface of CaO, and the peak at 1430-1450 cm^{-1} correspond to calcite. Above 600 °C microcrystalline calcite decomposes, and the quicklime is formed, after 800 °C calcareous clay minerals are rehydroxylated to $Ca(OH)_2$, above 900 °C dehydroxylation, dehydration and decarbonation occur up to 1000 °C with disapperance of all the calcite peaks and -OH bands.

It is known that if the cooling process of the glaze is fast, then it solidifies transparently, together with the contribution of formation of Al_2O_3, ZrO_2 and MgO and yields an amorphous XRD spectrum. On the other hand, slow cooling makes the crystals to grow, as well as addition of ZnO, TiO_2, CaO, Fe_2O_3, SiO_2, BaO, B_2O_3. As revealed by the XRF spectrometry results, Al_2O_3 content rising up to 7% and MgO contributions up to 2% made the potsherd glazes transparent and amorphous, with almost no signals in XRD spectra, and probably occurred because of the fast cooling process of the glazes. On the other hand, XRD signals of the tiles were easily identified with the help of their crystalline content in the glaze probably contributed by ZnO (around 0.014%), TiO_2 (0.19-0.22%), CaO (around 15%), Fe_2O_3 (2-2.5%) and SiO_2 (44-54%) being in great amounts and occurred by slowly cooling of the glazes. Anatase, calcite, albite, quartz, graphite, epidote, carbon iron silicon, siderite, magnetoplumbite, ramsdellite were identified in the turquoise tile by XRD

spectroscopy. The XRD analysis results were also consistent with the oxides detected by XRF spectrometry, such as 44% SiO_2, 15% PbO, 15% CO_2, 7% Al_2O_3, 6.7% SnO_2, 5% CaO, 2% Fe_2O_3, 1.6% CuO, 0.6% MgO, 0.2% TiO_2, 0.08% MnO for the turquoise tile. Due to the observance of anatase and calcite signals in XRD, the firing temperature was estimated between 600-850 °C, which is also parallel with the temperature found as 600-700 °C by FTIR spectroscopy. Moreover, pyroxene, quartz, graphite, albite, tin oxide, carbon iron silicon, tridymite, magnetoplumbite and ramsdellite were discovered by XRD spectrum of the glaze of the black tile, in which pyroxene is known to be formed at around 900 °C and tridymite occurs at temperatures higher than 870 °C, yielding the firing temperature as at least 900 °C, which is also relevant to the same temperature range calculated by FTIR spectroscopy, as well as the similar data of 54% SiO_2, 9.6% Na_2O, 4.7% CaO, 4.1% Al_2O_3, 4% MnO, 1.7% MgO, 0.2% TiO_2, 0.08% SnO_2 detected by XRF spectrometry. According to the XRF analysis results, the pyroxene determined by XRD was thought to be rich in Mg and Na. Crystalline structures of the tile glazes made them non-transparent most probably opacified by SnO_2, which was determined as 6.7% in K001 and 0.084% in K002, and occurred by slowly cooling of the glazes. Moreover, the colorant for the yellow glazes was assumed mostly to be lead antimonate ($Pb_2Sb_2O_7$) and green glazes as copper oxide, since according to the XRF analysis results, both the most PbO (with 49.7%) and the most Sb_2O_3 (with 0.361%) were determined in the yellow glaze of K149, as well as 1.12% CuO in the green glaze of K161. Moreover by XRD spectroscopy, olivine, epidote and siderite were examined in both tiles, additionally with augite and fayalite in K002 black tile, which also supports the idea that glazing traditions in the Seljukids-Danishmendids periods were a mixture of those of the Byzantines and the Ottomans, since olivine, epidote, augite and fayalite were typical mostly to the Byzantines as well as siderite to the Ottomans.

Due to the positive slope of the trend line in the chart of estimated average firing temperatures of the glazed ceramics differentiated by periods of production dates, the firing temperatures of the glazed ceramics of Comana Pontica were estimated to be increasing from the 12^{th} till 14^{th} centuries.

With the XRF analysis results, characterization of the samples could be made easily. Even though the observed deficiency of some important elements like Sn in the contents of the glazes makes the comparisons difficult, ratios of weight percentages of some metal oxides could be calculated and compared with the literature values in drawn biplots and ternary diagrams. From the biplot of SnO_2/PbO ratios, K002 black tile was found to be extremely similar to the Iznik (Nicaea) tiles of the Ottoman Empire from the 17th century and K001 turquoise tile was observed to be similar to the tiles of an Ottoman mosque (1429) in Edirne and those of the Timurids (2nd half of the 14th century – first quarter of the 16th century) where Iran might be the possible origin of influence [90].

With respect to the biplot of ratios of Pb/Si vs. Sn/Si, the potsherd K149 with yellow glaze from 13th century was determined to be close to the tiles from the mosques of the 15th and 16th centuries in Edirne, while K161 with green glaze and K172 with orange glaze from the 12-13th centuries were found to be close to the 15th century mosque in Edirne, which could bring the consideration that pottery making tradition with addition of similar proportions of lead and quartz might have continued from the periods of Seljukids in the 12th century to the Ottomans in the 16th century. This consideration is consistent with the information that continued workshop of ceramic arts and techniques of the Seljuks initiated the tile production in the Ottoman Empire [33, 87]. Furthermore, mineral natron was identified to be added as the flux during firing the glazes, that is also consistent with the traditional method in Anatolia in that period.

From the characterization biplot of PbO/SiO_2 vs. CaO/SiO_2, both tiles were closest to the 12th century Islamic Iran and the turquoise-glazed K223 was closest to the 11-12th century Islamic Syria which could find an estimation where it could be imported from if this is the case as recommended from Dr. Er [47]. The locations of the Comana potsherds in the biplots were consistent with the other previously analyzed glazes from Seljukid Era and the same time periods were condensed in close positions, which could make the glazes found in the layer of the Seljukids unique and its differentiation possible with respect to the oxide contents. Also this uniqueness could be seen from Figure 122 that the FTIR and Raman spectra of the potsherds display

both high PbO content similar to Byzantine Era as well as specified by addition of more NaO that also cause a change in the shape with a shoulder in the wavenumber region on the stretching modes.

Characterization analysis with respect to ternary plots gave also accurate information. By XRF, it could be seen that most of the samples contain high levels of lead. Also, calcareous samples could be detected by both XRF spectrometry and FTIR spectroscopy and give information that the firing temperature is below 850 °C.

Ternary diagrams also contributed to the possibility of the turquoise glazed sample K223 to be brought from Egypt or Iraq. From the ternary diagrams, the yellow glaze of K149 from the 13th century was found to be closer to Islamic glazes of Iran from the 10-11th centuries. On the other hand, since all the clay minerals were detected to be similar for the potsherds with respect to the 3600-3700 cm^{-1} region in FTIR spectra, it might be possible to produce all the pottery locally from the basin of Iris River, but influenced by different traditions or made by different potters.

Almost two-thirds of the glazed ceramic samples were found to be glazed on both the interior and exterior sides and almost quarter of the all glazed samples were glazed on a single side. 95% of the single-sided glazes were glazed on the interior part, which might assert that people at that time paid attention to the impermeability of the pottery more than its decorative purposes, in case glazing was to be done on a single side. Almost half of the one-sided and single-colored glazes were found to be colored in green, almost quarter of them in yellow, while turquoise, black, brown and orange could also be seen. Green was also the most preferred color (more than half) in all the glazes. Most of the glazed pottery samples (around three quarters) were preferred to be glazed on both sides. If the average firing temperatures calculated for just the glaze on one side are associated with the two-sided glazed samples, it could be found that majority (37%) of the glazed ceramics were estimated to be fired at 800-899 °C, followed by 27.4% at 700-799, 23.3% at 600-699 °C and 12.3% at 900-925 °C.

Coloring agents were also resolved. By Raman spectrum, the presence of magnetite and hematite were identified in the brown-glazed potsherd samples. Also, with the

help of the I_p calculations, more accurate firing temperatures are estimated compared to the ones calculated by FTIR spectra. Moreover, XRF data showed that manganese is responsible for the color of the black tile, copper (3% for the turquoise potsherd glaze) and 6.7% SnO_2 +1.6% CuO are the reasons for the turquoise coloring together with the high content of calcium oxide. This information is also supported by XRD spectrum of the turquoise glaze of the potsherd sample of K223, where Plagioclase [$Na(AlSi_3O_8)$,$Ca(Al_2Si_2O_8)$], Portlandite [$Ca(OH)_2$], Quartz (SiO_2) and Verdigris [$Cu(CH_3COO)_2.H_2O$] might be possibly included in the glaze.

CuO is attributed to be responsible for the turquoise and green colors of the glazes as well as the yellow glaze is the result of Fe_2O_3 together with $Pb_2Sb_2O_7$ and Sb_2O_3. For the turquoise color, the paste was preferred to be rich in calcite. For the color tones of green, it could be stated that increase in concentration of CuO could result in the yellow color of the glaze to turn into green. Dark colors, namely as brown, on the glazes mostly occur in reducting atmosphere and with low temperatures. Yellow color of the glazes could be proposed to be reached with very low concentration (around 0.5%) of Fe_2O_3 in the oxidizing atmosphere and by addition of Sb_2O_3, PbO and TiO_2. If the Fe_2O_3 concentration is increased to twice and 0.5% CuO and 0.06% As_2O_3 added in an oxidative environment, then its color turns into green. Glaze color of orange could be arisen from about 4% Fe_2O_3, 0.5% TiO_2 and 0.13% CdO. CuO addition between 1.5-3.4% is thought to be the reason for the turquoise glaze and on a calcite paste. Purple color on the glaze of K117 potsherd could be due to the mixture of colors of red due to the reduced Cu_2O and bluish green due to the oxidized CuO. Brown color could probably be occurred by FeO in the reductive atmosphere at lower temperatures together with around 0.2% TiO_2, and also related with the high CO_2 content. Black color by MnO and FeO, also by contributions of Na_2O and MgO. In tiles, SnO_2 was used for the opacification. Cobalt is known to be responsible for the dark blue color of the glaze, but no cobalt is detected in any sample.

The two tile samples are determined to be in the group of tin-opacified lead-alkali glaze, whereas the glazed potsherds are in the high lead and lead-alkali types.

The results of XRF analysis of the glazes of both the potsherds and tiles showed that lead-oxide was preferred as the fluxing agent with natron.

If the tin-opacified lead alkali type glaze is desired to be turquoise, then lead also should be in the medium, as could be understood from XRF data for the tiles.

Gas bubbles observed on the turquoise glaze, which could lead to consider no bisque-firing was applied prior to the glazing. Reddish color of the paste, occurred due to the clay and iron oxide, is an indicator for the atmosphere used in an oxidizing way in the kilns and its homogeneity is the result of the bisque-firing applied under high temperatures, whose temperature was estimated as around 900-925 °C from the FTIR Spectroscopy wavenumber data.

Firing temperatures were also estimated by using the information of shifts of the maximum peaks of the FT-IR spectra of each of the glaze samples and specified to be mostly in the range of 700-900 °C. Moreover, the glazes were determined to be produced using quartz, from not only calcareous but also non-calcareous clays. Body parts of the sherds investigated in the previous studies (Er, 2020) have already been suggested that the pottery samples were produced mostly in the local specialist centers which were limited in quantity during the Seljuks period in Anatolia. The similar temperature range was also determined not from the body but from the glaze parts of the sherds this time. PbO is thought to be added most probably to lower the firing temperature, which was supported by FTIR spectroscopy that it was as low as 600-700 °C for some pottery samples. Also, the estimated firing temperatures from Raman spectra are more or less in accordance with the FTIR data, in which Raman results are more trustworthy, which also yields Comana Pontica glazed potsherds are fired in changing temperatures from 600 to 900 °C.

Lead-oxide-based glazes and colorants were characterized by XRF spectrometry and FTIR spectroscopy. As revealed by the XRD analyses, most of the examined potsherd specimens were composed of polycrystalline materials with different phases. On the other hand, it also has complications due to its amorphous character.

FTIR spectroscopy is useful to estimate the firing temperatures with the help of the shifts of Si-O stretching peaks with increasing temperature. By FTIR, the characteristic stretching vibrations of M-O, Si–O, O-H, C-O and calcite vibrations could easily be detected. In FTIR spectra, the reason for the occurrence of the band at 3000-3700 cm^{-1} might be not related with water but because of the hydroxyls in crystals of azurite ($2CuCO_3.Cu(OH)_2$) mineral in turquoise-glazed and malachite ($CuCO_3.Cu(OH)_2$) in green-glazed samples.

Firing temperatures estimated by FTIR spectra were mostly consistent with those determined by the positions of samples on the isothermal curves in the bivariate chart of PbO vs. (Na_2O+K_2O) acquired by XRF spectrometry. Whereas, isothermal curves were found generally 50-100 °C higher than the firing temperatures estimated by FTIR spectra.

All in all, XRF spectrometry is a significant analytical tool to characterize both the glazes of potsherds and tiles, as well as Raman spectroscopy is good in calculations of the firing temperatures with the help of the I_p calculations. Also, the similarities between the estimated firing temperatuers that are calculated by I_p values of Raman spectra and wavenumber locations of FTIR spectra show that such approaches are consistent with each other, with an advantage on the side of Raman than FTIR spectra since Raman signals are narrower and yield more accurate results.

Just one type of an instrument may not be sufficient enough to analyze the contents of the materials inside the glazed ceramic objects, therefore combination of different techniques, such as FTIR, Raman and XRD spectroscopy along with XRF spectrometry, is a good way to determine the oxide contents, firing temperatures and to characterize the samples.

Analysis of ceramics and glazes are important in not only describing and dating the archaeological remains, but also providing information about the sociocultural structure and economic relationships [111]. The results of the thesis could be expected to contribute to the comprehension of the glazing of pottery and tiles of Comana Pontica during 11-14th centuries and also the pottery trading in and near Anatolia in

this period. Hope this research would provide beneficial information to the following generations.

All in all, every second I have spent on this thesis, from wondering to searching for answers, and from reading articles to conducting experiments, was really invaluable, enthusiastic and enjoyable for me.

REFERENCES

[1] M. S. Walton and M. S. Tite, 'Production technology of roman lead-glazed pottery and its continuance into late antiquity', *Archaeometry*, vol. 52, no. 5, pp. 733–759, Oct. 2010, doi: 10.1111/J.1475-4754.2009.00506.X.

[2] Dictionary.Cambridge.org, 'ceramic', 2021. https://dictionary.cambridge.org/dictionary/english/ceramic.

[3] S. Breuer, 'The Chemistry of Pottery', *Educ. Chem.*, vol. 49, no. 4, pp. 17–20, 2012.

[4] W. D. Nesse, *Introduction to Mineralogy*. New York: Oxford University Press, 2000.

[5] V. Roux and P. de Miroschedji, 'Revisiting the History of the Potter's Wheel in the Southern Levant', *Levant*, vol. 41, no. 2, pp. 155–173, 2009, doi: 10.1179/007589109X12484491671095.

[6] M. Bellotto, A. Gualtieri, G. Artioli, and S. M. Clark, 'Kinetic Study of the Kaolinite-Mullite Reaction Sequence. Part I: Kaolinite Dehydroxylation', *Phys. Chem. Miner.*, vol. 22, no. 4, pp. 207–217, 1995, doi: 10.1007/BF00202253.

[7] P. B. Vandiver, O. Soffer, B. Klima, and J. Svoboda, 'The Origins of Ceramic Technology at Dolni Vestonice, Czechoslovakia', *Science (80-.).*, vol. 246, no. 4933, pp. 1002–1008, 1989.

[8] X. Wu *et al.*, 'Early Pottery at 20,000 Years Ago in Xianrendong Cave, China', *Science (80-.).*, vol. 336, no. 6089, pp. 1696–1700, 2012, doi: 10.1126/science.1218643.

[9] A. H. Streily, 'Early Pottery Kilns in the Middle East', *Paléorient*, vol. 26, no. 2, pp. 69–81, 2000, [Online]. Available: https://www.persee.fr/doc/paleo_0153-9345_2000_num_26_2_4711.

[10] M. Spataro, A. Fletcher, C. R. Cartwright, and D. Baird, 'Boncuklu Höyük: the Earliest Ceramics on the Anatolian Plateau', *J. Archaeol. Sci. Reports*, 2016, [Online]. Available: http://dx.doi.org/10.1016/j.jasrep.2016.10.011.

[11] E. Akça *et al.*, 'Clues of Production for the Neolithic Çatalhöyük (Central Anatolia) Pottery', *Sci. Res. Essays*, vol. 4, no. 6, 2009.

[12] A. Lucas, 'Glazed Ware in Egypt, India, and Mesopotamia', *J. Egypt. Archaeol.*, vol. 22, no. 2, pp. 141–164, 1936, doi: 10.2307/3854623.

[13] T. Pradell, J. Molera, N. Salvadó, and A. Labrador, 'Synchrotron Radiation Micro-XRD in the Study of Glaze Technology', *Appl. Phys. A*, vol. 99, no. 2, pp. 407–417, 2010, doi: 10.1007/s00339-010-5639-7.

[14] P. B. Vandiver, 'Ancient Glazes', *Sci. Am.*, vol. 262, no. 4, pp. 106–113, 1990.

[15] T. Hansen, 'Crystallization', *Digital Fire Reference Library*, 2013. .

[16] H. Shen, G. Ma, N. Xian, and J. Li, ‘Application of Crystal Glaze in Architectural Pottery’, *IOP Conf. Ser. Earth Environ. Sci. 233(2)022039*, vol. 233, no. 2, pp. 22–39, 2019, doi: 10.1088/1755-1315/233/2/022039.

[17] P. Holakooei, ‘A Technological Study of the Elamite Polychrome Glazed Bricks at Susa, South-Western Iran’, *Archaeometry*, vol. 56, no. 5, pp. 764–783, 2014, doi: 10.1111/arcm.12030.

[18] A. Sroha, ‘Roman Floor Mosaics: Stories in Stone and Glass’, *Daily Art Magazine*, 2020. .

[19] İ. Yardımcı, ‘The Glazed Tile Techniques of the Seljuk and Beylik Periods’, *J. Lit. Art Stud.*, vol. 3, no. 1, pp. 42–51, 2013.

[20] J. Carswell, *Iznik Pottery*. British Museum Press, 2006.

[21] M. S. Tite, I. Freestone, R. Mason, J. Molera, M. Vendrell-Saz, and N. Wood, ‘Lead Glazes in Antiquity - Methods of Production and Reasons for Use’, *Archaeometry*, vol. 40, no. 2, pp. 241–260, 1998, doi: 10.1111/j.1475-4754.1998.tb00836.x.

[22] O. L.A, Z. M.C., A.-O. A., M. X., and A. A., ‘Petrographic and Geochemical Evidence for Long-Standing Supply of Raw Materials in Neolithic Pottery (Mendandia Site, Spain)”’, *Archaeometry*, vol. 52, no. 6, pp. 987–1001, 2010.

[23] P. T. Craddock, *Scientific Investigation of Copies, Fakes and Forgeries*. 2009.

[24] M. S. Walton, ‘A Materials Chemistry Investigation of Archaeological Lead Glazes’, 2004.

[25] M. Milwright, ‘Modest Luxuries: Decorated Lead-Glazed Pottery in the South of Bilad al-Sham (Thirteenth and Fourteenth Centuries)’, *Muqarnas*, vol. 20, pp. 85–111, 2003, [Online]. Available: https://www.jstor.org/stable/1523328.

[26] M. Budak Ünaler, ‘“Fine-Sgraffito Ware”, “Aegean Ware” from Anaia: an Analytical Approach’, 2013.

[27] W. D. . Kingery and V. P. B., *Ceramic Masterpieces, Art, Structure and Technology*. the Free Press, Division of Macmillan, Inc, 1986.

[28] S. Y. Waksman, N. D. Kontogiannis, S. S. Skartsis, and G. Vaxevanis, ‘The Main “Middle Byzantine Production” and Pottery Manufacture in Thebes and Chalkis’, *Annu. Br. Sch. Athens*, vol. 109, pp. 379–422, 2014.

[29] J. M. Stevels, ‘New Light on the Structure of Glass’, *Philips Tech. Rev.*, vol. 22, p. 300.

[30] E. Ringdalen and M. Tangstad, ‘Softening and Melting of SiO2, an Important Parameter for Reactions with Quartz in Si Production’, *Adv. Molten Slags, Fluxes, Salts Proc. 10th Int. Conf. Molten Slags, Fluxes Salts*, pp. 43–51, 2016, doi: 10.1007/978-3-319-48769-4_4.

[31] P. Green, ‘Introductory Glaze Composition’, *Garfield Campus Continuing Education, Glendale, California, USA*, 2019. .

[32] C. Tomczyk, K. Costa, A. Giosa, P. Brun, and C. Petit, ‘Provenance studies

using lead isotopy: contribution of the consideration of geological contexts in archaeological databases', *Bull. la Société Géologique Fr.*, vol. 192, no. 1, 2021, doi: 10.1051/bsgf/2021008.

[33] G. Simsek, O. Unsalan, K. Bayraktar, and P. Colomban, 'On-site pXRF analysis of glaze composition and colouring agents of "Iznik" tiles at Edirne mosques (15th and 16th-centuries)', *Ceram. Int.*, vol. 45, no. 1, pp. 595–605, 2019, doi: 10.1016/j.ceramint.2018.09.213.

[34] D. B. Arıkan Erciyas, 'Studies in the Archaeology of Hellenistic Pontus: the Settlements, Monuments, and Coinage of Mithrades VI and His Predecessors', Univ. of Cinninnati, 2001.

[35] M. N. Tatbul, 'Identifying Medieval Komana in the 12th-13th Centuries through Spatial Analysis of Archaeological Data with a Multidisciplinary Approach.', METU, 2017.

[36] B. Erciyas and E. Sökmen, 'An Overview of Byzantine Period Settlements around Comana Pontica in North-Central Turkey', *Byzantine Mod. Greek Stud.*, vol. 34, no. 2, pp. 119–141, 2010, doi: 10.1179/030701310X12572444129383.

[37] A. Öngül, 'Selçuklular Tarihi 2: Anadolu Selçukluları ve Beylikler. [Seljuk History 2: Anatolian Seljuks and Principalities]', *Çamlıca*, vol. 155, pp. 261–270, 2014.

[38] J. A. Cramer, *Geographical and Historical Description of Asia Minor*. 1832.

[39] W. J. Hamilton, *(1842) Researches in Asia Minor, Pontus, and Armenia*. London, 1842.

[40] D. G. Hogarth and J. A. R. Munro, *Modern and Ancient Roads in Eastern Asia Minor*. London, 1893.

[41] J. G. C. Anderson, *Studia Pontica I: A Journey of Exploration in Pontus*. Bruxelles, 1902.

[42] D. B. Erciyas, '27. Uluslararası Kazı, Araştırma ve Arkeometri Sempozyumu: Tokat İli Komana Antik Kenti Yüzey Araştırması 2004 [27th International Excavation, Research and Archaeometry Symposium: Surface Survey in 2014 on the Ancient City Comana Pontica in Tokat]', 2006.

[43] D. B. Erciyas, '28. Uluslararası Kazı, Araştırma ve Arkeometri Sempozyumu Komana Yüzey Araştırması 2005 [28th International Excavation, Research and Archaeometry Symposium: Surface Survey in 2005 on Comana]', 2007.

[44] Y. E. Karasu, 'Komana Anadolu Selçuklu Çağı Seramikleri [Ceramics of Comana from the Anatolian Seljuks' Period]', 2020.

[45] D. B. Erciyas and M. N. Tatbul, 'Komana'da 2016 Yılı Arkeolojik Araştırmaları, 35. Araştırma Sonuçları Toplantısı [Archaeological Research at Comana in 2016, 35th Research Results Meeting]', 2018.

[46] P. Ivanova, 'The Coins: Danishmend/Seljuk Phase', in *Comana Small Finds*, D. B. Erciyas and M. A. Eser, Eds. Istanbul, 2019, p. 257.

[47] M. B. Er, ‘An Archaeometrical Investigation on Provenance and Technological Properties of Seljuk Period Pottery from Komana (Tokat)’, 2020.

[48] A. E. Aydın, ‘A Preliminary Archaeometallurgical Examination of Some Bronze Coins from Komana’, METU, 2019.

[49] L. Stoch, ‘Infrared Spectroscopy in the Investigation of Oxide Glasses Structure’, *J. Mol. Struct.*, vol. 511–512, pp. 77–84, 1999.

[50] E. Grammatikakis, Kyriakidis, D. Demadis, Cabeza Diaz, and Leon-Reina, ‘Mineralogical Characterization and Firing Temperature Delineation on Minoan Pottery, Focusing on the Application of Micro-Raman Spectroscopy’, *Heritage*, vol. 2, no. 3, pp. 2652–2664, 2019, doi: 10.3390/heritage2030163.

[51] G. Simsek, ‘Alkali ve Kurşun Alkali Sırların Yapısının Raman Spektroskopisi ile Karakterizasyonu [Characterization of Structures of Alkaline and Lead-Alkali Glazes with Raman Spectroscopy]’, Istanbul Technical University, 2011.

[52] D. Domnisoru and M. Praisler, ‘Non-destructive Analysis of Ceramic Samples by FTIR-ATR and Standard SEM Methods’, in *ModTech International Conference - New face of TMCR*, 2011, pp. 345–348.

[53] P. Colomban and L. Bellot-gurlet, ‘Raman identification of glassy silicates used in ceramics , glass and jewellery : a tentative’, doi: 10.1002/jrs.1515.

[54] P. Colomban, ‘Polymerization degree and Raman identification of ancient glasses used for jewelry, ceramic enamels and mosaics’, *J. Non. Cryst. Solids*, vol. 323, no. 1–3, pp. 180–187, 2003, doi: 10.1016/S0022-3093(03)00303-X.

[55] V. Tanevska, P. Colomban, B. Minceva-Sukarova, and O. Grupce, ‘Characterization of Pottery from the Republic of Macedonia I: Raman Analyses of Byzantine Glazed Pottery Excavated from Prilep andSkopje (12th–14th Century)’, *J. Raman Spectrosc.*, vol. 40, pp. 1240–1248, 2009, doi: 10.1002/jrs.2273.

[56] S. Shoval and P. Beck, ‘Thermo-FTIR Spectroscopy Analysis as a Method of Characterizing Ancient Ceramic Technology’, *J. Therm. Anal. Calorim.*, vol. 82, no. 3, pp. 609–616, 2005, doi: 10.1007/s10973-005-0941-x.

[57] M. Özçatal, M. Yaygıngöl Özparpucu, A. İşçi, and A. Kara, ‘Characterization of Lead Glazed Potteries from Smyrna (Izmir/Turkey) Using Multiple Analytical Techniques; Part I: Glaze and Engobe’, *Ceram. Int.*, vol. 40, no. 1, pp. 2143–2151, 2014, doi: 10.1016/j.ceramint.2013.09.014.

[58] P. Colomban and L. Prinsloo, ‘Optical Spectroscopy of Silicates and Glasses’, *Spectrosc. Prop. Inorg. Organomet. Compds.*, pp. 1–22, 2009, doi: 10.1039/b715005a.

[59] P. Colomban, A. Tournie, and L. Bellot-Gurlet, ‘Raman Identification of Glassy Silicates Used in Ceramics, Glass and Jewellery: a Tentative Differentiation Guide’, *J. Raman Spectrosc.*, vol. 37, no. 8, pp. 841–852, 2006, doi: 10.1002/jrs.1515.

[60] P. Colomban, ‘On-site Raman Spectroscopic Analysis of Kütahya Fritwares’, *J. Raman Spectrosc.*, vol. 36, pp. 857–863, 2005, doi: 10.1002/jrs.1372.

[61] J. Senvaitiene, J. Smirnova, A. Beganskiene, and A. Kareiva, ‘XRD and FTIR Characterisation of Lead Oxide-Based Pigments and Glazes’, *Acta Chim. Slov.*, vol. 54, no. 1, pp. 185–193, 2007.

[62] E. S. A. Serrano, D. Á. Prado, F. L. Martinez-Viviente, I. Mártil, D. Bravo, and F. J. López, ‘Rapid Thermal Annealing Effects on the Structural Properties and Density of Defects in SiO2 and SiNx:H Films Deposited by Electron Cyclotron Resonance’, *J. Appl. Physics.*, vol. 87, pp. 1187–1192, 2000, doi: 10.1063/1.371996.

[63] M. Chen, A. K. Santra, and D. Goodman, ‘Structure of Thin SiO2 Films Grown on Mo(112)’, *Am. Phys. Soc.*, vol. 69, no. 15, 2004, doi: 10.1103/PHYSREVB.69.155404.

[64] H. Ouhaddouch, A. Cheikh, M. O. Idrissi, M. Draoui, and M. Bouatia, ‘FT-IR Spectroscopy Applied for Identification of a Mineral Drug Substance in Drug Products: Application to Bentonite’, *J. Spectrosc.*, 2019, doi: 10.1155/2019/2960845.

[65] M. Petrunin *et al.*, ‘Formation of Organosilicon Self-Organizing Nanolayers on an Iron Surface from Vapor Phase and Their Effect on Corrosion Behavior of Metal 1010-1017’, *Prot. Met. Phys. Chem. Surfaces*, vol. 51, 2015, doi: 10.1134/S2070205115060179.

[66] S. Vahur, A. Teearu, P. Peets, L. Joosu, and I. Leito, ‘ATR-FT-IR Spectral Collection of Conservation Materials in the Extended Region of 4000-80 cm–1’, *Anal. Bioanal. Chem.*, vol. 408, pp. 3373–3379, 2016, doi: 10.1007/s00216-016-9411-5.

[67] P. Djomgoue and D. Njopwouo, ‘FT-IR Spectroscopy Applied for Surface Clays Characterization’, *J. Surf. Eng. Mater. Adv. Technol.*, vol. 3, no. 4, pp. 275–282, 2013, doi: 10.4236/jsemat.2013.34037.

[68] R.-M. Ion *et al.*, *Ceramic Materials Based on Clay Minerals in Cultural Heritage Study*. 2016.

[69] A. A. Adeyemo, I. O. Adeoye, and O. S. Bello, ‘Adsorption of Dyes Using Different Types of Clay: a Review’, *Appl. Water Sci.*, vol. 7, pp. 543–568, 2017.

[70] W. W. Mar and E. Somsook, ‘Methanolysis of Soybean Oil over KCl/CaO Solid Basecatalyst for Biodiesel Production’, *ScienceAsia*, vol. 38, pp. 90–94, 1012.

[71] S. Shoval, ‘Using FT-IR spectroscopy for study of calcareous ancient ceramics’, *Opt. Mater. (Amst).*, vol. 24, no. 1–2, pp. 117–122, Oct. 2003, doi: 10.1016/S0925-3467(03)00114-9.

[72] L. Damjanović, V. Bikić, K. Šarić, S. Erić, and I. Holclajtner-Antunović, ‘Characterization of the Early Byzantine Pottery from Caričin Grad (South Serbia) in Terms of Composition and Firing Temperature’, *J. Archaeol. Sci.*,

vol. 46, pp. 156–172, 2014.

[73] A. Raškovska, B. Minčeva-Šukarova, O. Grupče, and P. Colomban, ‘Characterization of Pottery from Republic of Macedonia II. Raman and Infrared Analyses of Glazed Pottery Finds from Skopsko Kale’, *J. Raman Spectrosc.*, pp. 431–439, 2009, doi: 10.1002/jrs.2463.

[74] S. Shoval, ‘The Firing Temperature of a Persian-Period Pottery Kiln at Tel Michal, Israel, Estimated from the Composition of Its Pottery’, *J. Therm. Anal.*, vol. 42, no. 1, pp. 175–185, 1994.

[75] J. Rubio, J. . L. Oteo, S. Sánchez-Cortés, A. Tamayo, and F. Rubio, ‘Application of Raman and FT-IR Spectroscopy to the Study of Ceramic Glazes’, *Qualicer*, vol. Castellon, pp. 183–186, 2008.

[76] P. Benna, M. Tribaudino, and E. Bruno, ‘The Structure of Ordered and Disordered Lead Feldspar (PbAl2Si2O8)’, *Am. Mineral.*, vol. 81, no. 11, pp. 1337–1343, 1996.

[77] J. H. Pee, H. S. Choi, K. J. Kim, J. H. Ryu, G. I. Gang, and H. Katsuki, ‘Effects of Firing Atmosphere on the ColorManifestation of Celadon’, *IOP Conf. Ser. Mater. Sci. Eng.*, vol. 18, pp. 1–4, 2011, doi: 10.1088/1757-899X/18/22/222020.

[78] B. Peterson, ‘Ceramic and Glaze Colorants’, *The Spruce*, 2018. .

[79] L. Damjanović-Vasilić, V. Bikic, S. Stojanović, D. Bajuk-Bogdanović, Đ. Džodan, and S. Mentus, ‘Application of Analytical Techniques for Unveiling the Glazing Technology of Medieval Pottery from the Belgrade Fortress’, *J. Serbian Chem. Soc.*, vol. 85, pp. 1–15, 2020, doi: 10.2298/JSC200401036D.

[80] F. Schweizer and A. Rinuy, ‘Manganese Black as an Etruscan Pigment’, *Stud. Conserv.*, vol. 27, no. 3, pp. 118–123, 1982, doi: 10.2307/1506147.

[81] B. D. Çiftçi, ‘Archaeometrical Studies on Plasters of Some Historical Buildings’, Middle East Technical University, 2007.

[82] T. Hansen, ‘Opacifier’, *Reference Library*, 2023. https://digitalfire.com/glossary/opacifier.

[83] T. Hansen, ‘Sb2O3 (Antimony Oxide)’, *Reference Library*, 2023. https://digitalfire.com/oxide/sb2o3.

[84] G. W. Brindley and M. Nakahira, ‘The Kaolinite-Mullite Reaction Series: II, Metakaolin’, *J. Am. Ceram. Soc.*, vol. 42, no. 7, pp. 314–318, 2006, doi: 10.1111/j.1151-2916.1959.tb14315.x.

[85] H.-K. Mao and W. L. Mao, ‘Theory and Practice – Diamond-Anvil Cells and Probes for High P–T Mineral Physics Studies’, *Treatise Geophys.*, pp. 250–256, 2007, doi: 10.1016/b978-044452748-6.00037-7.

[86] G. Şimşek Franci, ‘Alkali ve Kurşun Alkali Sırların Yapısının Raman Spektroskopisi ile Karakterizasyonu’, 2011.

[87] Trinitat Pradell and J. Molera, ‘Ceramic technology. How to characterise ceramic glazes’, *Archaeol. Anthropol. Sci.*, vol. 12, no. 8, pp. 1–28, 2020, doi:

10.1007/s12520-020-01136-9.

[88] X. Zhang, ‘Preparation and Characterization of Calcium Phosphate Ceramics and Composites as Bone Substitutes’, University of California, San Diego, 2007.

[89] K. Dark, *Byzantine Pottery*. The History Press LTD, 2001.

[90] N. Kilic-Schubel, ‘Timurid Empire’, in *he Encyclopedia of Empire*, N. Dalziel and J. M. MacKenzie, Eds. 2016.

[91] H. Hatcher, A. Kaczmarczyk, A. Scherer, and R. P. Symonds, ‘Chemical Classification and Provenance of Some Roman Glazed Ceramics’, *Am. J. Archaeol.*, vol. 98, no. 3, pp. 431–456, 1994, [Online]. Available: https://www.jstor.org/stable/506438.

[92] I. C. Freestone, ‘An early Byzantine alkali glazing tradition? Discussion of P. Armstrong (2020). The earliest glazed ceramics in Constantinople: A regional or international phenomenon? , 29, 102,078’, *J. Archaeol. Sci. Reports*, vol. 35, 2021.

[93] J. R. Wood and M. Greenacre, ‘Making the most of expert knowledge to analyse archaeological data: a case study on Parthian and Sasanian glazed pottery’, *Archaeol. Anthropol. Sci.*, vol. 13, no. 7, 2021, doi: 10.1007/s12520-021-01341-0.

[94] M. S. Tite, ‘The technology of glazed Islamic ceramics using data collected by the late Alexander Kaczmarczyk’, *Archaeometry*, vol. 53, no. 2, pp. 329–339, 2010, doi: 10.1111/j.1475-4754.2010.00546.x.

[95] J. R. Wood and Y.-T. Hsu, ‘Recycling Roman Glass to Glaze Parthian Pottery’, *IRAQ*, pp. 1–12, 2020, doi: :10.1017/irq.2020.9.

[96] R. Gradmann, ‘Analysis of Historical Islamic Glazes and the Development of a Substitution Material’, Julius Maximilians University Würzburg, 2016.

[97] I. A. Kiseleva, L. P. Ogorodova, L. V. Melchakova, M. R. Bisengalieva, and N. S. Becturganov, ‘Thermodynamic properties of copper carbonates — malachite Cu2(OH)2CO3 and azurite Cu3(OH)2(CO3)2’, *Phys. Chem. Miner.*, vol. 19, pp. 322–333, 1992.

[98] T. Hansen, ‘Common ceramic oxides’, *Digital Fire Reference Library*, 2021. .

[99] Ş. Demirci, E. N. Caner-Saltık, A. Türkmenoğlu, S. Özçilingir-Akgün, and Ö. Bakırer, ‘Raw Material Characteristics and Technological Properties of Some Medieval Glazed Ceramics and Tiles in Anatolia’, *Key Eng. Mater.*, vol. 264–268, pp. 2395–2398, 2004, doi: 10.4028/www.scientific.net/kem.264-268.2395.

[100] F. J. Torres and J. Alarcon, ‘Mechanism of crystallization of pyroxene-based glass-ceramic glazes’, *J. Non. Cryst. Solids*, vol. 347, pp. 45–51, 2004.

[101] K. Kihara, T. Matsumoto, and M. Mamura, ‘Structural change of orthorhombic-I tridymite with temperature: A study based on second-order

thermal-vibrational parameters', *Zeitschrift für Krist.*, vol. 177, pp. 27–38, 1986, doi: 10.1524/zkri.1986.177.1-2.27.

[102] D. O. Testov, K. G. Gareev, I. K. Khmelnitskiy, A. Kosterov, E. V. Maraeva, and I. V. Klimtsova, 'Synthesis of High-Coercive Epsilon-Iron Oxide Nanoparticles for Biomedical Applications', in *Conference of Russian Young Researchers in Electrical and Electronic Engineering (ElConRus)*, 2022, pp. 1620–1623, [Online]. Available: 10.1109/ElConRus54750.2022.9755783.

[103] R. Akhter, L. Li, R. E. Edwards, and A. W. Gale, 'Porosity/bubble formation mechanism in laser surface enamelling', *Appl. Surf. Sci.*, vol. 208–209, pp. 447–452, 2003.

[104] A. T. Anderson, R. Friedman, J. Otto, T. Vander Wood, and J. Wyszynski, 'The Fractional Crystallization of Plagioclase in the Hat Creek Basalt: Observations and Theory', *J. Geol.*, vol. 90, no. 5, pp. 545–558, 1982.

[105] S. Coentro *et al.*, 'Mineralogical Characterization of Hispano-Moresque Glazes: A μ-Raman and Scanning Electron Microscopy with X-Ray Energy Dispersive Spectrometry (SEM-EDS) Study', *Microsc. Microanal.*, pp. 1–10, 2018, doi: 10.1017/S1431927618000338.

[106] D. Medeghini, L., Lottici, P. P., De Vito, C., Mignardi, S., & Bersani, 'Micro-Raman spectroscopy and ancient ceramics: applications and problems', *J. Raman Spectrosc.*, vol. 45, no. 11–12, pp. 1244–1250, 2014, doi: 10.1002/jrs.4583.

[107] S. M. Angel, N. R. Gomer, S. K. Sharma, and C. McKay, 'Remote Raman Spectroscopy for Planetary Exploration: A Review', *Appl. Spectrosc.*, vol. 66, no. 2, pp. 137–150, 2012, doi: 10.1366/11-06535.

[108] S. K. Sharma, A. K. Misra, S. Ismail, and U. N. Singh, 'Remote Raman Spectroscopy of Various Mixed and Composite Mineral Phases at 7.2 m Distance', 2006, [Online]. Available: https://ntrs.nasa.gov/citations/20060010179.

[109] L. Husby, 'Firing Temperatures & Cone Equivalents', 2013.

[110] R. M. Riefstahl, *Early Turkish tile revetments in Edirne*, vol. 4. Freer Gallery of Art, The Smithsonian Institution & Department. of the History of Art, University of Michigan, 1937.

[111] R. W. Grimshaw, *Reactions at High Temperatures, the Chemistry and Physics of Clays*. Techbooks, India, 1971.

[112] B. Downs, 'RRUFF Project Sample Data Search', *University of Arizona*, 2021. https://rruff.info/.

[113] S. Mutlu, 'Tanrıça Ma (Mã) ve Kappadokia Komana'sı [The Goddess Ma (Mã) and Comana in Cappadocia]', *Phaselis - Disiplinlerarası Akdeniz Araştırmaları Derg. [Journal Interdiscip. Mediterr. Stud.*, vol. 2, pp. 311–322, 2016.

[114] M. Ackermann *et al.*, *Putzger Historischer Weltatlas [Putzger Historical World Atlas]*. Cornelsen Publishing, 1985.

[115] W. D. Callister. and D. G. Rethwisch, *Fundamentals of Materials Science and Engineering: An Integrated Approach*, 5th Editio. 2018.

APPENDICES

A.1. Appendix of Images and Code Numbers of the Glazed Samples

The images of tiles and potsherds are listed in Table 11 and Table 12 below, respectively. Indications of interior and exterior sides are expressed as seen in the Figure 72 below. The length of the bar, consisting of red and black squares with 1 cm^2 each, is totally 10 cm.

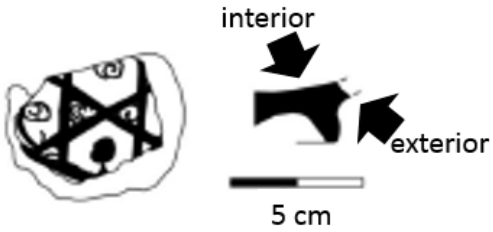

Figure 72. Pottery drawing of the base of K128 and its side view with expressions of interior and exterior sides. Adapted from [47].

Table 11. Images of the tiles.

K001 interior | K001 exterior | K002 interior | K002 exterior

Table 12. Images of the potsherds.

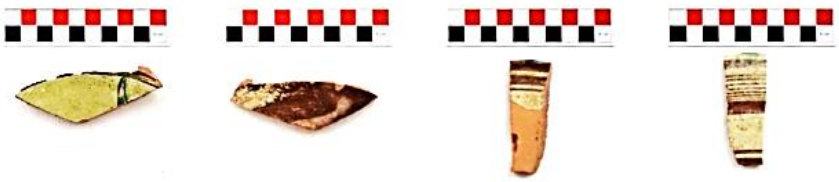

K101 interior | K101 exterior | K102 interior | K102 exterior

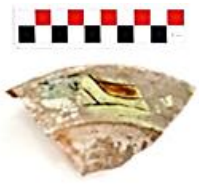

K103 interior

K103 exterior

K104 interior

K104 exterior

K105 interior

K105 exterior

K106 interior

K106 exterior

K108 interior

K108 exterior

K109 interior

K109 exterior

K110 interior

K110 exterior

K111 interior

K111 exterior

K112 interior

K112 exterior

K113 interior

K113 exterior

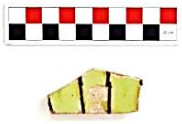

K114 interior

K114 exterior

K115 interior

K115 exterior

K117 interior

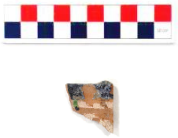

K117 exterior

K118 interior

K118 exterior

K119 interior

K119 exterior

K122 interior

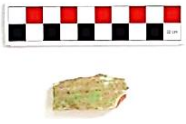

K122 exterior

K123 interior

K123 exterior

K124 interior

K124 exterior

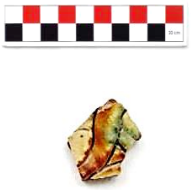

K125 interior

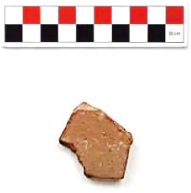

K125 exterior

K128 interior

K128 exterior

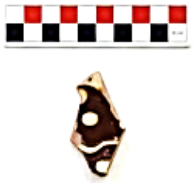

K129 interior

K129 exterior

K130 interior

K130 exterior

K131 interior

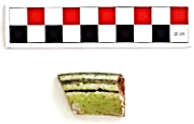

K131 exterior

K132 interior

K132 exterior

K143 interior

K143 exterior

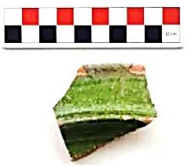

K144 interior

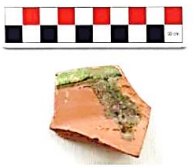

K144 exterior

K145 interior

K145 exterior

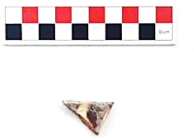

K146 interior

K146 exterior

K147 interior

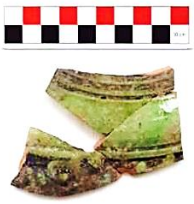

K147 exterior

K148 interior

K148 exterior

K149 interior

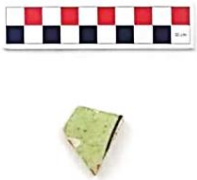

K149 exterior

K150 interior

K150 exterior

K151 interior

K151 exterior

K152 interior

K152 exterior

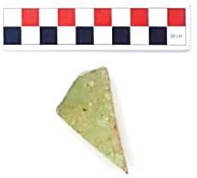

K153 interior

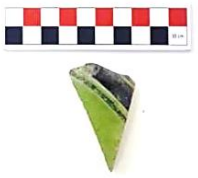

K153 exterior

K154 interior

K154 exterior

K155 interior

K155 exterior

K156 interior

K156 exterior

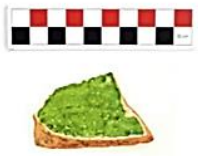

K157 interior

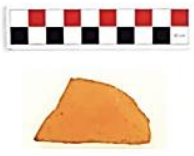

K157 exterior

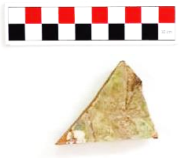

K158 interior

K158 exterior

K159 interior

K159 exterior

K160 interior

K160 exterior

K161 interior

K161 exterior

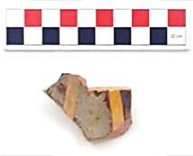

K164 interior

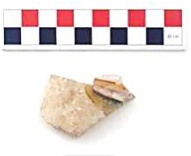

K164 exterior

K167 interior

K167 exterior

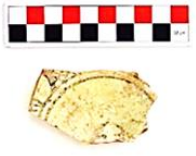

K168 interior

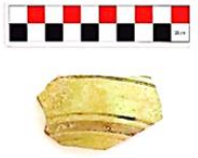

K168 exterior

K169 interior

K169 exterior

K170 interior

K170 exterior

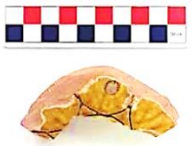

K171 interior

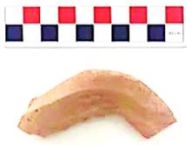

K171 exterior

K172 interior

K172 exterior

K173 interior

K173 exterior

K184 interior

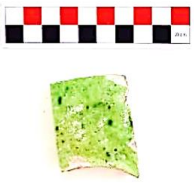

K184 exterior

K185 interior

K185 exterior

K199 interior

K199 exterior

K200 interior

K200 exterior

K201 interior

K201 exterior

K203 interior

K203 exterior

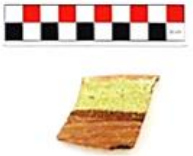

K204 interior

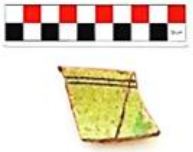

K204 exterior

K210 interior

K210 exterior

K211 interior

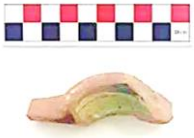

K211 exterior

K212 interior

K212 exterior

K213 interior

K213 exterior

K215 interior

K215 exterior

K220 interior

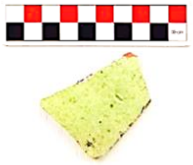

K220 exterior

K221 interior

K221 exterior

K222 interior

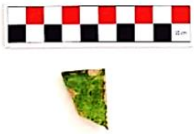

K222 exterior

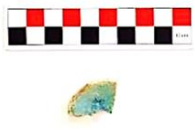

K223 interior

K223 exterior

K226 interior

K226 exterior

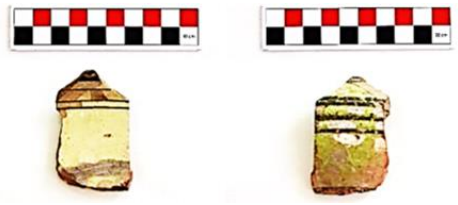

K228 interior K228 exterior

A.2. Appendix of FTIR Spectroscopy Results and Estimated Firing Temperatures of the Glazed Samples

Below, the graphs of the FTIR spectroscopy of the glazed samples are drawn with respect to the percent transmittance vs. wavenumber (cm^{-1}) (without baseline correction) together with the magnified view of the maximum peak point put in the box placed on the right below corners of each spectrum and the estimated firing temperatures calculated by the equations corresponding to the wavenumber of the local maxima. For each local maximum, there are 3 temperature values written hyphenated, such as 670-770-825 °C, which means the value in the middle is the corresponding temperature of the maximum wavenumber, however due to the resolution with 4 cm^{-1}, the wavenumber region falling within ±4 cm^{-1} frame becomes important and the temperature values corresponding to the end points of the frame may also contribute to the determination of the firing temperature, so that these values are also added before and after the middle value separated by hyphens. In each table below the spectrum, name of the sample with its code number and color are written in the box of "pellet" and the numbers at the end of the color represents from which replicate experiment that spectrum is taken. Moreover, if there are two peaks observed in the Si-O stretching band, the one with the greater area and lower percent transmittance is written more below on the spectrum, on which estimation of firing temperatures are referred to.

A.2.1. FTIR Spectra of the Yellow Glazes

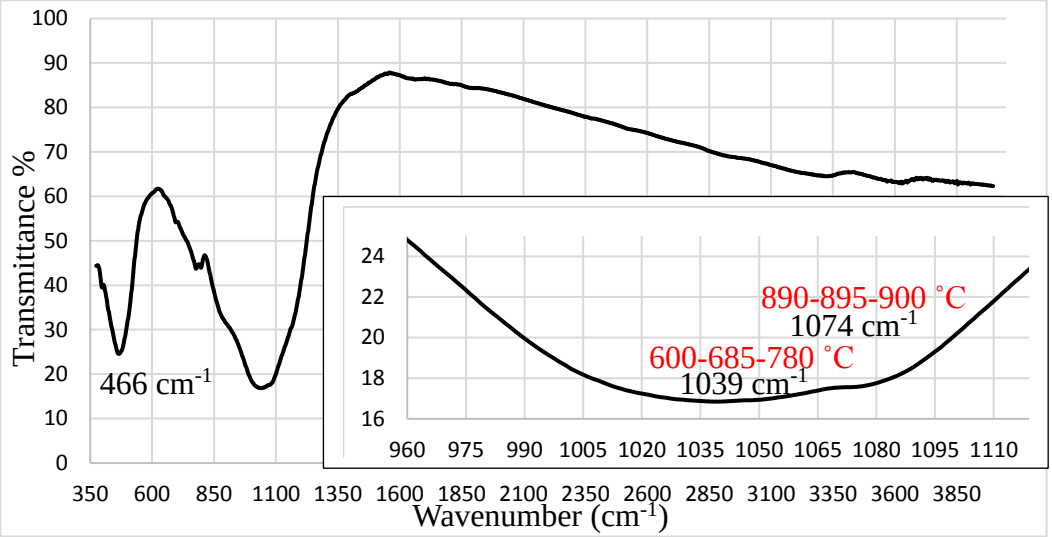

Figure 73. FTIR spectrum of the yellow glaze of the sample K102.

Even though the maximum peak is at 1039 cm^{-1} which corresponds to the 685 °C, it is observed that the maximum point of the peak is changing within the range of ±4 cm^{-1} when the number of the different pellets gathered from the same glaze with different locations is increased. Since at least 600 °C is needed for the occurrence of the glaze, the temperature values, that are found below 600 °C because of the addition of Pb, are considered in the range of 600-700 °C.

Hence, the final decision of the firing temperature for the yellow glaze of K102 below is made by rounding the numbers placed in the middle (685 °C) and the latter (780 °C) of the greatest peak, for instance it is rounded to 700-800 °C for this case.

Table 13. Estimation of the firing temperature of the yellow glaze of K102.

Pellet	Res	# of Scans	ν (cm^{-1})	T_{firing} (˚C)
K102.yellow.01	4	128	1039 & 1074	700-800

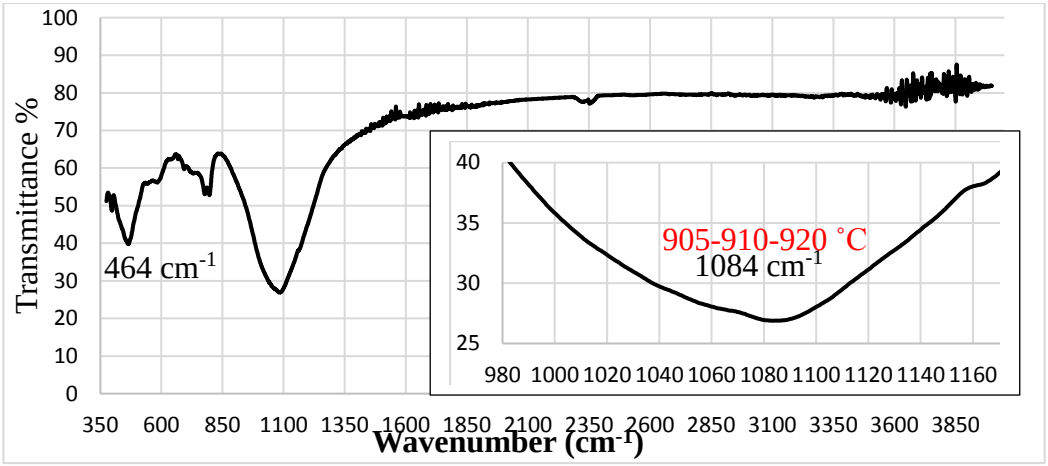

Figure 74. FTIR spectrum of the yellow glaze of the sample K104.

Table 14. Estimation of the firing temperature of the yellow glaze of K104.

Pellet	Res	# of Scans	ν (cm^{-1})	T_{firing} (˚C)
K104.yellow.02	4	512	1084	900-925

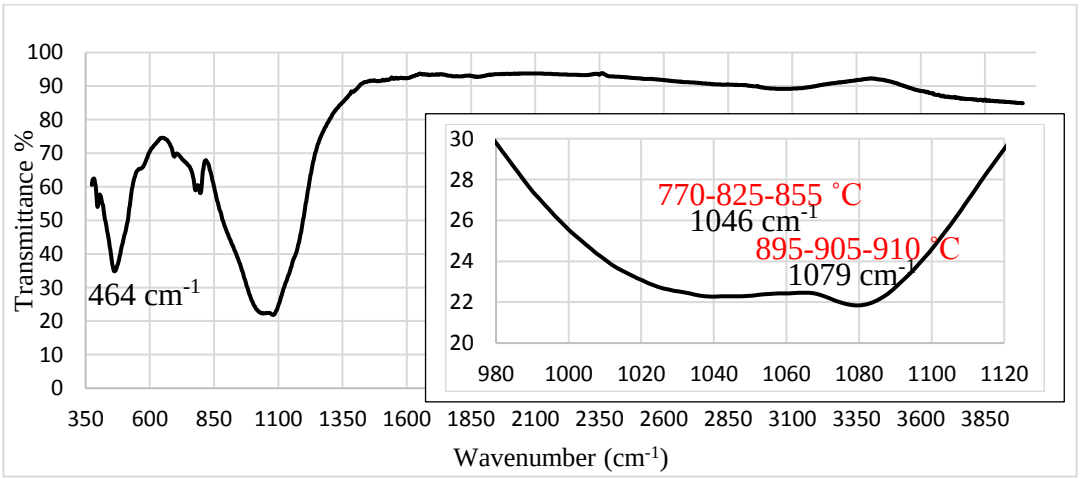

Figure 75. FTIR spectrum of the yellow glaze of the sample K106.

Table 15. Estimation of the firing temperature of the yellow glaze of K106.

Pellet	Res	# of Scans	ν (cm^{-1})	T_{firing} (˚C)
K106.yellow.01	4	128	1079	900-925

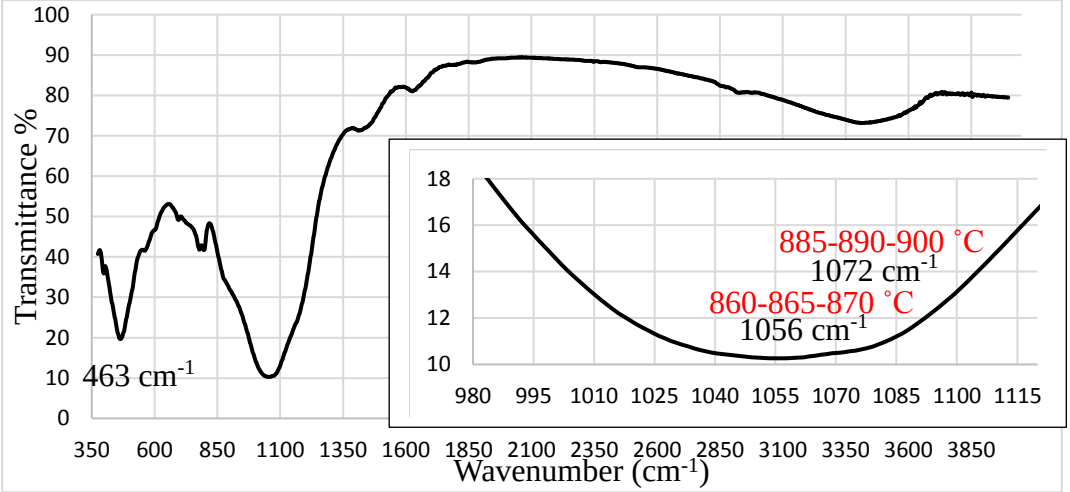

Figure 76. FTIR spectrum of the yellow glaze of the sample K108.

Table 16. Estimation of the firing temperature of the yellow glaze of K108.

Pellet	Res	# of Scans	ν (cm^{-1})	T_{firing} (˚C)
K108.yellow.01	4	128	1056 & 1072	850-900

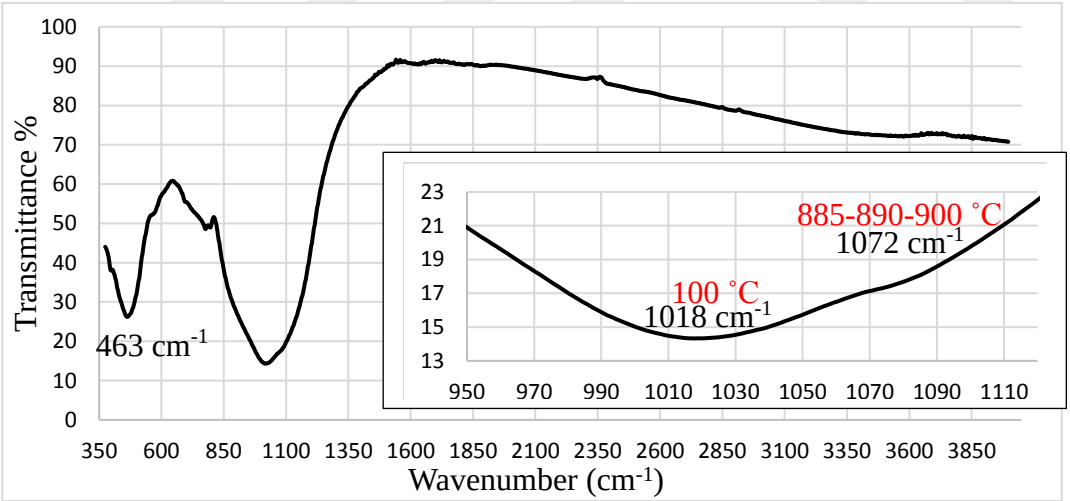

Figure 77. FTIR spectrum of the yellow glaze of the sample K111.

Table 17. Estimation of the firing temperature of the yellow glaze of K111.

Pellet	Res	# of Scans	ν (cm^{-1})	T_{firing} (˚C)
K111.yellow.01	4	128	1018 & 1072	600-700

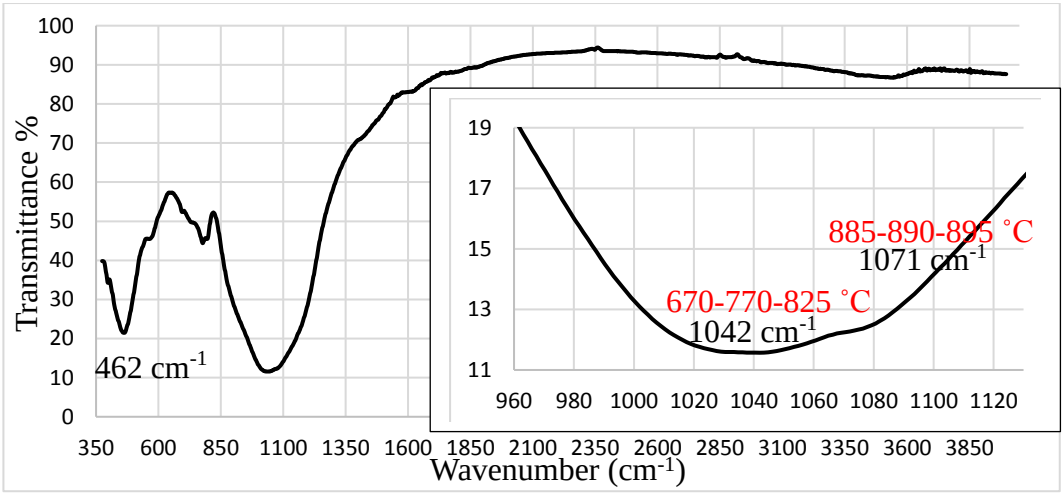

Figure 78. FTIR spectrum of the yellow glaze of the sample K112.

Table 18. Estimation of the firing temperature of the yellow glaze of K112.

Pellet	Res	# of Scans	v (cm^{-1})	T_{firing} (˚C)
K112.yellow.04	4	128	1042 & 1071	775-825

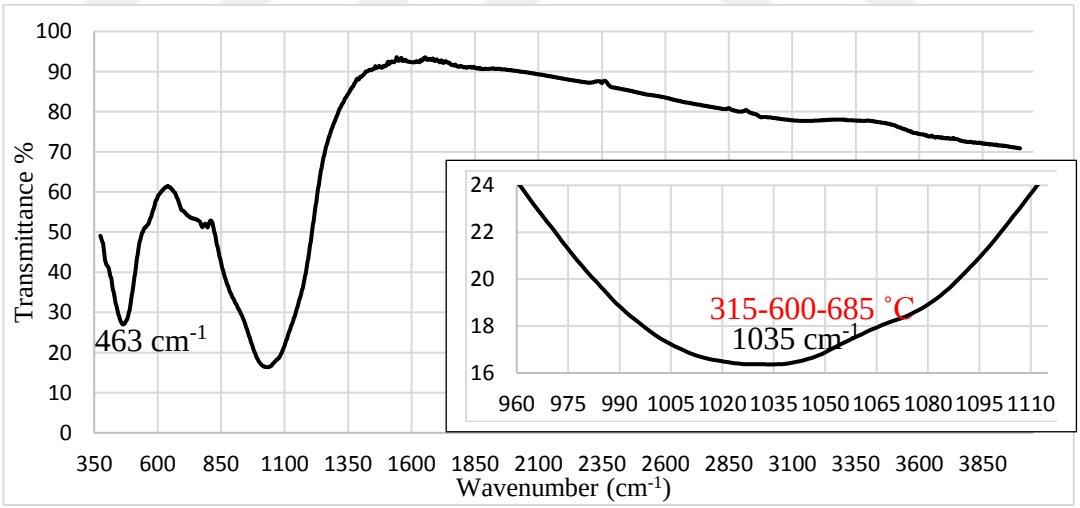

Figure 79. FTIR spectrum of the yellow glaze of the sample K113.

Table 19. Estimation of the firing temperature of the yellow glaze of K113.

Pellet	Res	# of Scans	v (cm^{-1})	T_{firing} (˚C)
K113.yellow.01	4	128	1035	600-700

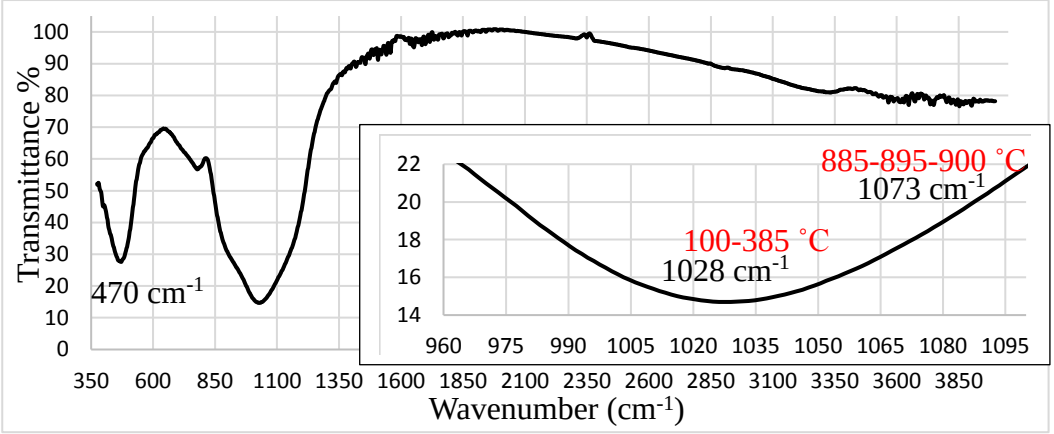

Figure 80. FTIR spectrum of the yellow glaze of the sample K115.

Table 20. Estimation of the firing temperature of the yellow glaze of K115.

Pellet	Res	# of Scans	ν (cm^{-1})	T_{firing} (˚C)
K115.yellow.01	4	128	1028 & 1073	600-700

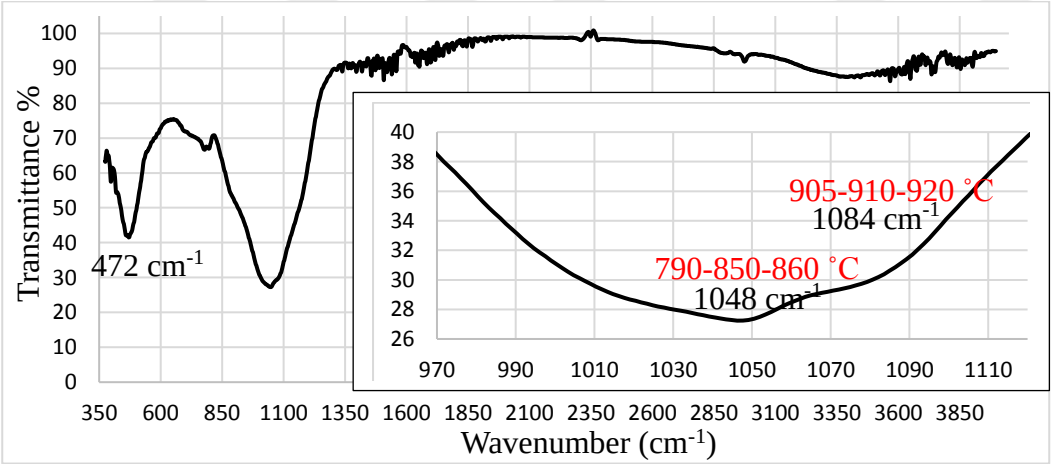

Figure 81. FTIR spectrum of the yellow glaze of the sample K122.

Table 21. Estimation of the firing temperature of the yellow glaze of K122.

Pellet	Res	# of Scans	ν (cm^{-1})	T_{firing} (˚C)
K122.yellow.01	4	128	1048 & 1084	850-900

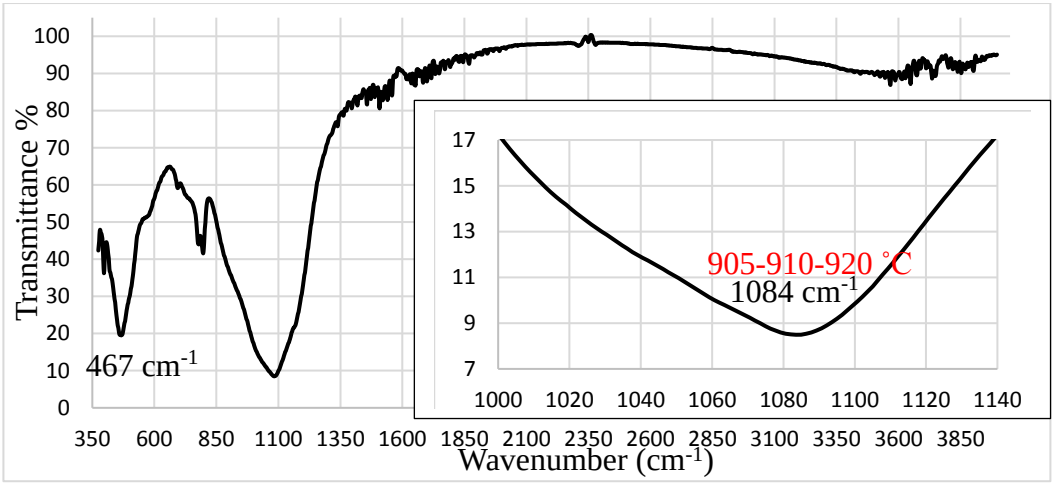

Figure 82. FTIR spectrum of the yellow glaze of the sample K125.

Table 22. Estimation of the firing temperature of the yellow glaze of K125.

Pellet	Res	# of Scans	ν (cm^{-1})	T_{firing} (˚C)
K125.yellow.01	4	128	1084	900-925

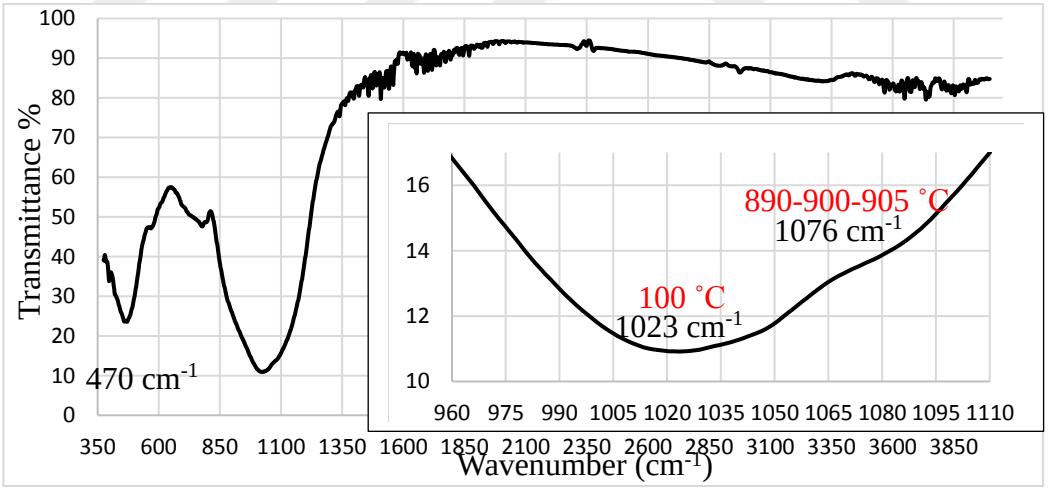

Figure 83. FTIR spectrum of the yellow glaze of the sample K128.

Table 23. Estimation of the firing temperature of the yellow glaze of K128.

Pellet	Res	# of Scans	ν (cm^{-1})	T_{firing} (˚C)
K128.yellow.01	4	128	1023 & 1076	600-700

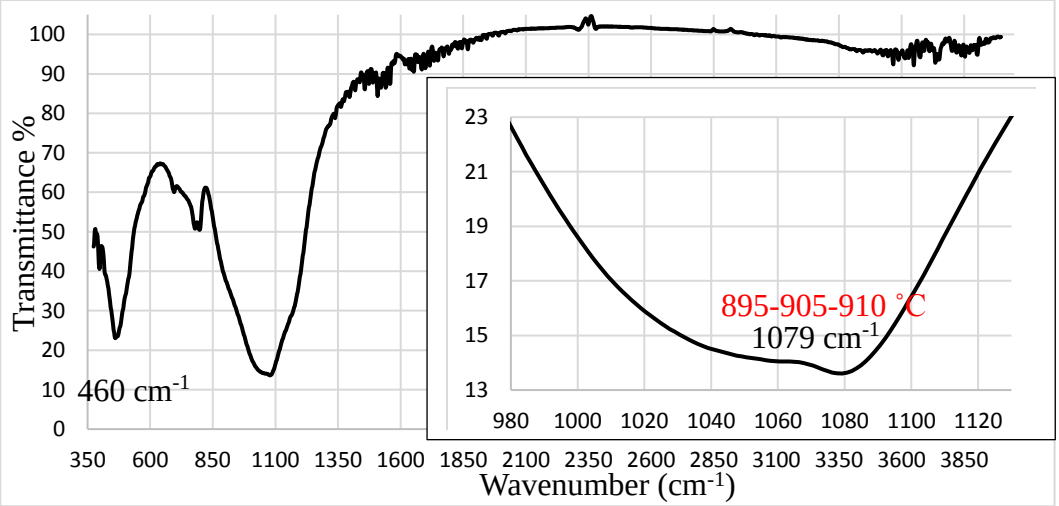

Figure 84. FTIR spectrum of the yellow glaze of the sample K129.

Table 24. Estimation of the firing temperature of the yellow glaze of K129.

Pellet	Res	# of Scans	ν (cm^{-1})	T_{firing} (˚C)
K129.yellow.01	4	128	1079	900-925

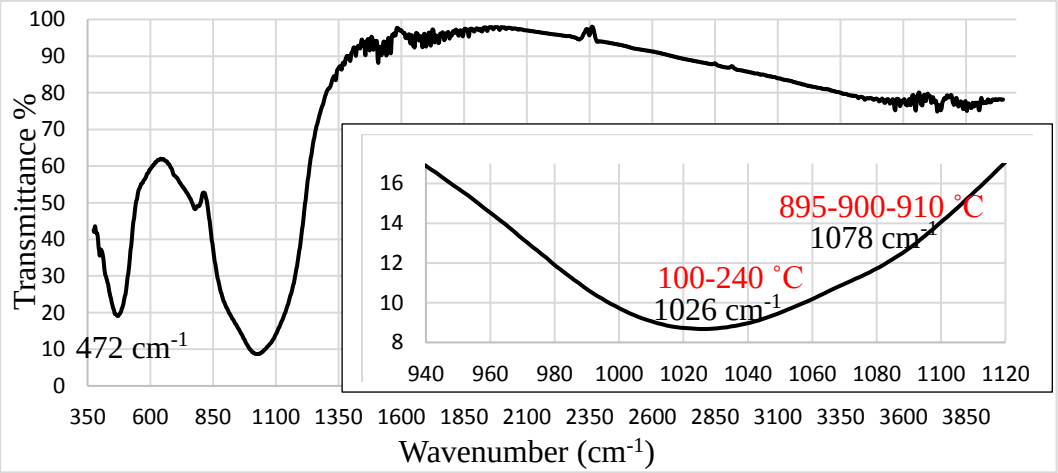

Figure 85. FTIR spectrum of the yellow glaze of the sample K130.

Table 25. Estimation of the firing temperature of the yellow glaze of K130.

Pellet	Res	# of Scans	ν (cm^{-1})	T_{firing} (˚C)
K130.yellow.01	4	128	1026 & 1078	600-700

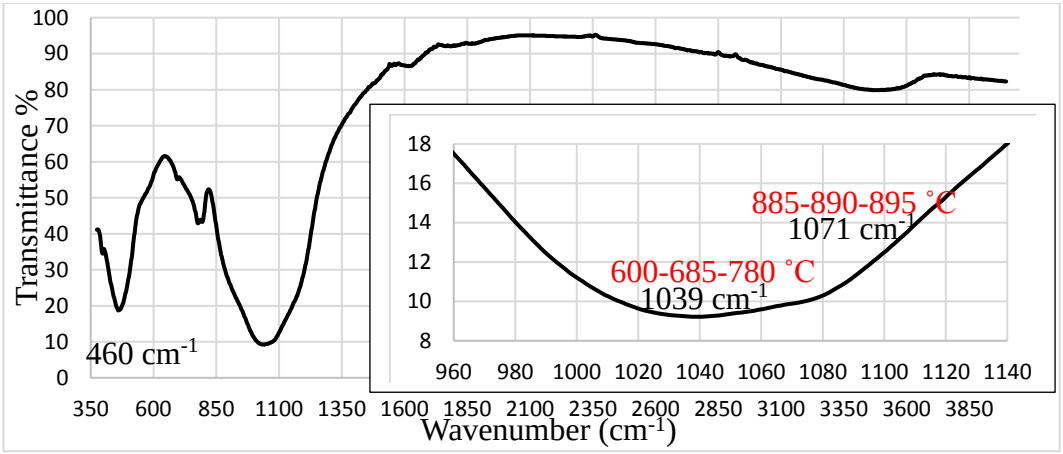

Figure 86. FTIR spectrum of the yellow glaze of the sample K131.

Table 26. Estimation of the firing temperature of the yellow glaze of K131.

Pellet	Res	# of Scans	v (cm^{-1})	T_{firing} (˚C)
K131.yellow.03	4	128	1039 & 1071	700-800

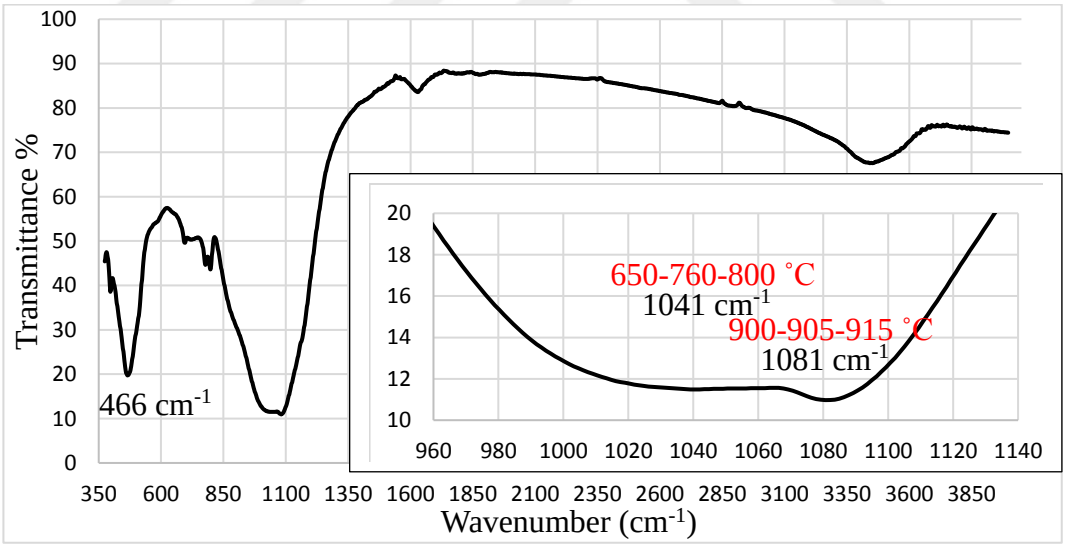

Figure 87. FTIR spectrum of the yellow glaze of the sample K132.

Table 27. Estimation of the firing temperature of the yellow glaze of K132.

Pellet	Res	# of Scans	v (cm^{-1})	T_{firing} (˚C)
K132.yellow.02	4	128	1081	900-925

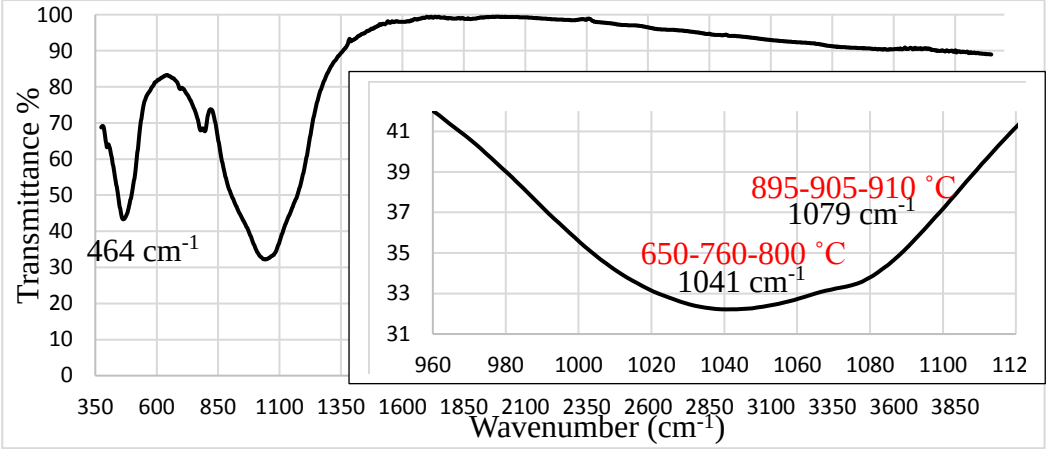

Figure 88. FTIR spectrum of the yellow glaze of the sample K148.

Table 28. Estimation of the firing temperature of the yellow glaze of K148.

Pellet	Res	# of Scans	v (cm^{-1})	T_{firing} (˚C)
K148.yellow.02	4	128	1041 & 1079	750-800

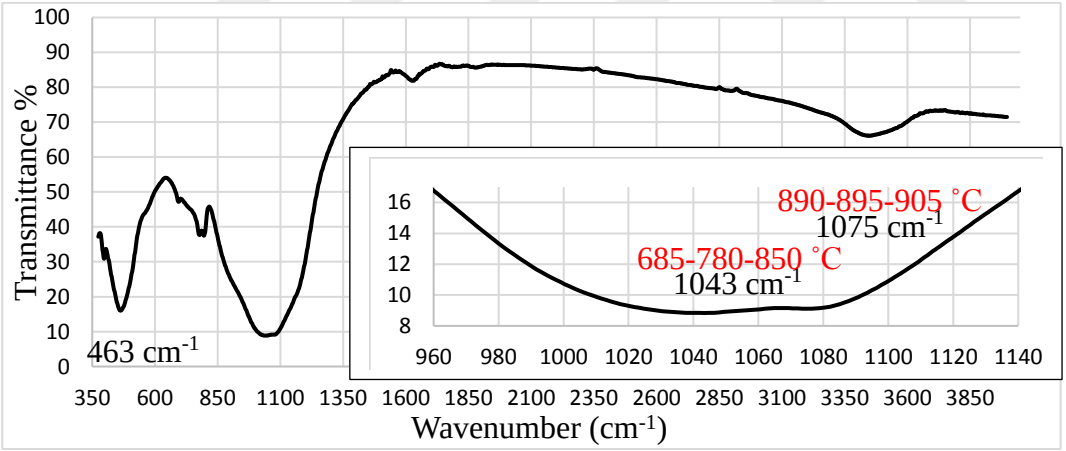

Figure 89. FTIR spectrum of the yellow glaze of the sample K149.

Table 29. Estimation of the firing temperature of the yellow glaze of K149.

Pellet	Res	# of Scans	v (cm^{-1})	T_{firing} (˚C)
K149.yellow.03	4	128	1043 & 1075	775-850

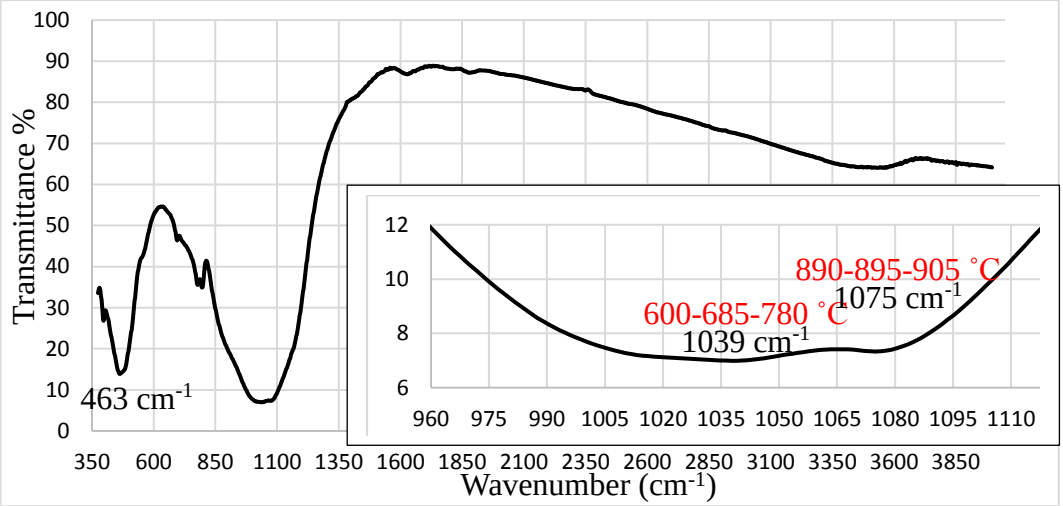

Figure 90. FTIR spectrum of the yellow glaze of the sample K151.

Table 30. Estimation of the firing temperature of the yellow glaze of K151.

Pellet	Res	# of Scans	ν (cm^{-1})	T_{firing} (˚C)
K151.yellow.02	4	128	1039 & 1075	700-800

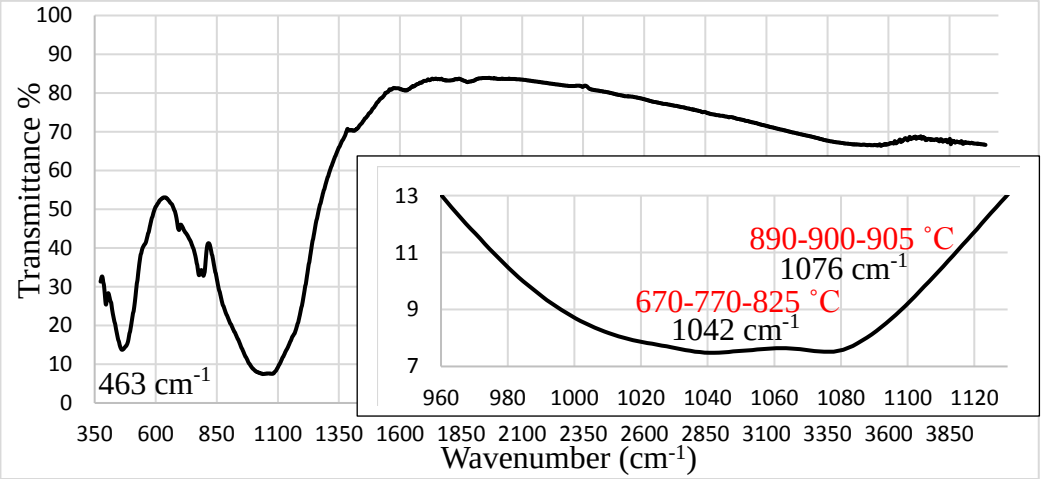

Figure 91. FTIR spectrum of the yellow glaze of the sample K152.

Table 31. Estimation of the firing temperature of the yellow glaze of K152.

Pellet	Res	# of Scans	ν (cm^{-1})	T_{firing} (˚C)
K152.yellow.02	4	128	1042 & 1076	775-825

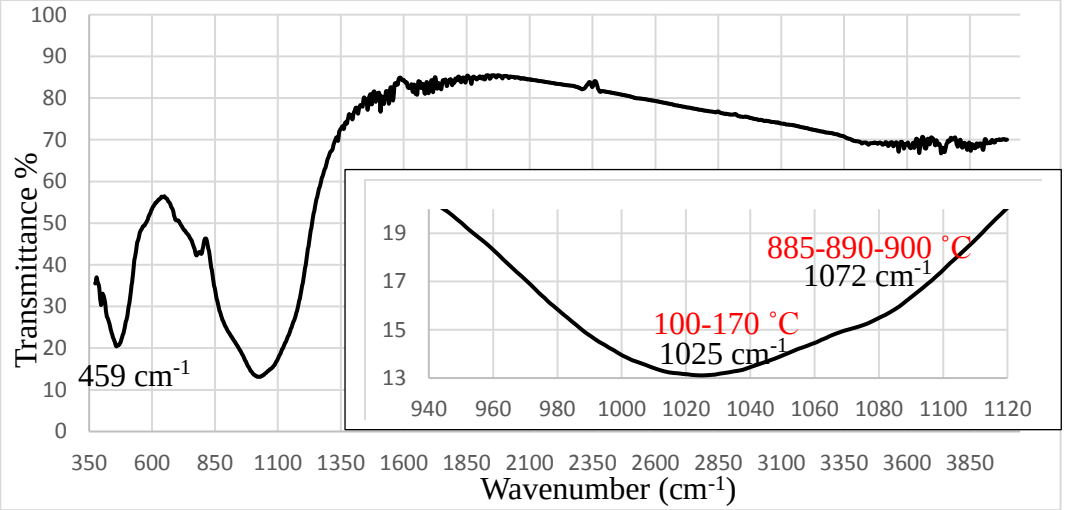

Figure 92. FTIR spectrum of the yellow glaze of the sample K154.

Table 32. Estimation of the firing temperature of the yellow glaze of K154.

Pellet	Res	# of Scans	v (cm^{-1})	T_{firing} (˚C)
K154.yellow.01	4	128	1025 & 1072	600-700

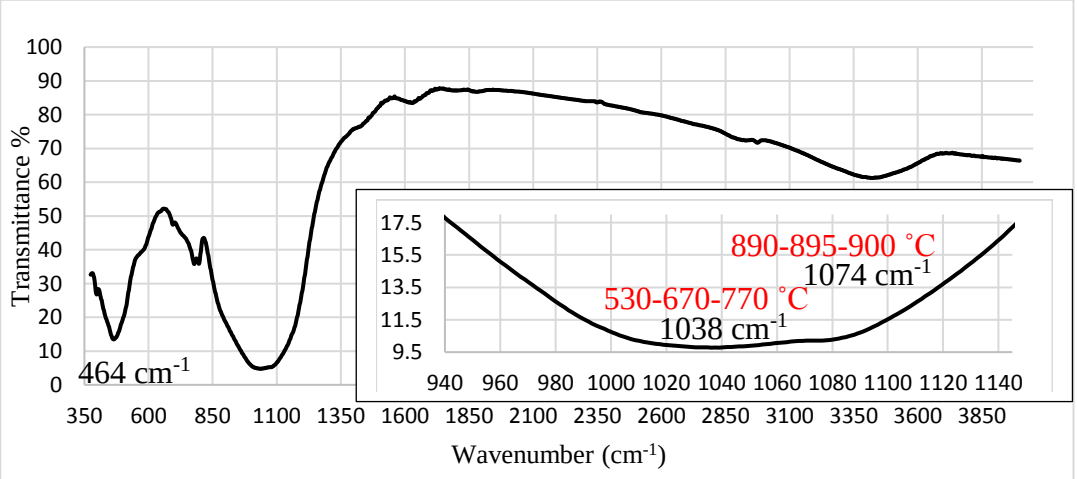

Figure 93. FTIR spectrum of the yellow glaze of the sample K155.

Table 33. Estimation of the firing temperature of the yellow glaze of K155.

Pellet	Res	# of Scans	v (cm^{-1})	T_{firing} (˚C)
K155.yellow.01	4	128	1038	675-775

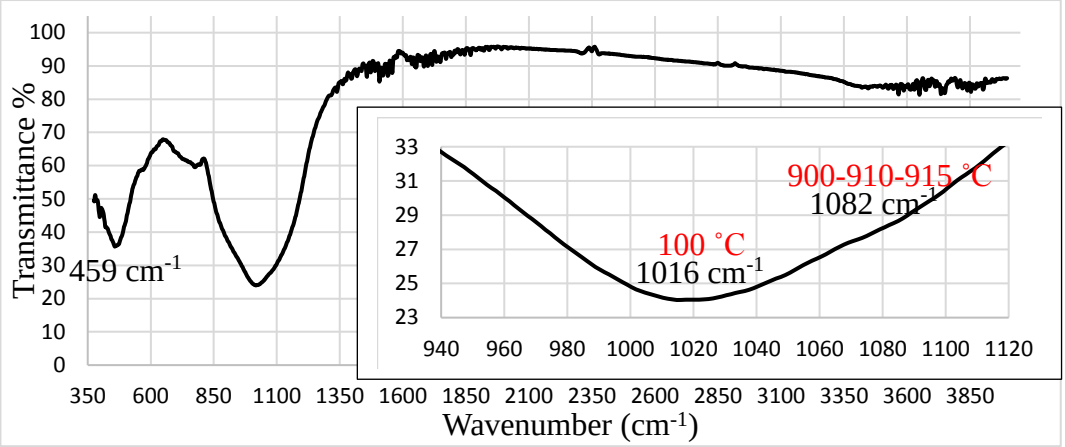

Figure 94. FTIR spectrum of the yellow glaze of the sample K156.

Table 34. Estimation of the firing temperature of the yellow glaze of K156.

Pellet	Res	# of Scans	v (cm^{-1})	T_{firing} (˚C)
K156.yellow.01	4	128	1016 & 1082	600-700

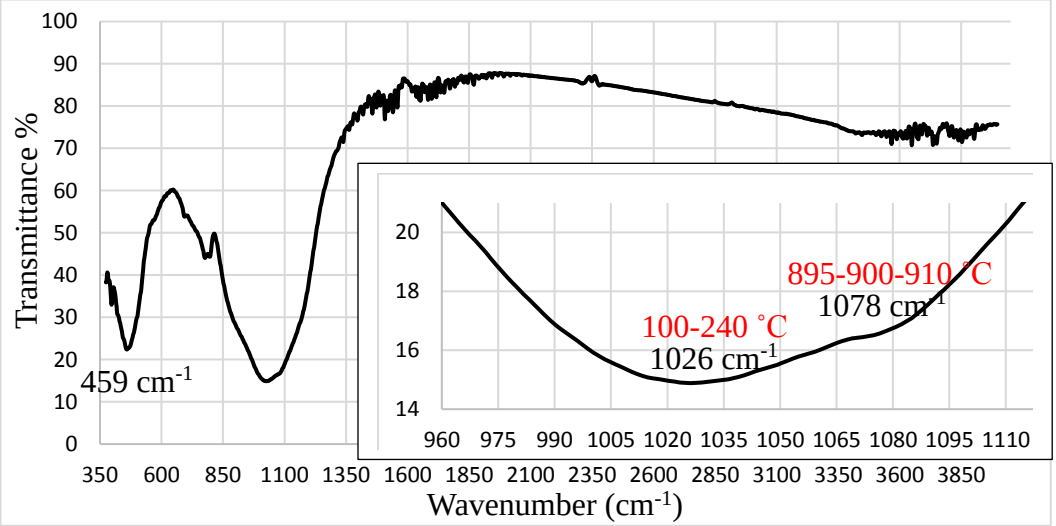

Figure 95. FTIR spectrum of the yellow glaze of the sample K160.

Table 35. Estimation of the firing temperature of the yellow glaze of K160.

Pellet	Res	# of Scans	v (cm^{-1})	T_{firing} (˚C)
K160.yellow.01	4	128	1026 & 1078	600-700

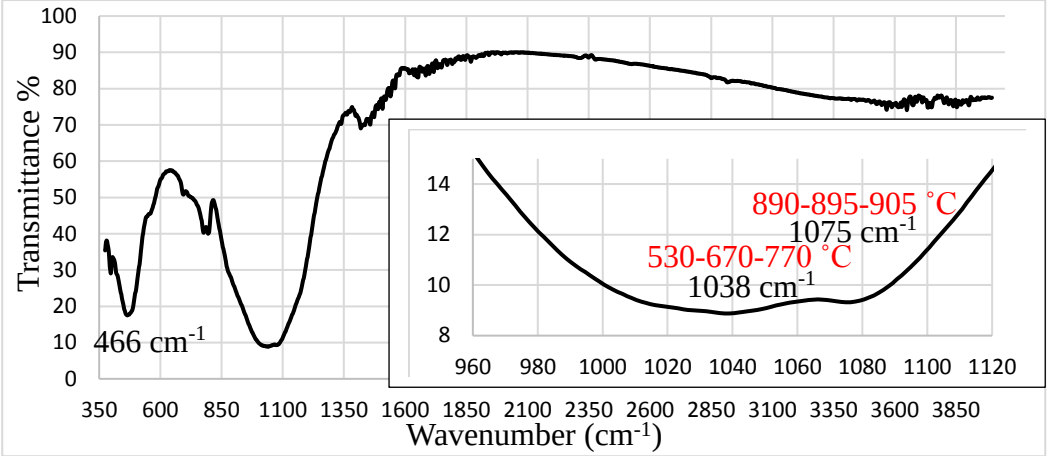

Figure 96. FTIR spectrum of the yellow glaze of the sample K167.

Table 36. Estimation of the firing temperature of the yellow glaze of K167.

Pellet	Res	# of Scans	v (cm^{-1})	T_{firing} (˚C)
K167.yellow.01	4	128	1038 & 1075	675-775

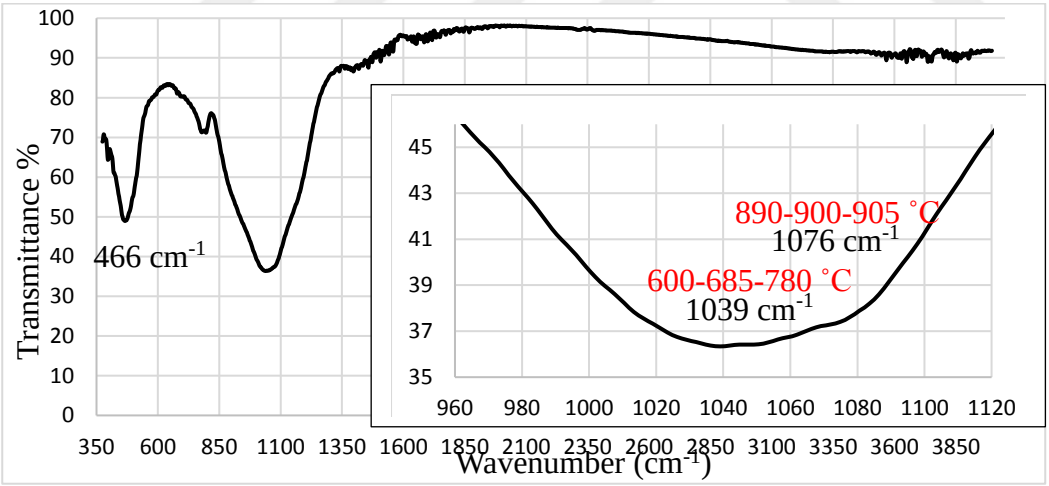

Figure 97. FTIR spectrum of the yellow glaze of the sample K168.

Table 37. Estimation of the firing temperature of the yellow glaze of K168.

Pellet	Res	# of Scans	v (cm^{-1})	T_{firing} (˚C)
K168.yellow.01	4	128	1039 & 1076	700-800

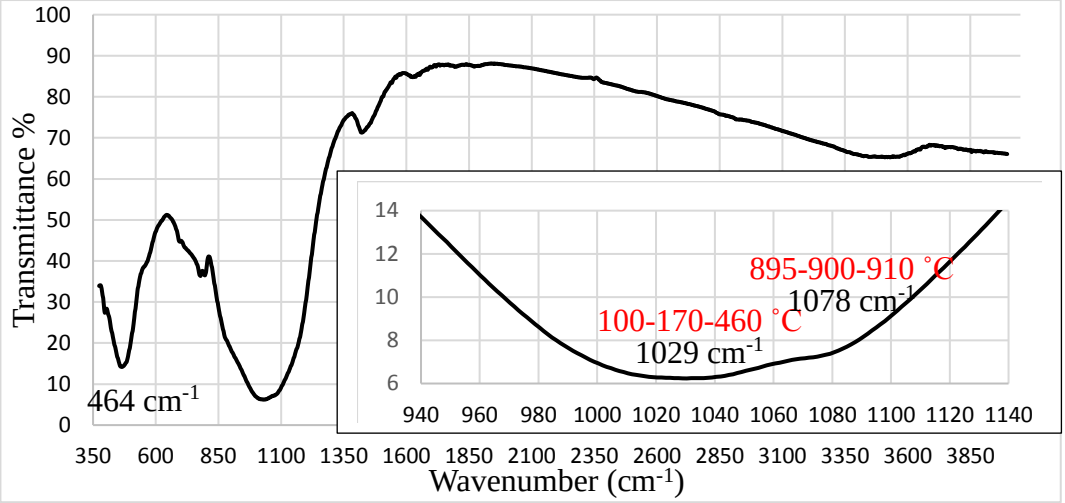

Figure 98. FTIR spectrum of the yellow glaze of the sample K170.

Table 38. Estimation of the firing temperature of the yellow glaze of K170.

Pellet	Res	# of Scans	v (cm^{-1})	T_{firing} (˚C)
K170.yellow.03	4	128	1029 & 1078	600-700

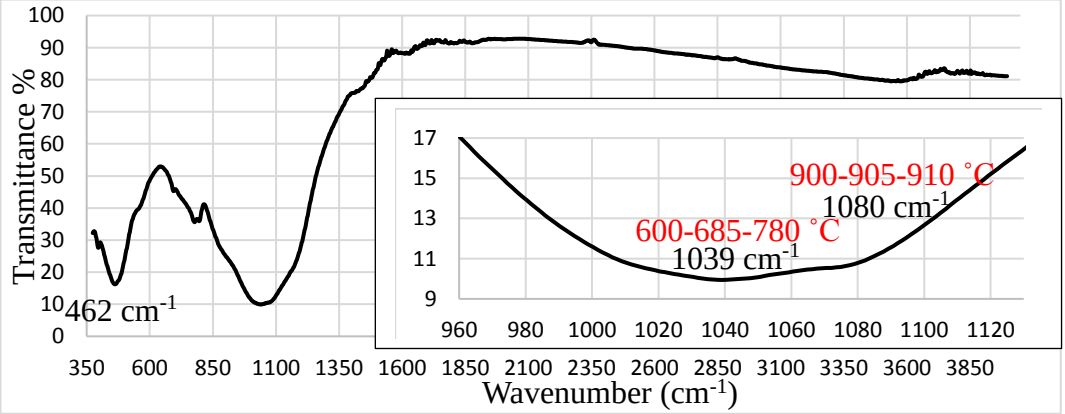

Figure 99. FTIR spectrum of the yellow glaze of the sample K184.

Table 39. Estimation of the firing temperature of the yellow glaze of K184.

Pellet	Res	# of Scans	v (cm^{-1})	T_{firing} (˚C)
K184.yellow.01	4	128	1039 & 1080	700-800

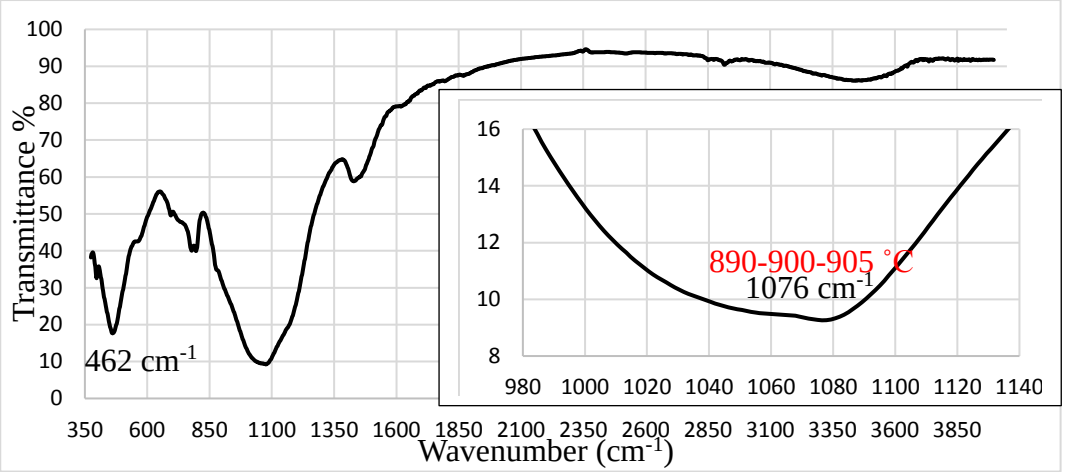

Figure 100. FTIR spectrum of the yellow glaze of the sample K185.

Table 40. Estimation of the firing temperature of the yellow glaze of K185.

Pellet	Res	# of Scans	ν (cm^{-1})	T_{firing} (°C)
K185.yellow.02	4	128	1076	850-900

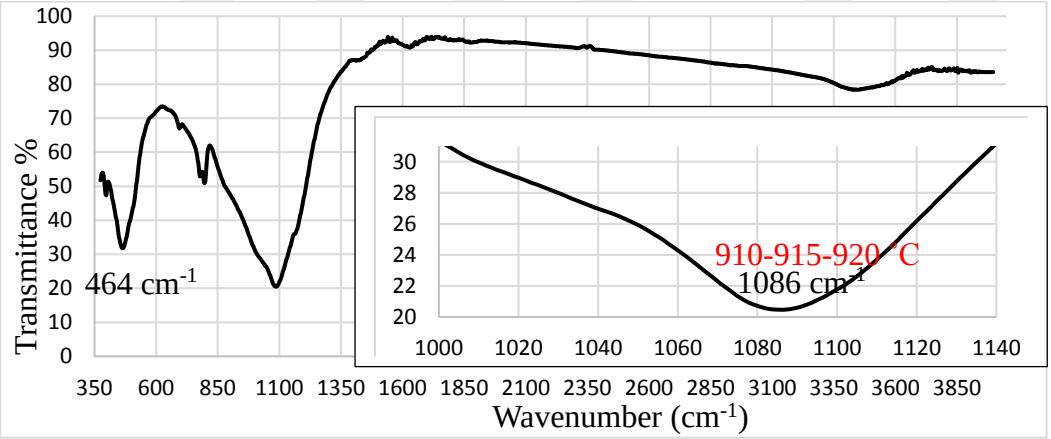

Figure 101. FTIR spectrum of the yellow glaze of the sample K199.

Table 41. Estimation of the firing temperature of the yellow glaze of K199.

Pellet	Res	# of Scans	ν (cm^{-1})	T_{firing} (°C)
K199.yellow.01	4	128	1086	900-925

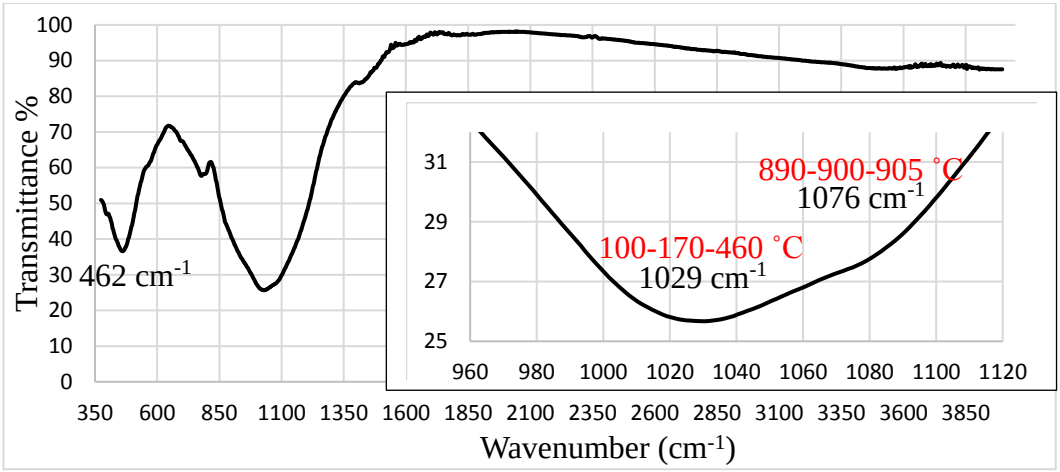

Figure 102. FTIR spectrum of the yellow glaze of the sample K200.

Table 42. Estimation of the firing temperature of the yellow glaze of K200.

Pellet	Res	# of Scans	v (cm^{-1})	T_{firing} (˚C)
K200.yellow.01	4	128	1029 & 1076	600-700

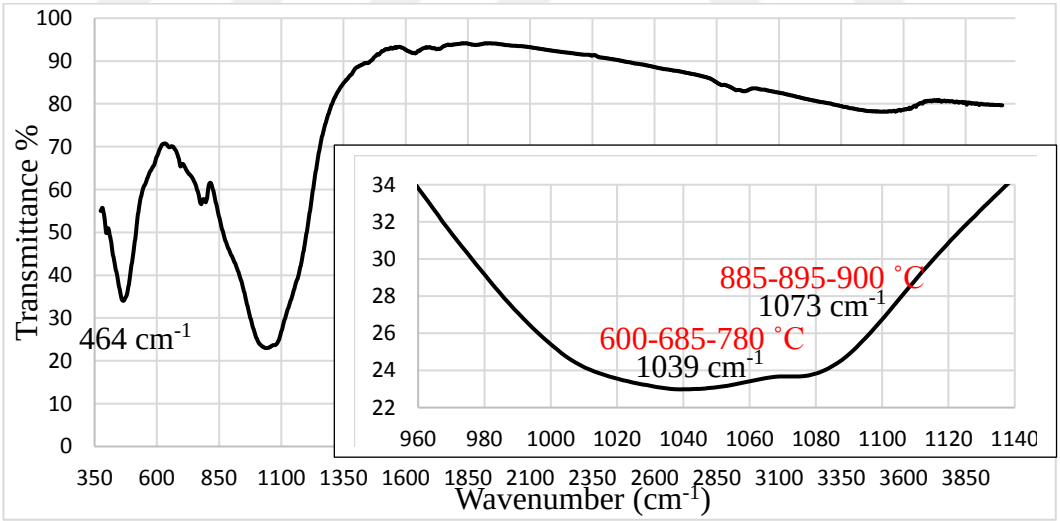

Figure 103. FTIR spectrum of the yellow glaze of the sample K203.

Table 43. Estimation of the firing temperature of the yellow glaze of K203.

Pellet	Res	# of Scans	v (cm^{-1})	T_{firing} (˚C)
K203.yellow.01	4	128	1039 & 1073	700-800

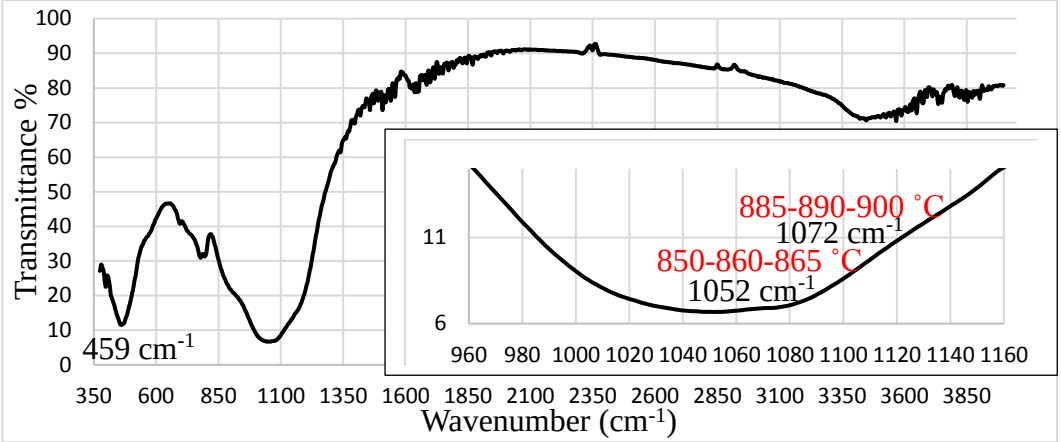

Figure 104. FTIR spectrum of the yellow glaze of the sample K211.

Table 44. Estimation of the firing temperature of the yellow glaze of K211.

Pellet	Res	# of Scans	ν (cm^{-1})	T_{firing} (˚C)
K211.yellow.01	4	128	1052 & 1072	850-900

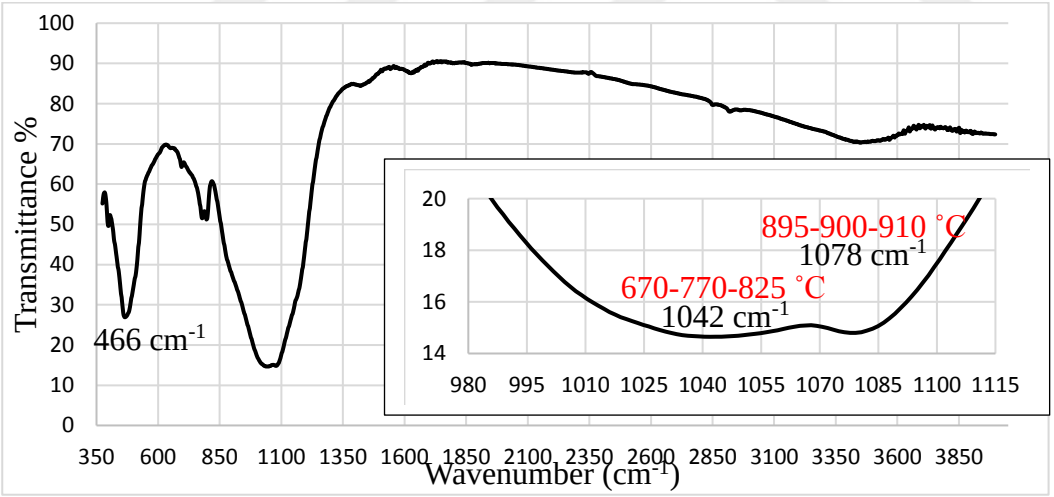

Figure 105. FTIR spectrum of the yellow glaze of the sample K215.

Table 45. Estimation of the firing temperature of the yellow glaze of K215.

Pellet	Res	# of Scans	ν (cm^{-1})	T_{firing} (˚C)
K215.yellow.04	4	128	1042 & 1078	775-825

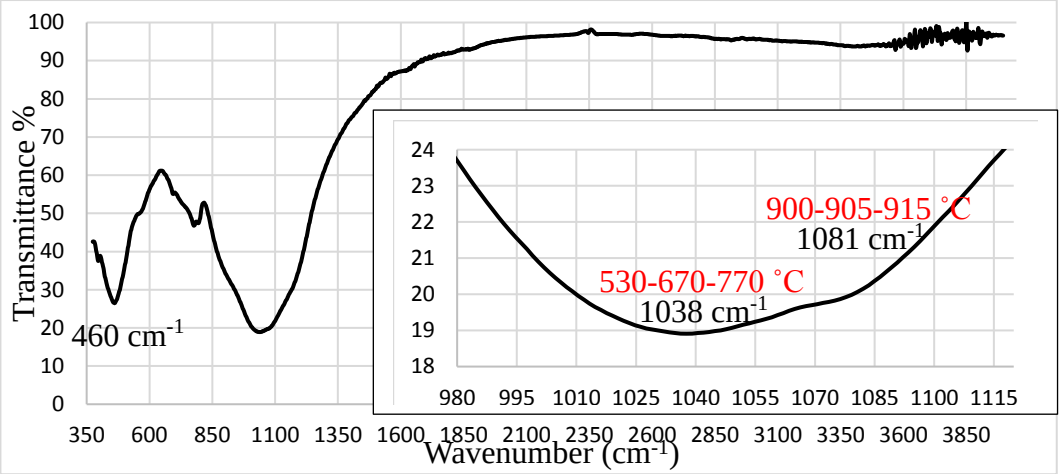

Figure 106. FTIR spectrum of the yellow glaze of the sample K220.

Table 46. Estimation of the firing temperature of the yellow glaze of K220.

Pellet	Res	# of Scans	v (cm^{-1})	T_{firing} (˚C)
K220.yellow.02	4	128	1038 & 1081	675-775

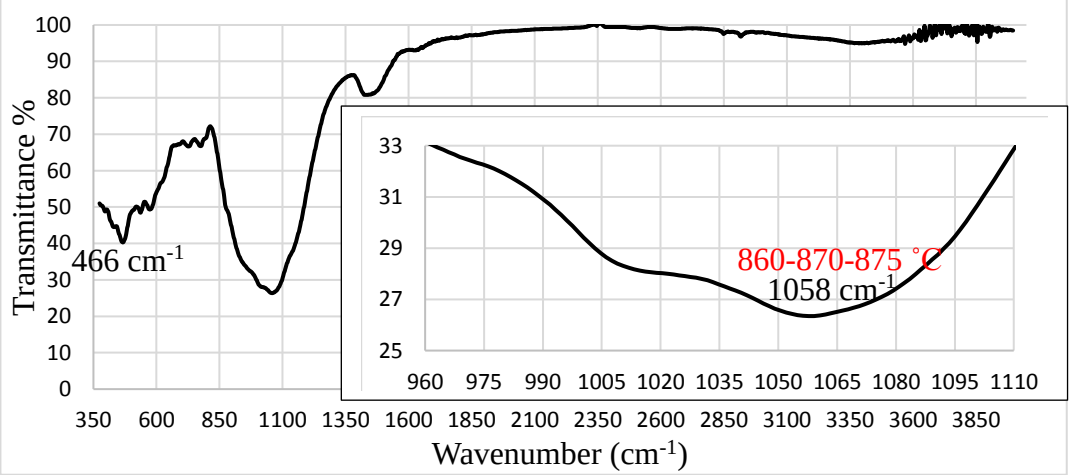

Figure 107. FTIR spectrum of the yellow glaze of the sample K221.

Table 47. Estimation of the firing temperature of the yellow glaze of K221.

Pellet	Res	# of Scans	v (cm^{-1})	T_{firing} (˚C)
K221.yellow.02	4	128	1058	850-900

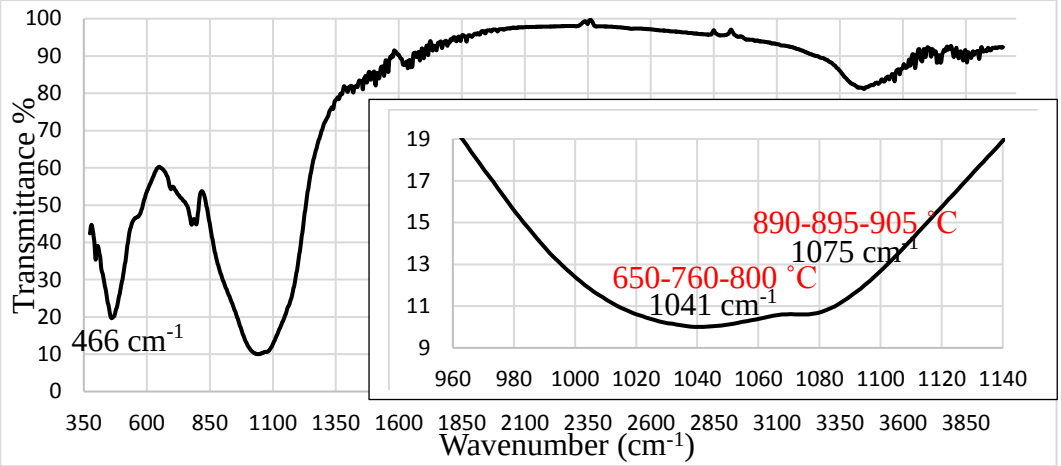

Figure 108. FTIR spectrum of the yellow glaze of the sample K228.

Table 48. Estimation of the firing temperature of the yellow glaze of K228.

Pellet	Res	# of Scans	v (cm^{-1})	T_{firing} (˚C)
K228.yellow.01	4	128	1041 & 1075	750-800

A.2.2. FTIR Spectra of the Green Glazes

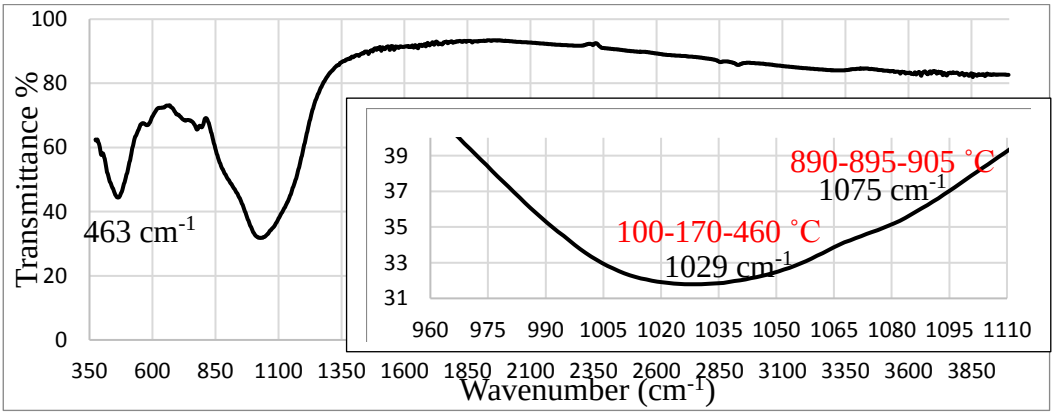

Figure 109. FTIR spectrum of the green glaze of the sample K101.

Table 49. Estimation of the firing temperature of the green glaze of K101.

Pellet	Res	# of Scans	v (cm^{-1})	T_{firing} (˚C)
K101.green.07	4	512	1029 & 1075	600-700

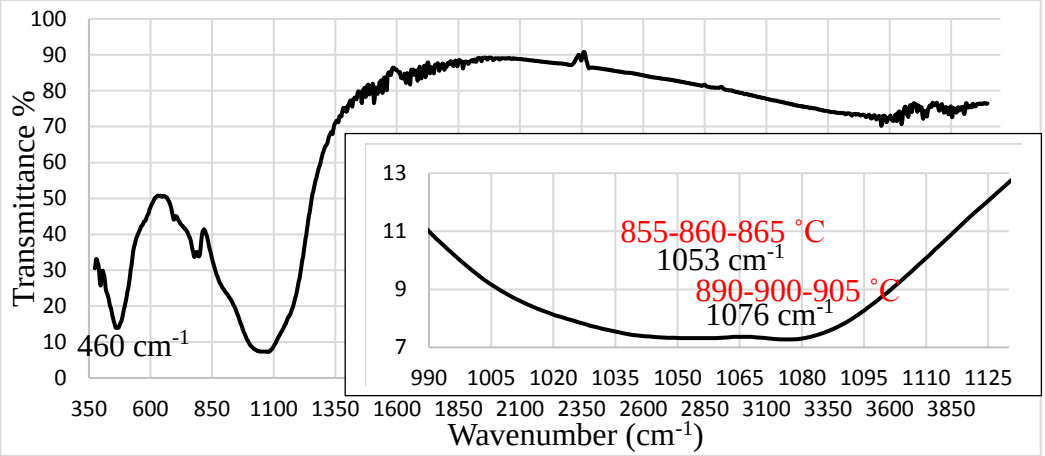

Figure 110. FTIR spectrum of the green glaze of the sample K103.

Table 50. Estimation of the firing temperature of the green glaze of K103.

Pellet	Res	# of Scans	v (cm^{-1})	T_{firing} (˚C)
K103.green.01	4	128	1053 & 1076	850-900

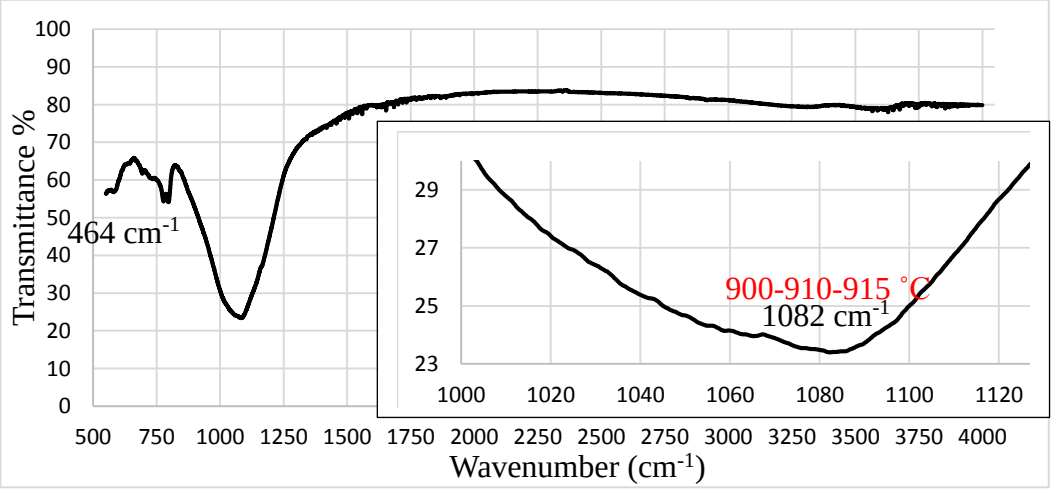

Figure 111. FTIR spectrum of the green glaze of the sample K104.

Table 51. Estimation of the firing temperature of the green glaze of K104.

Pellet	Res	# of Scans	v (cm^{-1})	T_{firing} (˚C)
K104.green.05	4	128	1082	900-925

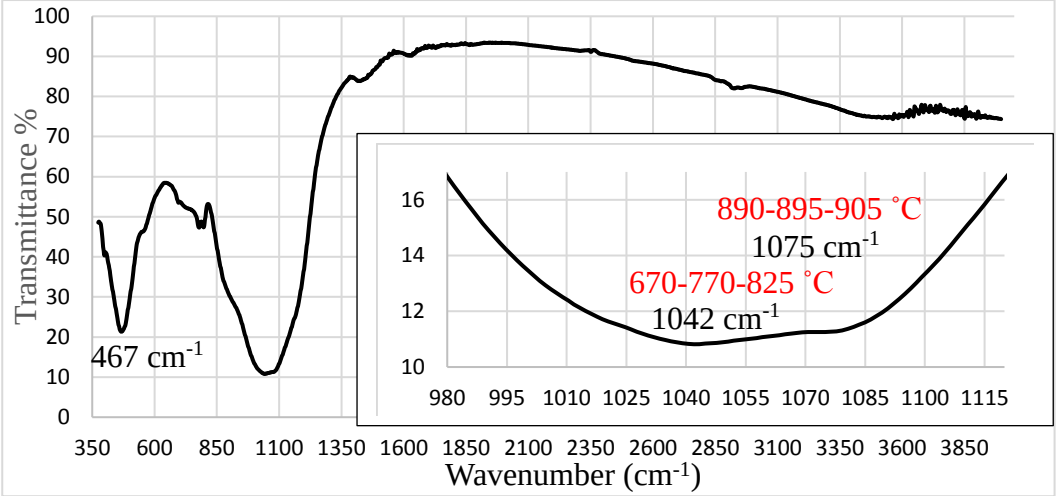

Figure 112. FTIR spectrum of the green glaze of the sample K105.

Table 52. Estimation of the firing temperature of the green glaze of K105.

Pellet	Res	# of Scans	v (cm^{-1})	T_{firing} (˚C)
K105.green.04	4	128	1042 & 1075	775-825

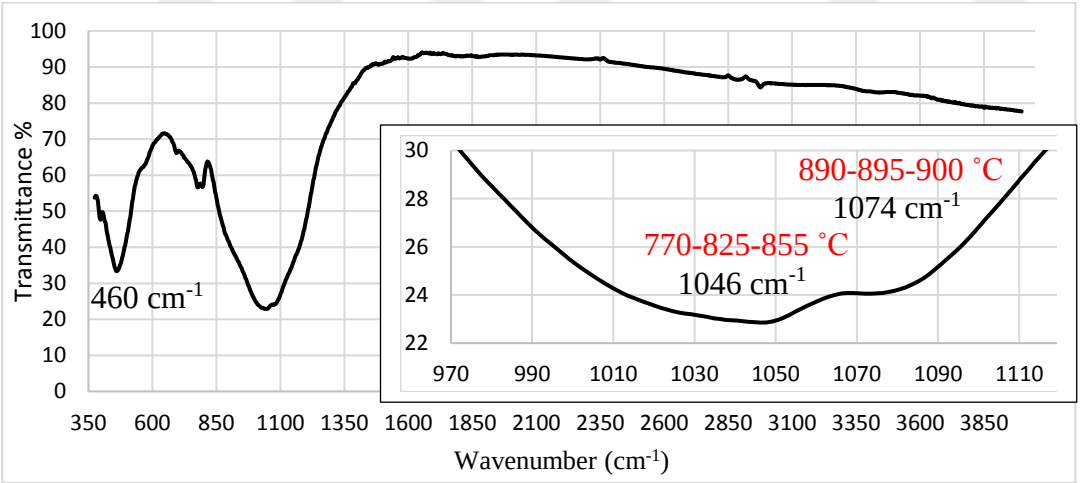

Figure 113. FTIR spectrum of the green glaze of the sample K106.

Table 53. Estimation of the firing temperature of the green glaze of K106.

Pellet	Res	# of Scans	v (cm^{-1})	T_{firing} (˚C)
K106.green.01	4	128	1046 & 1074	800-850

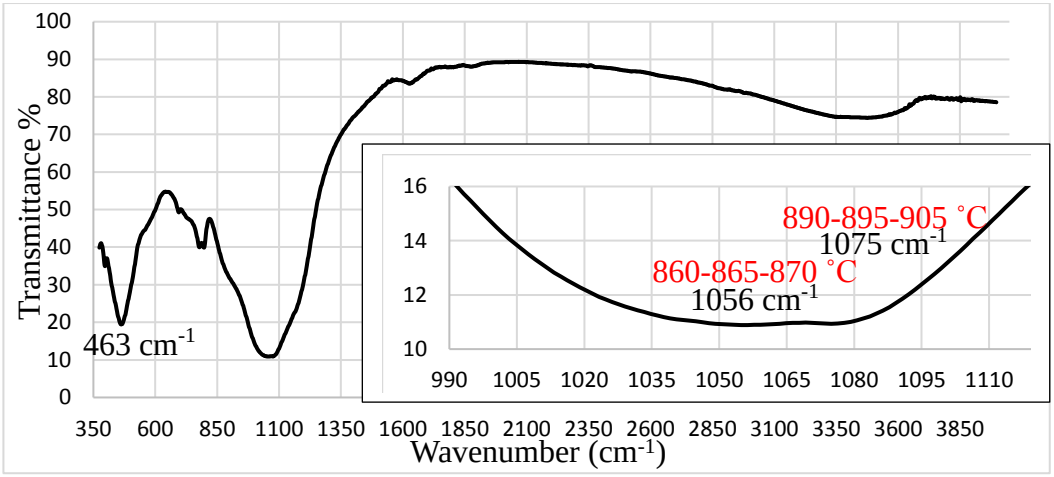

Figure 114. FTIR spectrum of the green glaze of the sample K108.

Table 54. Estimation of the firing temperature of the green glaze of K108.

Pellet	Res	# of Scans	ν (cm^{-1})	T_{firing} (˚C)
K108.green.01	4	128	1056 & 1075	850-900

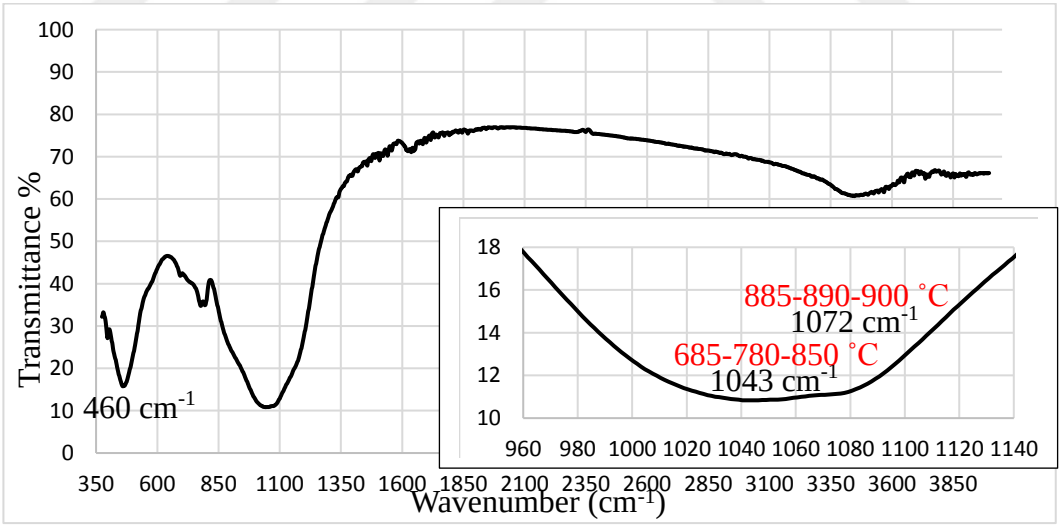

Figure 115. FTIR spectrum of the green glaze of the sample K109.

Table 55. Estimation of the firing temperature of the green glaze of K109.

Pellet	Res	# of Scans	ν (cm^{-1})	T_{firing} (˚C)
K109.green.02	4	128	1043 & 1072	775-850

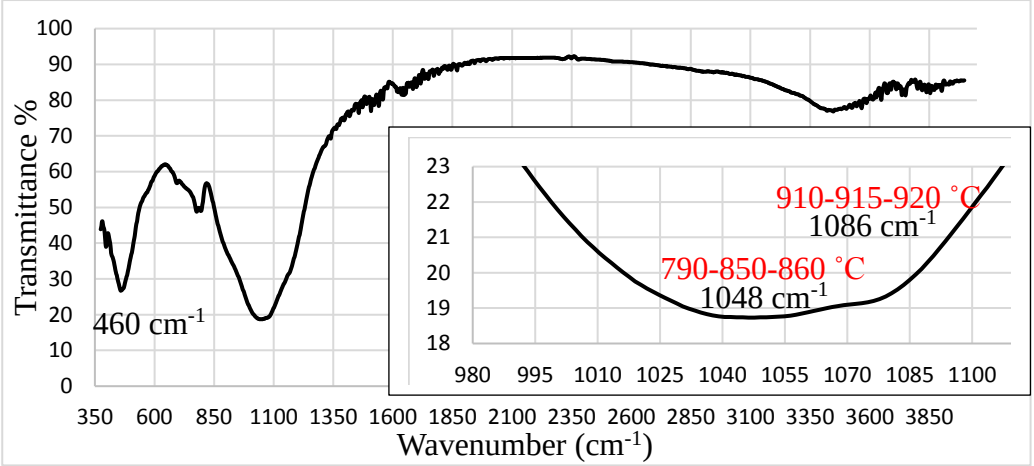

Figure 116. FTIR spectrum of the green glaze of the sample K110.

Table 56. Estimation of the firing temperature of the green glaze of K110.

Pellet	Res	# of Scans	ν (cm^{-1})	T_{firing} (˚C)
K110.green.02	4	128	1048 & 1086	850-900

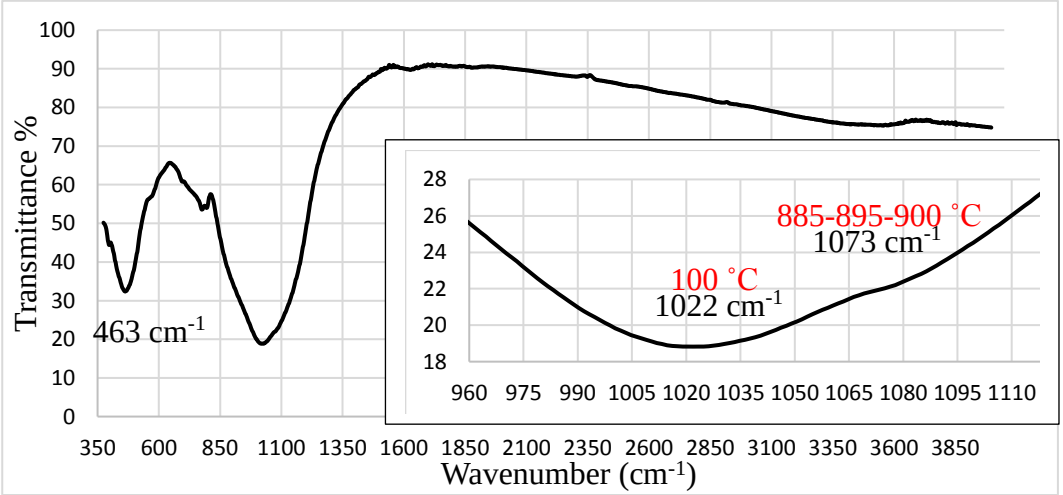

Figure 117. FTIR spectrum of the green glaze of the sample K111.

Table 57. Estimation of the firing temperature of the green glaze of K111.

Pellet	Res	# of Scans	ν (cm^{-1})	T_{firing} (˚C)
K111.green.01	4	128	1022 & 1073	600-700

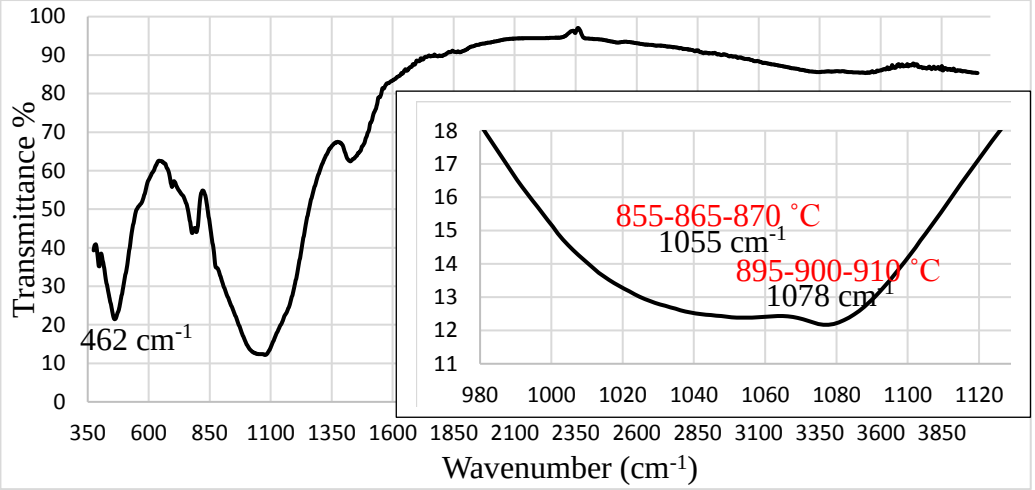

Figure 118. FTIR spectrum of the green glaze of the sample K112.

Table 58. Estimation of the firing temperature of the green glaze of K112.

Pellet	Res	# of Scans	ν (cm^{-1})	T_{firing} (˚C)
K112.green.01	4	128	1078	900-925

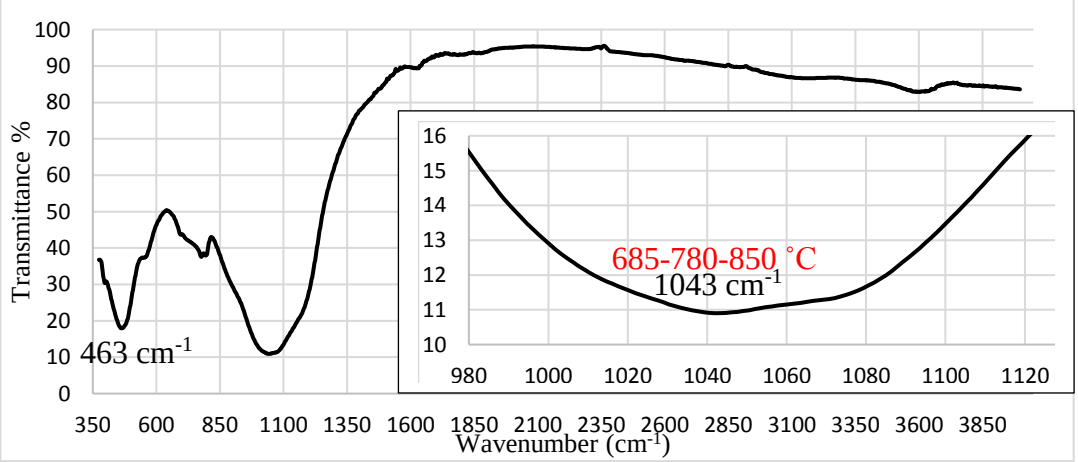

Figure 119. FTIR spectrum of the green glaze of the sample K113.

Table 59. Estimation of the firing temperature of the green glaze of K113.

Pellet	Res	# of Scans	ν (cm^{-1})	T_{firing} (˚C)
K113.green.01	4	128	1043	775-850

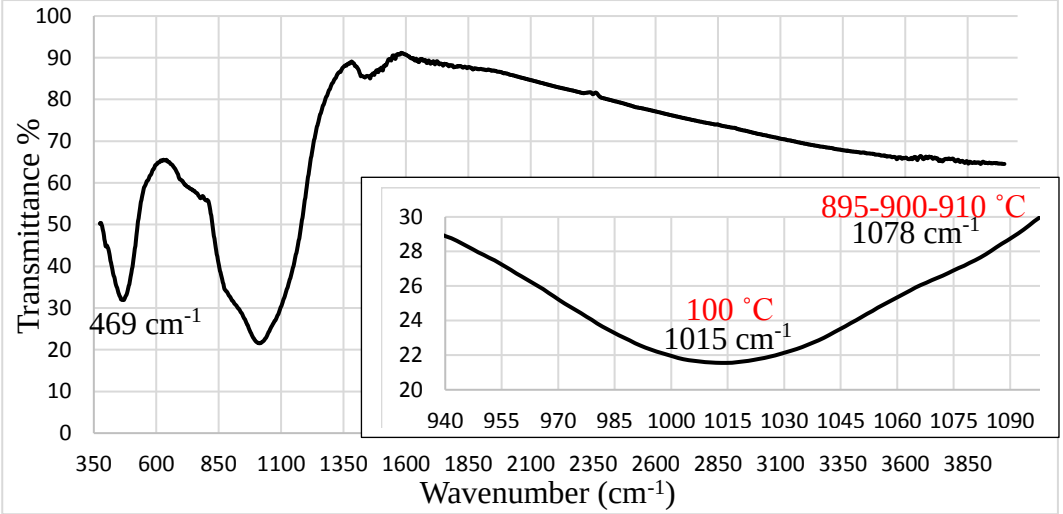

Figure 120. FTIR spectrum of the green glaze of the sample K114.

Table 60. Estimation of the firing temperature of the green glaze of K114.

Pellet	Res	# of Scans	v (cm^{-1})	T_{firing} (˚C)
K114.green.01	4	128	1078	600-700

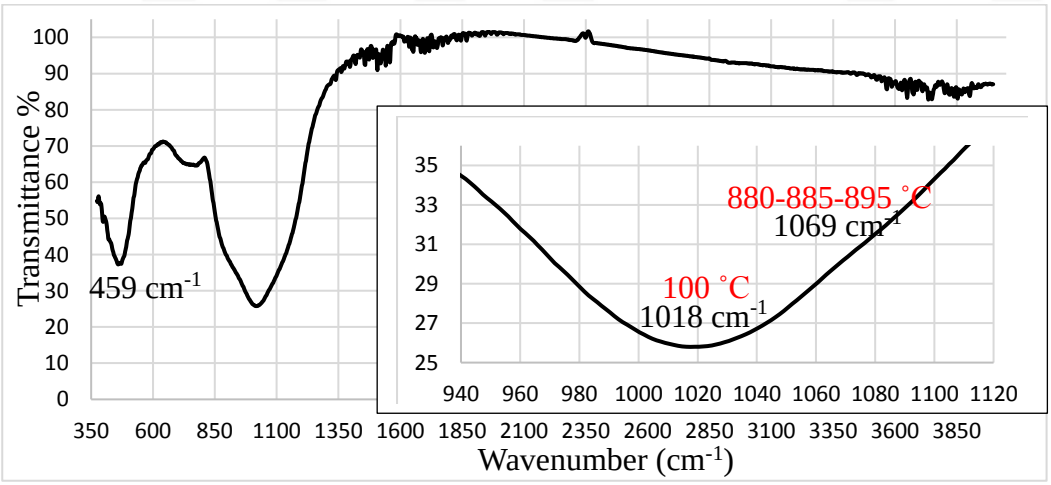

Figure 121. FTIR spectrum of the green glaze of the sample K115.

Table 61. Estimation of the firing temperature of the green glaze of K115.

Pellet	Res	# of Scans	v (cm^{-1})	T_{firing} (˚C)
K115.green.01	4	128	1069	600-700

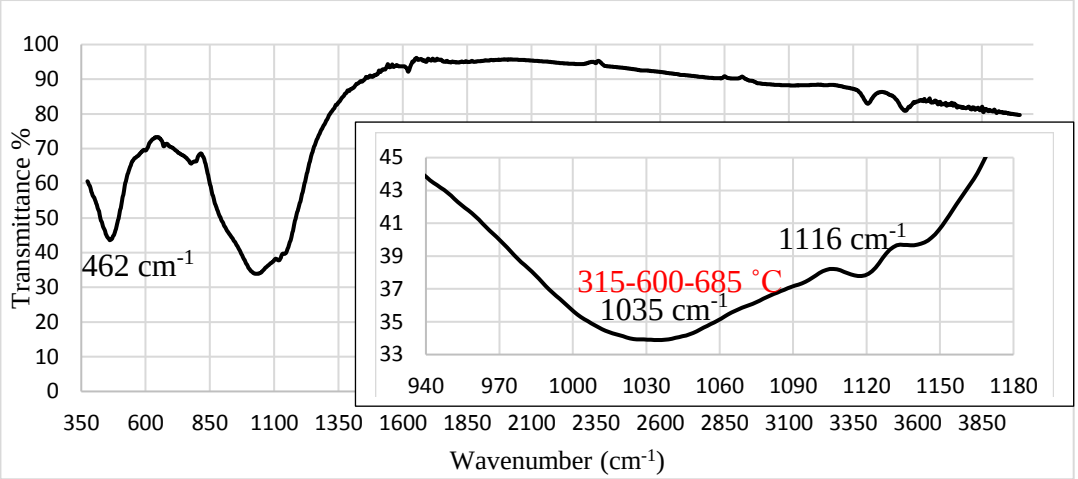

Figure 122. FTIR spectrum of the green glaze of the sample K119.

Table 62. Estimation of the firing temperature of the green glaze of K119.

Pellet	Res	# of Scans	v (cm^{-1})	T_{firing} (˚C)
K119.green.01	4	128	1035	600-700

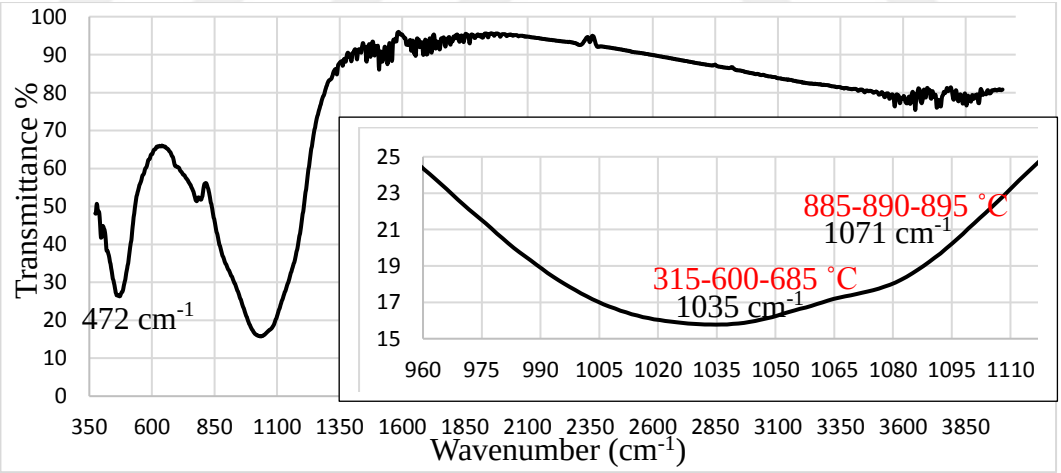

Figure 123. FTIR spectrum of the green glaze of the sample K122.

Table 63. Estimation of the firing temperature of the green glaze of K122.

Pellet	Res	# of Scans	v (cm^{-1})	T_{firing} (˚C)
K122.green.01	4	128	1035 & 1071	600-700

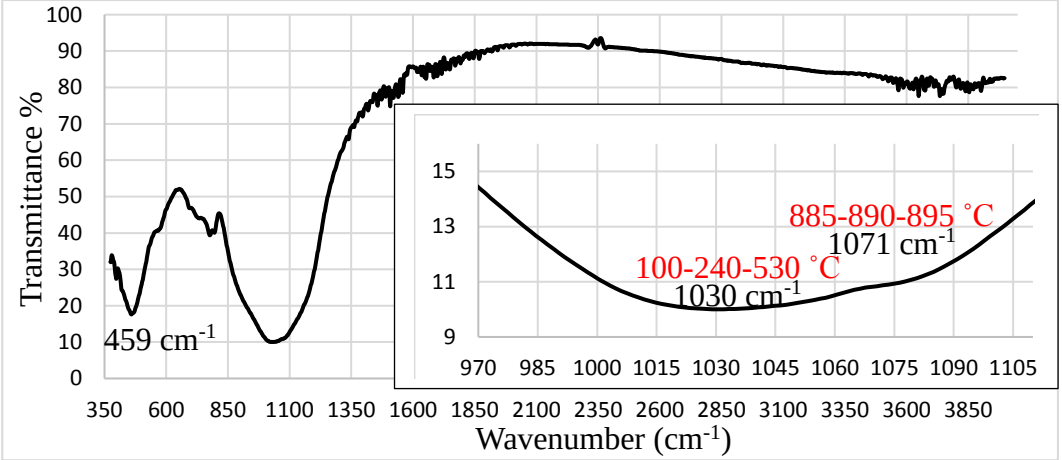

Figure 124. FTIR spectrum of the exterior green glaze of the sample K123.

Table 64. Estimation of the firing temperature of the exterior green glaze of K123.

Pellet	Res	# of Scans	v (cm^{-1})	T_{firing} (˚C)
K123.green.exterior.01	4	128	1030 & 1071	600-700

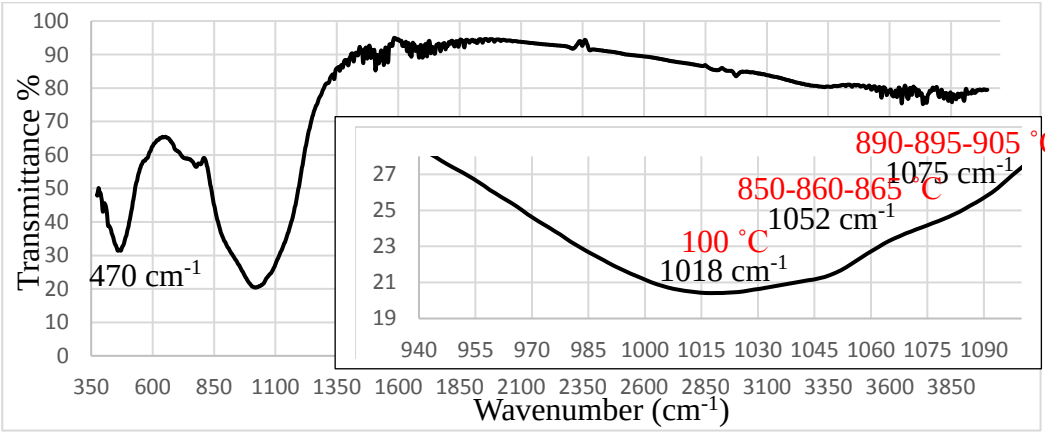

Figure 125. FTIR spectrum of the interior green glaze of the sample K123.

Table 65. Estimation of the firing temperature of the interior green glaze of K123.

Pellet	Res	# of Scans	v (cm^{-1})	T_{firing} (˚C)
K123.green.interior.01	4	128	1018	600-700

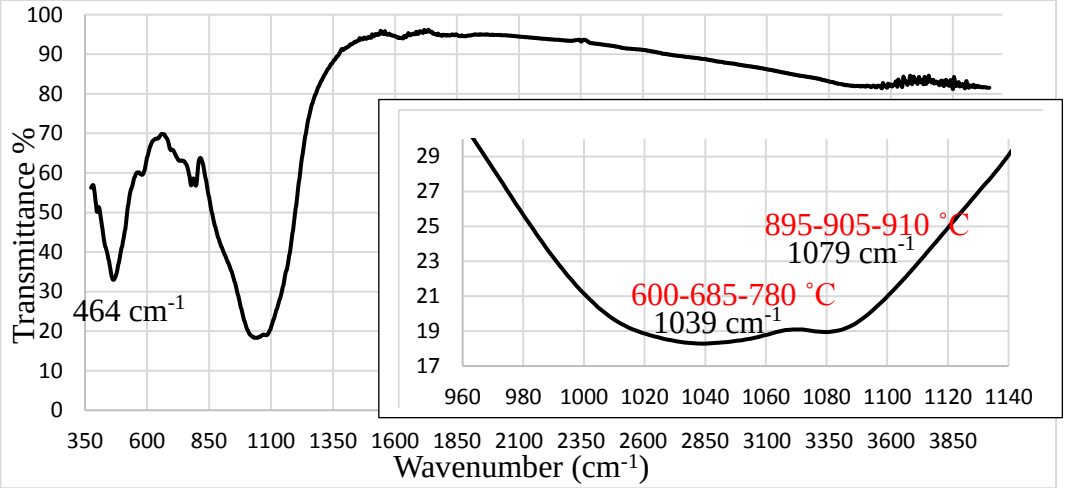

Figure 126. FTIR spectrum of the green glaze of the sample K124.

Table 66. Estimation of the firing temperature of the green glaze of K124.

Pellet	Res	# of Scans	ν (cm^{-1})	T_{firing} (˚C)
K124.green.02	4	128	1039 & 1079	700-800

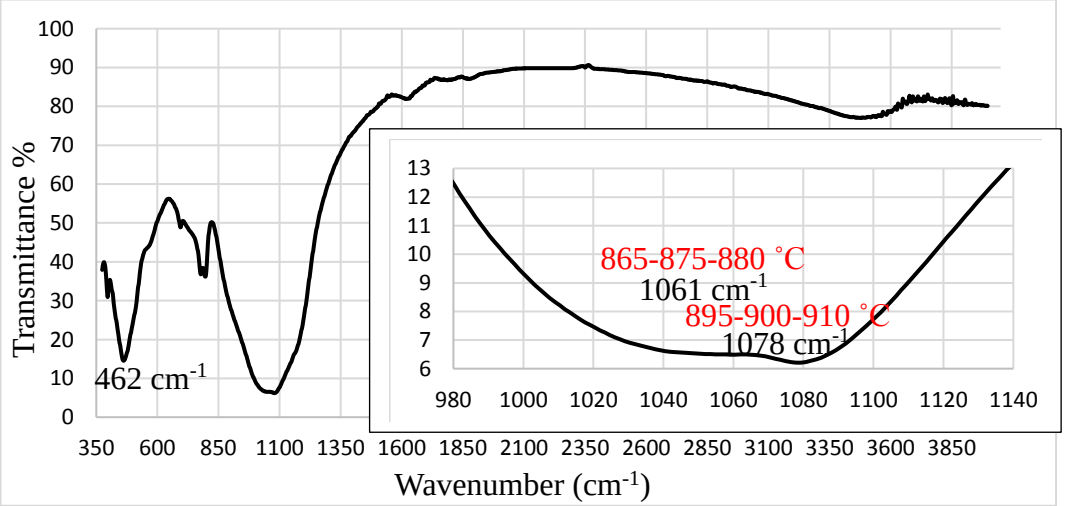

Figure 127. FTIR spectrum of the green glaze of the sample K131.

Table 67. Estimation of the firing temperature of the green glaze of K131.

Pellet	Res	# of Scans	ν (cm^{-1})	T_{firing} (˚C)
K131.green.03	4	128	1061 & 1075	900-925

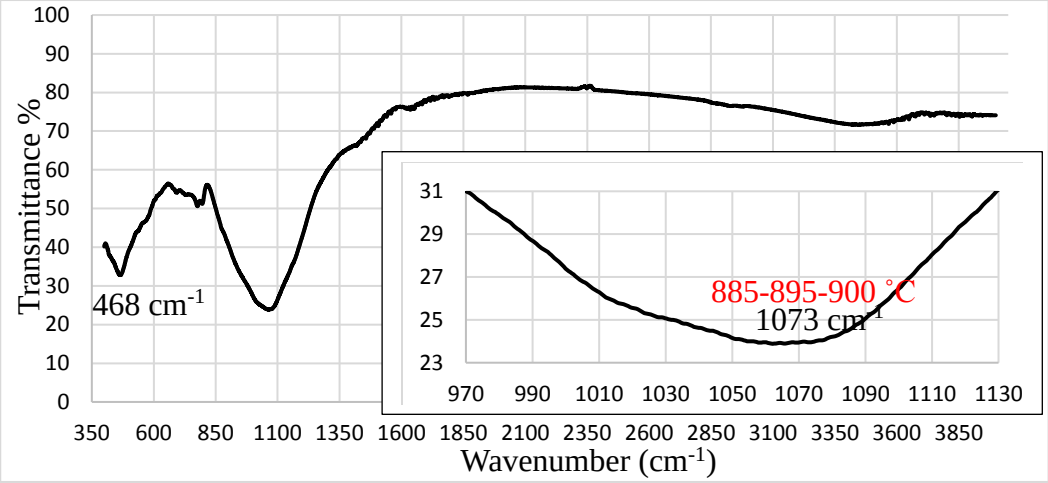

Figure 128. FTIR spectrum of the green glaze of the sample K143.

Table 68. Estimation of the firing temperature of the green glaze of K143.

Pellet	Res	# of Scans	v (cm^{-1})	T_{firing} (°C)
K143.green.04	4	128	1073	850-900

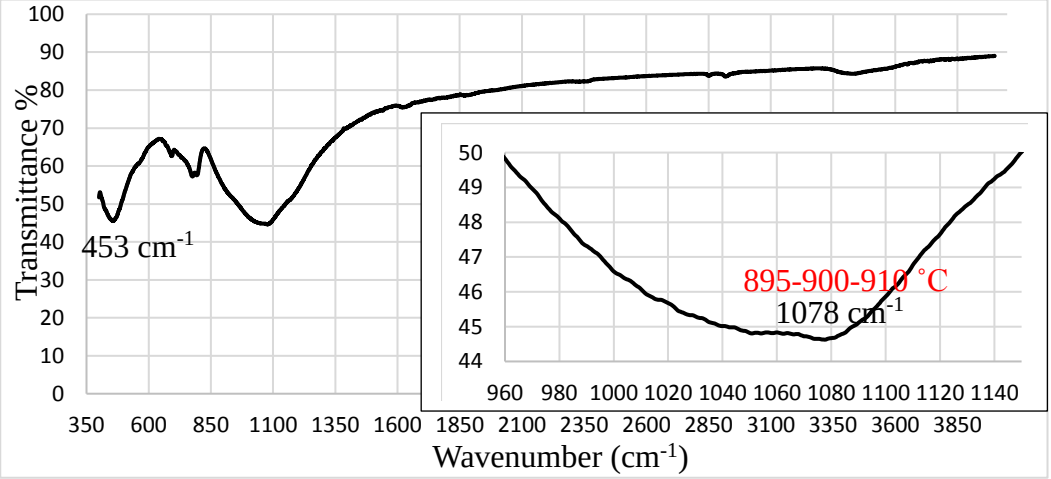

Figure 129. FTIR spectrum of the green glaze of the sample K144.

Table 69. Estimation of the firing temperature of the green glaze of K144.

Pellet	Res	# of Scans	v (cm^{-1})	T_{firing} (°C)
K144.green.04	4	128	1078	900-925

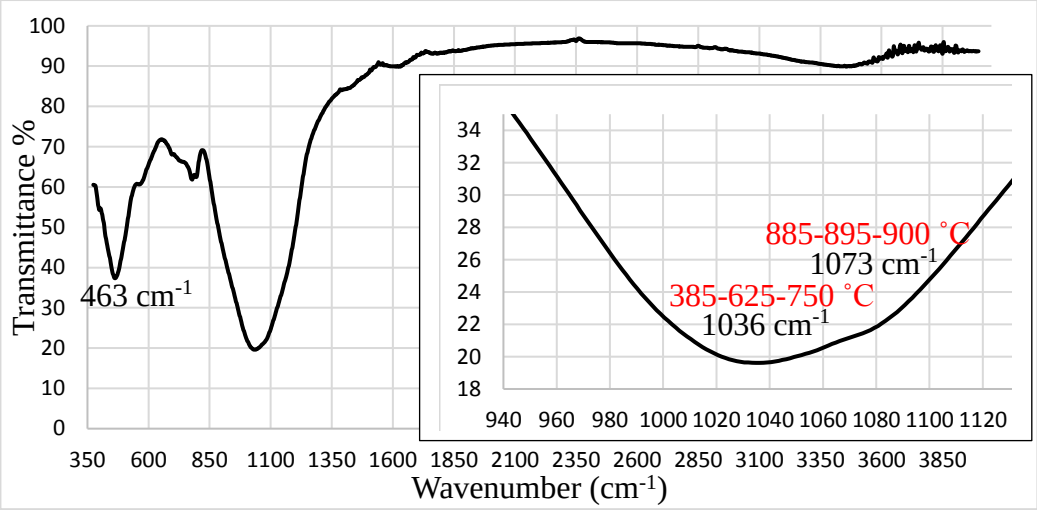

Figure 130. FTIR spectrum of the green glaze of the sample K145.

Table 70. Estimation of the firing temperature of the green glaze of K145.

Pellet	Res	# of Scans	ν (cm^{-1})	T_{firing} (˚C)
K145.green.02	4	128	1036 & 1073	650-750

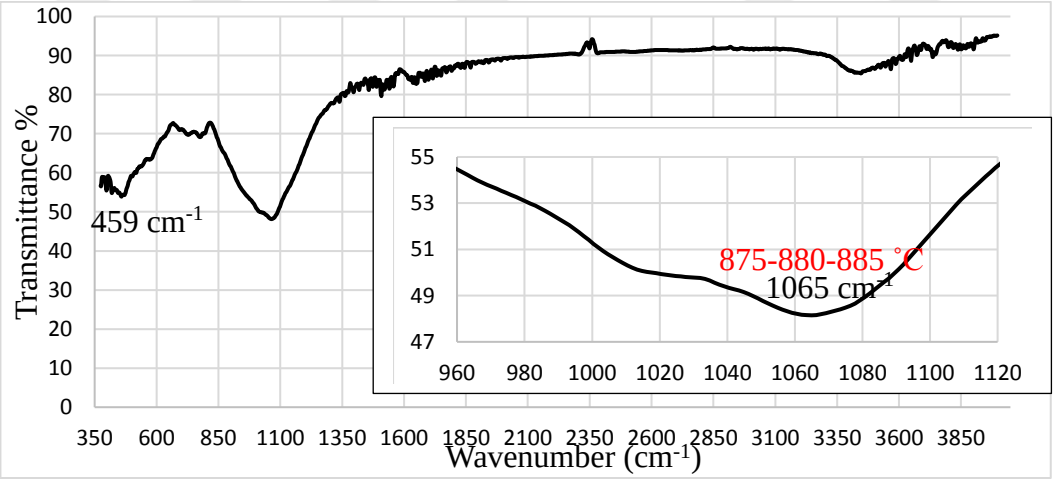

Figure 131. FTIR spectrum of the green glaze of the sample K147.

Table 71. Estimation of the firing temperature of the green glaze of K147.

Pellet	Res	# of Scans	ν (cm^{-1})	T_{firing} (˚C)
K147.green.01	4	128	1065	850-900

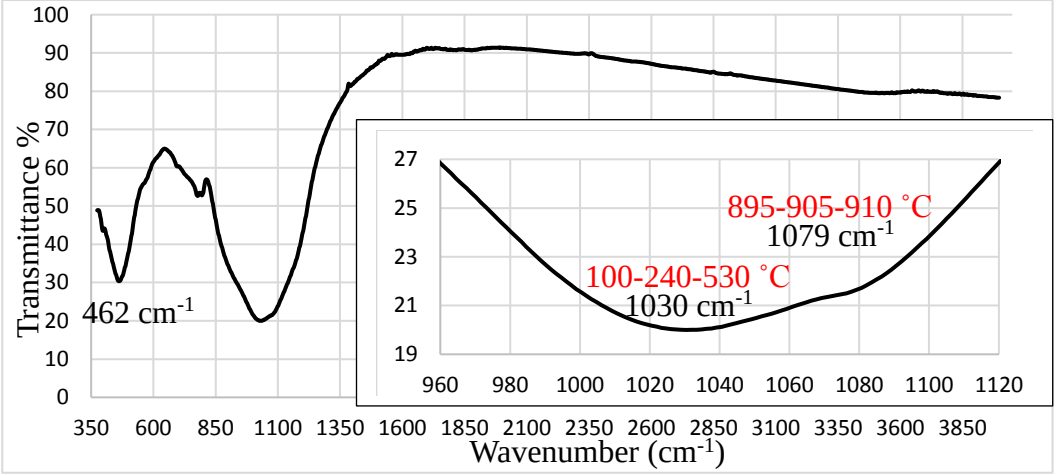

Figure 132. FTIR spectrum of the green glaze of the sample K148.

Table 72. Estimation of the firing temperature of the green glaze of K148.

Pellet	Res	# of Scans	ν (cm^{-1})	T_{firing} (˚C)
K148.green.02	4	128	1030 & 1079	600-700

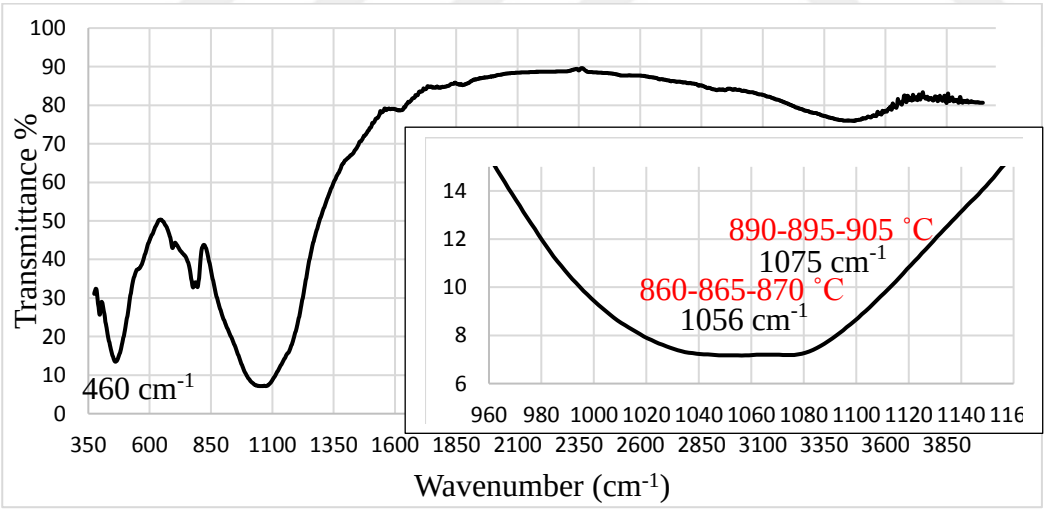

Figure 133. FTIR spectrum of the green glaze of the sample K149.

Table 73. Estimation of the firing temperature of the green glaze of K149.

Pellet	Res	# of Scans	ν (cm^{-1})	T_{firing} (˚C)
K149.green.03	4	128	1056 & 1075	850-900

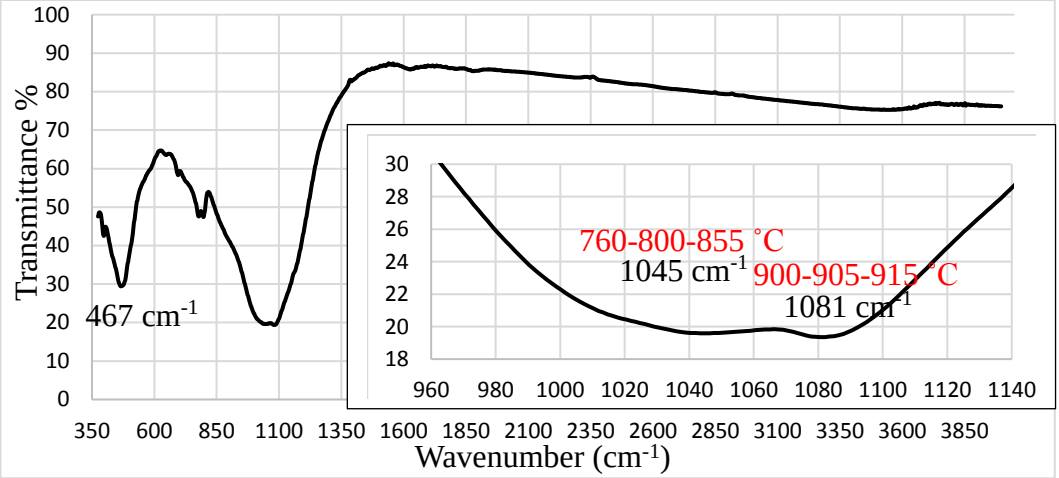

Figure 134. FTIR spectrum of the green glaze of the sample K150.

Table 74. Estimation of the firing temperature of the green glaze of K150.

Pellet	Res	# of Scans	v (cm^{-1})	T_{firing} (˚C)
K150.green.02	4	128	1045 & 1081	900-925

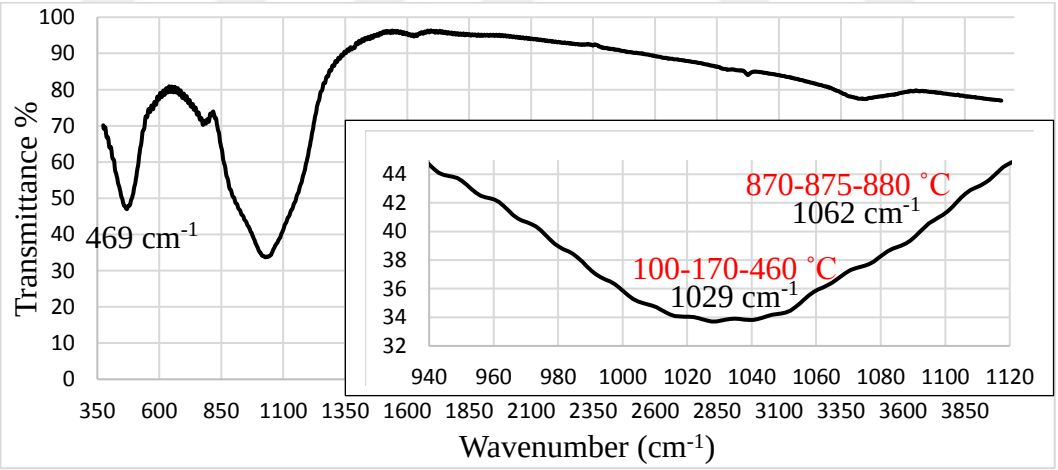

Figure 135. FTIR spectrum of the green glaze of the sample K153.

Table 75. Estimation of the firing temperature of the green glaze of K153.

Pellet	Res	# of Scans	v (cm^{-1})	T_{firing} (˚C)
K153.green.03	4	128	1029 & 1062	600-700

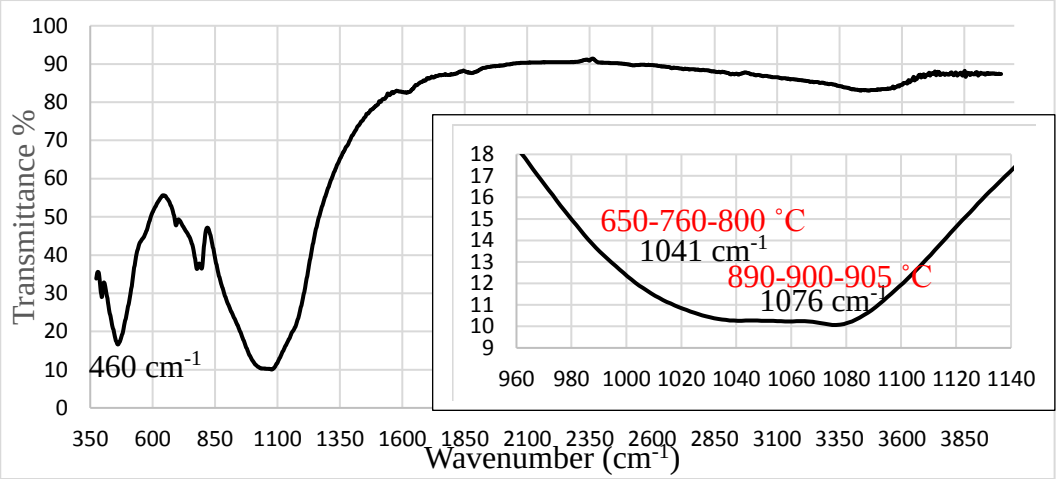

Figure 136. FTIR spectrum of the green glaze of the sample K154.

Table 76. Estimation of the firing temperature of the green glaze of K154.

Pellet	Res	# of Scans	v (cm^{-1})	T_{firing} (˚C)
K154.green.03	4	128	1076	850-900

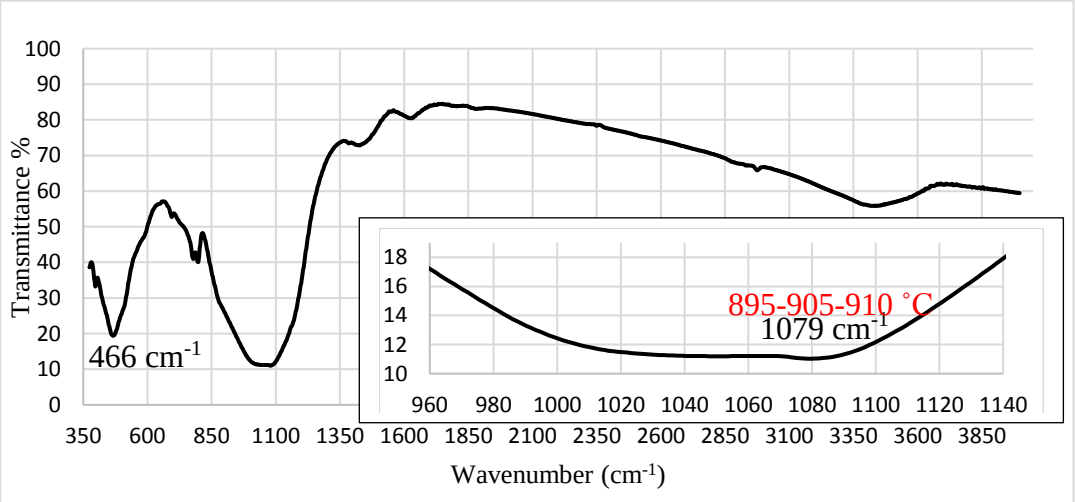

Figure 137. FTIR spectrum of the green glaze of the sample K155.

Table 77. Estimation of the firing temperature of the green glaze of K155.

Pellet	Res	# of Scans	v (cm^{-1})	T_{firing} (˚C)
K155.green.01	4	128	1079	900-925

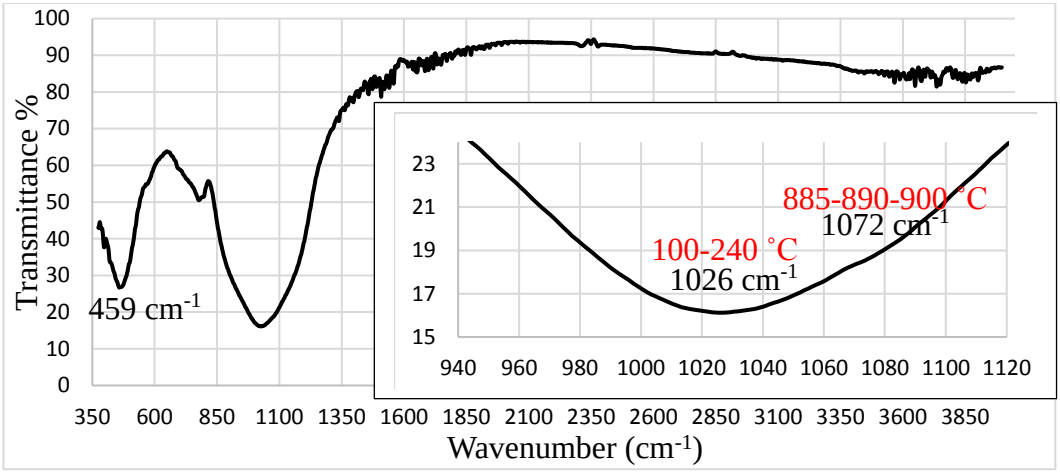

Figure 138. FTIR spectrum of the green glaze of the sample K156.

Table 78. Estimation of the firing temperature of the green glaze of K156.

Pellet	Res	# of Scans	v (cm^{-1})	T_{firing} (˚C)
K156.green.01	4	128	1026	600-700

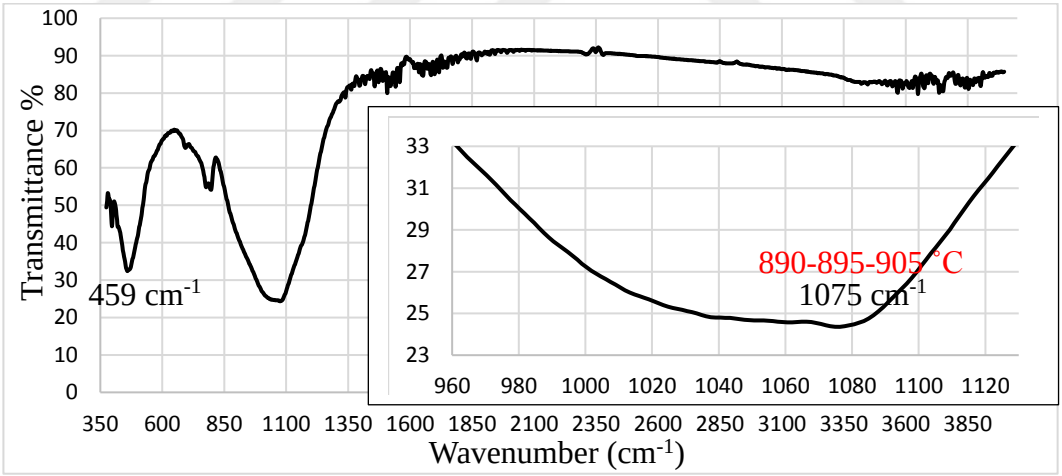

Figure 139. FTIR spectrum of the green glaze of the sample K157.

Table 79. Estimation of the firing temperature of the green glaze of K157.

Pellet	Res	# of Scans	v (cm^{-1})	T_{firing} (˚C)
K157.green.01	4	128	1075	850-900

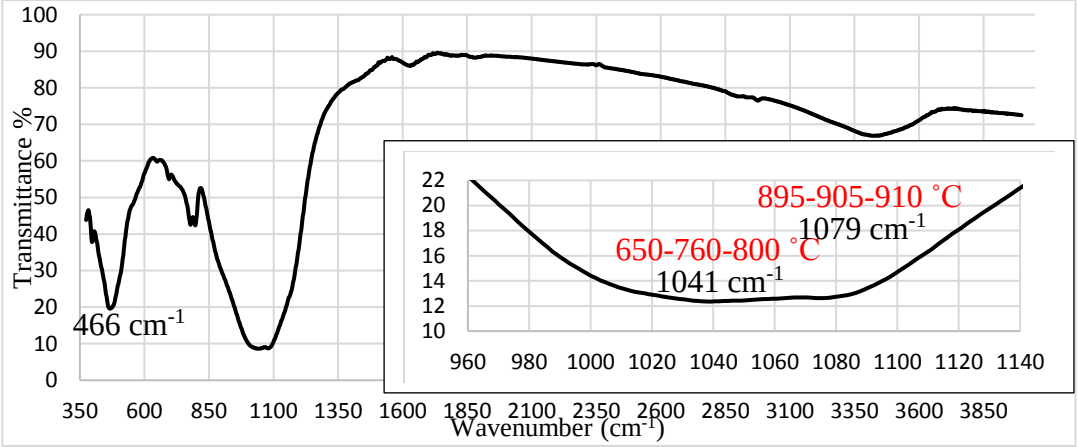

Figure 140. FTIR spectrum of the green glaze of the sample K158.

Table 80. Estimation of the firing temperature of the green glaze of K158.

Pellet	Res	# of Scans	v (cm^{-1})	T_{firing} (˚C)
K158.green.01	4	128	1041	750-800

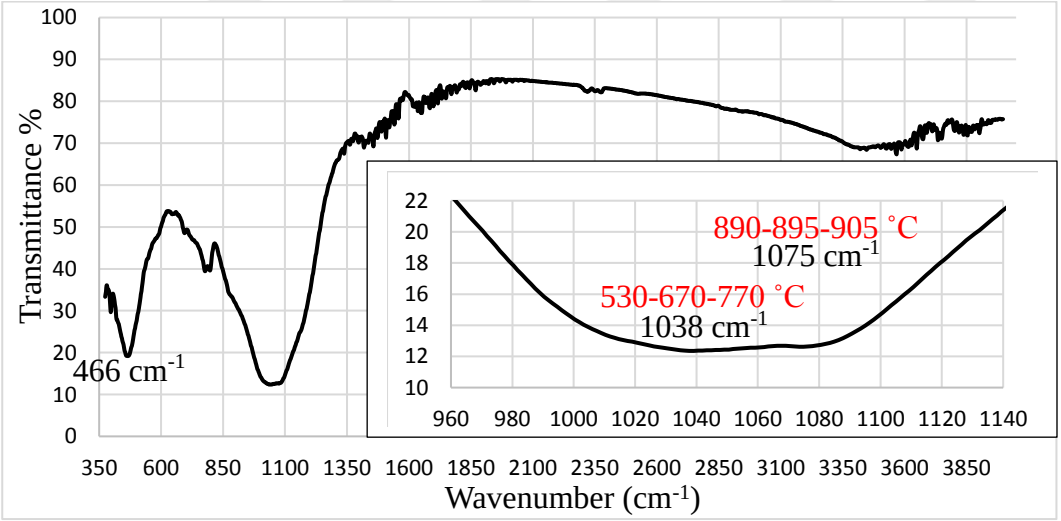

Figure 141. FTIR spectrum of the green glaze of the sample K159.

Table 81. Estimation of the firing temperature of the green glaze of K159.

Pellet	Res	# of Scans	v (cm^{-1})	T_{firing} (˚C)
K159.green.01	4	128	1038 & 1075	675-775

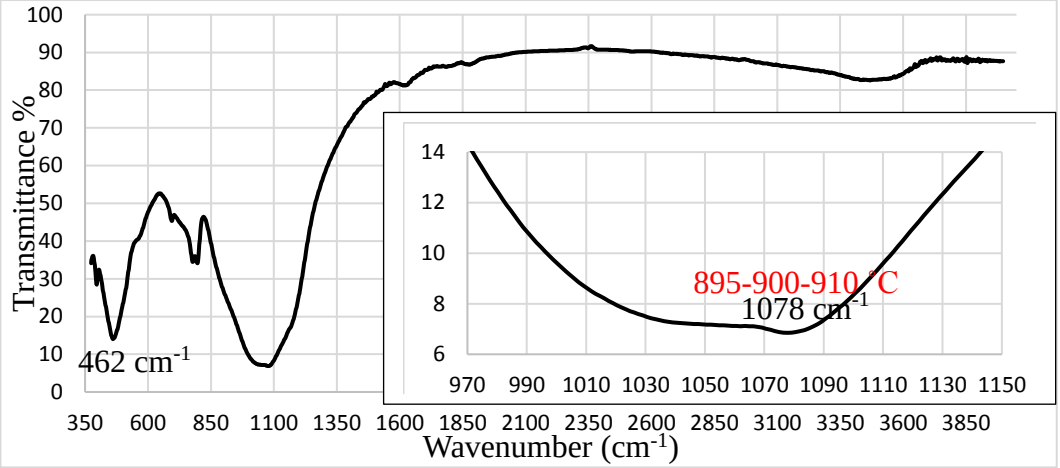

Figure 142. FTIR spectrum of the green glaze of the sample K160.

Table 82. Estimation of the firing temperature of the green glaze of K160.

Pellet	Res	# of Scans	v (cm^{-1})	T_{firing} (˚C)
K160.green.03	4	128	1078	900-925

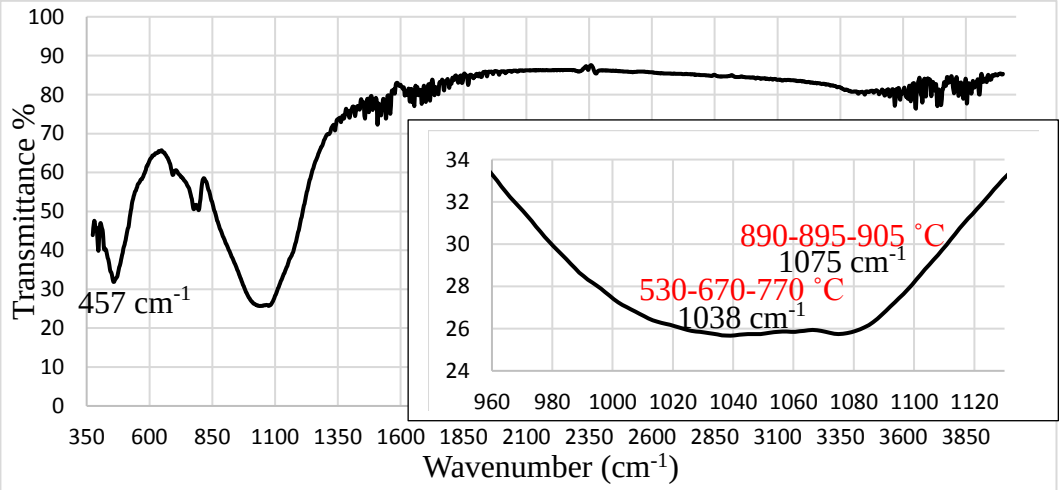

Figure 143. FTIR spectrum of the green glaze of the sample K161.

Table 83. Estimation of the firing temperature of the green glaze of K161.

Pellet	Res	# of Scans	v (cm^{-1})	T_{firing} (˚C)
K161.green.01	4	128	1038 & 1075	675-775

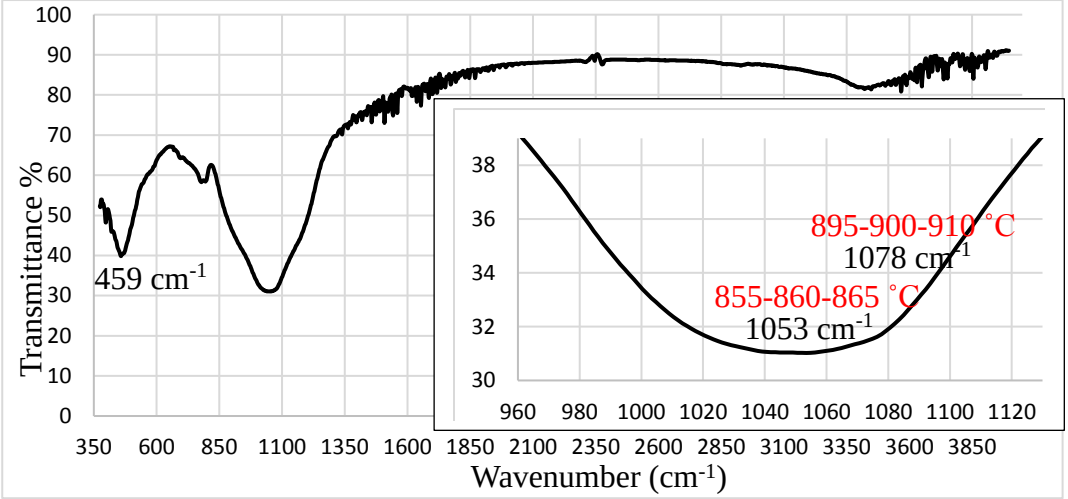

Figure 144. FTIR spectrum of the green glaze of the sample K168.

Table 84. Estimation of the firing temperature of the green glaze of K168.

Pellet	Res	# of Scans	ν (cm^{-1})	T_{firing} (˚C)
K168.green.01	4	128	1053	850-900

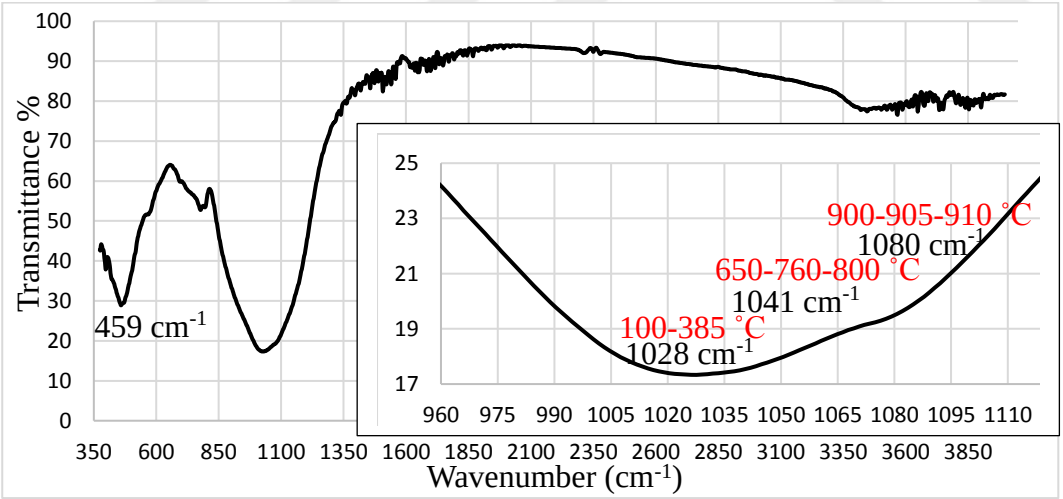

Figure 145. FTIR spectrum of the green glaze of the sample K169.

Table 85. Estimation of the firing temperature of the green glaze of K169.

Pellet	Res	# of Scans	ν (cm^{-1})	T_{firing} (˚C)
K169.green.01	4	128	1041 & 1080	600-700

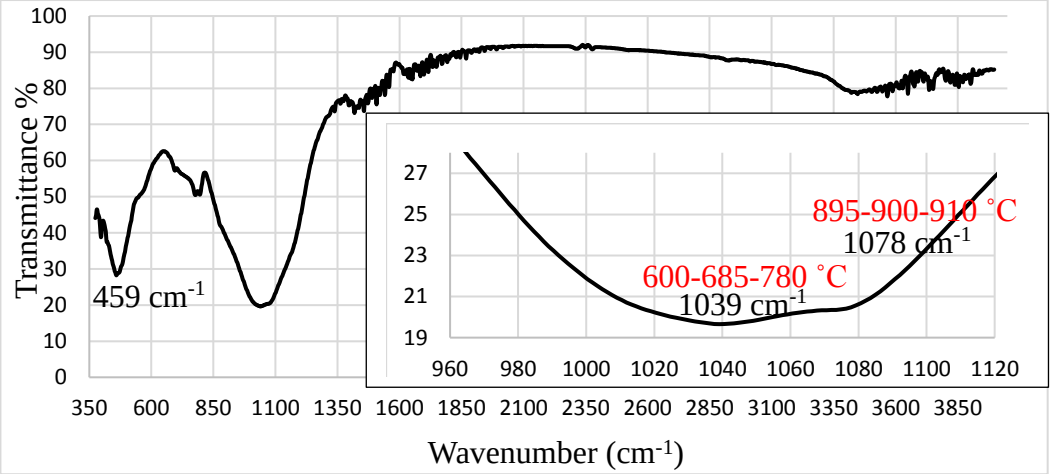

Figure 146. FTIR spectrum of the green glaze of the sample K170.

Table 86. Estimation of the firing temperature of the green glaze of K170.

Pellet	Res	# of Scans	v (cm^{-1})	T_{firing} (˚C)
K170.green.01	4	128	1039 & 1078	700-800

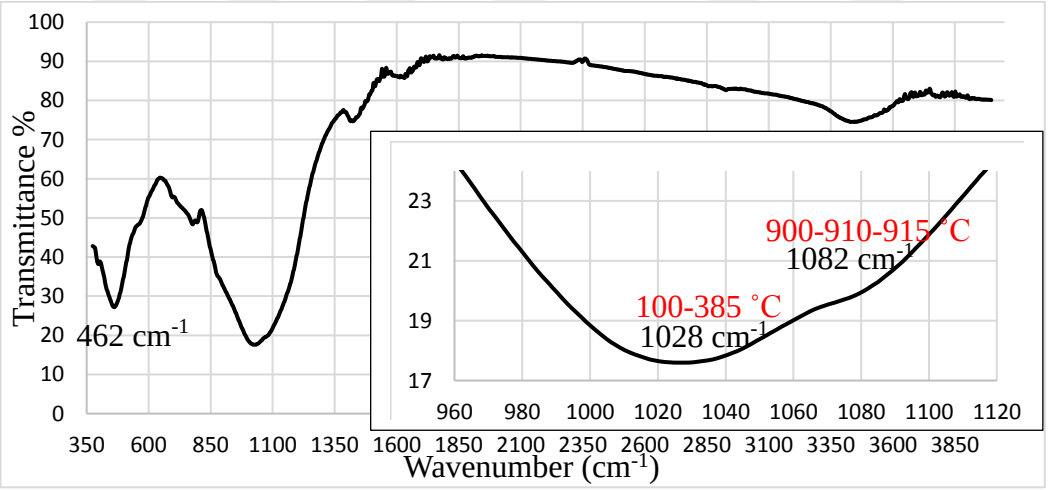

Figure 147. FTIR spectrum of the green glaze of the sample K184.

Table 87. Estimation of the firing temperature of the green glaze of K184.

Pellet	Res	# of Scans	v (cm^{-1})	T_{firing} (˚C)
K184.green.01	4	128	1028 & 1082	600-700

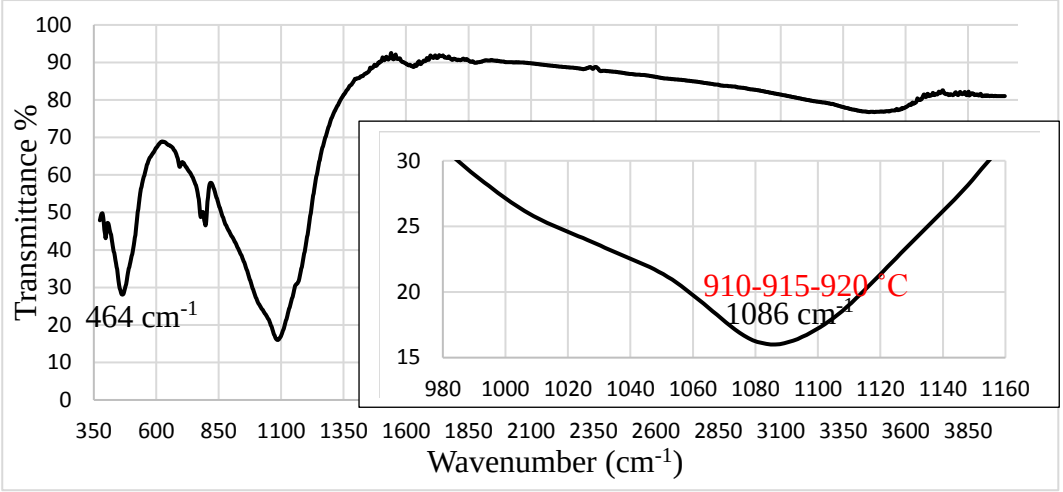

Figure 148. FTIR spectrum of the green glaze of the sample K199.

Table 88. Estimation of the firing temperature of the green glaze of K199.

Pellet	Res	# of Scans	v (cm^{-1})	T_{firing} (˚C)
K199.green.01	4	128	1086	900-925

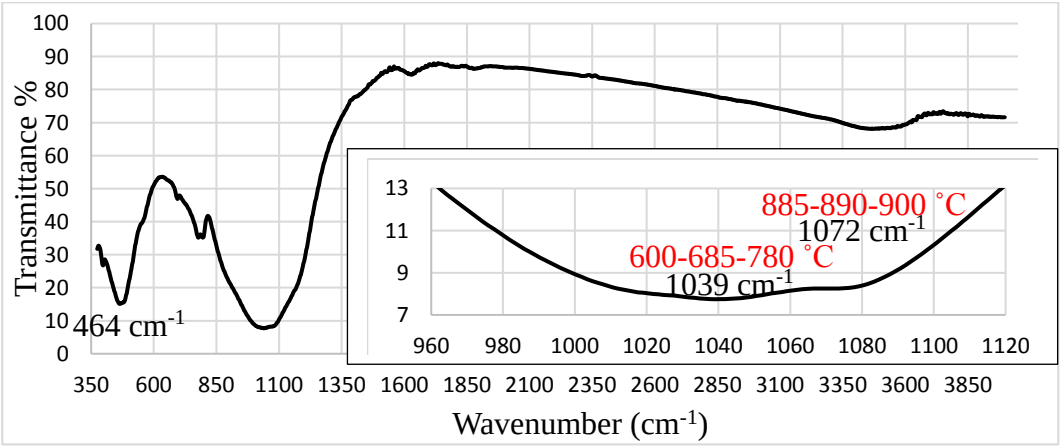

Figure 149. FTIR spectrum of the interior green glaze of the sample K201.

Table 89. Estimation of the firing temperature of the interior green glaze of K201.

Pellet	Res	# of Scans	v (cm^{-1})	T_{firing} (˚C)
K201.green.interior.01	4	128	1039 & 1072	700-800

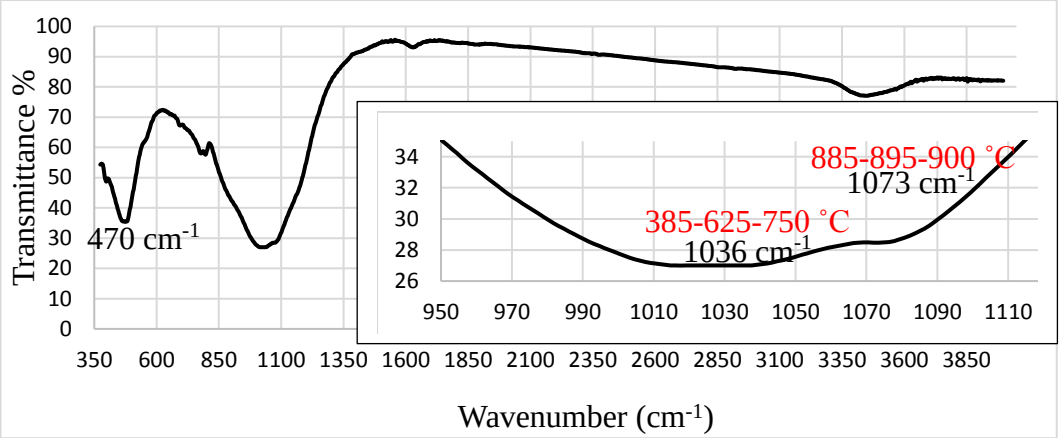

Figure 150. FTIR spectrum of the exterior green glaze of the sample K201.

Table 90. Estimation of the firing temperature of the exterior green glaze of K201.

Pellet	Res	# of Scans	ν (cm^{-1})	T_{firing} (˚C)
K201.green.exterior.01	4	128	1036 & 1073	650-750

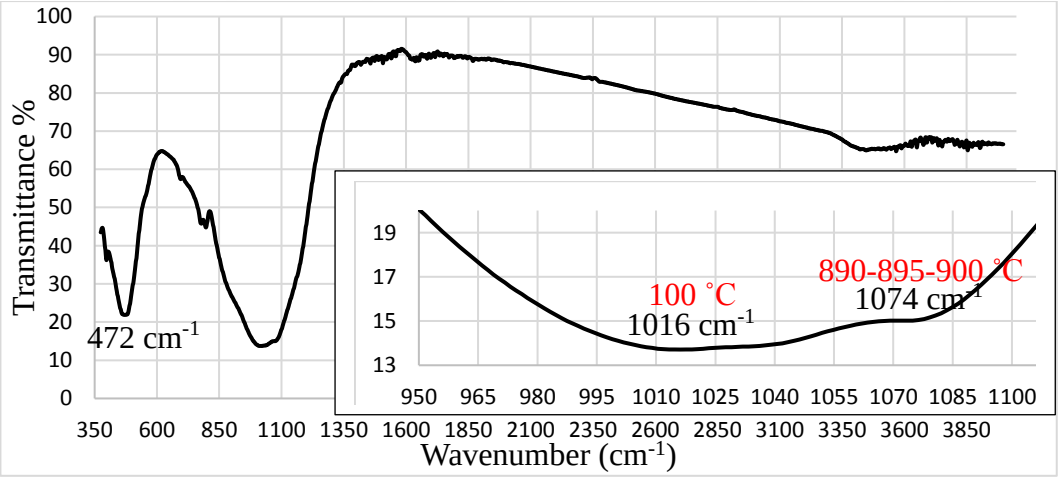

Figure 151. FTIR spectrum of the green glaze of the sample K204.

Table 91. Estimation of the firing temperature of the green glaze of K204.

Pellet	Res	# of Scans	ν (cm^{-1})	T_{firing} (˚C)
K204.green.01	4	128	1016 & 1074	600-700

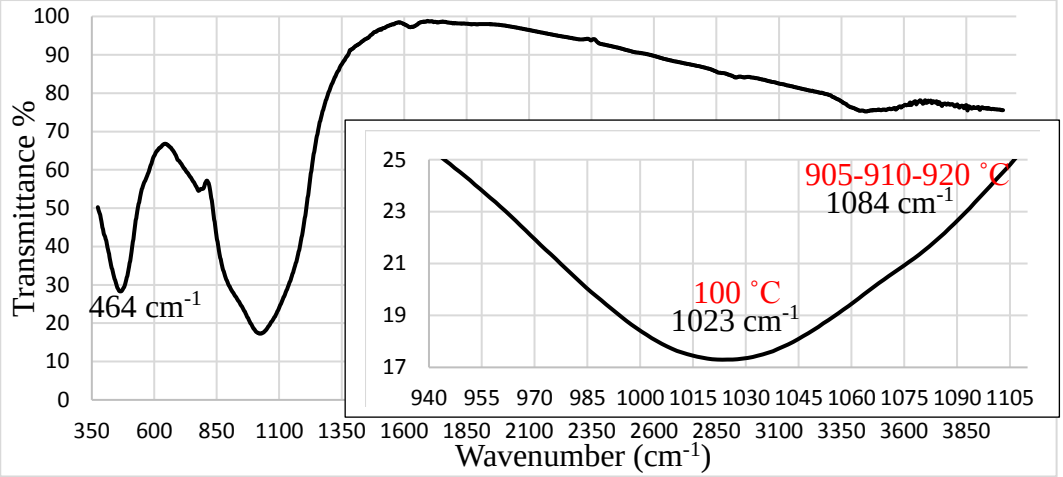

Figure 152. FTIR spectrum of the green glaze of the sample K210.

Table 92. Estimation of the firing temperature of the green glaze of K210.

Pellet	Res	# of Scans	ν (cm^{-1})	T_{firing} (˚C)
K210.green.01	4	128	1023 & 1084	600-700

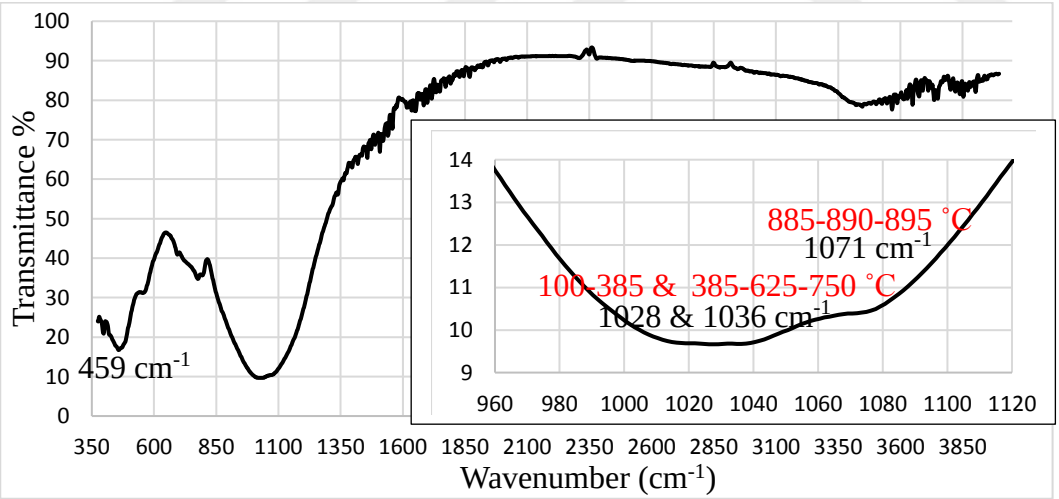

Figure 153. FTIR spectrum of the green glaze of the sample K212.

Table 93. Estimation of the firing temperature of the green glaze of K212.

Pellet	Res	# of Scans	ν (cm^{-1})	T_{firing} (˚C)
K212.green.01	4	128	1036 & 1071	650-750

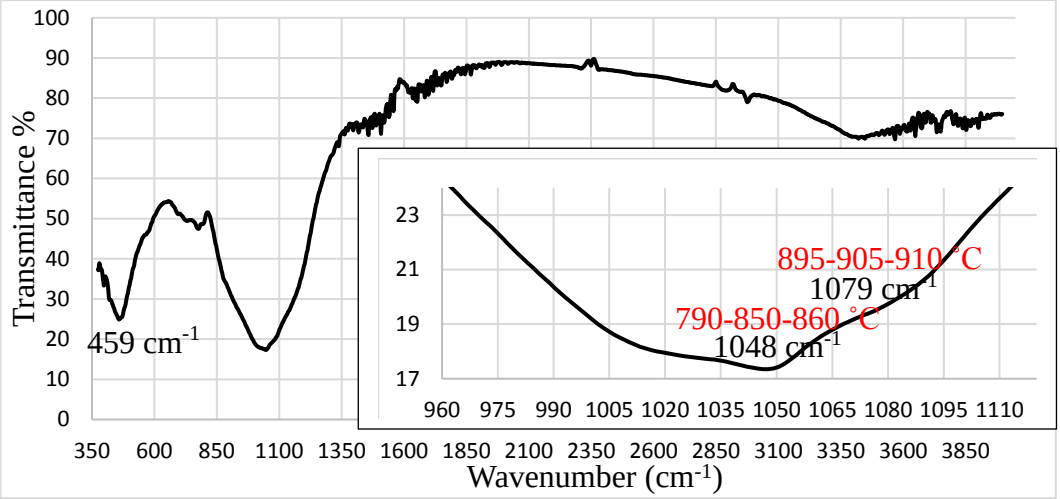

Figure 154. FTIR spectrum of the green glaze of the sample K213.

Table 94. Estimation of the firing temperature of the green glaze of K213.

Pellet	Res	# of Scans	v (cm^{-1})	T_{firing} (˚C)
K213.green.01	4	128	1048 & 1079	850-900

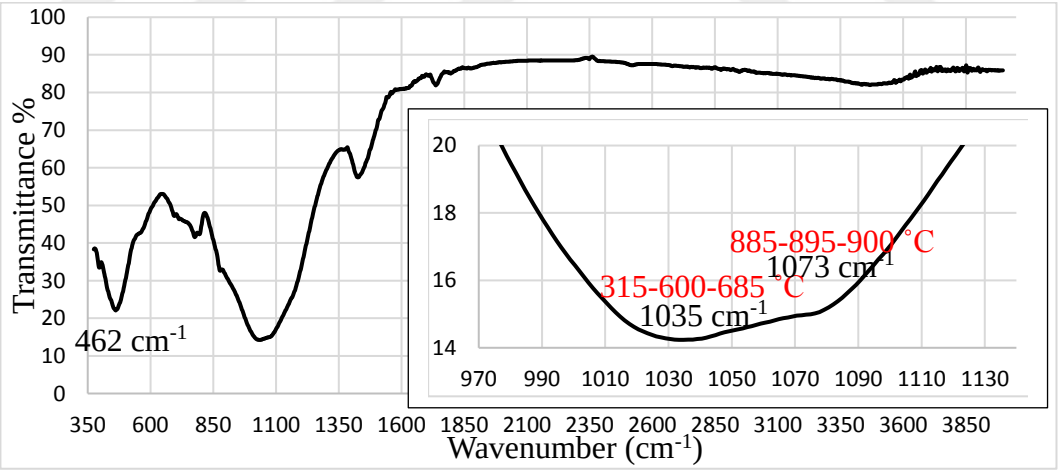

Figure 155. FTIR spectrum of the green glaze of the sample K220.

Table 95. Estimation of the firing temperature of the green glaze of K220.

Pellet	Res	# of Scans	v (cm^{-1})	T_{firing} (˚C)
K220.green.03	4	128	1035 & 1073	600-700

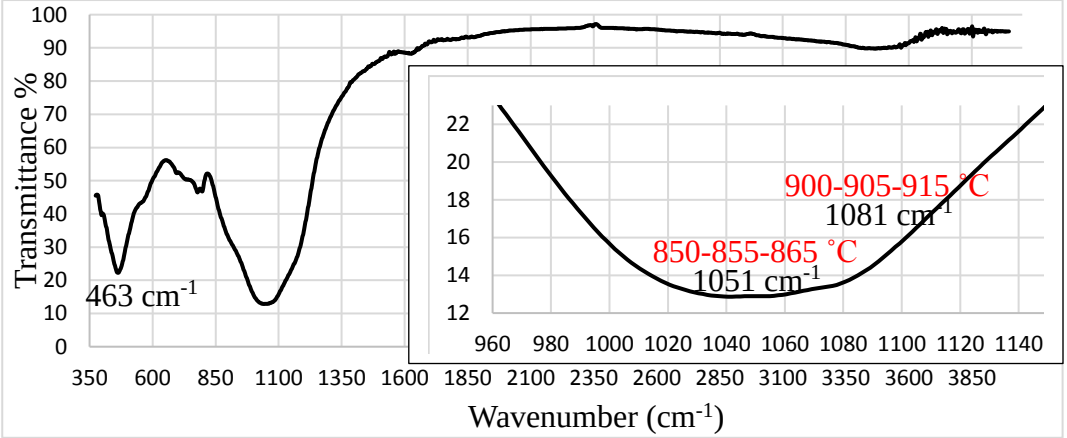

Figure 156. FTIR spectrum of the interior green glaze of the sample K222.

Table 96. Estimation of the firing temperature of the K222 interior green glaze.

Pellet	Res	# of Scans	v (cm^{-1})	T_{firing} (˚C)
K222.green.interior.03	4	128	1051 & 1081	850-900

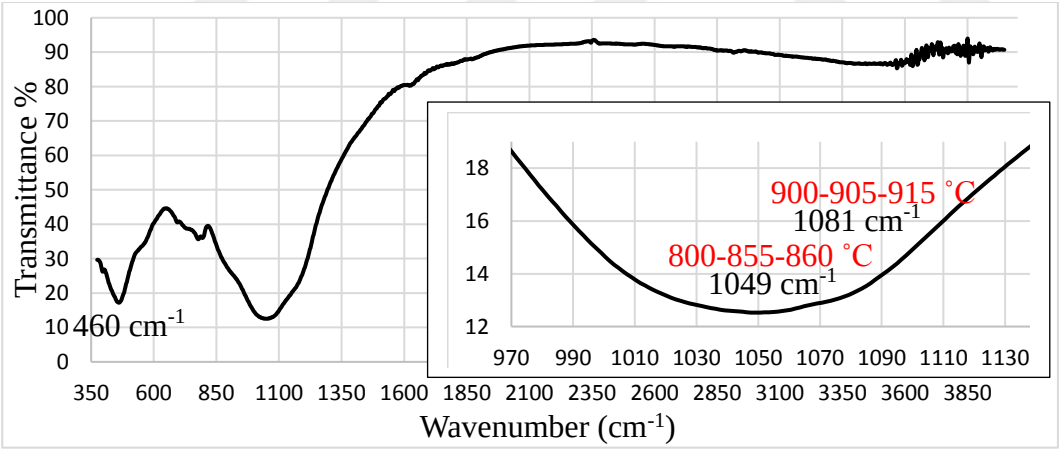

Figure 157. FTIR spectrum of the exterior green glaze of the sample K222.

Table 97. Estimation of the firing temperature of the exterior green glaze of K222.

Pellet	Res	# of Scans	v (cm^{-1})	T_{firing} (˚C)
K222.green.exterior.02	4	128	1049 & 1081	850-900

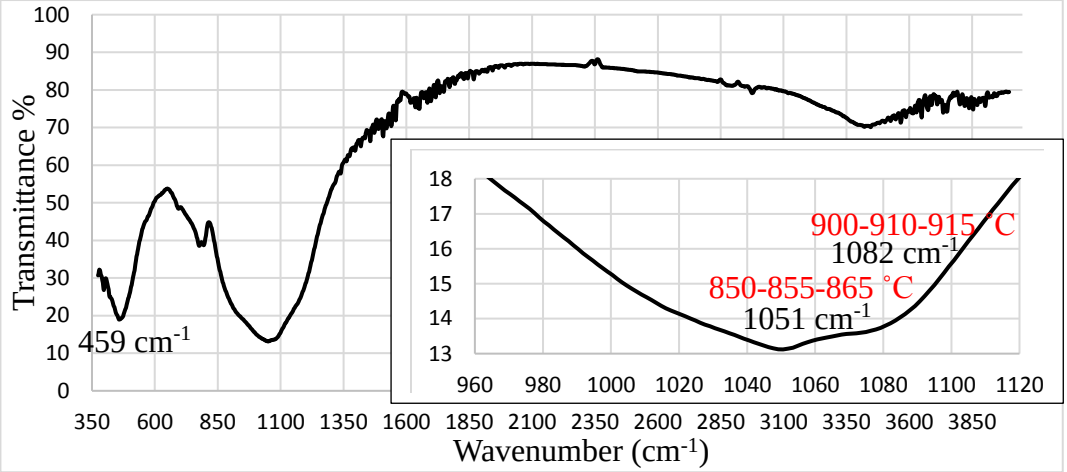

Figure 158. FTIR spectrum of the green glaze of the sample K226.

Table 98. Estimation of the firing temperature of the green glaze of K226.

Pellet	Res	# of Scans	v (cm^{-1})	T_{firing} (˚C)
K226.green.01	4	128	1051 & 1082	850-900

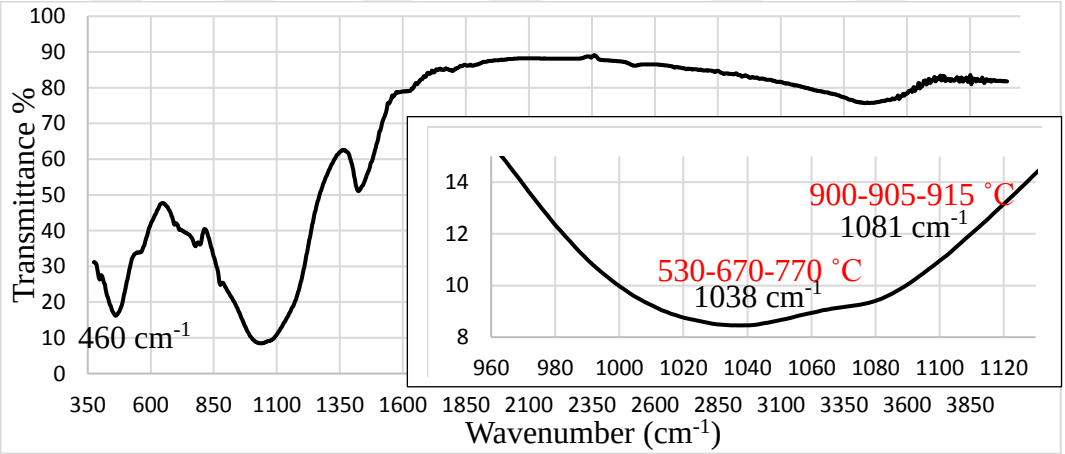

Figure 159. FTIR spectrum of the green glaze of the sample K228.

Table 99. Estimation of the firing temperature of the green glaze of K228.

Pellet	Res	# of Scans	v (cm^{-1})	T_{firing} (˚C)
K228.green.03	4	128	1038 & 1081	675-775

A.2.3. FTIR Spectra of the Orange Glazes

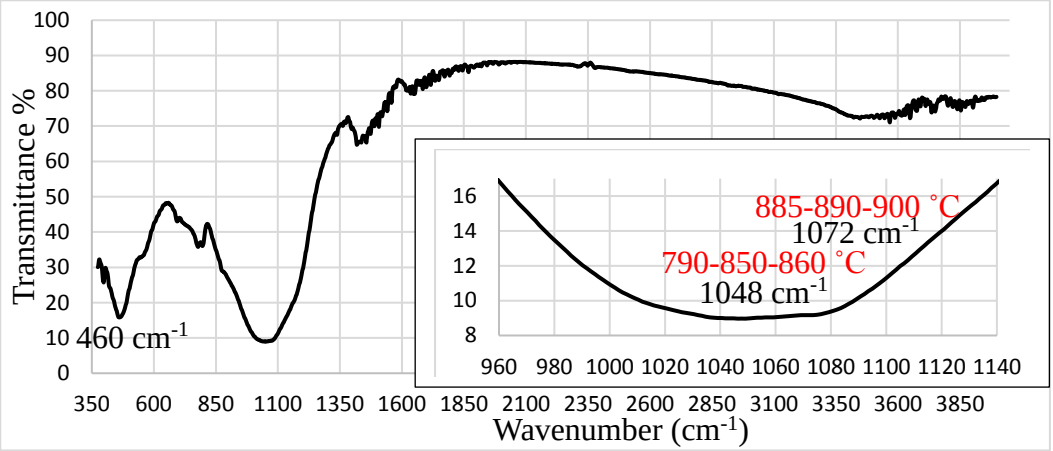

Figure 160. FTIR spectrum of the orange glaze of the sample K164.

Table 100. Estimation of the firing temperature of the orange glaze of K164.

Pellet	Res	# of Scans	ν (cm^{-1})	T_{firing} (˚C)
K164.orange.01	4	128	1048 & 1072	850-900

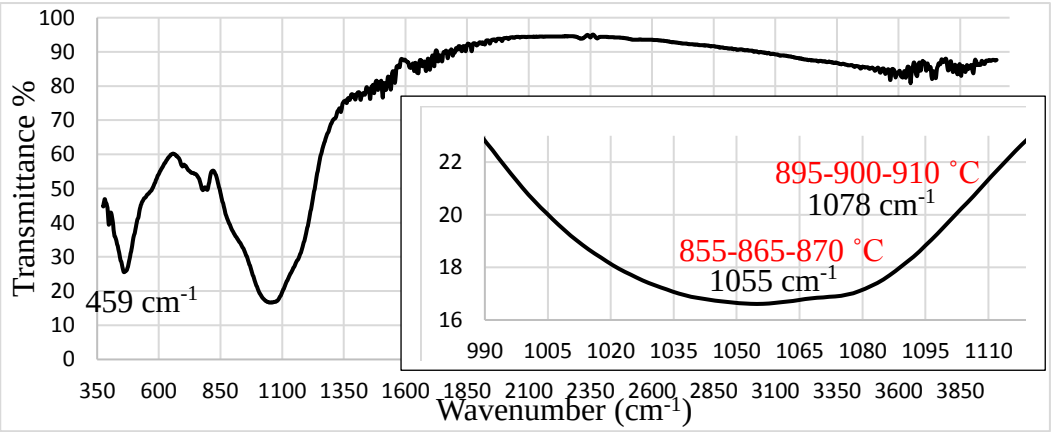

Figure 161. FTIR spectrum of the orange glaze of the sample K171.

Table 101. Estimation of the firing temperature of the orange glaze of K171.

Pellet	Res	# of Scans	ν (cm^{-1})	T_{firing} (˚C)
K171.orange.01	4	128	1055 & 1078	850-900

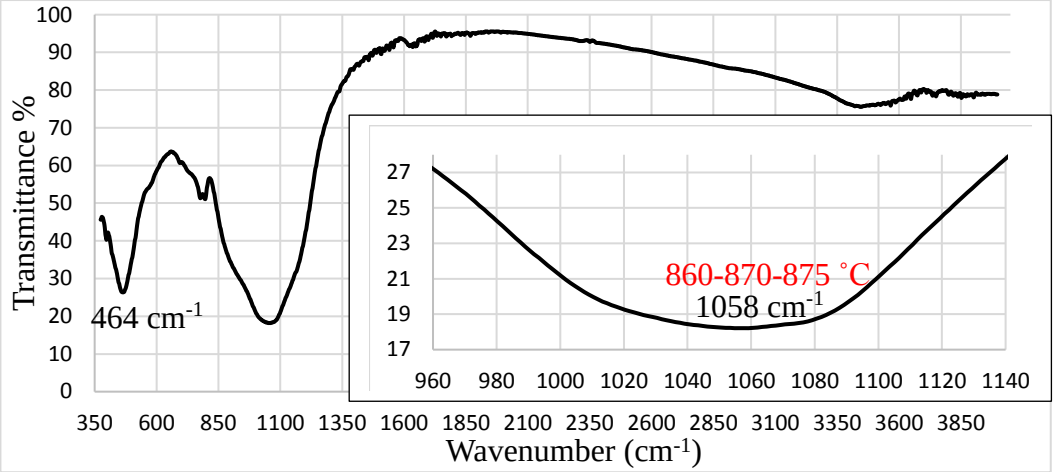

Figure 162. FTIR spectrum of K172 interior orange glaze.

Table 102. Estimation of the firing temperature of K172 interior orange glaze.

Pellet	Res	# of Scans	v (cm^{-1})	T_{firing} (°C)
K172.orange.interior.01	4	128	1058 & 1086	850-900

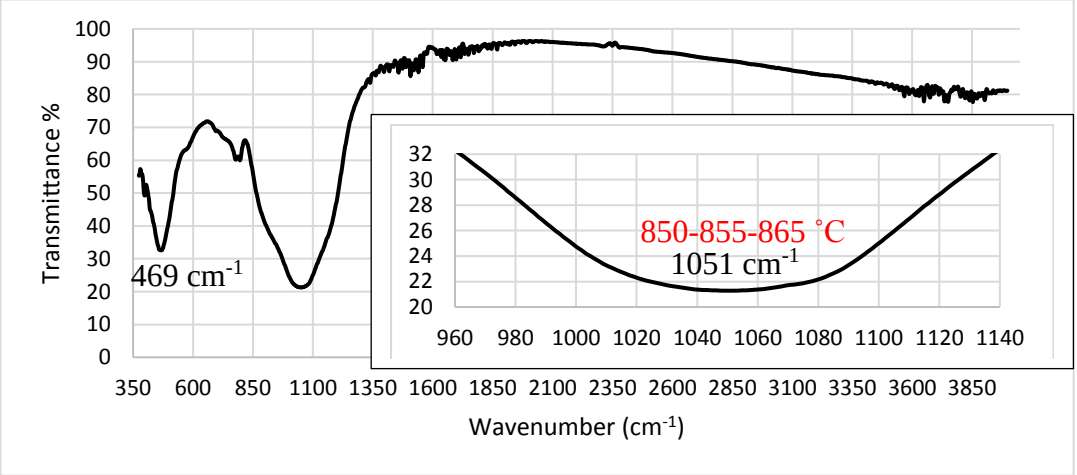

Figure 163. FTIR spectrum of the exterior orange glaze of the sample K172.

Table 103. Estimation of the firing temperature of K172 exterior orange glaze.

Pellet	Res	# of Scans	v (cm^{-1})	T_{firing} (°C)
K172.orange.exterior.01	4	128	1051	850-900

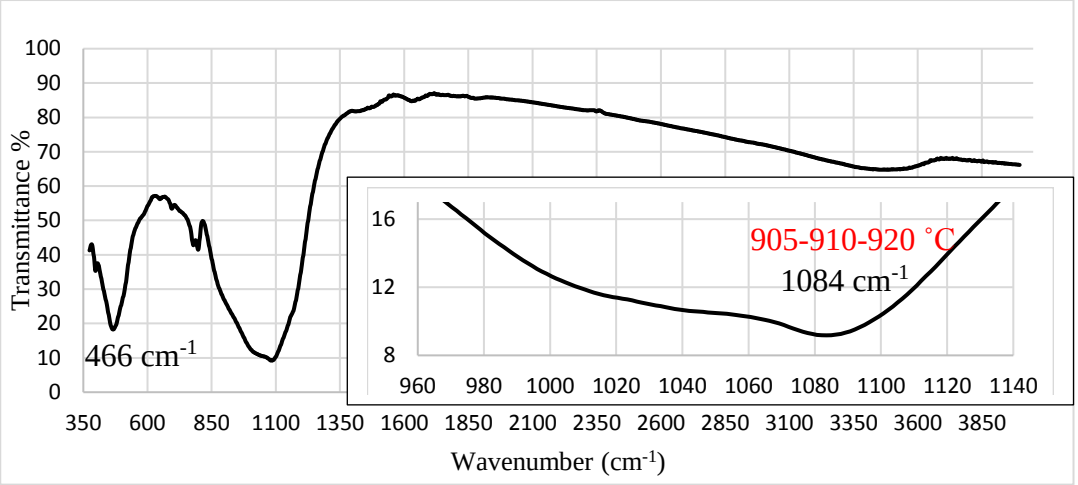

Figure 164. FTIR spectrum of the interior orange glaze of the sample K173.

Table 104. Estimation of the firing temperature of K173 interior orange glaze.

Pellet	Res	# of Scans	v (cm^{-1})	T_{firing} (˚C)
K173.orange.interior.01	4	128	1084	900-925

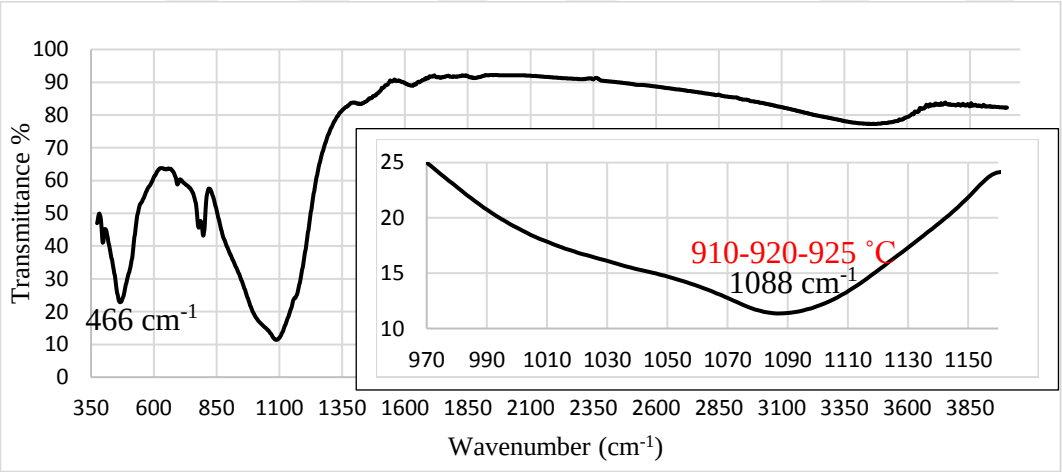

Figure 165. FTIR spectrum of the exterior orange glaze of the sample K173.

Table 105. Estimation of the firing temperature of K173 exterior orange glaze.

Pellet	Res	# of Scans	v (cm^{-1})	T_{firing} (˚C)
K173.orange.exterior.01	4	128	1088	900-925

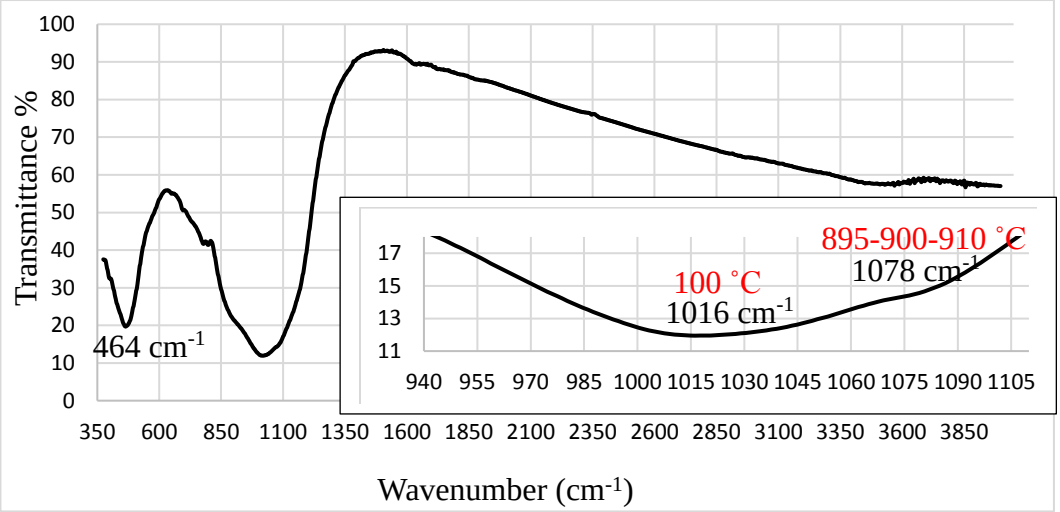

Figure 166. FTIR spectrum of the orange glaze of the sample K203.

Table 106. Estimation of the firing temperature of the orange glaze of K203.

Pellet	Res	# of Scans	ν (cm^{-1})	T_{firing} (˚C)
K203.orange.01	4	128	1043 & 1078	600-700

A.2.4. FTIR Spectra of the Turquoise Glazes

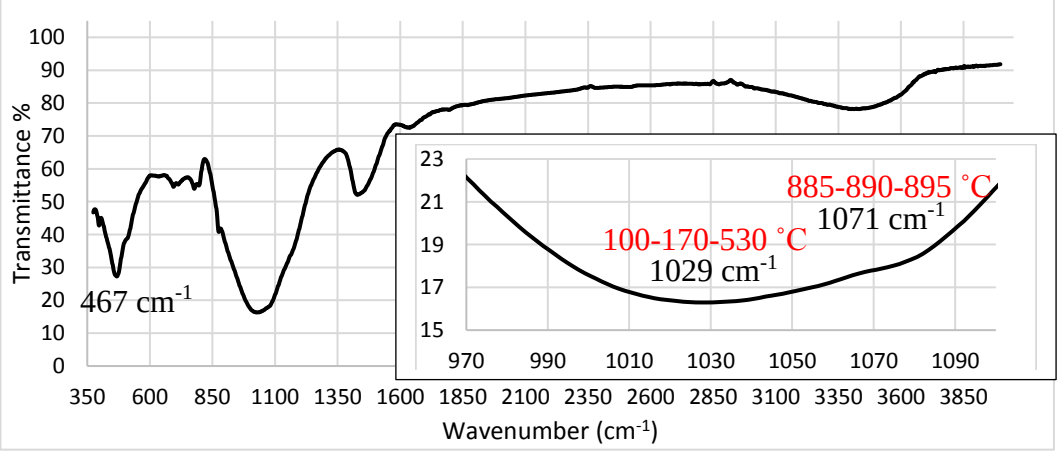

Figure 167. FTIR spectrum of the turquoise glaze of the tile sample K001.

Table 107. Estimation of the firing temperature of K001 tile turquoise glaze.

Pellet	Res	# of Scans	ν (cm^{-1})	T_{firing} (˚C)
K001.tq.01	4	128	1029	600-700

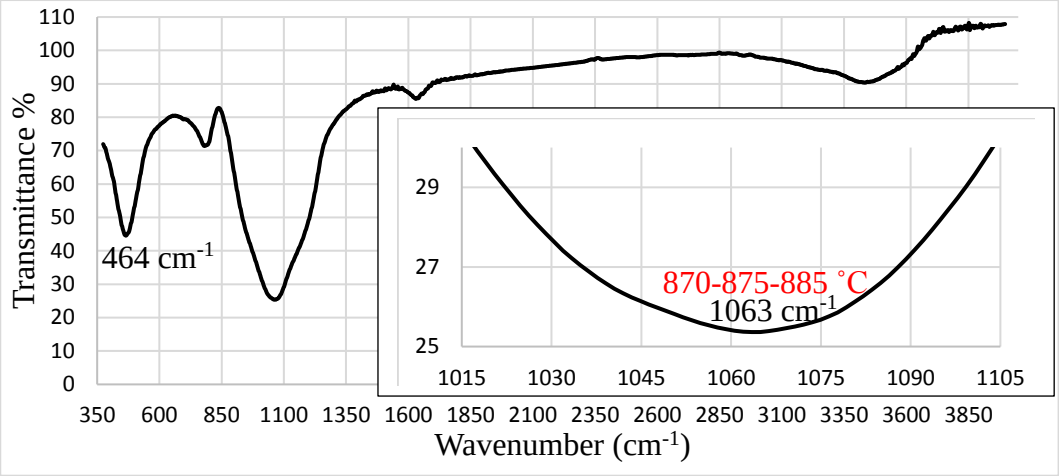

Figure 168. FTIR spectrum of the turquoise glaze of the sample K223.

Table 108. Estimation of the firing temperature of the turquoise glaze of K223.

Pellet	Res	# of Scans	ν (cm^{-1})	T_{firing} (˚C)
K223.tq.03	4	128	1063	850-900

A.2.5. FTIR Spectra of the Brown Glazes

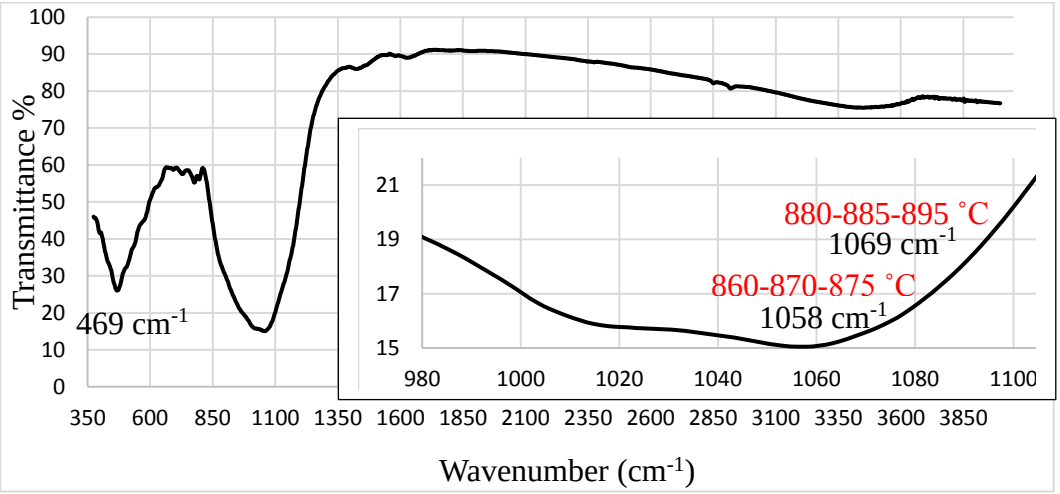

Figure 169. FTIR spectrum of the brown glaze of the sample K102.

Table 109. Estimation of the firing temperature of the brown glaze of K102.

Pellet	Res	# of Scans	ν (cm^{-1})	T_{firing} (˚C)
K102.brown.01	4	128	1058	850-900

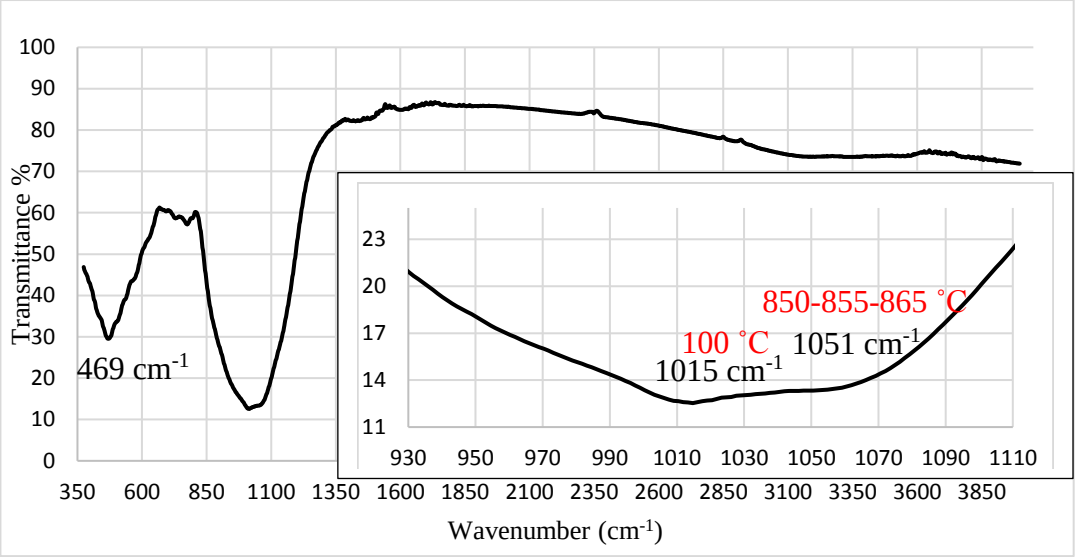

Figure 170. FTIR spectrum of the brown glaze of the sample K108.

Table 110. Estimation of the firing temperature of the brown glaze of K108.

Pellet	Res	# of Scans	v (cm^{-1})	T_{firing} (˚C)
K108.brown.01	4	128	1015 &1051	600-700

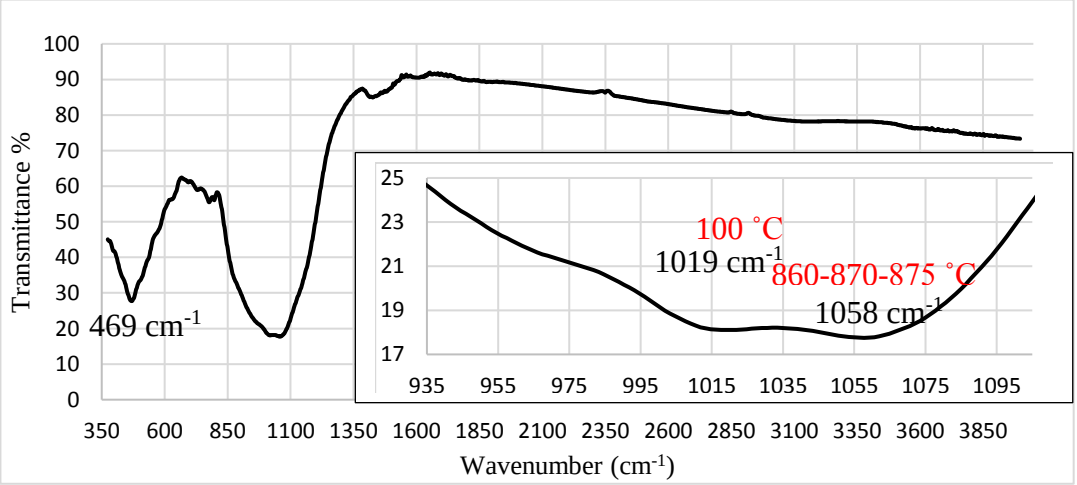

Figure 171. FTIR spectrum of the brown glaze of the sample K117.

Table 111. Estimation of the firing temperature of the brown glaze of K117.

Pellet	Res	# of Scans	v (cm^{-1})	T_{firing} (˚C)
K117.brown.interior.01	4	128	1058	850-900

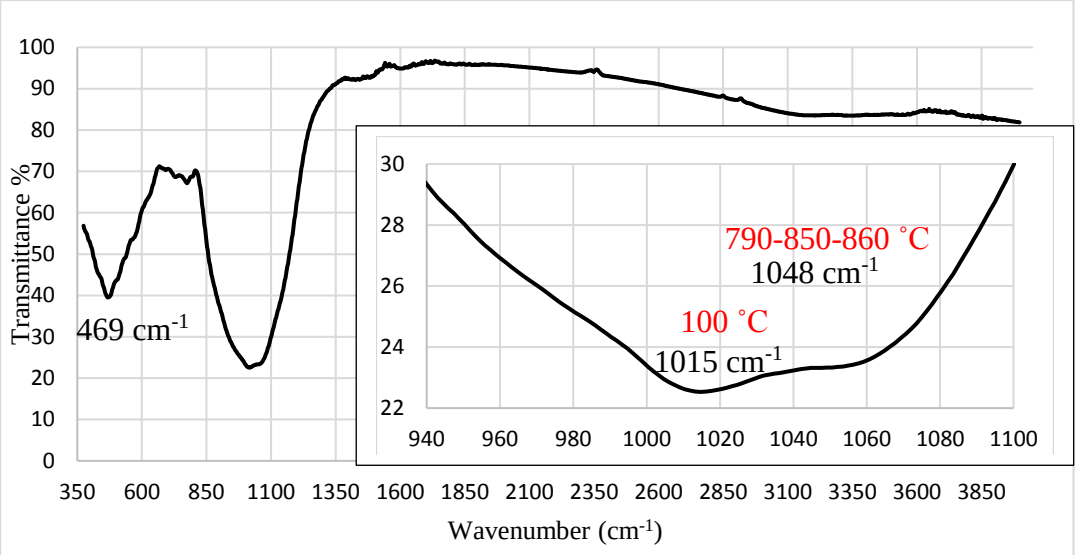

Figure 172. FTIR spectrum of the brown glaze of the sample K118.

Table 112. Estimation of the firing temperature of the brown glaze of K118.

Pellet	Res	# of Scans	ν (cm^{-1})	T_{firing} (˚C)
K118.brown.interior.01	4	128	1015 & 1048	600-700

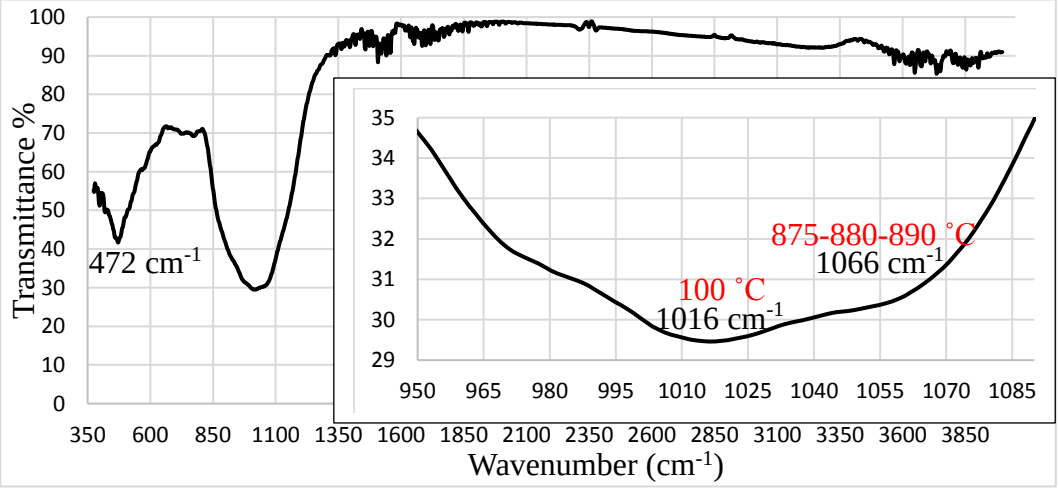

Figure 173. FTIR spectrum of the brown glaze of the sample K129.

Table 113. Estimation of the firing temperature of the brown glaze of K129.

Pellet	Res	# of Scans	ν (cm^{-1})	T_{firing} (˚C)
K129.brown.01	4	128	1016 & 1066	600-700

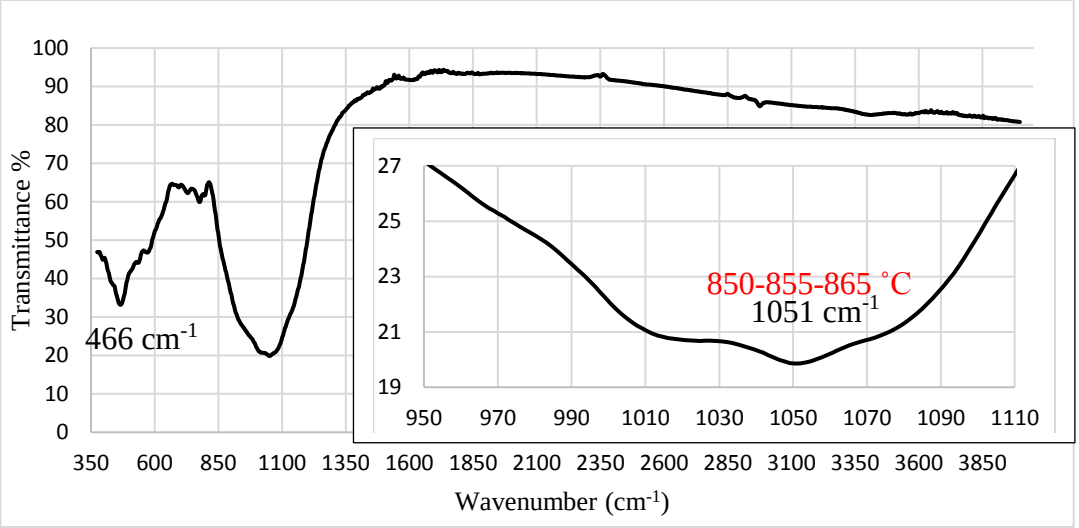

Figure 174. FTIR spectrum of the brown glaze of the sample K146.

Table 114. Estimation of the firing temperature of the brown glaze of K146.

Pellet	Res	# of Scans	ν (cm^{-1})	T_{firing} (˚C)
K146.brown.01	4	128	1051	850-900

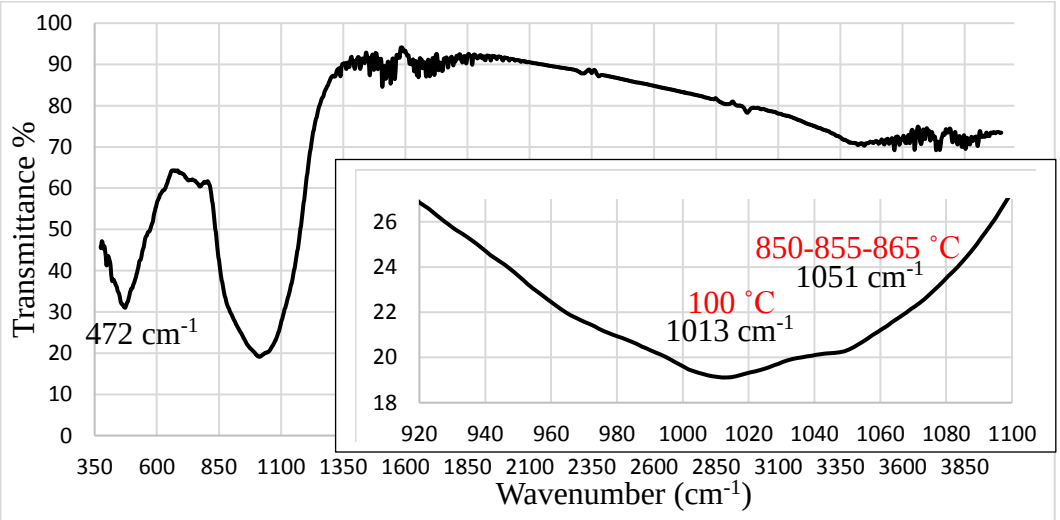

Figure 175. FTIR spectrum of the brown glaze of the sample K164.

Table 115. Estimation of the firing temperature of the brown glaze of K164.

Pellet	Res	# of Scans	ν (cm^{-1})	T_{firing} (˚C)
K164.brown.01	4	128	1013 & 1051	600-700

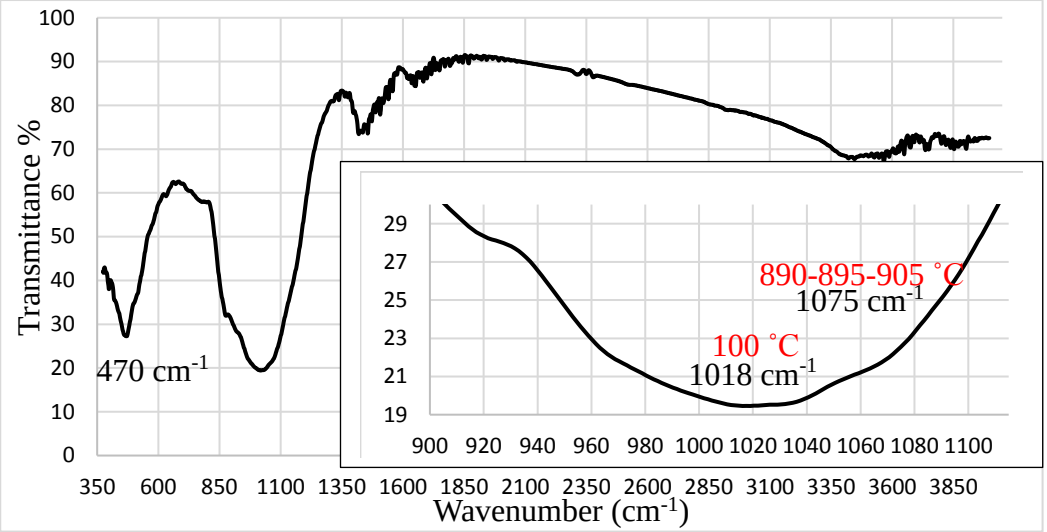

Figure 176. FTIR spectrum of the brown glaze of the sample K169.

Table 116. Estimation of the firing temperature of the brown glaze of K169.

Pellet	Res	# of Scans	ν (cm^{-1})	T_{firing} (˚C)
K169.brown.01	4	128	1018 & 1075	600-700

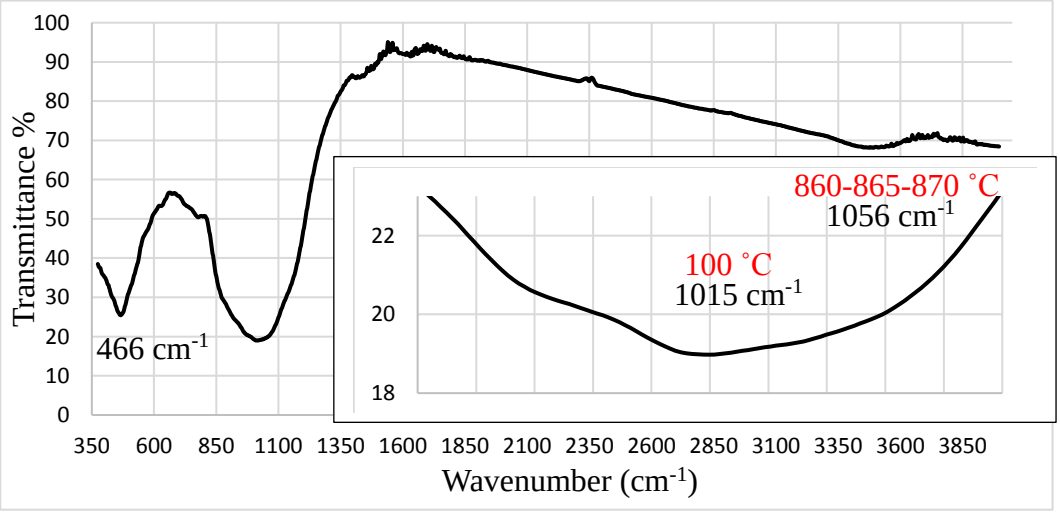

Figure 177. FTIR spectrum of the brown glaze of the sample K184.

Table 117. Estimation of the firing temperature of the brown glaze of K184.

Pellet	Res	# of Scans	ν (cm^{-1})	T_{firing} (˚C)
K184.brown.01	4	128	1015 & 1056	600-700

A.2.6. FTIR Spectrum of the Black Glaze

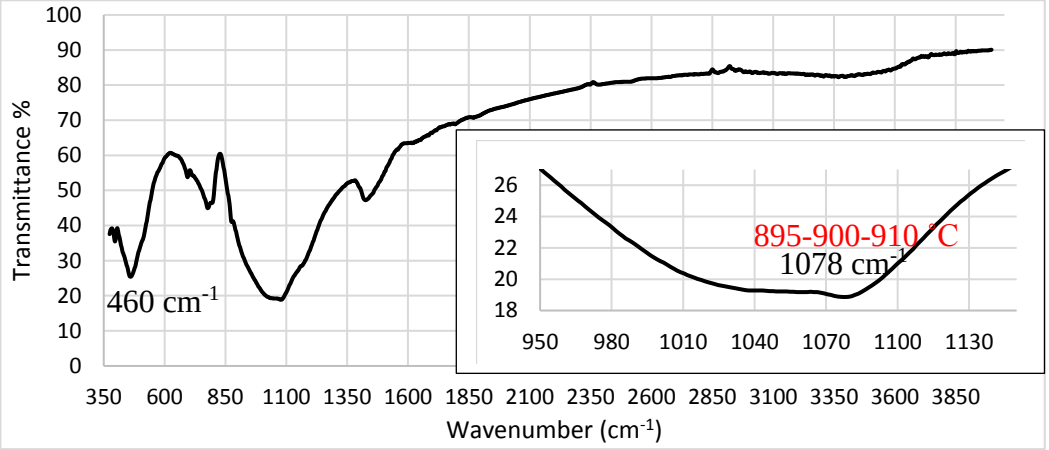

Figure 178. FTIR spectrum of the black glaze of the tile sample K002.

Table 118. Estimation of the firing temperature of the black glaze of K002.

Pellet	Res	# of Scans	v (cm^{-1})	T_{firing} (˚C)
K002.black.tile.01	4	128	1078	900-925

A.2.7. FTIR Spectra of the Red and White Pastes under the Glazes

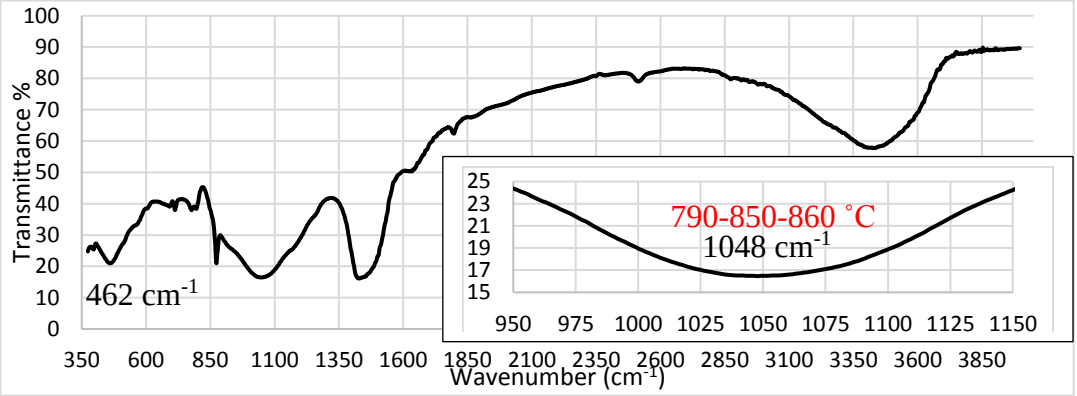

Figure 179. FTIR spectrum of the white paste of the turquoise tile sample K001.

Table 119. Estimation of the firing temperature of the white paste of K001.

Pellet	Res	# of Scans	v (cm^{-1})	T_{firing} (˚C)
K001.white.paste.01	4	128	1048	850-900

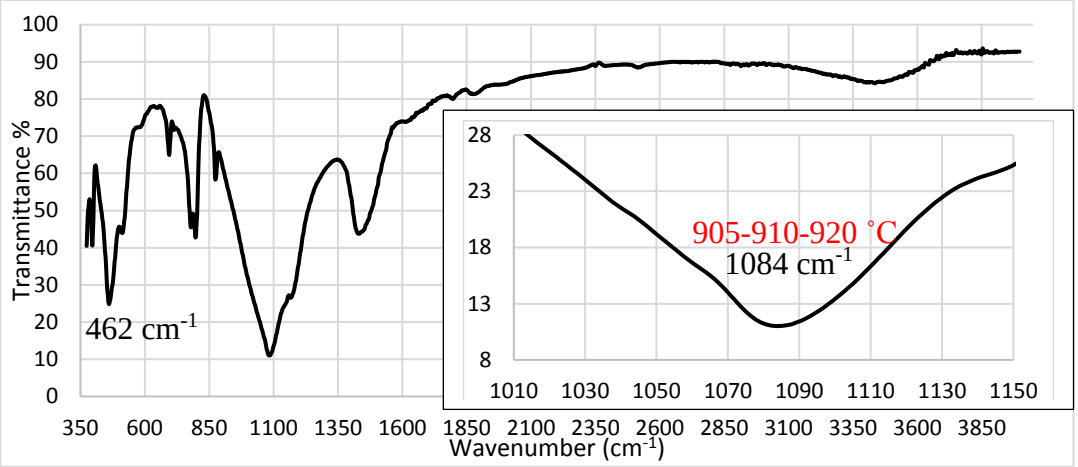

Figure 180. FTIR spectrum of the white paste of the black tile sample K002.

Table 120. Estimation of the firing temperature of the white paste of K002.

Pellet	Res	# of Scans	v (cm^{-1})	T_{firing} (°C)
K002.white.paste.01	4	128	1084	900-925

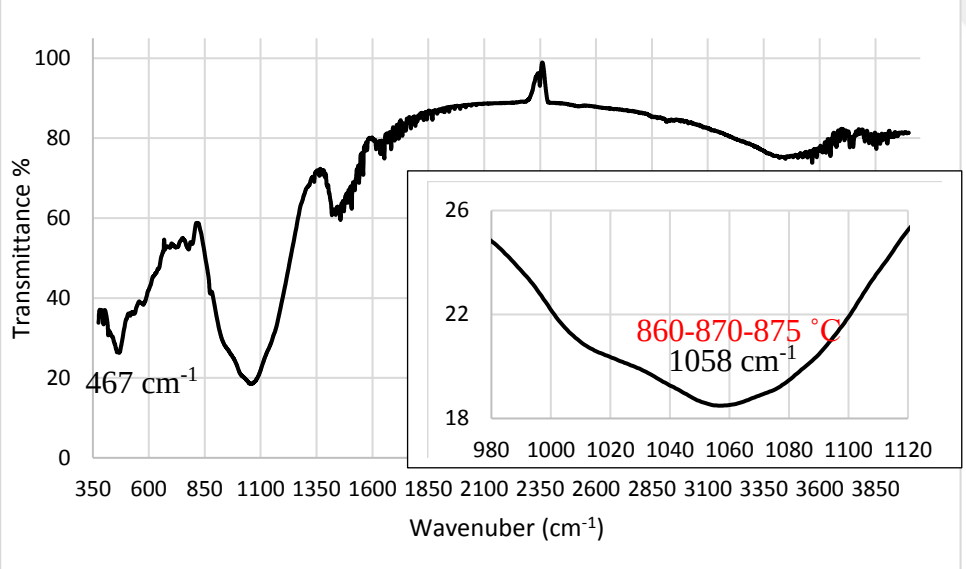

Figure 181. FTIR spectrum of the red paste of the sample K101.

Table 121. Estimation of the firing temperature of the red paste of K101.

Pellet	Res	# of Scans	v (cm^{-1})	T_{firing} (°C)
K101.red.paste.01	4	128	1058	850-900

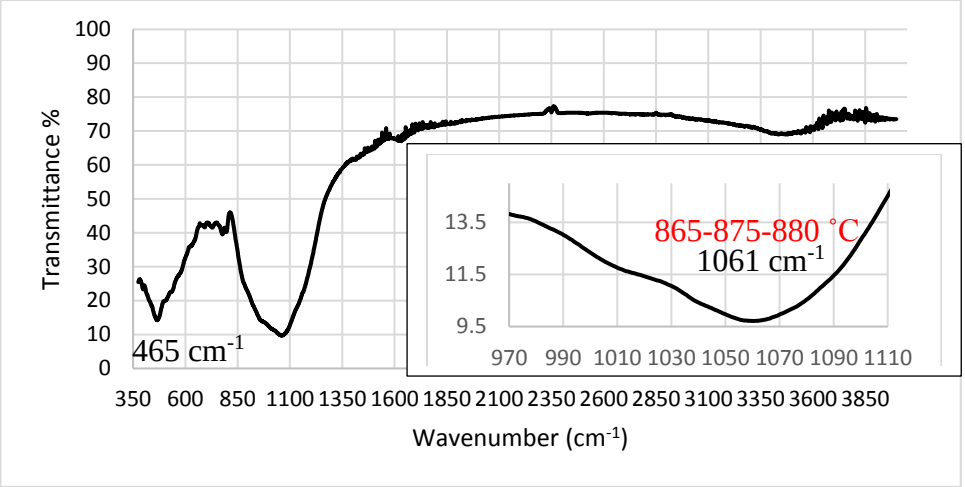

Figure 182. FTIR spectrum of the red paste of the sample K104.

Table 122. Estimation of the firing temperature of the red paste of K104.

Pellet	Res	# of Scans	v (cm^{-1})	T_{firing} (˚C)
K104.red.paste.01	4	128	1061	850-900

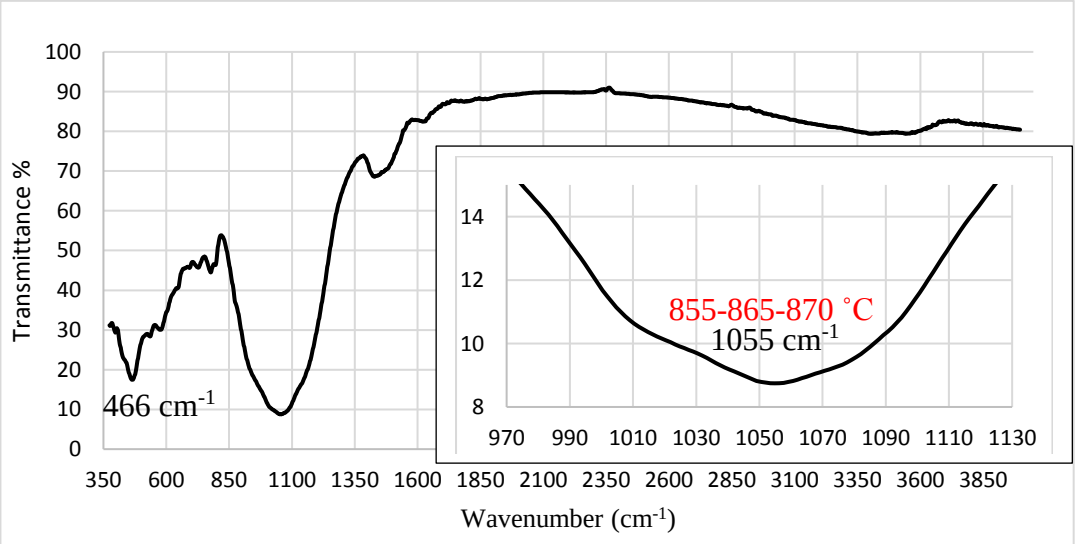

Figure 183. FTIR spectrum of the red paste of the sample K106.

Table 123. Estimation of the firing temperature of the red paste of K106.

Pellet	Res	# of Scans	v (cm^{-1})	T_{firing} (˚C)
K106.red.paste.01	4	128	1055	850-900

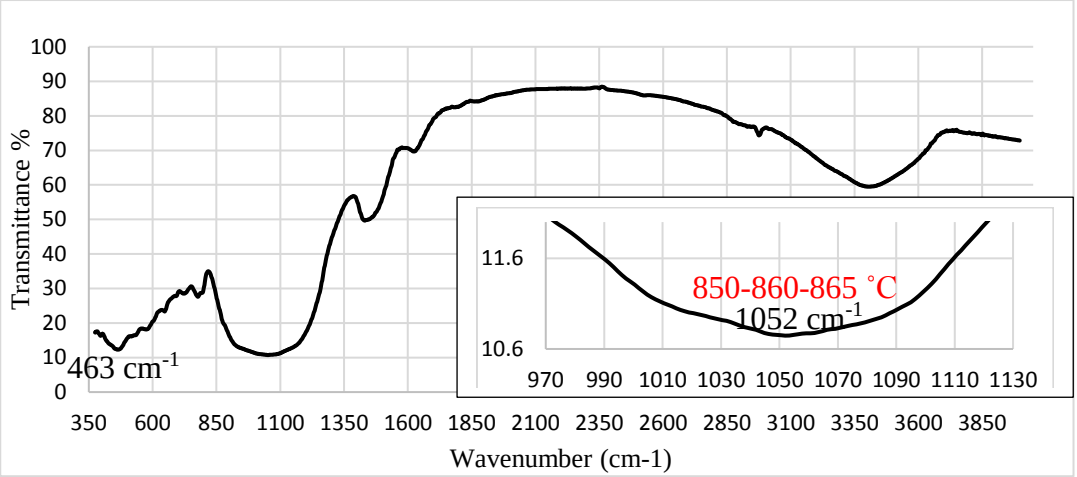

Figure 184. FTIR spectrum of the red paste of the sample K149.

Table 124. Estimation of the firing temperature of the red paste of K149.

Pellet	Res	# of Scans	ν (cm^{-1})	T_{firing} (˚C)
K149.red.paste.01	4	128	1052	850-900

A.2.8. FTIR Spectra of the White Slips under the Glazes

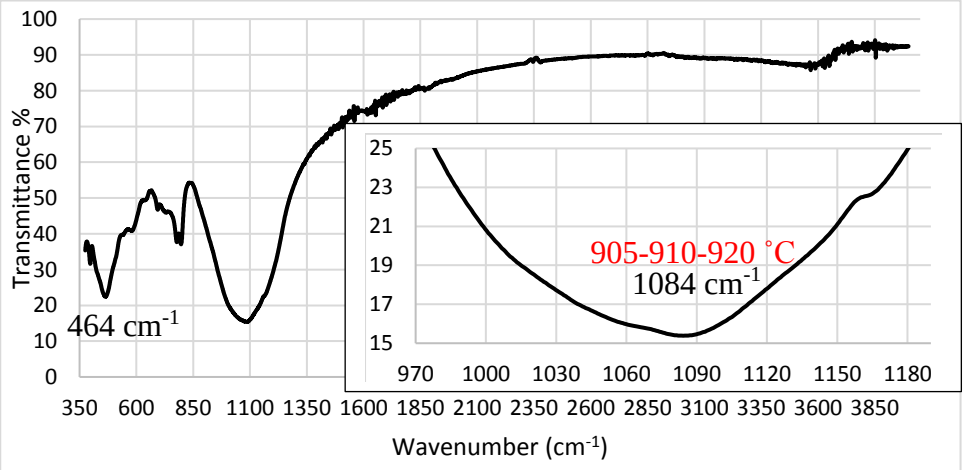

Figure 185. FTIR spectrum of the white slip of the sample K104.

Table 125. Estimation of the firing temperature of the white slip of K104.

Pellet	Res	# of Scans	ν (cm^{-1})	T_{firing} (˚C)
K104.white.slip.02	4	128	1084	900-925

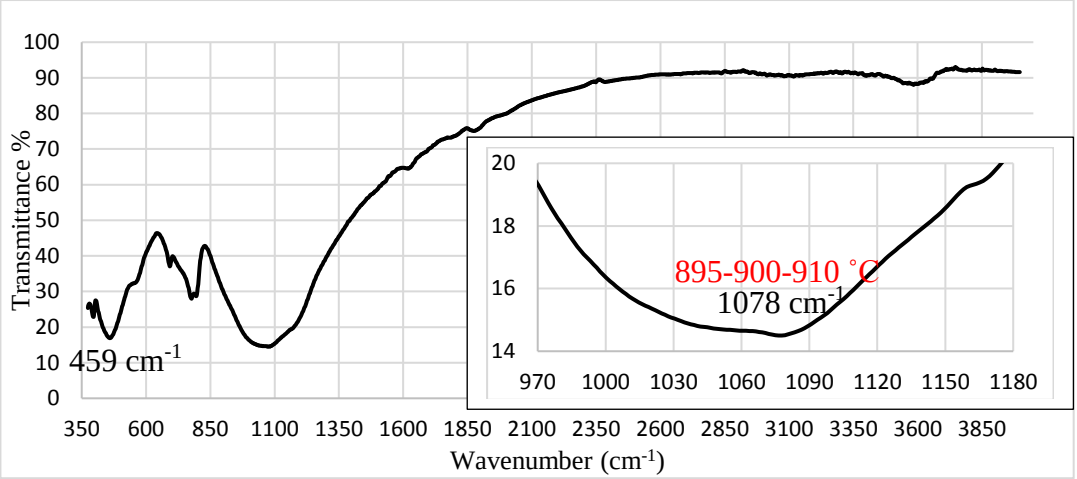

Figure 186. FTIR spectrum of the white slip of the sample K106.

Table 126. Estimation of the firing temperature of the white slip of K106.

Pellet	Res	# of Scans	v (cm^{-1})	T_{firing} (˚C)
K106.white.slip.01	4	128	1078	900-925

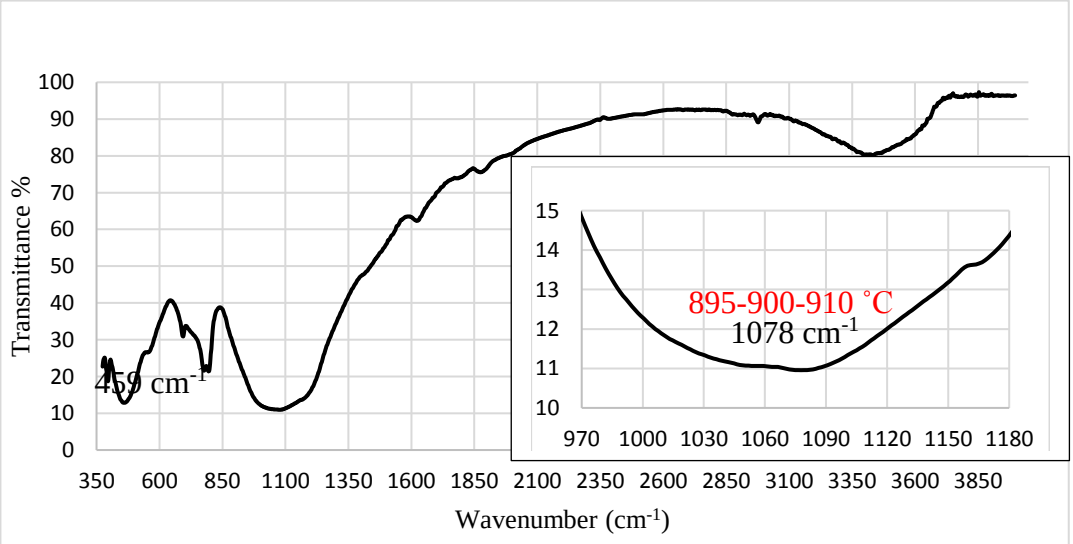

Figure 187. FTIR spectrum of the white slip of the sample K149.

Table 127. Estimation of the firing temperature of the white slip of K149.

Pellet	Res	# of Scans	v (cm^{-1})	T_{firing} (˚C)
K149.white.slip.01	4	128	1078	900-925

A.2.9. Comparison of the FTIR Spectra of Glazes of Various Colors with Each Other

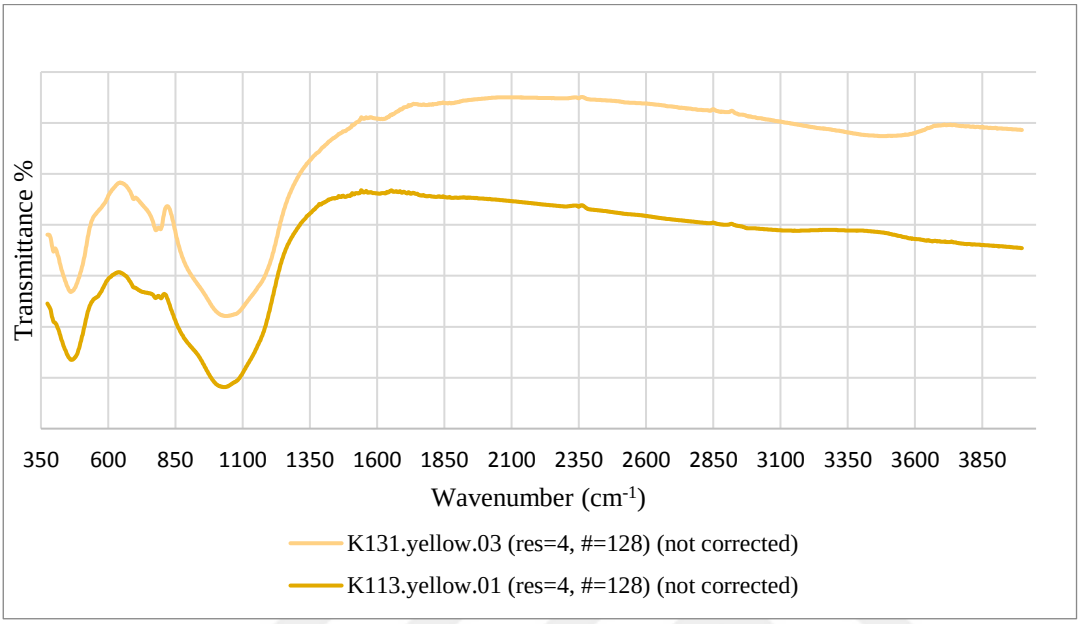

Figure 188. Comparison of the FTIR spectra of yellow glazes.

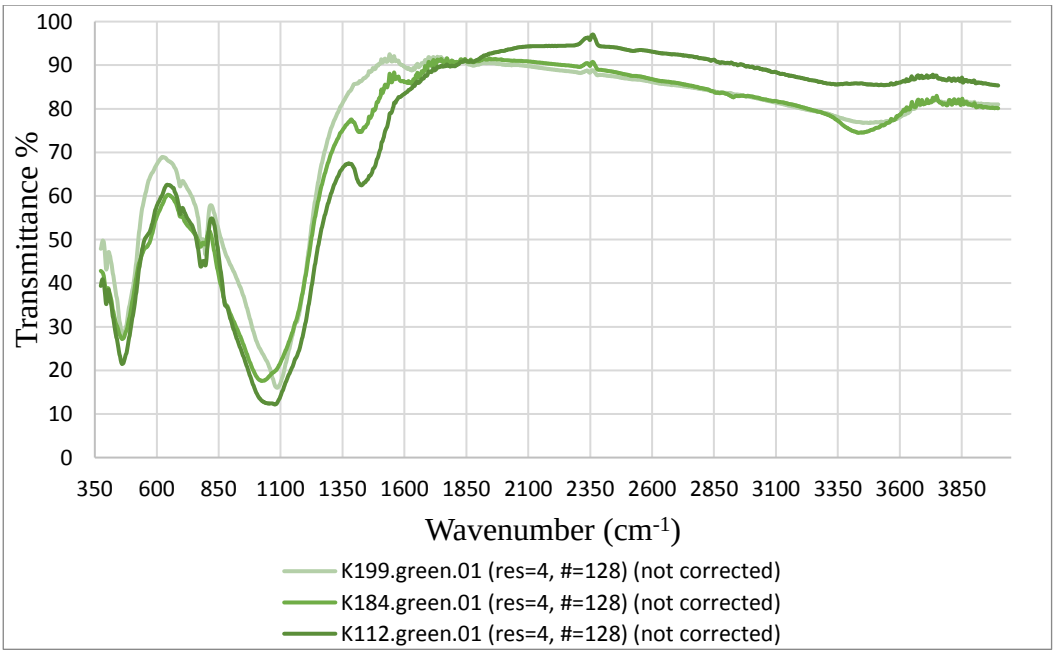

Figure 189. Comparison of the FTIR spectra of green glazes.

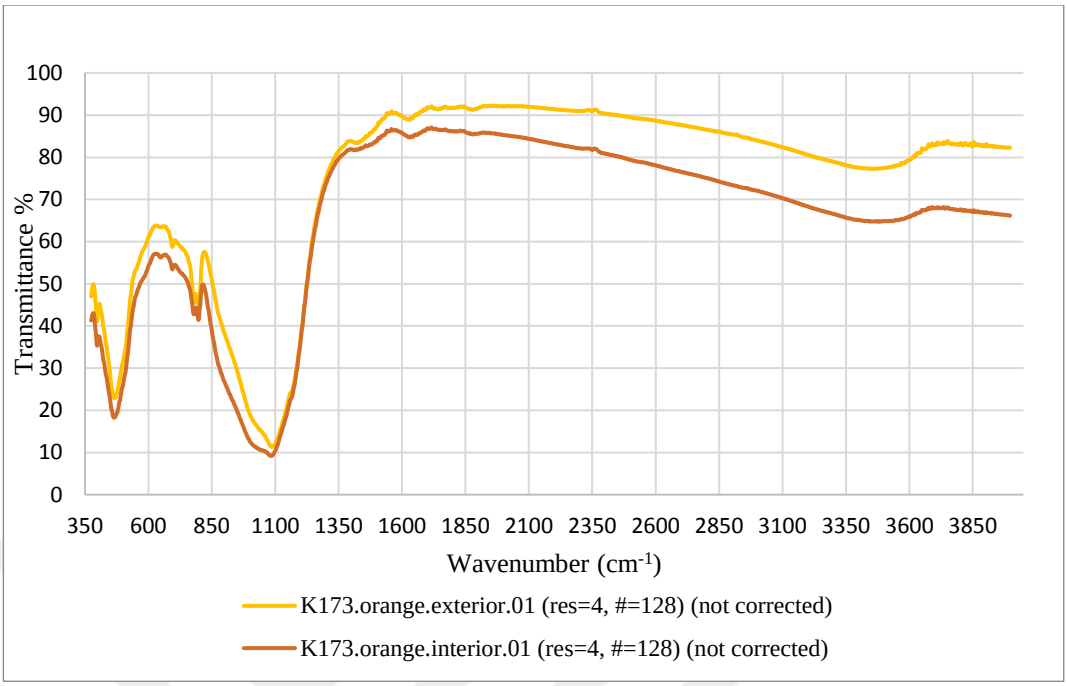

Figure 190. Comparison of the FTIR spectra of orange glazes.

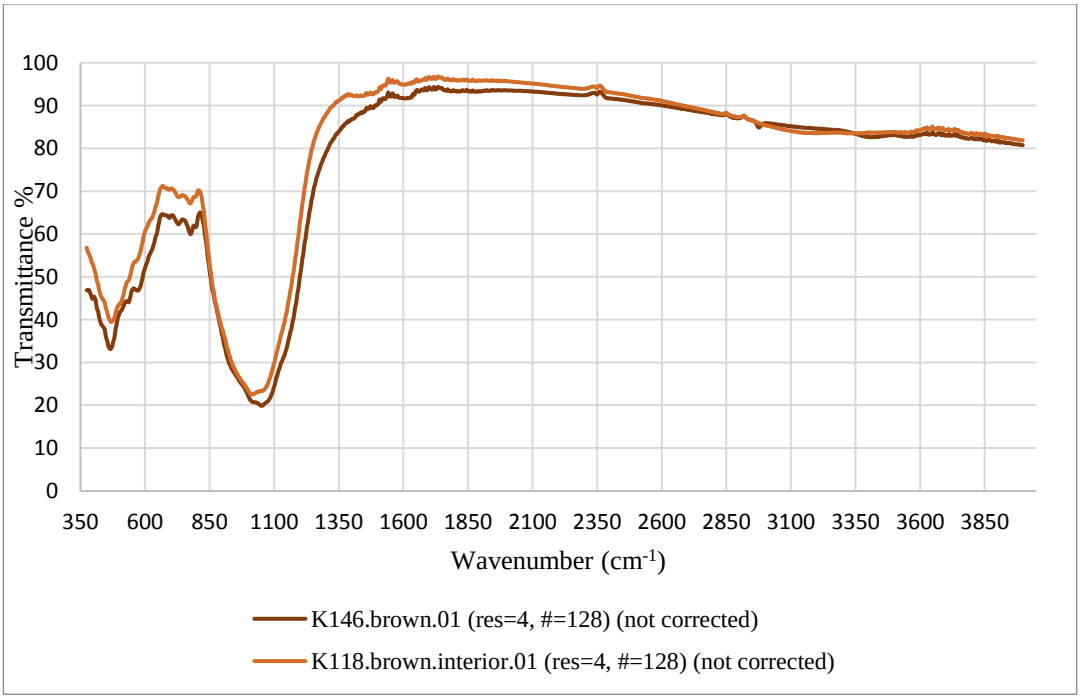

Figure 191. Comparison of the FTIR spectra of brown glazes.

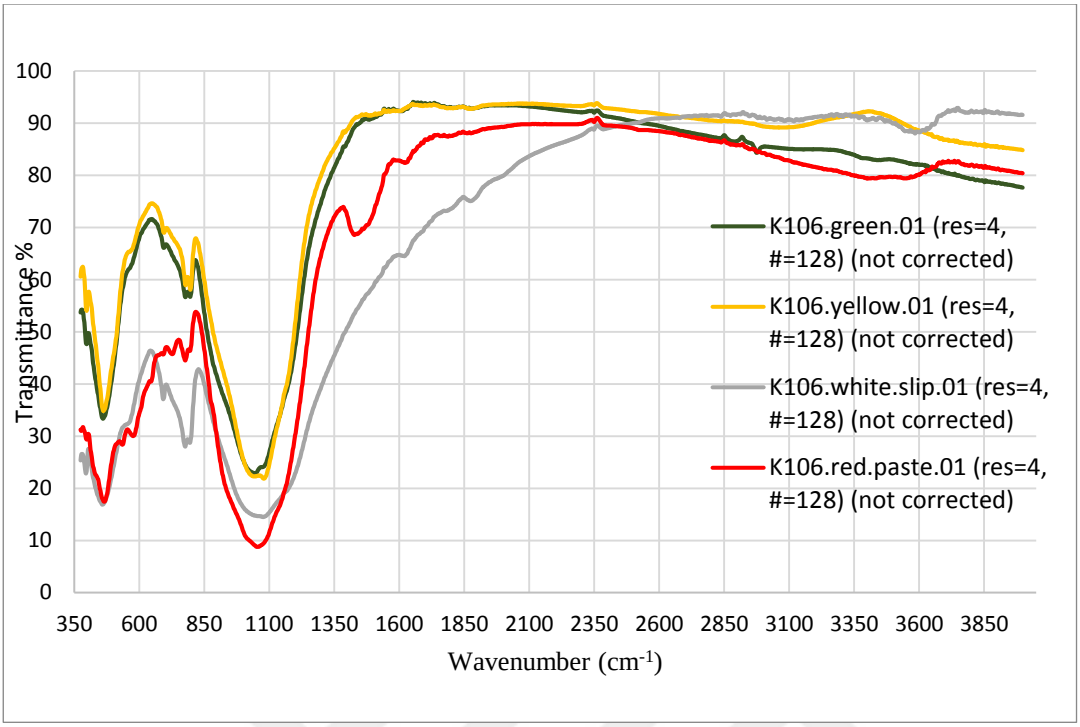

Figure 192. Comparison of the FTIR spectra of all the glazes with different colors and the sub-glaze samples (slip and paste) on the same potsherd.

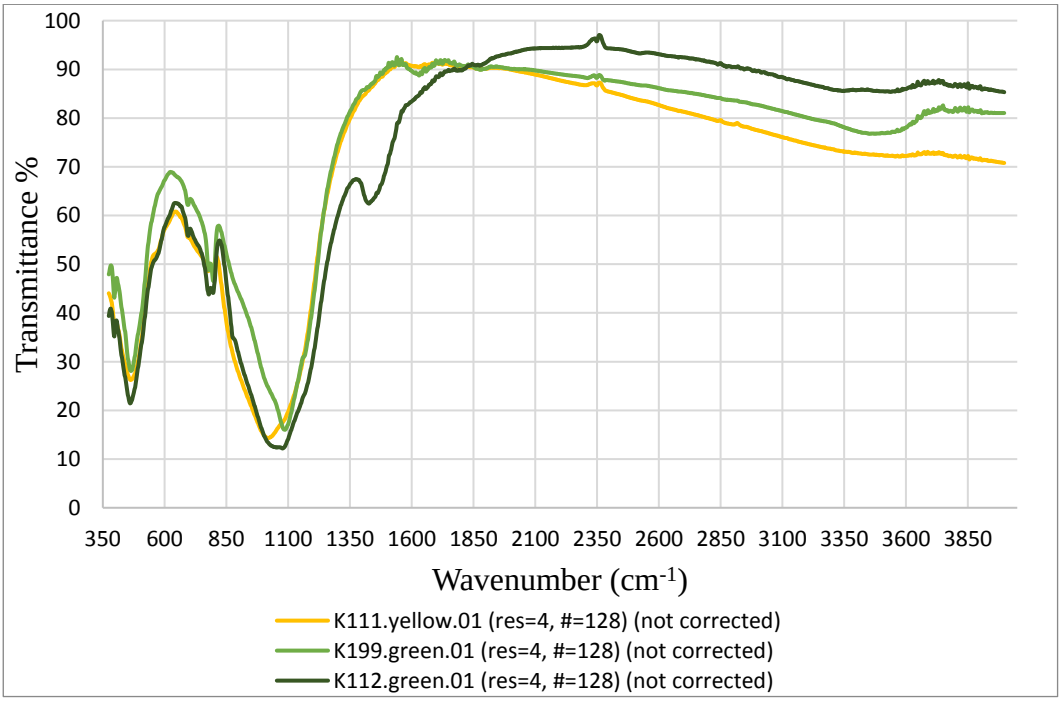

Figure 193. Comparison of the FTIR spectra of yellow and green glazes.

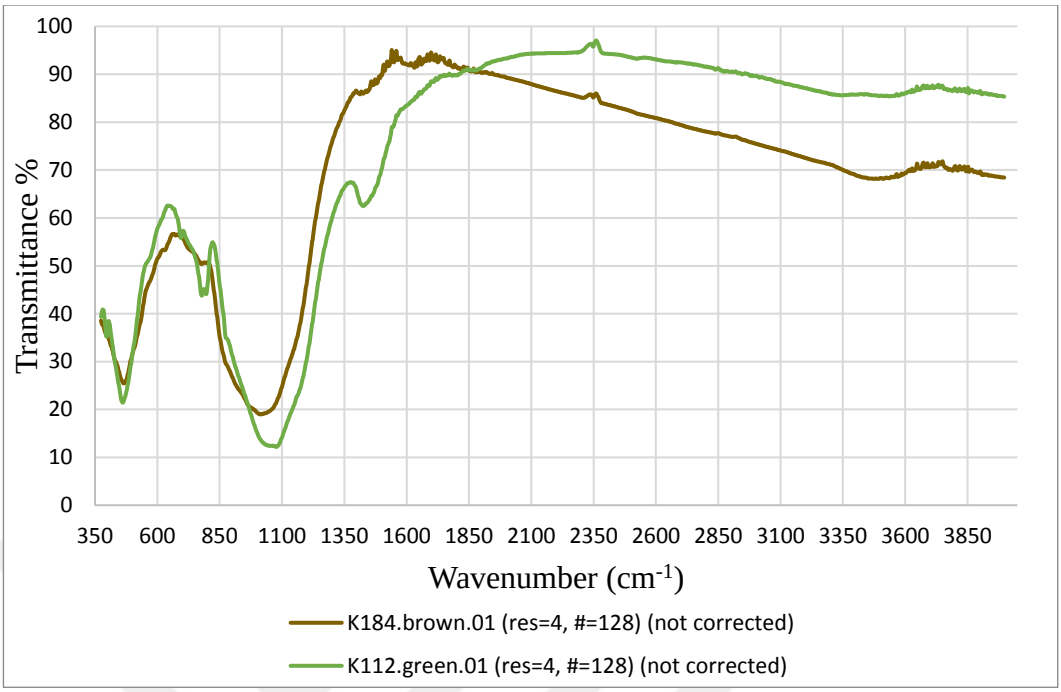

Figure 194. Comparison of the FTIR spectra of green and brown glazes.

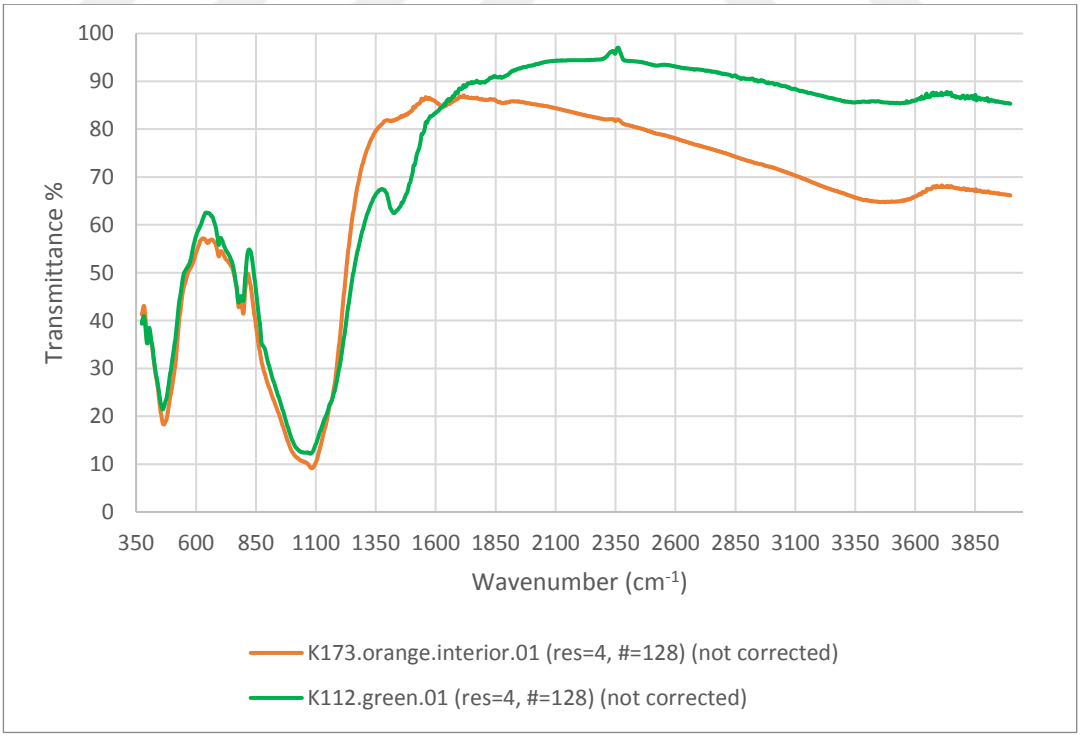

Figure 195. Comparison of the FTIR spectra of green and orange glazes.

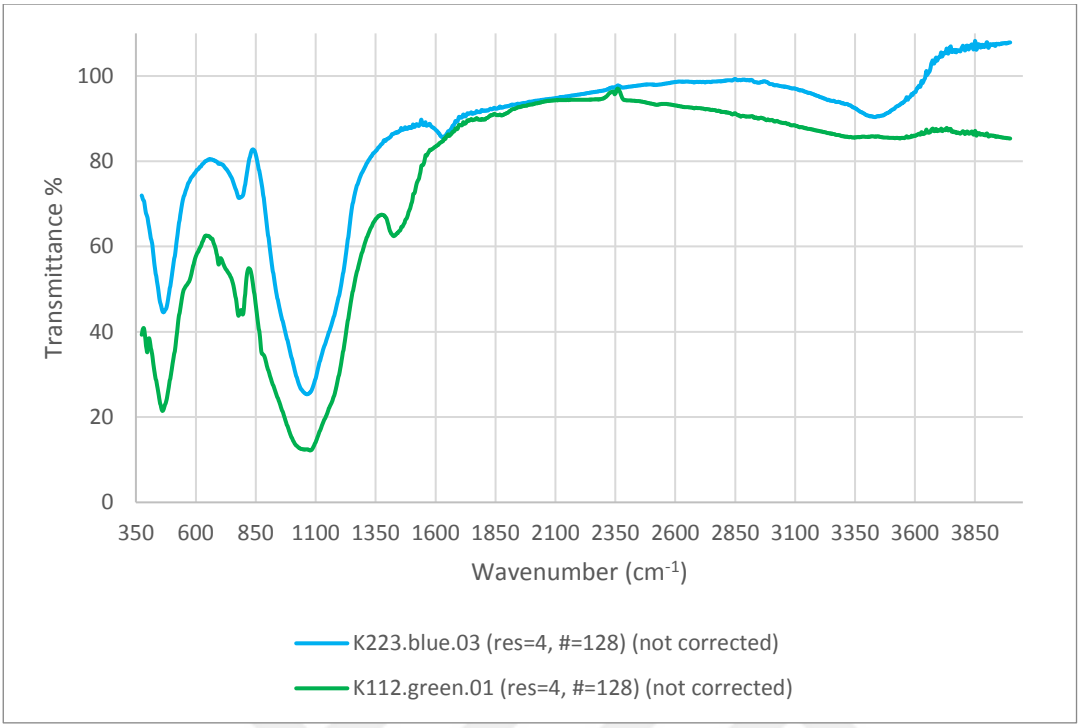

Figure 196. Comparison of the FTIR spectra of green and blue/turquoise glazes.

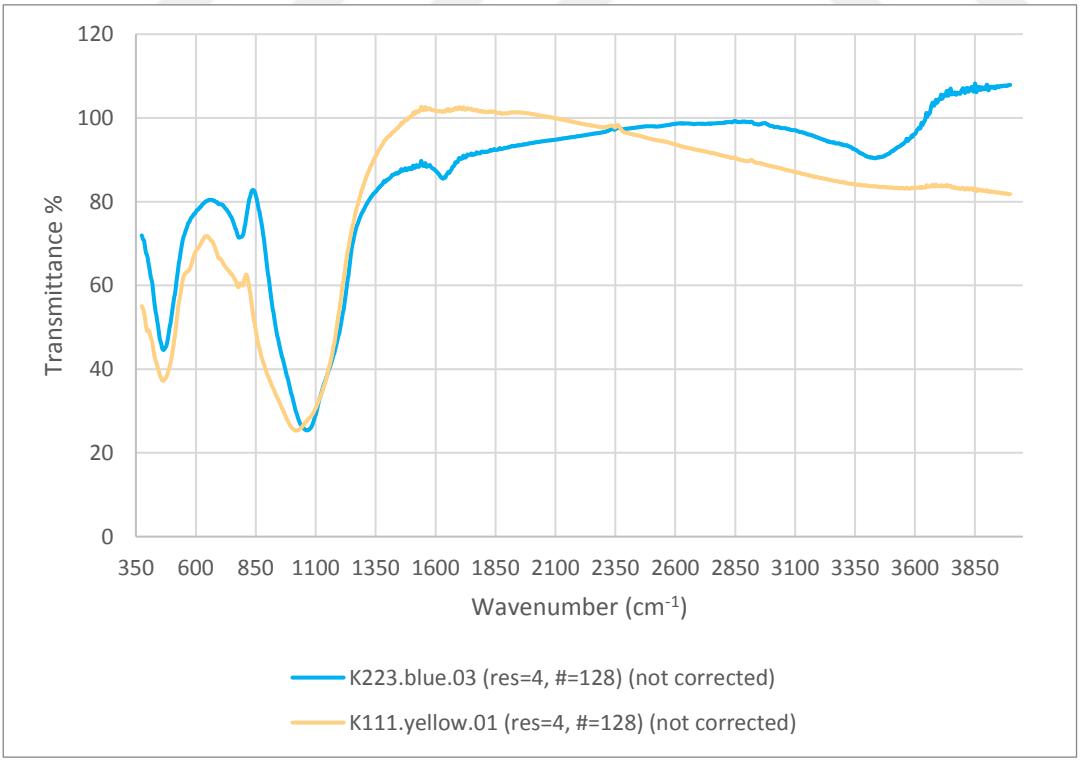

Figure 197. Comparison of the FTIR spectra of yellow and blue/turquoise glazes.

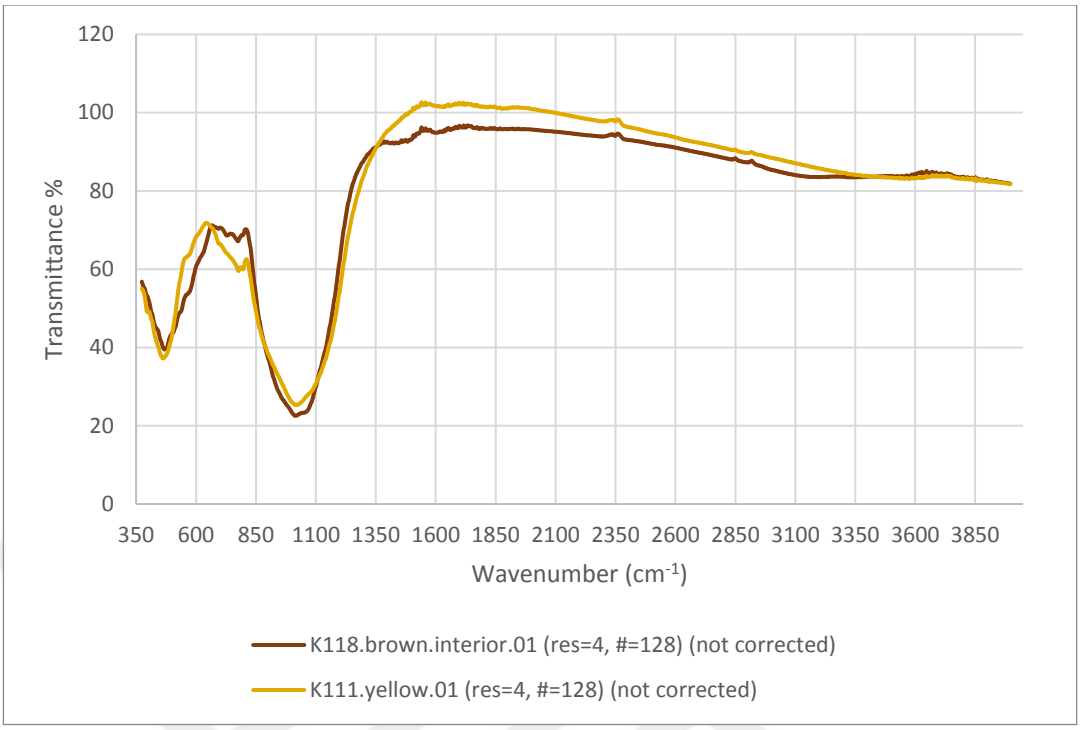

Figure 198. Comparison of the FTIR spectra of yellow and brown glazes.

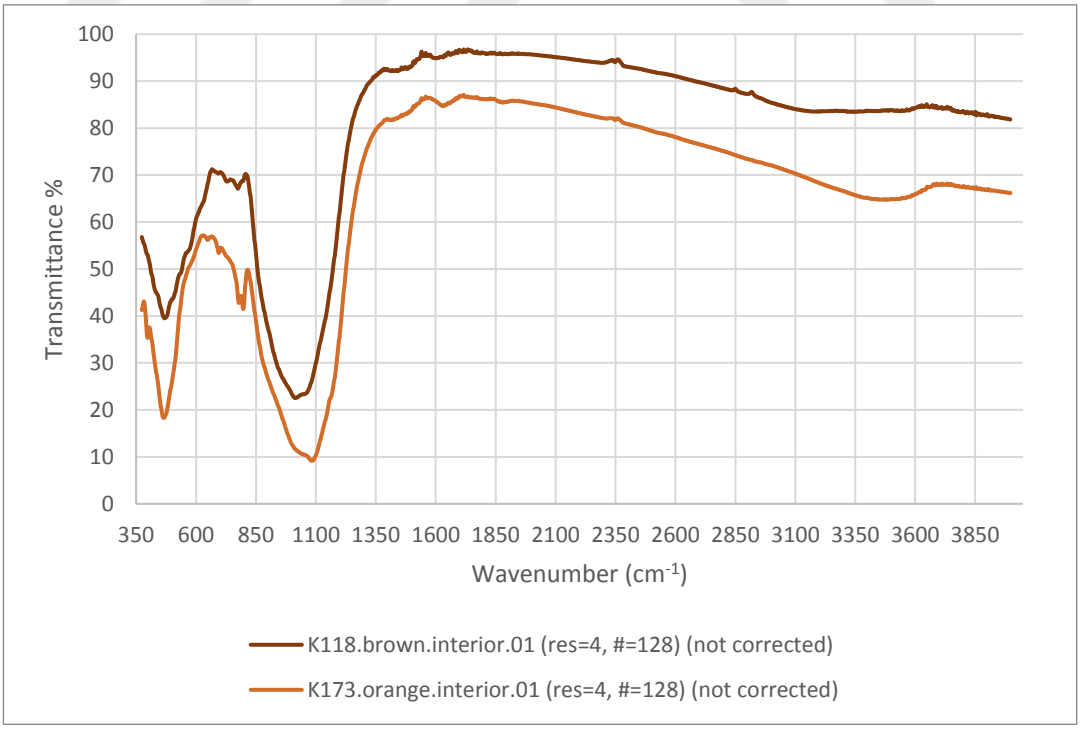

Figure 199. Comparison of the FTIR spectra of orange and brown glazes.

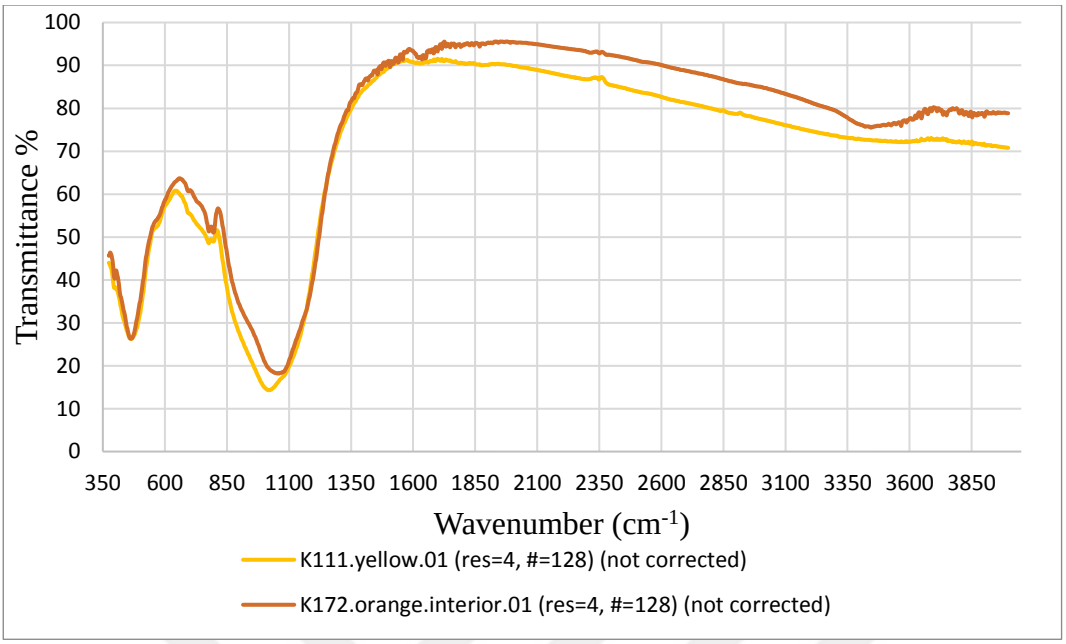

Figure 200. Comparison of the FTIR spectra of yellow and orange glazes.

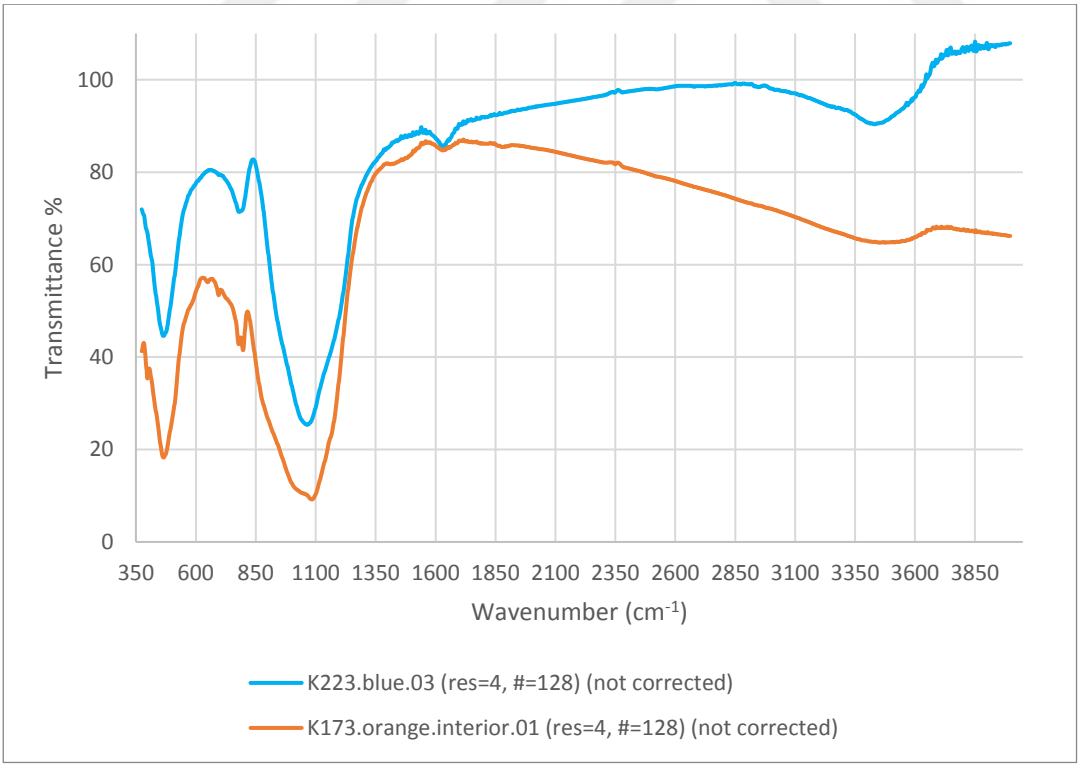

Figure 201. Comparison of the FTIR spectra of orange and blue/turquoise glazes.

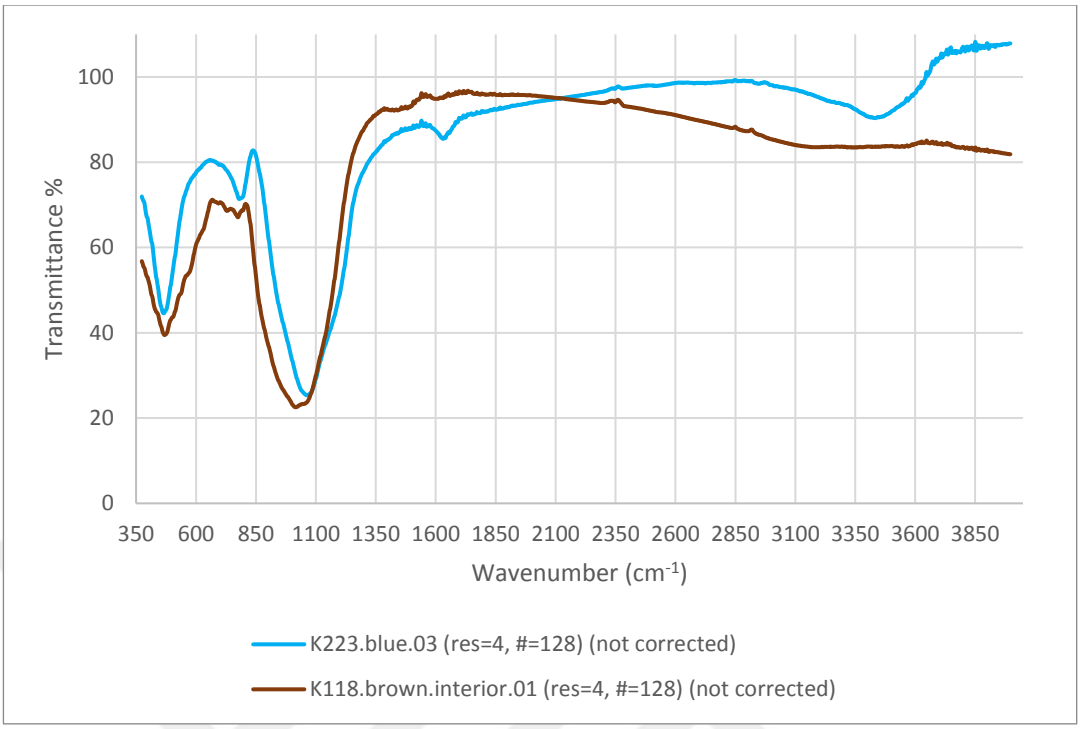

Figure 202. Comparison of the FTIR spectra of blue/turquoise and brown glazes.

A.3. Appendix of XRF Spectra

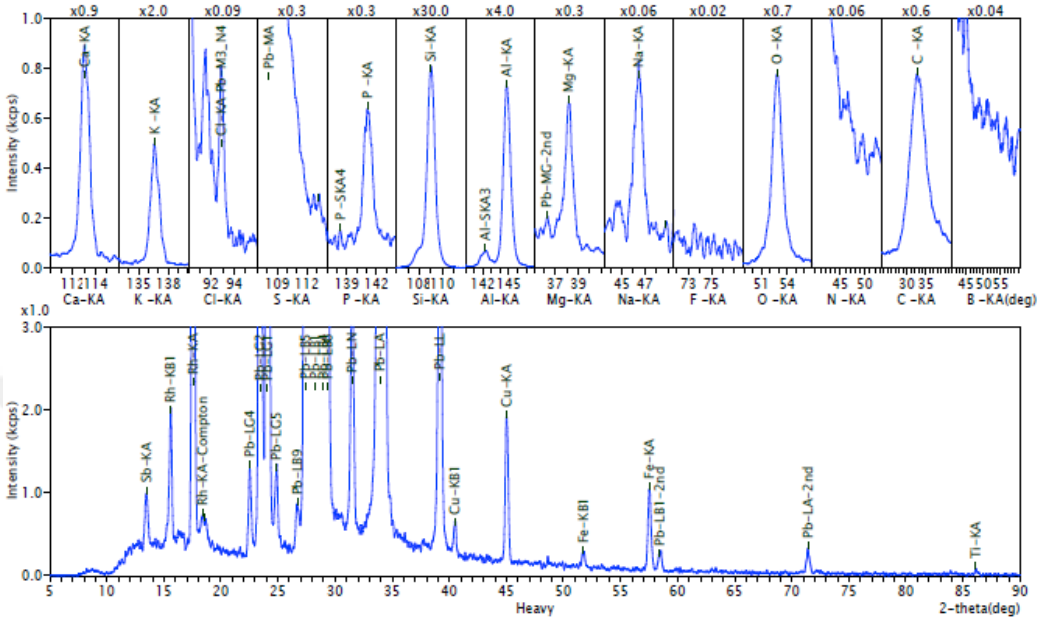

Figure 203. XRF spectrum of the yellow glaze of K149.

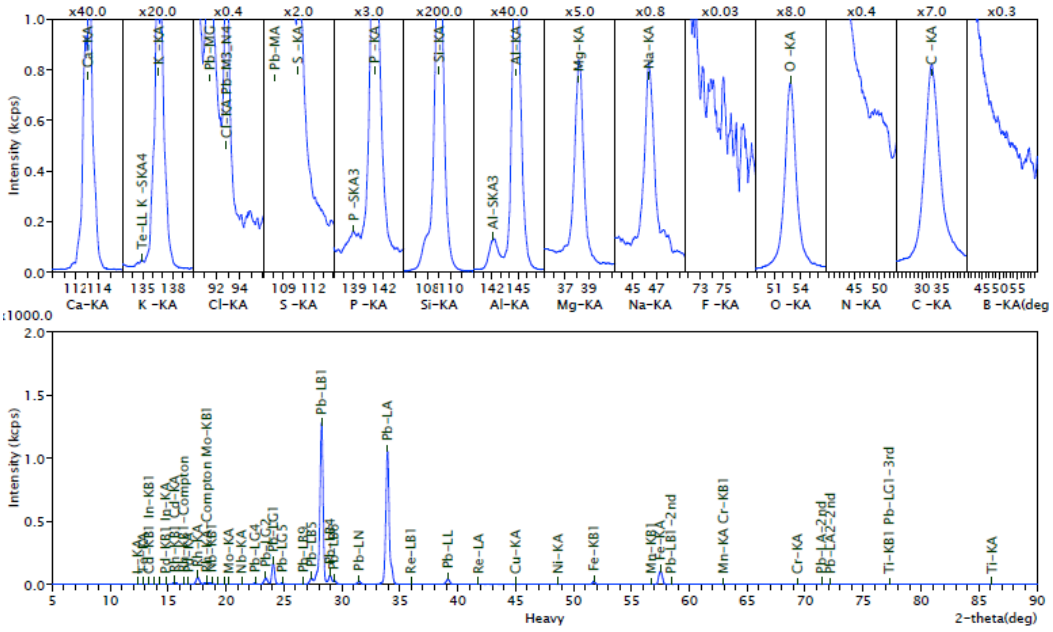

Figure 204. XRF spectrum of the orange glaze of K172.

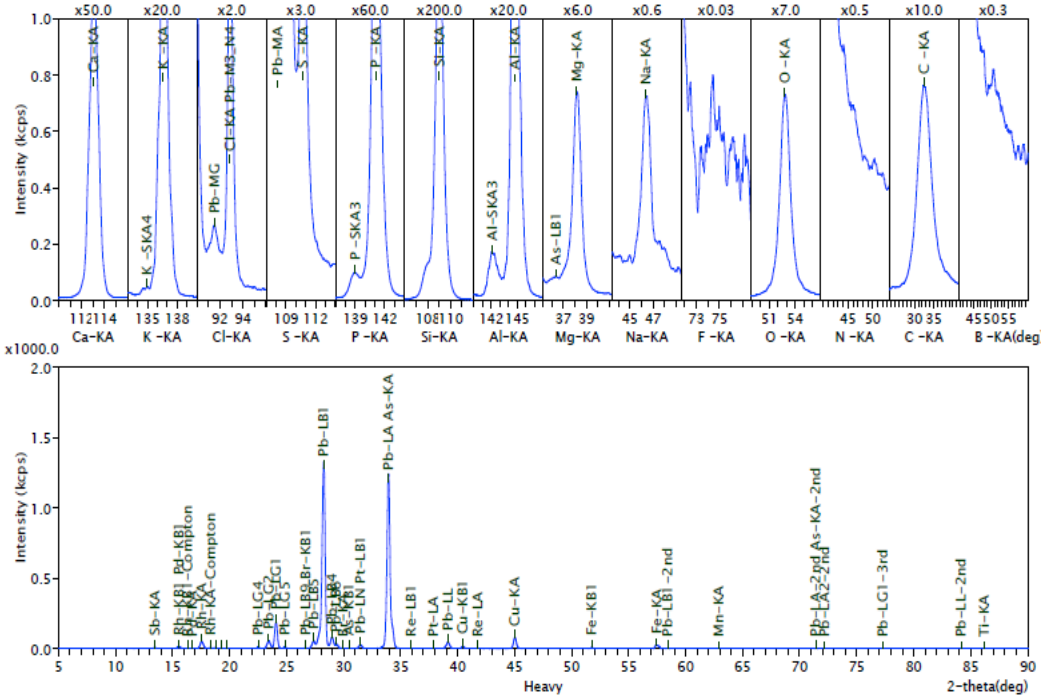

Figure 205. XRF spectrum of the green glaze of K161.

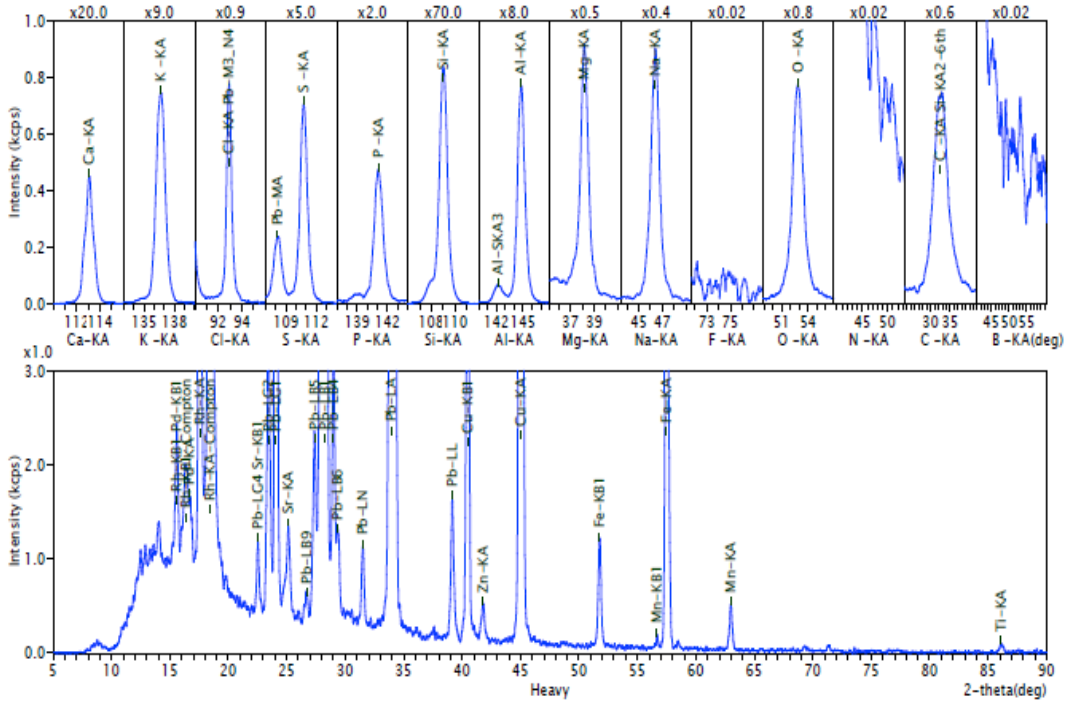

Figure 206. XRF spectrum of the turquoise glaze of K123.

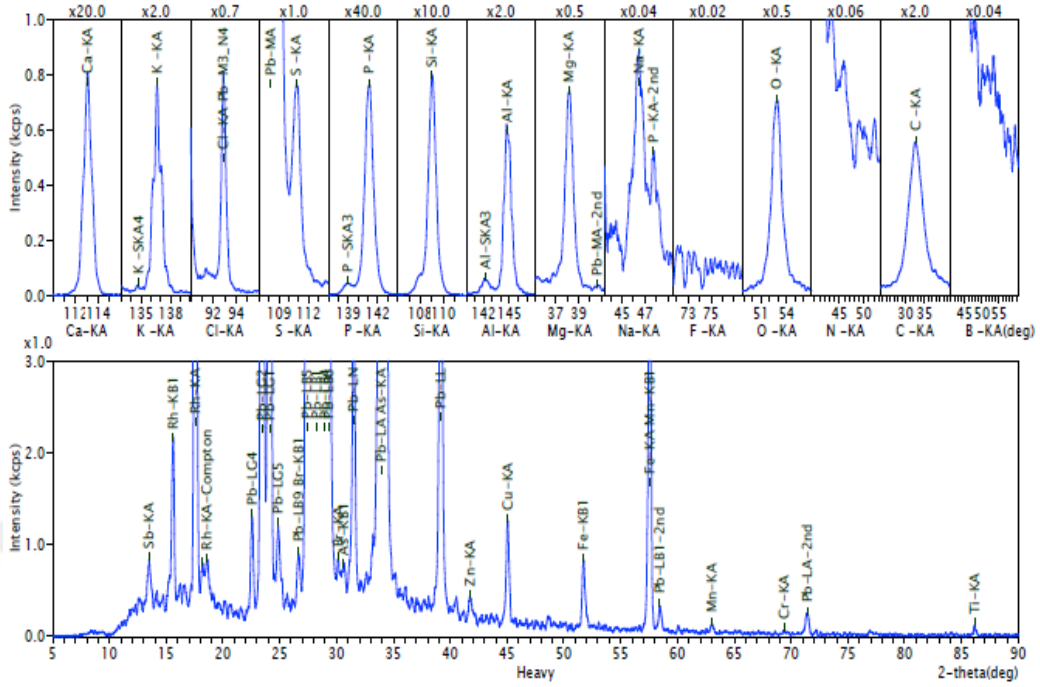

Figure 207. XRF spectrum of the brown glaze of K108.

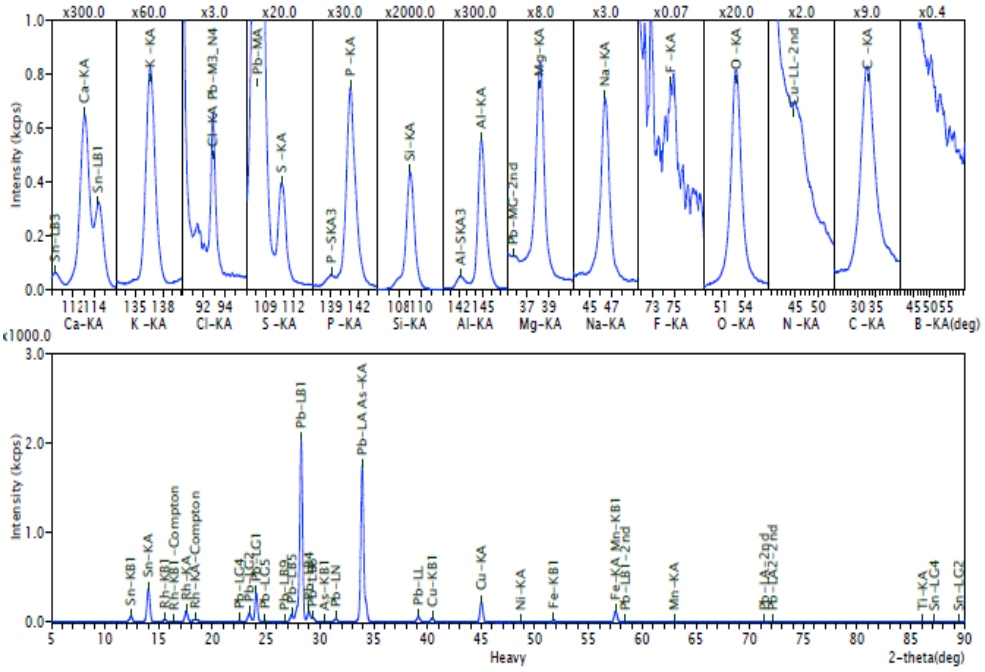

Figure 208. XRF spectrum of the turquoise tile of K001.

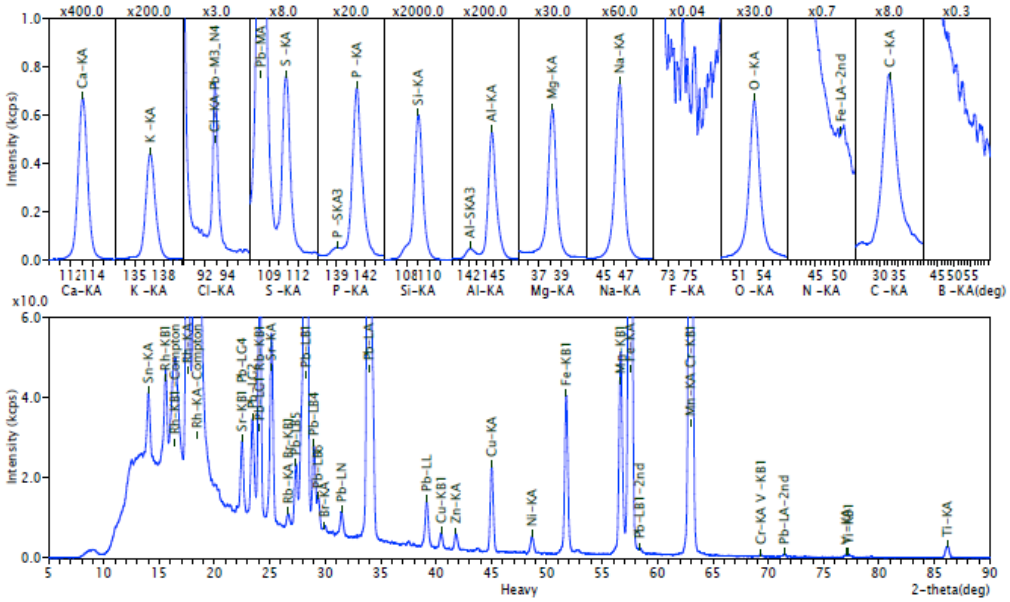

Figure 209. XRF spectrum of the black tile of K002.

A.4. Appendix of Characterization Data Points

Table 128. Characterization Data of the Glaze Contents in the World. MO (Metal Oxide) is calculated by addition of the columns from Na_2O to Fe_2O_3.

Sample	SiO_2	PbO	Na_2O	MgO	Al_2O_3	K_2O	CaO	Fe_2O_3	MO
Comana Pontica K001 turquoise tile, 14th c.	43.9	15.3	0.503	0.593	6.92	1.01	5.04	2.16	16.23
Comana Pontica K002 black tile, 14th c.	54.2	1.67	9.57	1.67	4.13	1.23	4.68	2.50	23.78
Comana Pontica K108 brown glaze, 13th c.	7.08	32.2	0.137	0.607	0.87	0.692	9.78	1.34	13.43
Comana Pontica K149 yellow glaze, 13th c.	28.9	49.7	0.227	0.367	2.76	0.688	0.687	0.458	5.19
Comana Pontica K161 green glaze, 12-13th c.	27.2	21.6	0.189	0.833	3.32	1.24	3.63	0.815	10.03
Comana Pontica K172 orange glaze, 12-13th c.	34.2	23.3	0.333	0.847	5.39	1.06	2.77	4.17	14.57
Seljukid Sahib Ata Mosque in Konya, black glaze, 13-14th c.	65.5	0.1	16.3	0.6	3.4	2	4.3	2.1	28.70
Seljukid Sahib Ata Mosque in Konya, ochre glaze, 13-14th c.	69.5	0.5	10.8	0.3	5.7	2.4	4	2.1	25.30
Seljukid Sahib Ata Mosque in Konya, turquoise glaze, 13-14th c.	63.1	12.2	7.2	0.2	4.7	1.2	3.2	1.6	18.10
Seljukid Sahib Ata Mosque in Konya, turquoise glaze, 13-14th c.	56.4	12.2	12.6	0.6	2.1	1.9	6.2	1.2	24.60
Seljukid turquoise glaze, found in Kayseri, late 13th c.	58.9	15.6	10.5	0.6	0.5	2.1	6.9	0.6	21.20
Seljukid Sahib Ata Mosque in Konya, turquoise glaze, 13-14th c.	55.6	27.5	6.1	0.1	1	2.3	1.5	2.2	13.20
Seljukid Sahib Ata Mosque in Konya, turquoise glaze, 12-13th c.	48.3	36	3	1.4	1	1.6	2.9	0.5	10.40
Seljukid Sahib Ata Mosque in Konya, turquoise glaze, 12-13th c.	50	36.2	2	0.5	0.9	0.7	3.7	1.2	9.00
Seljukid Sahib Ata Mosque in Konya, turquoise glaze, 12-13th c.	49.7	37	3	1.3	1.2	1.4	2.8	0.9	10.60

Table 128 (Cont'd)

Sample	SiO_2	PbO	Na_2O	MgO	Al_2O_3	K_2O	CaO	Fe_2O_3	MO
Comana Pontica K223 turquoise glaze, 12-13th c.	53.0	4.24	1.7	0.764	4.56	2.2	3.85	1.08	14.15
Alexandria, Roman Egypt	29.9	56	0	0	0	4	5.6	2.3	11.9
Xanthos, Lycia, Roman Anatolia	28.7	61	0	0	0	1	4.9	1.8	7.7
Paphos, Roman Cyprus, green	37.2	55	0	0	0	2	2.5	1.4	5.9
Paphos, Roman Cyprus, transparent	20.6	64	0	0	0	7	4.2	3.7	14.9
Ain Tab, Roman Anatolia, green	28.5	57	0	0	0	5	3.3	0.4	8.7
Ain Tab, Roman Anatolia, green	33.2	51	0	0	0	6	3.8	0.6	10.4
Ain Tab, Roman Anatolia, transparent	42.8	44	0	0	0	8	2.5	2.3	12.8
Dura Eiropos, Roman Syria, transparent	15.5	72	0	0	0	1	6.1	5.1	12.2
Dura Eiropos, Roman Syria, black	19.9	66	0	0	0	1	2.2	10.6	13.8
Kition, Roman Cyprus, green	25.5	63	0	0	0	1	5.3	2.5	8.8
Kition, Roman Cyprus, transparent	35.6	58	0	0	0	1	1.9	3.3	6.2
Iznik tiles, work of İbrahim from Kütahya	56.9	25.7	11.4	0.7	0.9	1.2	2.7	0.3	17.2
Iznik tiles, work of İbrahim from Kütahya	54.4	22	12.7	0	0.4	1.4	0.6	0	15.1
Iznik tiles, work of İbrahim from Kütahya	57.9	19.1	11.6	0	0.4	1	1.1	0.3	14.4
Iznik tiles, work of İbrahim from Kütahya	49.8	30.5	8.8	0.2	0.4	1.7	1	1.9	14
Iznik tiles, work of İbrahim from Kütahya	54.2	24.1	10	0	0.8	1	1	0	12.8
Iznik tiles, work of İbrahim from Kütahya	53.4	28.2	9.2	0	0.5	1.1	0.7	0.5	12
Iznik tiles, work of İbrahim from Kütahya	55.7	26.8	8.9	0.4	0.4	1	1	0	11.7

Table 128 (Cont'd)

Sample	SiO_2	PbO	Na_2O	MgO	Al_2O_3	K_2O	CaO	Fe_2O_3	MO
Average, Iznik tiles, work of İbrahim from Kütahya	54.61	25.20	10.37	0.19	0.54	1.20	1.16	0.43	13.89
Blue-white Iznik tiles	58.4	22	10.2	0.2	0.4	1.1	0.7	0.3	12.9
Blue-white Iznik tiles	47.1	28.9	8.5	0.2	0.3	0.8	1	0.7	11.5
Blue-white Iznik tiles	48.6	31.8	8.6	0.2	0.9	0.9	1.1	0.6	12.3
Average, blue-white Iznik tiles	51.37	27.57	9.10	0.20	0.53	0.93	0.93	0.53	12.23
Blue-turquoise Iznik tiles	53.5	28.3	9.2	0	0.5	1	0.7	0	11.4
Iznik tiles, work of Golden Horn	53.9	27.9	8.7	0	0.3	0.9	1	0.5	11.4
Iznik tiles, work of Golden Horn	48.2	35.6	9.1	0.3	0	0.8	0.5	0.4	11.1
Iznik tiles, work of Golden Horn	51.9	27.5	13.9	0.1	0.5	1	1.1	0.3	16.9
Average, Iznik tiles, work of Golden Horn	51.33	30.33	10.57	0.13	0.27	0.90	0.87	0.40	13.13
Iznik tiles, work of Damascus	49.4	33.3	9.2	0	0.5	0.8	1	0	11.5
Iznik tiles, work of Damascus	50.7	36.2	5.7	0.1	0.4	0.9	0.9	0.6	8.6
Iznik tiles, work of Damascus	55.1	28.5	8	0.2	0.5	1	1	0.4	11.1
Average, Iznik tiles, work of Damascus	51.73	32.67	7.63	0.10	0.47	0.90	0.97	0.33	10.4
Polychrome Iznik tiles	45.8	38.9	8.3	0	0.2	0.8	0.7	0.4	10.4
Polychrome Iznik tiles	21.6	34.2	6	0.1	0.4	0.9	1.6	0.5	9.5
Polychrome Iznik tiles	39.9	34.5	10.9	0.4	0.6	0.7	1	0.7	14.3
Average, polychrome Iznik tiles	35.77	35.87	8.40	0.17	0.40	0.80	1.10	0.53	11.4
Iznik tiles, Rhodes work	46.1	37	9.3	0.4	0.7	1	1.3	0.4	13.1
Iznik tiles, Rhodes work	54.3	29.2	10.9	0	0.3	1	0.4	0	12.6
Iznik tiles, Rhodes work	37.7	42.6	12.3	0	0.4	1	0.9	0.4	15
Iznik tiles, Rhodes work	48.6	37	9.4	0	0.4	0.7	0.9	0.3	11.7
Iznik tiles, Rhodes work	49.9	31.1	11.4	0.2	0.3	0.8	0.7	0.3	13.7

Table 128 (Cont'd)

Sample	SiO_2	PbO	Na_2O	MgO	Al_2O_3	K_2O	CaO	Fe_2O_3	MO
Iznik tiles, Rhodes work	50.2	30.5	11.6	0.1	0.4	0.8	0.5	0.5	13.9
Average, Iznik tiles, Rhodes work	47.80	34.57	10.82	0.12	0.42	0.88	0.78	0.32	13.33
Colchester transparent	30.46	62	0	0.4	0	0	4.9	2.2	7.50
Smyrna transparent glaze	37.68	56	0	0.2	0	0	3.2	2.7	6.10
Clazomenae transparent glaze	36.2	58	0	0.2	0	0	3	2.4	5.60
Tarsus transparent glaze	39.4	54	0	0	0	0	2.9	3.4	6.30
Smyrna green	36.6	53	0	0.1	0	0	4.1	1	5.20
Clazomenae green	36.9	53	0	0.1	0	0	2.8	0.8	3.70
Tarsus green	32.38	59	0	0.02	0	0	3.2	0.9	4.12
Roman Forum, 8-10th	31.24	57.96	0.22	0.93	4.53	0.89	1.95	1.94	10.46
Roman Forum, 8-10th	19.41	69.97	0.3	0.72	5.77	0.35	0.98	2.17	10.29
Roman Forum, 8-10th	26.36	61.21	0.19	1	5.83	0.52	1.82	2.59	11.95
Roman Forum, average, 8-10th	25.67	63.05	0.24	0.88	5.38	0.59	1.58	2.23	10.90
Byzantine, 9-10th	19.43	67.41	0.11	0.27	6.49	0.15	0.3	0.66	7.98
Byzantine, 9-10th	18.9	74.18	0.04	0.16	5.59	0.2	0.14	0.35	6.48
Byzantine, 9-10th	28.93	63.41	0.56	0.26	1.06	0.32	1.49	3.39	7.08
Byzantine, 9-10th	27.24	65.6	0.85	0.08	0.74	0.19	0.62	4.37	6.85
Byzantine, 9-10th	32.98	59.44	0.27	0.11	0.41	0.17	0.74	5.08	6.78
Byzantine, average, 9-10th	25.50	66.01	0.37	0.18	2.86	0.21	0.66	2.77	7.03
Byzantine, 11-12th	27.94	62.67	0.36	0.36	6.28	0.68	0.63	0.58	8.89
Byzantine, 11-12th	20.43	63.74	0.28	0.5	5.38	0.45	0.96	1.04	8.61
Byzantine, 11-12th	37.75	51.7	0.47	0.57	3.54	1.94	2.8	0.79	10.11

Table 128 (Cont'd)

Sample	SiO_2	PbO	Na_2O	MgO	Al_2O_3	K_2O	CaO	Fe_2O_3	MO
Byzantine, average, 11-12th	28.71	59.37	0.37	0.48	5.07	1.02	1.46	0.80	9.20
Byzantine, 13th	33.08	61.22	0.17	0.56	1.9	0.58	1.59	0.77	5.57
Byzantine, 13th	30.2	60.47	0.59	0.44	1.81	1.63	2.65	0.59	7.71
Byzantine, average, 13th	31.64	60.845	0.38	0.5	1.855	1.105	2.12	0.68	6.64
Byzantine, average, 11-13th	27.688	62.984	0.37	0.331	3.32	0.631	1.192	1.762	7.61
Chinese sancai, 8-9th	33.31	53.62	0.23	0.25	6.09	0.3	0.77	0.4	8.04
Chinese sancai, 8-9th	36.49	55.67	0.11	0.41	3.47	0.3	1.07	0.27	5.63
Chinese sancai, 8-9th	32.09	57.18	0.64	0.48	5.71	1.13	2.32	0.14	10.42
Chinese sancai, 8-9th	34.9	55.8	0.17	0.5	4.22	0.29	0.94	0.44	6.56
Chinese sancai, 8-9th	44.24	42.41	0.36	0.57	9.11	0.84	0.85	0.4	12.13
Chinese sancai, average, 8-9th	36.21	52.94	0.30	0.44	5.72	0.57	1.19	0.33	8.56
Diana, Serbia, 1st-2nd	19.34	68.53	0.17	0.34	9.25	0.78	0.37	0.83	11.74
Diana, Serbia, 1st-2nd	18.75	70.36	0.15	0.28	8.35	0.57	0.32	0.74	10.41
Diana, Serbia, 1st-2nd	17.67	71.47	0.19	0.3	8.42	0.52	0.36	0.7	10.49
Diana, Serbia, 1st-2nd	20.3	68.08	0.07	0.35	9.21	0.47	0.27	0.77	11.14
Diana, Serbia, 1st-2nd	18.66	69.77	0.18	0.32	8.78	0.81	0.42	0.67	11.18
Diana, Serbia, 1st-2nd	17.98	71.07	0.17	0.28	8.52	0.56	0.43	0.66	10.62
Diana, Serbia, 1st-2nd	18.69	69.65	0.21	0.34	9.04	0.66	0.39	0.73	11.37
Diana, Serbia, 1st-2nd	19.46	68.96	0.14	0.38	9.05	0.52	0.39	0.69	11.17
Diana, Serbia, 2nd	18.5	70.02	0.17	0.33	8.53	0.73	0.59	0.72	11.07
Diana, Serbia, ?	18.32	70.18	0.21	0.3	8.76	0.78	0.31	0.67	11.03
Diana, Serbia, 2nd	17.69	70.48	0.36	0.36	8.75	0.65	0.54	0.74	11.40
Diana, Serbia, 3rd-4th	18.35	70.5	0.07	0.25	8.41	0.3	0.53	0.94	10.50

Table 128 (Cont'd)

Sample	SiO_2	PbO	Na_2O	MgO	Al_2O_3	K_2O	CaO	Fe_2O_3	MO
Diana, Serbia, average, 1st-2nd	18.832	69.823	0.210	0.398	8.290	0.606	0.460	0.921	10.885
Singidunum, Serbia, 2nd	17.86	70.56	0.27	0.3	8.85	0.55	0.49	0.79	11.25
Singidunum, Serbia, 2nd	17.81	71.17	0.18	0.36	8.53	0.46	0.37	0.69	10.59
Singidunum, Serbia, 2nd	17.19	71.26	0.11	0.37	8.9	0.54	0.39	0.89	11.20
Singidunum, average, Serbia, 2nd	19.94	69.34	0.21	0.49	7.33	0.58	0.49	1.16	10.27
Lezoux, France, 1st	16.94	72.44	0.34	0.32	6.91	0.62	0.65	0.94	9.78
Lezoux, France, 1st	13.24	77.46	0.17	0.23	6.55	0.42	0.55	0.81	8.73
Lezoux, average, France, 1st	15.1	75.0	0.3	0.3	6.7	0.5	0.6	0.9	9.26
Vichy, France, 1st	22.25	66.15	0.01	0.16	8.87	0.59	0.43	0.67	10.73
London, England, 1st	18.61	69.19	0.35	0.42	8.37	0.69	0.74	1.15	11.72
London, England, 1st	16.82	72.58	0.26	0.31	7.14	0.64	0.65	0.95	9.95
London, England, ?	20.1	67.58	0.07	0.29	8.46	0.89	1.08	0.87	11.66
London, England, ?	17.5	70.95	0.15	0.25	8.66	0.79	0.51	0.81	11.17
London, England, 2nd	22.01	67.12	0.1	0.6	7.06	0.55	0.51	1.55	10.37
London, England, 3rd	24.03	66.82	0.22	0.71	4.68	0.63	0.4	2.11	8.75
London, England, 3rd	20.71	70.17	0.15	0.71	4.59	0.64	1.55	0.78	8.42
London, average, England, 1st-4th	20.32	67.81	0.18	0.40	5.42	0.58	1.18	1.11	8.87
Diana, Serbia, 1st-2nd	19.71	69.34	0.36	0.73	5.85	0.49	0.8	1.95	10.18
Diana, Serbia, ?	16.38	74.8	0.35	0.67	4.94	0.39	0.42	1.58	8.35
Diana, Serbia, 3rd-4th	20.46	68.6	0.38	0.57	6.15	0.1	0.91	1.98	10.09
Diana, Serbia, 3rd-4th	18.48	71.57	0.29	0.66	5.23	0.18	0.53	2.33	9.22
Diana, Serbia, 3rd-4th	25.85	61.29	0.34	0.86	7.24	0.24	0.8	2.71	12.19
Diana, Serbia, ?	23.98	63.43	0.41	0.97	7.32	0.83	0.72	1.83	12.08
Diana, average, Serbia, 3rd-4th	21.67	68.36	0.28	0.58	5.70	0.22	0.75	1.69	9.22

Table 128 (Cont'd)

Sample	SiO_2	PbO	Na_2O	MgO	Al_2O_3	K_2O	CaO	Fe_2O_3	MO
Diana, average, Serbia, 1st-4th	20.15	68.75	0.23	0.49	7.22	0.50	0.63	1.26	10.33
Singidunum, Serbia, 2nd	18.18	71.83	0.34	0.63	5.66	0.53	0.74	1.57	9.47
Singidunum, Serbia, 2nd	23.09	64.16	0.34	0.95	7.22	0.67	0.71	2.33	12.22
Apulum Partos, Romania, 2nd	22.53	66.24	0.46	0.87	5.87	0.12	1.06	1.81	10.19
Apulum Partos, Romania, 2nd	27.46	60.62	0.65	0.64	4.04	1.71	2.7	1.3	11.04
Apulum Partos, Romania, 2nd	27.34	59.09	0.46	1.14	6.94	0.22	1.46	2.35	12.57
Apulum Partos, Romania, 2nd	29.61	55.3	0.61	1.19	8.02	0.22	1.34	2.36	13.74
Apulum Partos, Romania, 2nd	24.45	63.01	0.52	0.92	6.02	0.55	1.31	2.12	11.44
Apulum Partos, Romania, 2nd	19.86	69.47	0.41	0.83	5.3	0.22	1.13	1.9	9.79
Apulum Partos, Romania, 2nd	24.39	62.02	0.44	1.07	6.69	0.12	1.48	2.45	12.25
Apulum Partos, average, Romania, 2nd	24.38	63.17	0.49	0.93	6.01	0.42	1.53	2.03	11.41
London, England, ?	22.81	67.54	0.08	0.37	6	0.28	0.6	0.68	8.01
Diana, Serbia, 3rd-4th	20.5	70.86	0.38	0.4	5.58	0.12	0.37	1.02	7.87
Diana, Serbia, 3rd-4th	15.63	78.2	0.14	0.17	4.42	0.18	0.2	0.48	5.59
Singidunum, Serbia, 2nd	21.08	70.62	0.13	0.39	5.64	0.57	0.31	0.75	7.79
Singidunum, Serbia, 2nd	24.37	65.8	0.08	0.45	6.53	0.76	0.42	1.13	9.37
Diana, Serbia, 1st-2nd	19.23	70.14	0.35	0.77	5.73	0.51	0.64	1.85	9.85
Diana, Serbia, ?	28.9	55.81	0.35	0.74	6.63	0.54	2.97	3.03	14.26
Diana, Serbia, 3rd-4th	28.2	61.16	0.19	0.56	6.38	0.22	1.04	1.32	9.71
Diana, Serbia, 3rd-4th	22.58	66.82	0.26	0.85	4.92	0.47	1.39	2.01	9.90
Apulum Partos, Romania, 2nd	19.41	69.59	0.39	0.78	5.2	0.19	1.75	1.91	10.22
Ostia, Italy, 5th	28.74	60.91	0.14	0.52	5.18	0.93	0.98	2.05	9.80
Ostia, Italy, 5th	24.16	67.16	0.29	0.38	5.03	0.42	0.57	1.58	8.27
Ostia, Italy, 5th	26.67	61.82	0.22	0.64	5.73	0.57	1.36	2.51	11.03
Ostia, average, Italy, 5th	27.26	62.30	0.30	0.55	4.71	0.66	1.56	1.91	9.69
Carlino, Italy, 4-5th	28.51	59.82	0.46	0.97	5.56	0.82	1.61	1.88	11.30
Carlino, Italy, 4-5th	36.84	47.21	0.68	0.92	7.12	1	3.24	2.4	15.36
Carlino, Italy, 4-5th	32.09	56.74	0.36	0.66	6.24	0.9	0.93	1.77	10.86

Table 128 (Cont'd)

Sample	SiO_2	PbO	Na_2O	MgO	Al_2O_3	K_2O	CaO	Fe_2O_3	MO
Carlino, Italy, 4-5th	27.88	61.84	0.29	0.82	5.64	0.52	0.69	1.93	9.89
Carlino, Italy, 4-5th	22.77	67.73	0.27	0.77	4.98	0.58	0.8	1.85	9.25
Carlino, Italy, 4-5th	29.41	59.88	0.43	0.78	5.65	0.77	1.44	1.38	10.45
Carlino, average, Italy, 4-5th	29.58	58.87	0.42	0.82	5.87	0.77	1.45	1.87	11.19
Ostia, Italy, 2nd	25.93	68.78	0.04	0.25	0.59	0.31	1.67	0.85	3.71
Ostia, Italy, 3rd	35.36	56.64	0.25	0.46	1.26	0.58	2.05	1.74	6.34
Ostia, Italy, 5th	29.47	59.31	0.55	0.65	2.91	0.72	3.34	1.5	9.67
Ostia, average, Italy, 2nd-5th	28.07	64.08	0.21	0.39	2.58	0.47	1.65	1.66	6.96
London, England, 3rd-4th	30.12	62.91	0.15	0.35	1.09	0.3	2.53	0.62	5.04
London, England, ?	26.86	62.88	0.21	0.17	2.53	0.49	2.92	1.06	7.38
London, England, 2nd-3rd	25.19	68.19	0.21	0.22	1.06	0.48	1.49	1.61	5.07
Gaul, France, 3rd	29.98	57.47	0.37	0.55	3.25	0.81	3.43	2.45	10.86
Ostia, Italy, 2nd-3rd	26.08	68.05	0.19	0.27	1.01	0.29	2.2	0.62	4.58
Ostia, Italy, 2nd	27.28	69.43	0.1	0.09	0.36	0.15	0.87	1.5	3.07
Ostia, Italy, 2nd	28.93	64.61	0.12	0.29	1.14	0.25	1.78	2.58	6.16
Ostia, average, Italy, 2nd-3rd	28.716	65.502	0.14	0.272	0.872	0.316	1.714	1.458	4.77
Roman, Italy, 1st c. BCE	17.7	74.3	0.4	0.7	4.5	0.5	0.4	1.5	8.00
Roman, Italy, 1st-2nd c.	31.6	56	0.3	0.5	3.5	0.7	4.1	3.3	12.40
Islamic, Iraq, 8-10th c.	27.9	65.65	0.25	0.4	1.05	0.25	1.45	0.4	3.80
Islamic, Egypt, 10-11th c.	30.35	62.6	0.4	0.5	2.3	0.7	1.35	1.8	7.05
Islamic, Iran, 10-11th c.	36.95	56.15	0.7	0.7	3.2	1	1.25	0.4	7.25
Islamic, Spain, 10th c.	36.2	50.9	0.3	0.4	2.9	2.9	3.1	2.8	12.40
Hispano-Moresque, 13th c.	33	54.9	0.1	0.5	5.3	0.9	2.6	2.5	11.90
Hispano-Moresque, 14-15th c.	33.1	56.2	0.1	0.6	5.6	0.6	1.6	2.2	10.70
Anglo-Saxon (tile), 10-11th c.	29.65	63.2	0	0.2	4.95	0.35	0.55	0.7	6.75
Byzantine, 9-10th c.	24.25	67.65	0.6	0.2	3.6	0.3	0.75	2.8	8.25
Byzantine, 11-12th c.	32.25	57.45	0.4	0.5	5	1.2	2.3	0.9	10.30

Table 128. Cont'd.

Sample	SiO_2	PbO	Na_2O	MgO	Al_2O_3	K_2O	CaO	Fe_2O_3	MO
Byzantine, 13th c.	28	69.6	0.1	0.1	1.5	0.2	0.4	0.1	2.40
Medieval, England, 14th c.	28.25	57.6	0.4	1.4	5.4	1.2	0.4	2.5	11.30
Medieval, England, 15-16th c.	30.4	60.1	0	1.1	4.7	0.8	0.6	2.3	9.50
St. Porchaire, 16th c.	39.15	52.15	0.15	0.35	6.45	0.65	0.55	0.55	8.70
Palissy, 16th c.	45.7	45.6	2.3	0.3	2.3	0.8	2.5	0.5	8.70
English earthenware, 18th c.	40.85	52.05	0.4	0	5.3	0.3	0.35	0.2	6.55
Islamic, Iraq, 8th c.	71.5	1.4	8.3	3.9	2.2	5.1	6.8	0.8	27.10
Islamic, Iraq, 9th c.	66.6	8.5	9.5	3.9	1.8	4.5	4.5	0.8	25.00
Islamic, Iraq, 10th c.	62.7	16.6	6.7	2.5	2.1	4.7	4.2	0.6	20.80
Islamic, Iraq, 9th c.	50.7	36	4.4	1.5	1.5	2.7	2.7	0.4	13.20
Islamic, Iraq, 9th c.	42.2	49.3	2.7	1.2	0.6	1.7	2	0.4	8.60
Islamic, Egypt, 11th c.	47.1	41.8	3.3	0.3	1.9	2.9	2.4	0.4	11.20
Islamic, Egypt, 11th c.	50.2	38.7	4.1	0.2	1.9	2.6	1.7	0.4	10.90
Islamic, Egypt, 11th c.	54.8	29.8	6.5	0.9	1.5	1.1	3.3	1.5	14.80
Islamic, Spain, 10-12th c.	47	43.3	1.8	0.7	0.9	2.9	3.1	0.3	9.70
Islamic, Spain, 10-12th c.	44.6	41.9	2.4	0.9	2.1	3.3	3.9	0.7	13.30
Islamic, Spain, 10th c.	38	54.3	1.4	0.4	0.5	2.1	2.7	0.6	7.70
Hispano-Moresque, 13th c.	40.3	47.4	1.3	0.6	2.7	4.9	2.5	0.2	12.20
Hispano-Moresque, 13th c.	40.5	48.2	1	0.6	2.6	4.4	2.4	0.3	11.30
Islamic, Iran, 12th c.	57.6	19.5	9.3	2.3	2.7	1.7	5.5	1.3	22.80
Islamic, Iran, 12th c.	56.4	24.3	9.4	2.4	1.4	1.3	4.1	0.7	19.30
Islamic, Iran, 12th c.	61.1	22.1	7.6	1.6	1.9	1.6	3.2	0.7	16.60
Islamic, Iznik, 15-16th c.	54.1	33.2	9.6	0.2	0.4	1.1	1.1	0.3	12.70
Islamic, Iznik, 15-16th c.	58.6	28.3	9.4	0.4	0.4	1.2	1.1	0.5	13.00
Islamic, Iznik, 15-16th c.	50.7	37.5	9.6	0.3	1.5	0.9	0.5	0.5	13.30
Maiolica, Pavia, 13th c.	44.2	51	0.5	0.7	2.5	0	1.5	0.7	5.90
Maiolica, Ferrara, 14th c.	43.3	45.6	1.2	1.5	4.9	2.4	2.8	0.7	13.50

Table 128 (Cont'd)

Sample	SiO_2	PbO	Na_2O	MgO	Al_2O_3	K_2O	CaO	Fe_2O_3	MO
Maiolica, Urbina, 16th c.	58.9	26.2	1.4	0.4	4	5.3	2	0.5	13.60
Maiolica, Deruta, 15th c.	58.9	25.4	2	0.7	0	5.8	3.1	0.4	12.00
Maarrat al Numan, Syria, 11-12th c.	62.1	16.2	12.2	1.9	1.1	1.4	4.3	0.6	21.50
Maarrat al Numan, Syria, 11-12th c.	73.2	0.6	13.5	2.4	1.8	1.8	5.4	1.2	26.10
Maarrat al Numan, Syria, 11-12th c.	71.1	0	19.7	0.7	0	1.8	5.2	1.5	28.90
Maarrat al Numan, Syria, 11-12th c.	70.3	0.1	18.2	2.5	1.5	1.8	4.8	0.8	29.60
Maarrat al Numan, Syria, 11-12th c.	67	0	21.8	0.4	0	2	7.9	0.9	33.00
Fustat, Egypt, 10-12th c.	45.7	29.3	2.6	0.2	2.2	2.5	1.3	0.6	9.40
Deh Luran, Sasanian, Iran, 3rd c.	67.21	0	8.68	2.12	4.44	4.46	6.28	0.85	26.83
Deh Luran, Sasanian, Iran, 3rd c.	70.75	0	11.39	1.95	2.97	2.9	4.2	0.76	24.17
Deh Luran, Parthian, Iran, 3rd c.	62.54	0	8.17	3.2	2.57	4.82	7.78	3.71	30.25
Nippur, Iraq, Parthian, 3rd c.	66.07	0	10.27	4.09	3.66	4.64	7.27	1.43	31.36
Nippur, Iraq, Parthian, 3rd c.	62.99	0	13.37	3.67	5.95	5.61	6.32	1.16	36.08
Nippur, Iraq, Parthian, 3rd c.	62.19	0	5.9	6.34	6.01	3.87	11.16	2.7	35.98
Nippur, Iraq, Parthian, 3rd c.	61.78	0	12.87	3.38	5.88	4.94	5.4	2.72	35.19
Nippur, Iraq, Parthian, 3rd c.	69.92	0	6.41	2.51	7.26	5.74	5.17	1.08	28.17
Nippur, Iraq, Parthian, 3rd c.	65.18	0	9.88	3	4.94	5.44	7.3	1.68	32.24
Nippur, Iraq, Parthian, 3rd c.	66.54	0	11.28	3.47	2.19	5.12	6.32	5	33.38
Nippur, Iraq, Parthian, 3rd c.	58.46	0	8.55	3.31	12.93	5.56	6.87	3.31	40.53
Nippur, Iraq, Parthian, 3rd c.	60.3	0	13.93	3.04	3.15	4.74	6.33	3.98	35.17
Nippur, Iraq, Parthian, 3rd c.	63	0	10.15	5.27	4.08	3.57	9.25	2.79	35.11
Nippur, Iraq, Parthian, 3rd c.	59.84	0	10.75	4.15	2.19	6.54	7.33	4.84	35.80
Nippur, Iraq, Parthian-Sasanian, 3rd c.	62.11	0	16.3	4.12	3.28	4.36	7.29	0.96	36.31

Table 128 (Cont'd)

Sample	SiO_2	Na_2O	MgO	Al_2O_3	K_2O	CaO	Fe_2O_3	MO
Nippur, Iraq, Parthian-Sasanian, 3rd c.	66.19	13.88	3.7	3.23	5.38	5.41	1.32	32.92
Nippur, Iraq, Sasanian, 3rd c.	64.26	14.76	4.38	3.51	3.73	7.2	1.05	34.63
Nippur, Iraq, Sasanian, 3rd c.	65.94	10.47	3.69	3.11	4.86	6.99	0.89	30.01
Nippur, Iraq, Parthian, 3rd c.	62.2	19.6	2.4	2.8	4.5	7.3	1.3	37.90
Nippur, Iraq, Sasanian, 3rd c.	67.4	9.6	3.3	2.6	5.7	8.4	3	32.60
Nippur, Iraq, Parthian, 3rd c.	63.4	16.2	3.9	4.4	4.2	7.1	0.8	36.60
Nippur, Iraq, Parthian, 3rd c.	65.8	13.2	4	3.8	4.2	7.9	0.9	34.00
Aksum, Ethiopia, Sasanian, 3rd c.	66.3	10.29	3.74	1.49	4.71	7.81	1.42	29.46
Aksum, Ethiopia, Sasanian, 3rd c.	65.19	9.46	4.44	1.57	4.31	8.76	1.87	30.41
Aksum, Ethiopia, Sasanian, 3rd c.	67.11	7.85	4.91	2.02	4.34	10.05	2.54	31.71
Aksum, Ethiopia, Sasanian, 3rd c.	66.16	10.09	4.33	1.75	5.04	8.58	2.32	32.11
Aksum, Ethiopia, Sasanian, 3rd c.	65.51	9.42	4.48	1.59	5.15	8.12	0.81	29.57
Aksum, Ethiopia, Sasanian, 3rd c.	65.05	13.31	3.83	2.14	3.95	7.48	0.97	31.68
Aksum, Ethiopia, Sasanian, 3rd c.	65.54	10.17	4.27	1.53	4.86	8.85	2.32	32.00
Babylon/Susa/Warka/Sippar/Nineveh, Parthian-Sasanian, 3rd c.	60.39	8.4	5.61	3.13	3.59	10.3	1.54	32.57
Babylon/Susa/Warka/Sippar/Nineveh, Parthian-Sasanian, 3rd c.	70.4	8.98	2.03	1.5	6.68	6.11	0.78	26.08
Babylon/Susa/Warka/Sippar/Nineveh, Parthian-Sasanian, 3rd c.	63.97	10.68	3.33	1.56	4.7	7.09	0.89	28.25
Babylon/Susa/Warka/Sippar/Nineveh, Parthian-Sasanian, 3rd c.	68.55	12.54	3.4	2.3	3.58	6.3	0.71	28.83
Babylon/Susa/Warka/Sippar/Nineveh, Parthian-Sasanian, 3rd c.	64.31	11.27	3.55	4.22	3.45	6.36	1.33	30.18
Babylon/Susa/Warka/Sippar/Nineveh, Parthian-Sasanian, 3rd c.	64.03	11.44	2.79	3.73	5.18	5.96	4.16	33.26
Babylon/Susa/Warka/Sippar/Nineveh, Parthian-Sasanian, 3rd c.	64.44	10.03	4.36	4.21	4.39	8.28	1.99	33.26
Babylon/Susa/Warka/Sippar/Nineveh, Parthian-Sasanian, 3rd c.	63.94	11.54	2.85	5.79	5.69	5.08	2.87	33.82
Nishapur, Iran, Sasanian, 3rd c.	67.07	11.03	3.23	2.45	5.56	5.96	1.14	29.37
Nishapur, Iran, Sasanian, 3rd c.	65.75	9.83	3.54	4.27	4.3	7.94	1.98	31.86
Seleucia, Iraq, 1st-3rd c.	69.1	6.4	3.1	3.6	7.8	7.7	1.5	30.10
Veh Ardasir, Iraq, Sasanian, 3rd c.	60.2	12.8	4.5	4.4	4.1	9.3	1.7	36.80
Veh Ardasir, Iraq, Sasanian, 3rd c.	60.5	13.4	4.9	4.2	4.7	9.8	1.3	38.30
Veh Ardasir, Iraq, Sasanian, 3rd c.	64.7	10.9	3.9	2.2	4	7.6	1.5	30.10
Veh Ardasir, Iraq, Sasanian, 3rd c.	63.5	12.8	4.7	3	4.5	7.7	1.4	34.10
Veh Ardasir, Iraq, Sasanian, 3rd c.	60.4	11.3	5.2	4	4.5	10	1.9	36.90
Veh Ardasir, Iraq, Sasanian, 3rd c.	63.9	12.9	4.3	2.3	4.6	7.8	1.1	33.00
Veh Ardasir, Iraq, Sasanian, 3rd c.	68.4	8.2	5	2.6	4.9	8.4	1.5	30.60
Veh Ardasir, Iraq, Sasanian, 3rd c.	68.3	9.4	3.6	1.9	3.9	7.1	1	26.90
Veh Ardasir, Iraq, Sasanian, 3rd c.	67.6	9.2	4.4	2.1	3.5	8	1.3	28.50
Veh Ardasir, Iraq, Sasanian, 3rd c.	67	8.6	3.9	3	3.7	8.5	1.4	29.10

Table 128 (Cont'd.)

Sample	SiO_2	PbO	Na_2O	MgO	Al_2O_3	K_2O	CaO	Fe_2O_3	MO
Veh Ardasir, Iraq, Sasanian, 3rd c.	67.6	0	10.8	3.8	1.5	4.1	6.9	0.9	28
Veh Ardasir, Iraq, Sasanian, 3rd c.	65.9	0	10.1	3.3	3.1	4.9	8.1	1.3	30.8
Veh Ardasir, Iraq, Sasanian, 3rd c.	67.2	0	8.8	4	3.6	3.6	7.8	1.9	29.70
Ain Sinu, Iraq, Parthian, 3rd c.	63.84	0.5	11.52	3.51	3.11	4.28	8.65	1.77	32.84
Ain Sinu, Iraq, Parthian, 3rd c.	69.27	0.59	12.25	0.77	1.98	2.74	9.29	0.66	27.69
Ain Sinu, Iraq, Parthian, 3rd c.	68.13	0	11.01	2.99	2.36	4.1	5.96	1.42	27.84
Ain Sinu, Iraq, Parthian, 3rd c.	68.12	0	14.24	0.86	1.87	1.8	7.96	0.83	27.56
Ain Sinu, Iraq, Parthian, 3rd c.	66.91	0.54	12.16	1.14	2.04	3.49	8.42	0.94	28.19
Ain Sinu, Iraq, Parthian, 3rd c.	64.98	1.09	11.88	2.81	2.35	3.41	5.8	1.82	28.07
Ain Sinu, Iraq, Parthian, 3rd c.	64.47	0.77	14.11	2.34	3.04	3.52	5.96	1.64	30.61
Ain Sinu, Iraq, Parthian, 3rd c.	62.8	0	11.14	3.75	3.38	4	8.49	2.1	32.86
Jordan, 5th	56	0	10.4	1.1	19.6	5.9	1.7	4	42.70
Jordan, 5th	56	0	15.3	1.5	13.2	4.1	4.2	3.8	42.10
Jordan, 5th	61.3	0	10.4	1.2	11.2	5.4	4.3	4.3	36.80
Jordan, 5th	68.3	0	9.4	1	10.1	5.6	1.6	3.3	31.00

A.5. Appendix of XRD Spectra

Table 129. XRD spectra of the yellow glazes of the potsherd samples of a. K128, b. K149, c. K152 without baseline corrections.

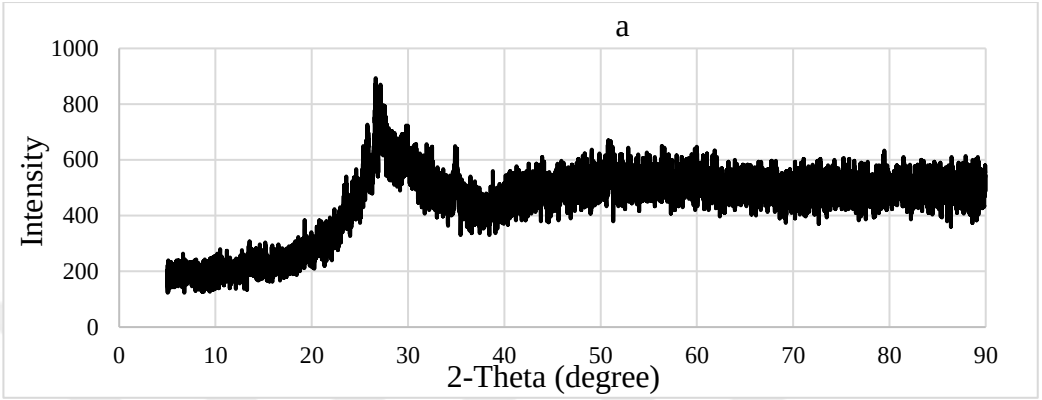

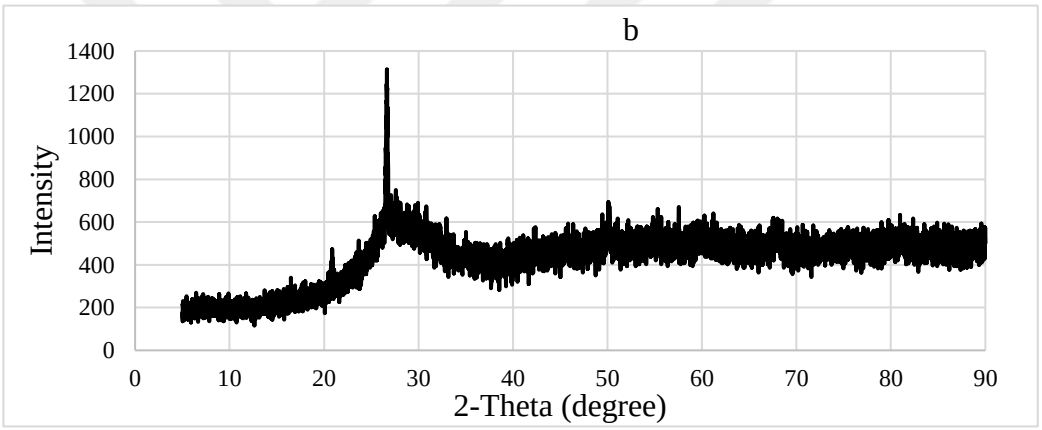

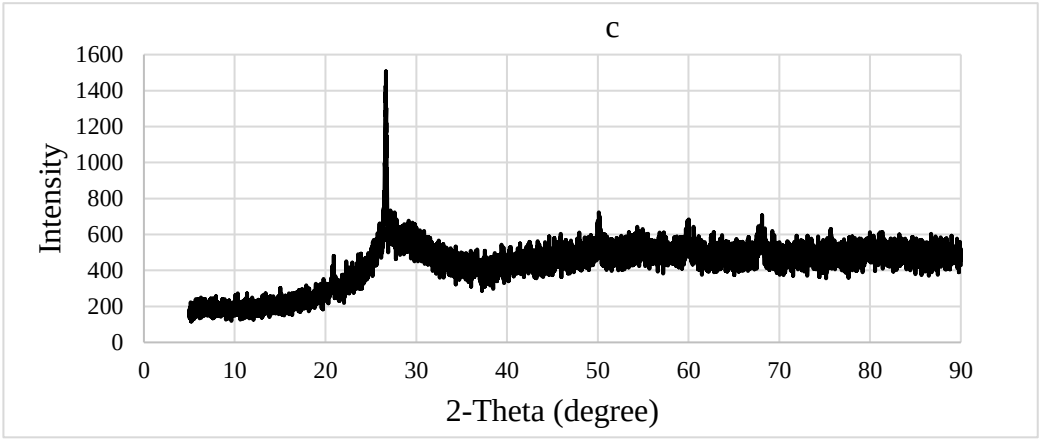

Table 130. XRD spectra of the green glazes of the potsherd samples of a. K115, b. K157, c. K160 without baseline corrections.

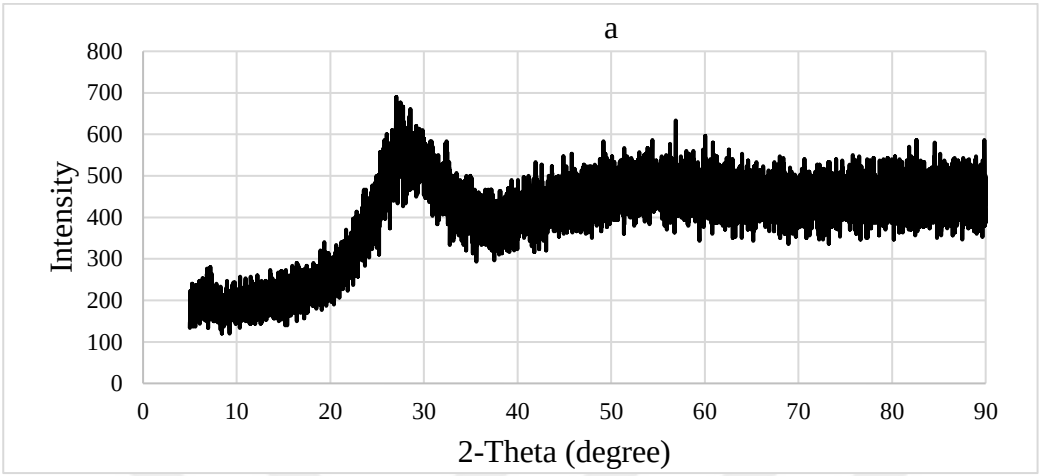

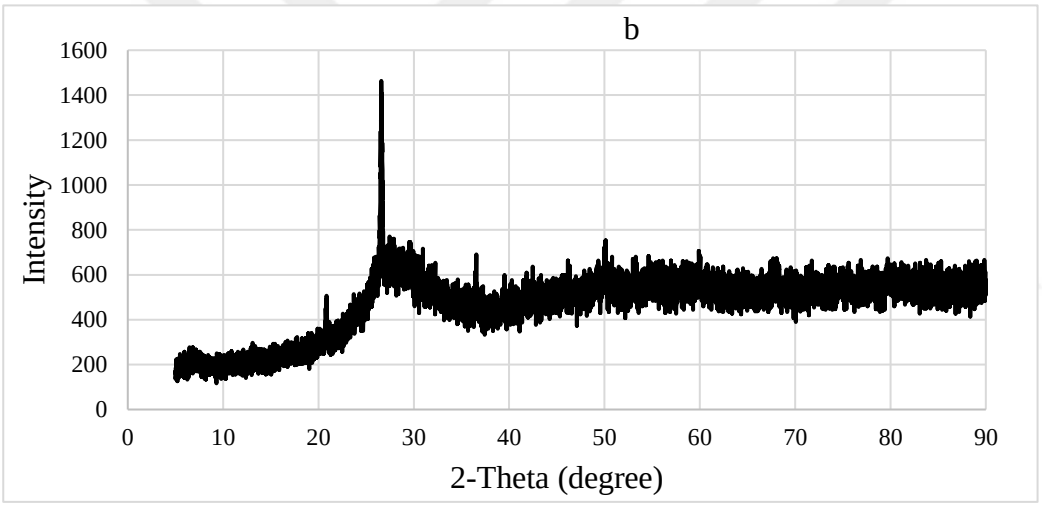

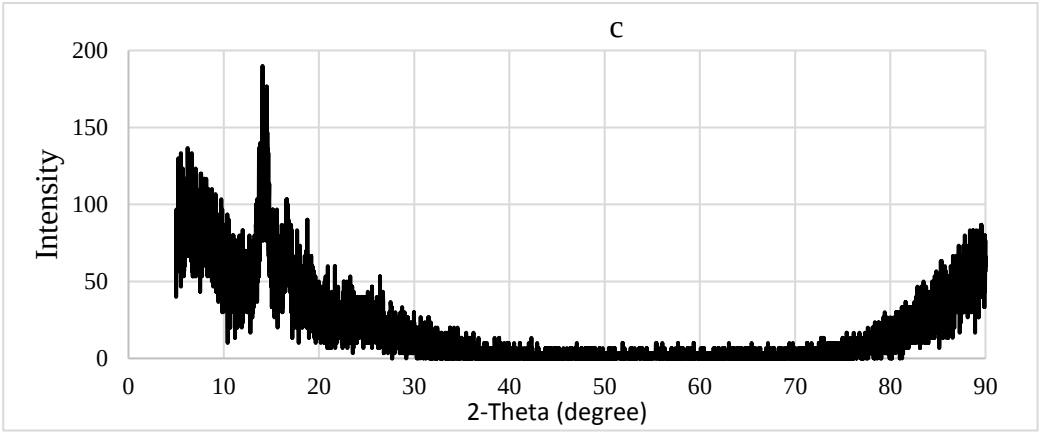

Table 131. XRD spectrum of the orange glaze of the potsherd sample of K172 without a baseline correction.

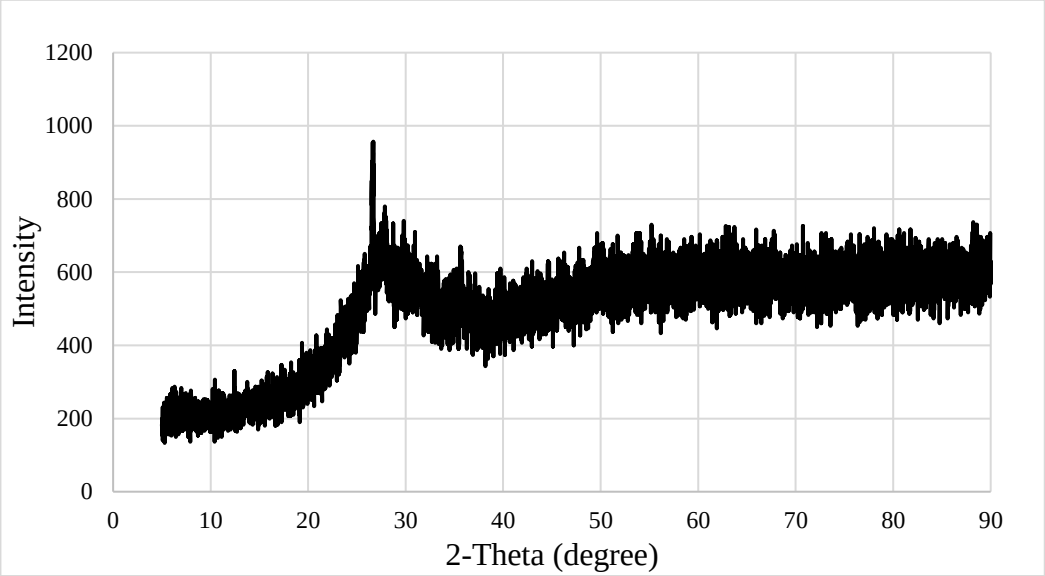

Table 132. XRD spectra of the turquoise glazes of a. the potsherd sample of K223, b. the tile sample of K001 without baseline corrections.

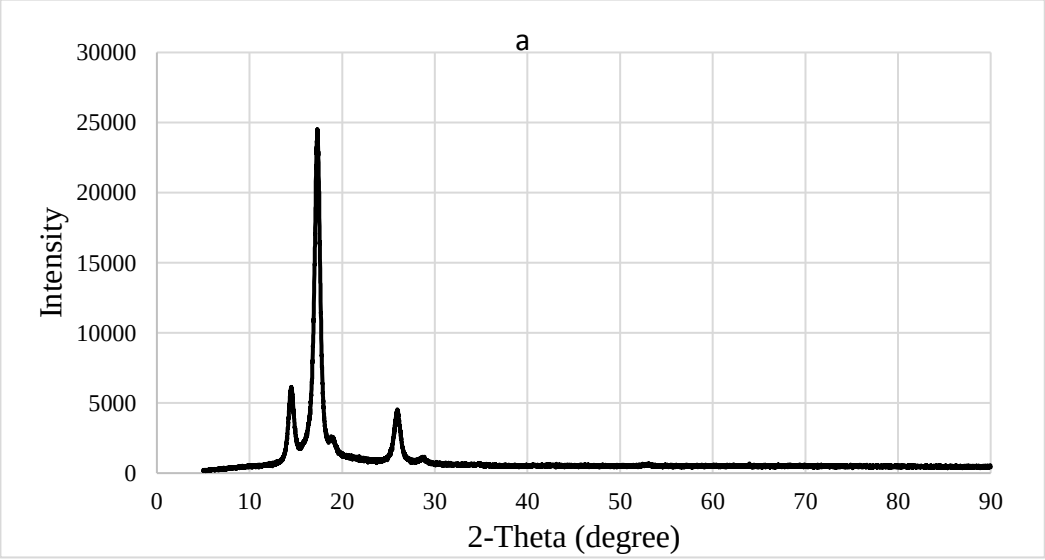

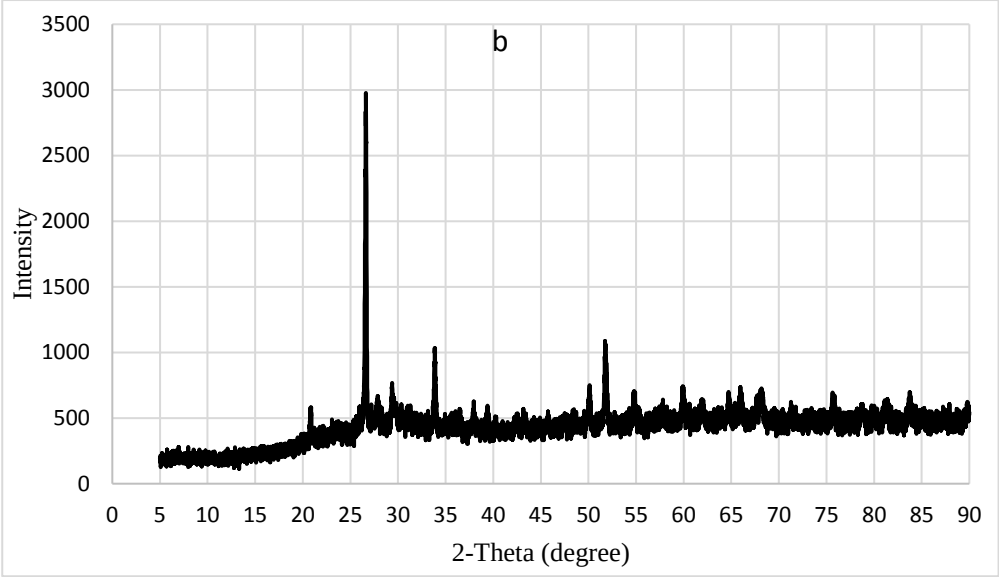

Table 133. XRD spectrum of the brown glaze of the potsherd sample of K129 without a baseline correction.

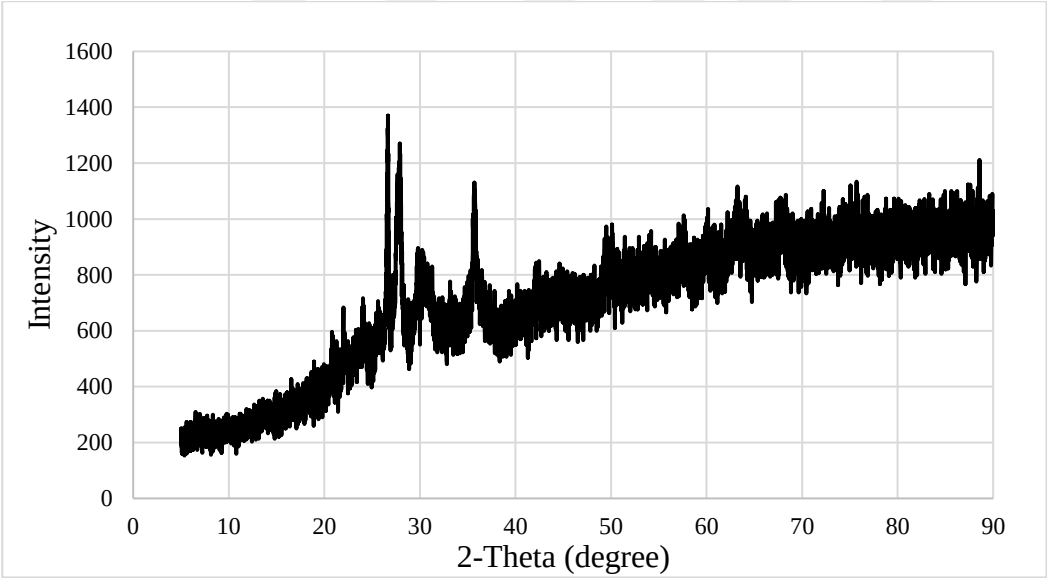

Table 134. XRD spectrum of the black glaze of the tile sample of K002 without a baseline correction.

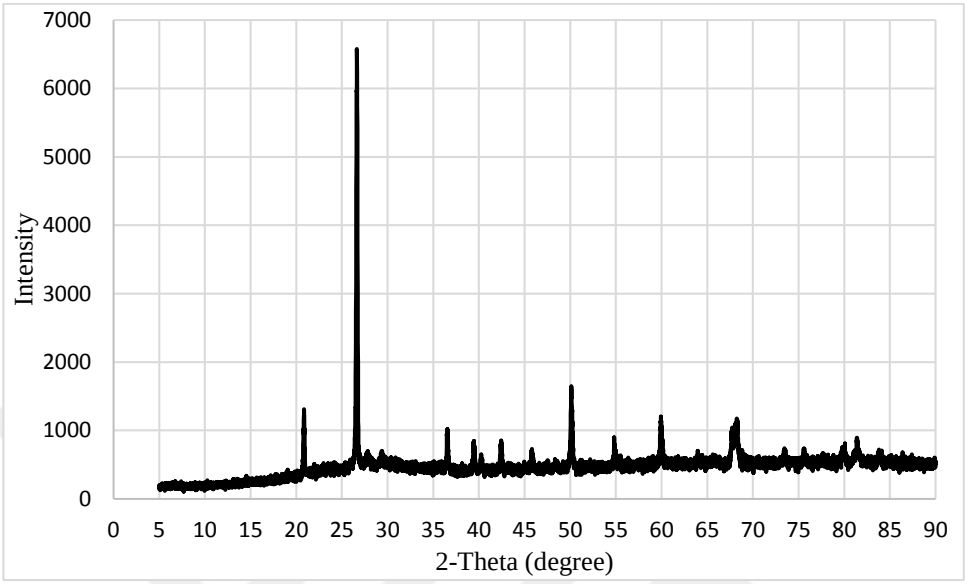

A.6. Appendix of Identification of Compounds by XRD Spectroscopy

Table 135. Identification of phases of the major glaze components, taken from ICDD (International Centre for Diffraction Data) card information for the ones starting with numbers and from RRUFF data set [112] for the ones beginning with R; d-values are calculated according to the Bragg's Law.

Compound Name	Peak Positions (2Θ)	d-value (Å)	Card Number
Monoclinic epidote, $Ca_2(Al,Fe)_3(Si_2O_7)(SiO_4)(OH)_2$	56.13	1.64	45-1446
Cubic carbon iron silicon, $C_{0.12}Fe_{0.79}Si_{0.09}$	43.13, 45.59	2.10, 1.99	43-1098
Tin oxide, SnO_2	38.00, 43.46, 51.92, 54.86	2.37, 2.08, 1.76, 1.65	41-1445
Orthorhombic olivine, $Mg_{1.8}Fe_2(SiO_4)$	36.46, 35.64, 32.25	2.46, 2.52, 2.77	79-1195
Cubic syn maghemite, Fe_2O_3	35.63, 30.24	2.52, 2.95	39-1346
Cubic ferroan spassartine, $(Mn_{2.58}Fe_{0.34}Ca_{0.08})(Al_{1.99}Fe_{0.01})Si_3O_{12}$	34.51	2.60	74-1554
Cubic vanadian spassartine, $(Mn,Ca)_3(Al,V)_2Si_3O_{12}$	34.24, 30.52	2.62, 2.93	47-1815
Hexagonal syn hematite, Fe_2O_3	33.18, 35.77	2.70, 2.51	73-0603
Hexagonal siderite, $FeCO_3$	32.0, 52.83	2.80, 1.73	29-0696
Syn hexagonal calcian siderite, $Ca_{0.1}Mg_{0.33}Fe_{0.57}(CO_3)$	31.89, 52.65, 42.20	2.80, 1.74, 2.14	80-0502
Orthorhombic magnesian fayalite, $(Fe,Mg)_2(SiO_4)$	31.82, 36.06, 35.18	2.81, 2.49, 2.55	31-0633
Hexagonal manganoan magnetoplumbite-5H, $Pb(Fe^{3+},Mn^{3+})_{12}O_{19}$	31.77, 33.78, 62.4, 36.73	2.81, 2.65, 1.49, 2.45	43-0666
Orthorhombic manganoan fayalite, $(Fe,Mn)_2SiO_4$	31.25, 35.45	2.86, 2.53	12-0220

Table 135 (Cont'd)

Component Name	Peak Positions (2Θ)	d-value (Å)	Card Number
Hexagonal dolomite, $CaMg(CO_3)_2$	30.94, 41.13, 51.07	2.89, 2.19, 1.79	36-0426
Hexagonal manganoan calcite, $(Ca,Mg)CO_3$	30.27, 49.21, 99.40, 40.23	2.95, 1.85, 1.01, 2.24	2-0714
Monoclinic diopside, $Ca(Mg,Al)(Si,Al)_2O_6$	29.91, 30.35, 27.68	2.99, 2.94, 3.22	41-1370
Monoclinic ferrous diopside	29.85, 35.74, 35.43	2.99, 2.51, 2.53	74-2424
Monoclinic aluminian titanite, $Ca(Ti,Al)(SiO_4)(O,F)$	29.83, 34.40, 27.49	2.99, 2.61, 3.24	50-1614
Monoclinic augite, $Ca(Fe,Mg)Si_2O_6$	29.77, 35.51, 30.16, 34.84	3.00, 2.53, 2.96, 2.57	24-0201
Hexagonal magnesian calcite, $(Ca,Mg)CO_3$	29.71, 48.13, 39.81	3.00, 1.89, 2.26	43-0697
Hexagonal syn calcite, $CaCO_3$	29.41, 39.40, 43.15	3.04, 2.29, 2.10	5-0586
Cubic syn sphalerite, ZnS	29.06, 48.37	3.07, 1.88	79-0043
Monoclinic syn coesite, SiO_2	28.87, 25.96	3.09, 3.43	14-0654
Pyroxene $[(Na,Ca,Fe^{2+},Mg,Zn,Mn,Li)(Mg, Fe^{3+}, Fe^{2+},Cr,Al,Co,Mn,Sc,Ti,Vn)(Si,Al)_2O_6]$	28.03, 29.67, 32.42, 35.33	3.18, 3.01, 2.76, 2.54	R110130.9
Triclinic ordered albite, $NaAlSi_3O_8$	27.89, 23.52, 24.14, 13.85	3.20, 3.78, 3.68, 6.39	9-0466
Triclinic syn disordered calcian albite, $(Na,Ca)(Si,Al)_4O_8$	27.86, 23.77, 22.09, 28.13	3.20, 3.74, 4.02, 3.17	9-0456
Monoclinic syn titanite ($CaTiSiO_5$)	27.51	3.24	25-0177
Tetragonal syn rutile, TiO_2	27.45, 54.32, 36.09	3.25, 1.69, 2.49	21-1276
Hexagonal syn graphite-3R, C	26.60, 43.45	3.35, 2.08	26-1079

Table 135 (Cont'd)

Component Name	Peak Positions (2Θ)	d-value (Å)	Card Number
Hexagonal beta quartz, SiO_2	26.27, 20.51, 50.42	3.39, 4.33, 1.81	89-8949
Hexagonal silica, SiO_2	26.19, 20.45, 49.58	3.40, 4.34, 1.84	11-0252
Tetragonal silica, SiO_2	26.03, 23.9, 26.75, 19.71	3.42, 3.72, 3.33, 4.5	13-0026
Orthorhombic plumbian barite, $(Ba,Pb)SO_4$	26.00, 24.99	3.42, 3.56	46-1415
Tetragonal syn anatase, TiO_2	25.28, 48.05	3.52, 1.89	21-1272
Monoclinic syn tridymite, SiO_2	21.62, 20.5, 23.28	4.11, 4.33, 3.82	18-1170
Triclinic ordered microcline, $KAlSi_3O_8$	21.03, 24.03, 23.21	4.22, 3.70, 3.08	19-0926
Hexagonal syn magnetoplumbite-5H, $PbO(Fe_2O_3)_6$	20.93, 30.39, 34.24	4.24, 2.94,2.62	76-1804
Plagioclase $Na(AlSi_3O_8)$,$Ca(Al_2Si_2O_8)$	13.858, 24.184, 27.97	6.39, 3.68, 3.19	METU Chemistry
Monoclinic hornblende, $Na_{0.9}K_{0.4}Ca_{1.6}Mg_{2.8}Fe_{1.4}Ti_5Al_{2.4}$-$Si_6O_{23}(OH)$	10.49, 28.52	8.42, 3.13	71-1060
Mica/illite	8.932, 26.854, 45.58	9.90, 3.32, 1.99	METU Chemistry
Hexagonal phlogopite-3T, $KMg_3(Si_3Al)O_{10}(OH)_2$	8.75, 33.08, 26.13	10.10, 3.41, 2.71	10-0492

Table 135 (Cont'd)

Component Name	Peak Positions (2Θ)	d-value (Å)	Card Number
Monoclinic tenorite, CuO	35.67, 38.83, 48.88, 53.68, 58.42, 61.65, 66.0, 66.52, 68.01, 68.37, 72.66, 75.06, 75.53, 80.33, 82.65, 83.33, 83.97, 86.93	2.52, 2.32, 1.86, 1.71, 1.58, 1.50, 1.42, 1.41, 1.38, 1.37, 1.30, 1.27, 1.26, 1.20, 1.17, 1.16, 1.15, 1.12	R-120076.9
Tetragonal cristobalite, SiO_2	22.03, 28.50, 31.50, 36.12, 42.69, 44.84, 47.07, 48.71, 57.1	4.04, 3.13, 2.84, 2.49, 2.12, 2.02, 1.93, 1.87, 1.61	R060648.1
Quartz, SiO_2	26.62, 20.84	3.3, 4.33	R100134
Gypsum, $CaSO_4.2H_2O$	11.67, 20.77	7.6, 4.3	R040029.1
Portlandite, $Ca(OH)_2$	16.1	5.5	R070210.1
Verdigris, $[Cu(CH_3COO)_2.H_2O]$	12.8, 24.7	6.9, 3.6	27-0145

A.7. Appendix of Macroscopic Examinations of Thin Section Samples of Glazes

D 1.6x/0.1 FWD 36mm Zeiss Objective was used at KUYTAM, Istanbul.

Figure 210. Thin section of K115 potsherd magnified by 34x.

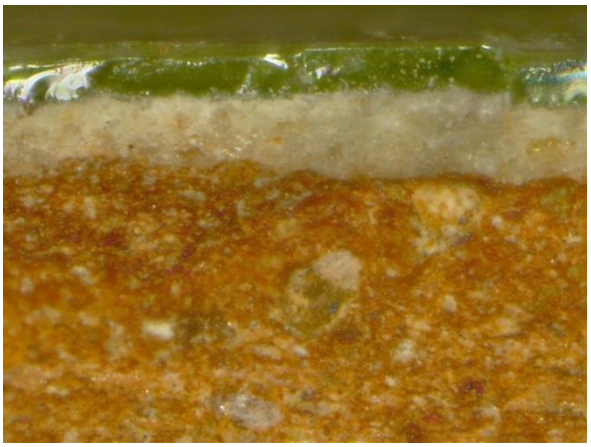

Figure 211. Thin section of K115 interior green glaze magnified by 335x.

Figure 212. Thin section of K115 exterior green glaze magnified by 335x.

Figure 213. Thin section of K128 potsherd magnified by 34x.

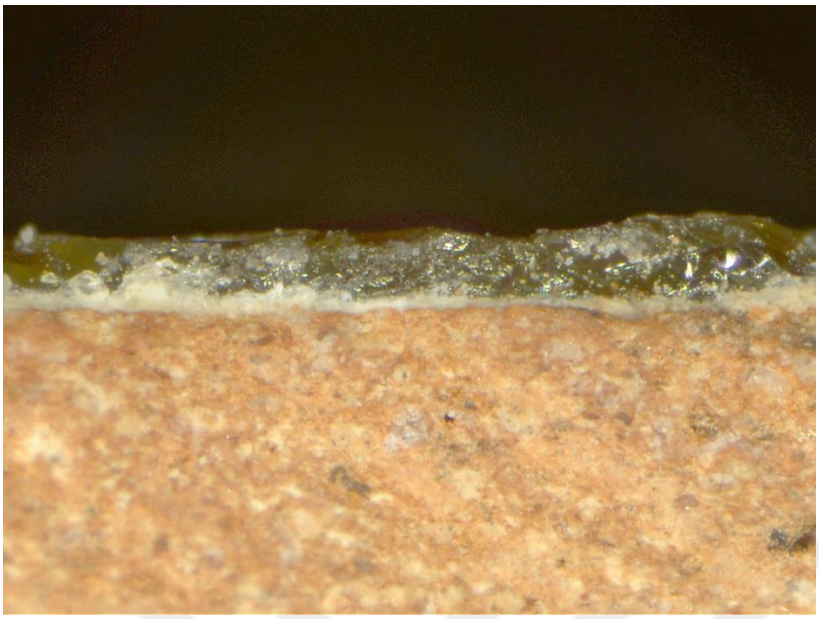

Figure 214. Thin section of K128 interior brown glaze magnified by 240x.

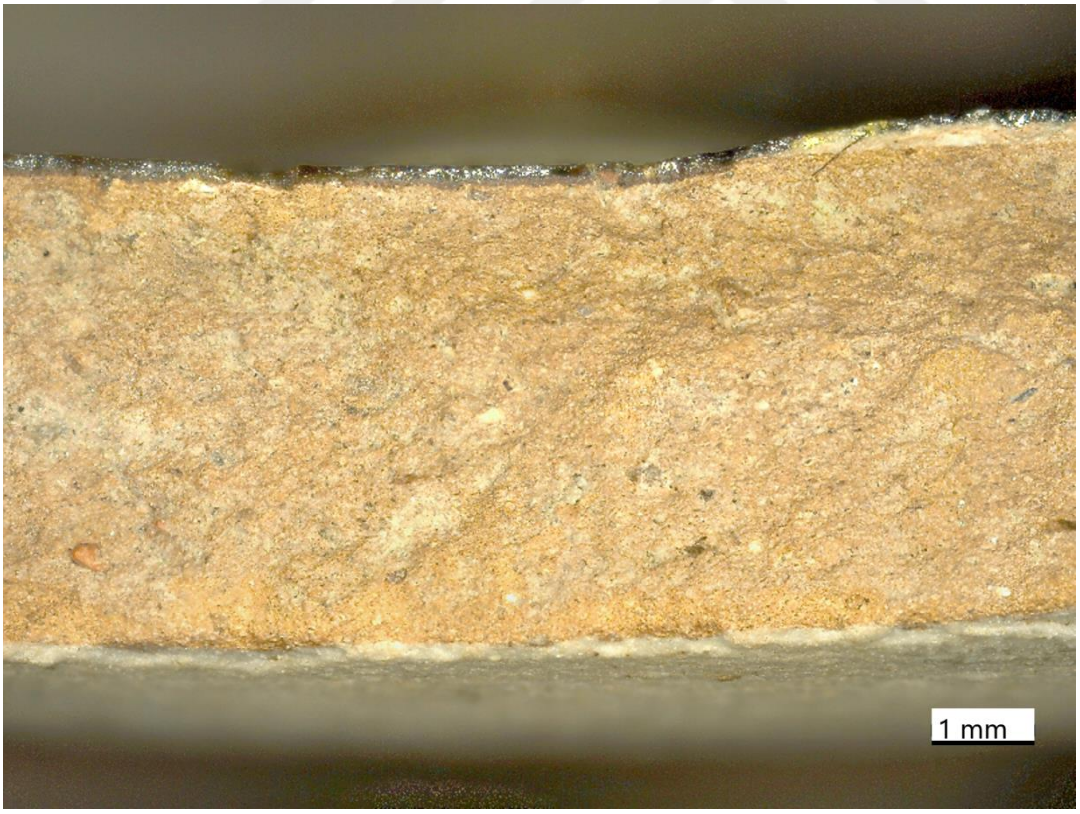

Figure 215. Thin section of K129 potsherd magnified by 34x.

Figure 216. Thin section of K129 interior brown glaze magnified by 335x.

Figure 217. Thin section of K149 potsherd magnified by 34x.

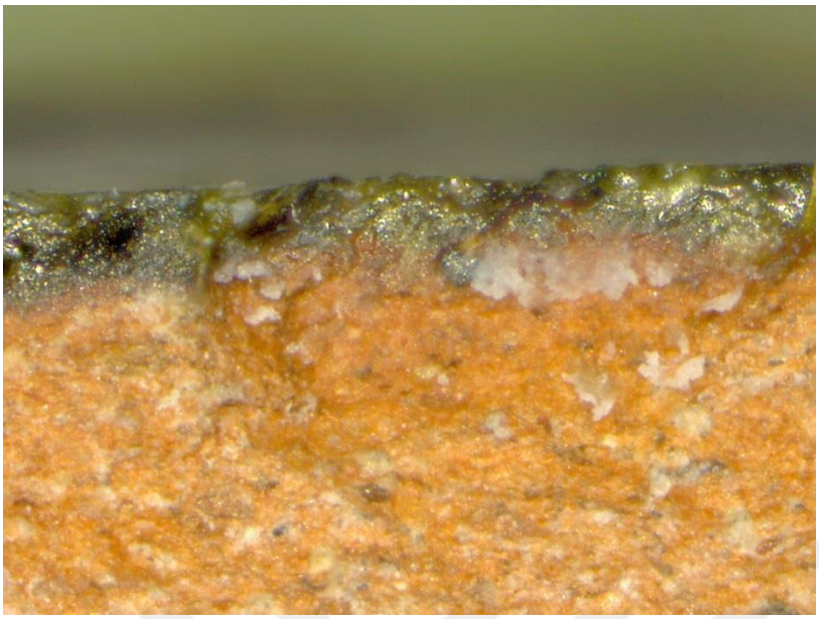

Figure 218. Thin section of K149 exterior green glaze magnified by 335x.

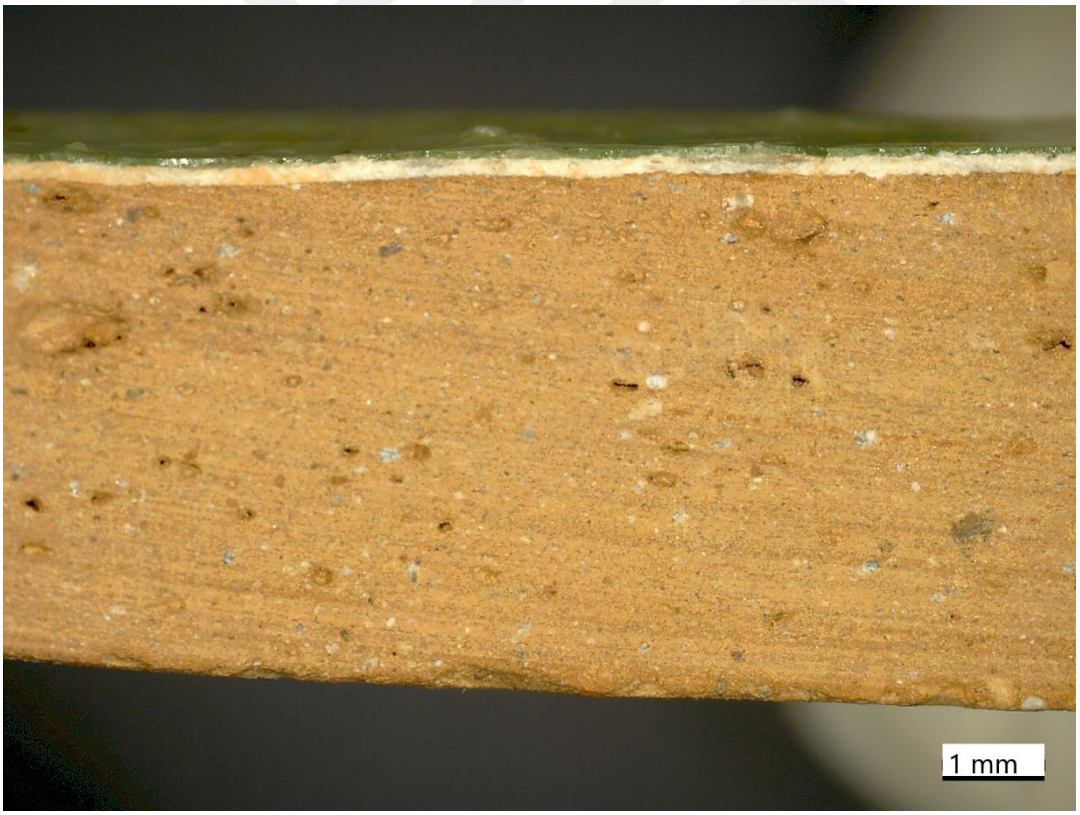

Figure 219. Thin section of K152 potsherd magnified by 34x.

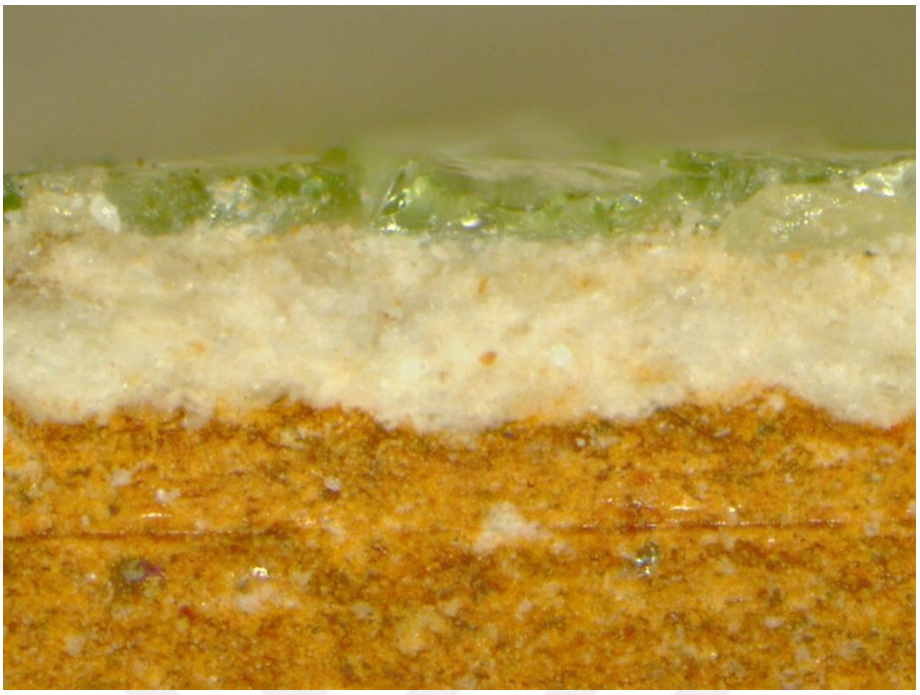

Figure 220. Thin section of K152 interior green glaze magnified by 335x.

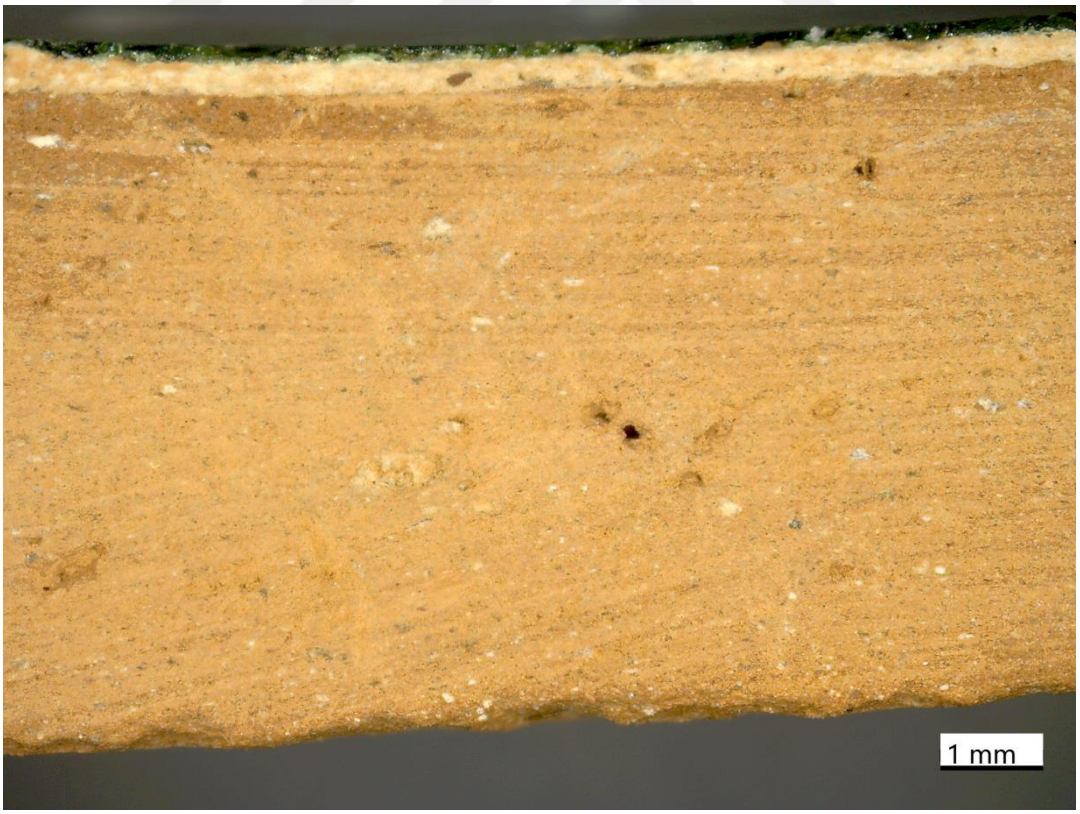

Figure 221. Thin section of K157 potsherd magnified by 34x.

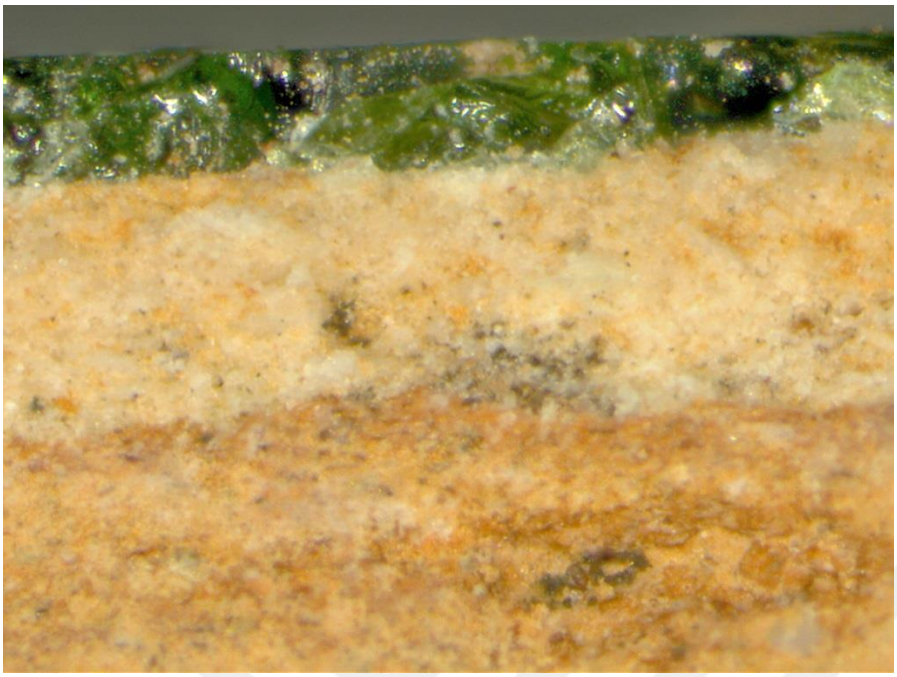

Figure 222. Thin section of K157 interior green glaze magnified by 335x.

Figure 223. Thin section of K160 potsherd magnified by 34x.

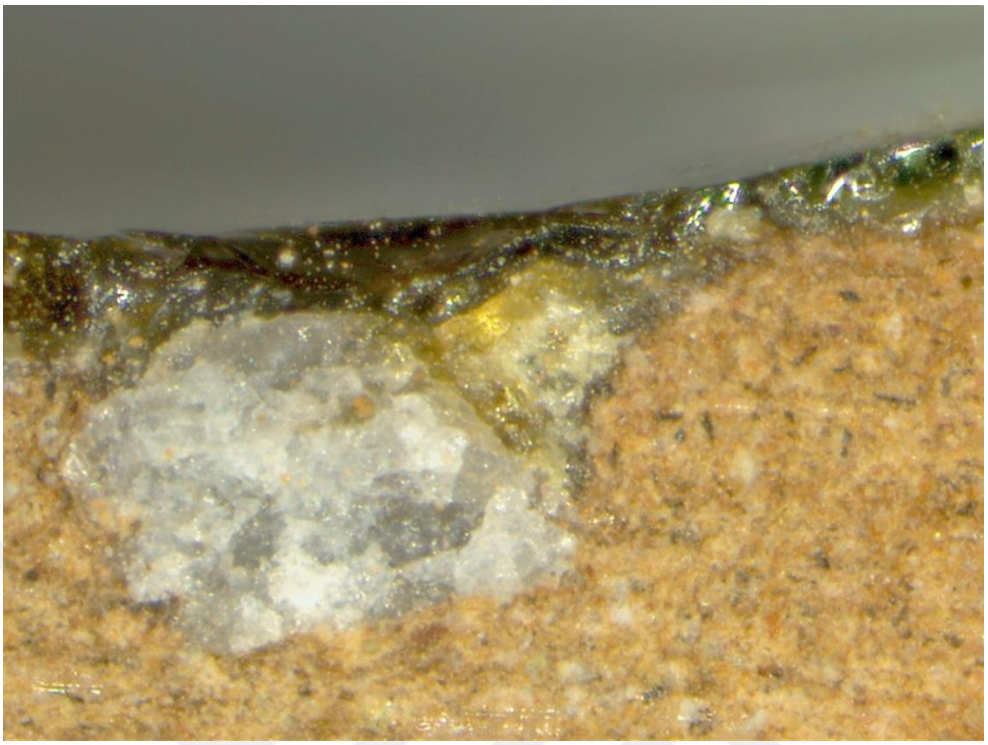

Figure 224. Thin section of K160 interior yellowish green glaze magnified by 335x.

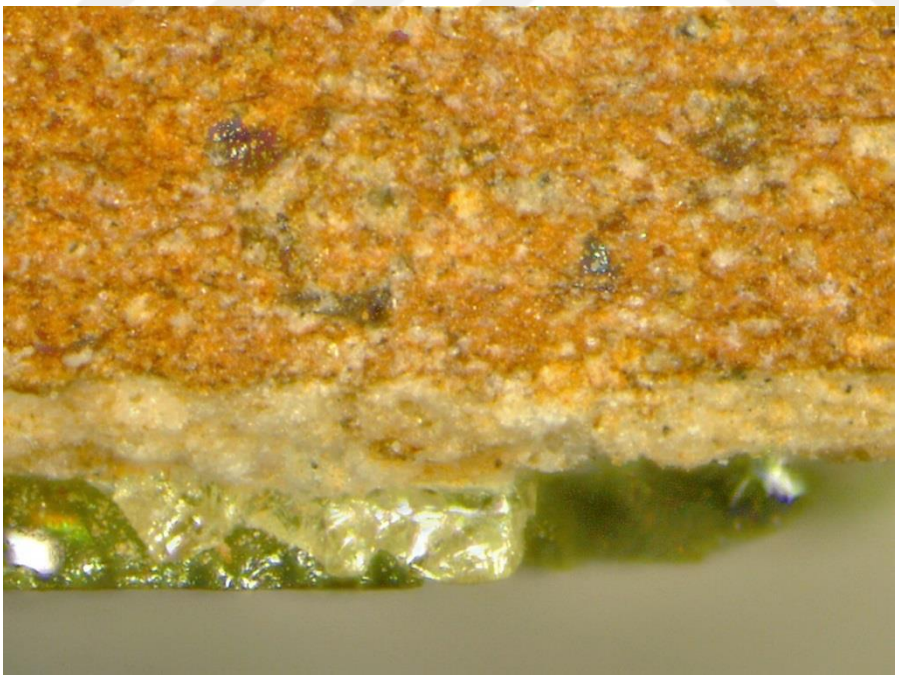

Figure 225. Thin section of K160 exterior green glaze magnified by 335x.

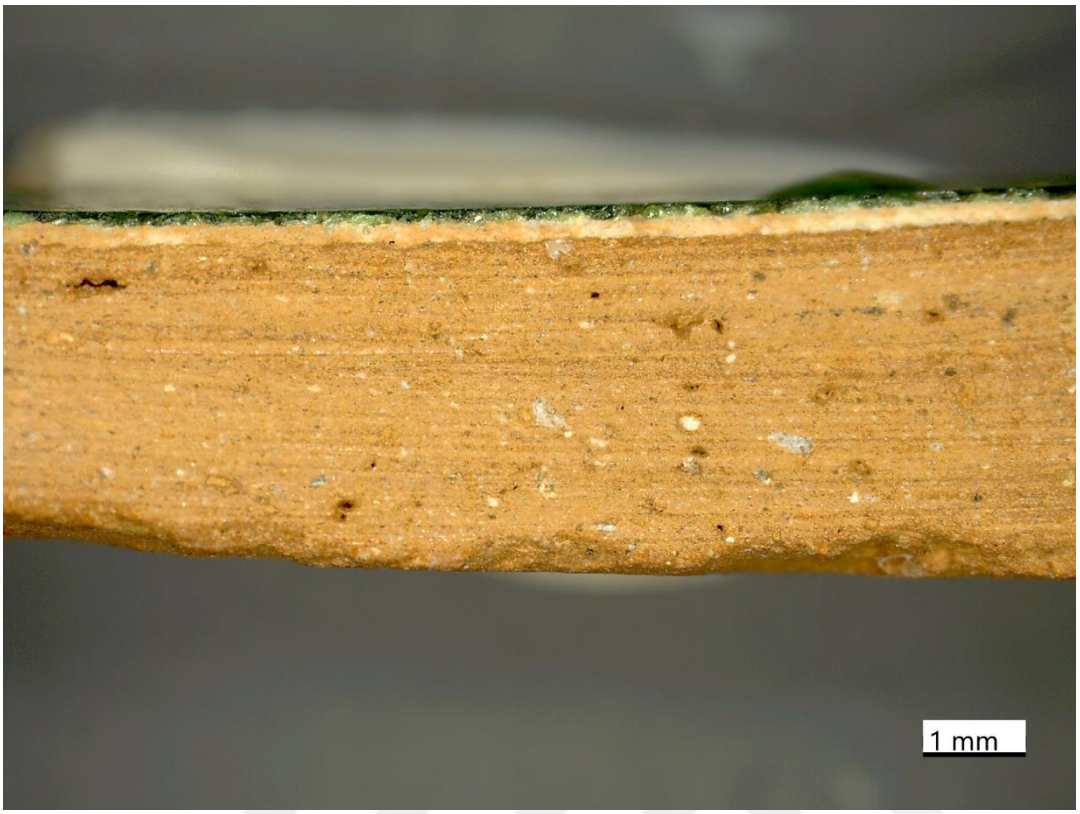

Figure 226. Thin section of K161 potsherd magnified by 34x.

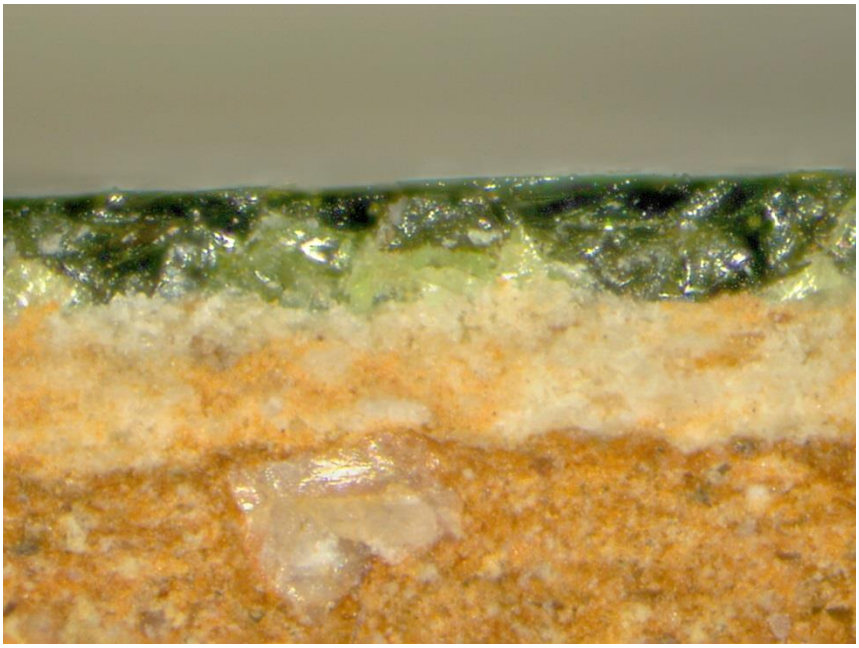

Figure 227. Thin section of K161 interior green glaze magnified by 335x.